Delft University of Technology

Investigation of Temperature Tolerance in Saccharomyces cerevisiae under Anaerobic Conditions

Lip, K.Y.F.

DOI
10.4233/uuid:a2f06688-c74a-4160-ac50-62fecc9a5f8b

Publication date
2022

Document Version
Final published version

Citation (APA)
Lip, K. Y. F. (2022). *Investigation of Temperature Tolerance in Saccharomyces cerevisiae under Anaerobic Conditions*. [Dissertation (TU Delft), Delft University of Technology]. https://doi.org/10.4233/uuid:a2f06688-c74a-4160-ac50-62fecc9a5f8b

Important note
To cite this publication, please use the final published version (if applicable).
Please check the document version above.

INVESTIGATION OF
TEMPERATURE TOLERANCE IN
SACCHAROMYCES CEREVISIAE
UNDER ANAEROBIC CONDITIONS

KA YING FLORENCE LIP

PROPOSITIONS
ACCOMPANYING THE THESIS

"Investigation of Temperature Tolerance in Saccharomyces cerevisiae under Anaerobic Conditions"

by Ka Ying Florence Lip

1/ Acquired thermotolerance in yeast does not result in a higher growth rate but a lower death rate at supra-optimal temperatures (Chapter 4 of this thesis).

2/ Temperature tolerance is determined by a definite set of genes which differs between strains (Chapters 2 and 3 of this thesis).

3/ Too much emphasis on planning hampers creativity.

4/ To efficiently address environmental issues, the development of empathetic skills should be reinforced.

5/ Being verbally less expressive is not a sign of disinterest or lack of opinion.
M. Kawabata, D. Gastaldo, The Less Said, the Better: Interpreting Silence in Qualitative Research, International Journal of Qualitative Methods. 14 (2015) 1609406915618123. https://doi.org/10.1177/1609406915618123.

6/ Integrative multi-omics analysis provides more questions than answers. (This thesis)

7/ Finishing a PhD project during the pandemic outbreak of COVID19 put's one to the proof of either flexibility or indifference

8/ Artificial intelligence has no guarantee to provide objective and rational decisions and always relies on human intelligence.
C. de Saint Laurent, In Defence of Machine Learning: Debunking the Myths of Artificial Intelligence, Eur J Psychol. 14 (2018) 734–747. https://doi.org/10.5964/ejop.v14i4.1823.

9/ An agreement is by no means effective unless there is consensual commitment and proper evaluation of the final achievements.

10/ Disregarding seemingly useless data is like throwing away an appealing piece of furniture which does not fit in your house anymore.

These propositions are considered opposable and defendable, and have been approved as such by the promotor Prof.dr.ir. M. C. M. van Loosdrecht and co-promotor Dr. W. M. van Gulik.

Investigation of Temperature Tolerance in *Saccharomyces cerevisiae* under Anaerobic Conditions

Dissertation

for the purpose of obtaining the degree of doctor
at Delft University of Technology
by the authority of the Rector Magnificus, Prof.dr.ir. T.H.J.J. van der Hagen;
Chair of the Board for Doctorates
to be defended publicly on
Monday, 28 March 2022 at
at 10:00 o'clock

by

Ka Ying Florence LIP

Master of Science in Biotechnology, Wageningen University,
The Netherlands

born in Hong Kong, China

This dissertation has been approved by the promotor and the copromotor.

Composition of the doctoral committee

Rector Magnificus	Chairperson
Prof.dr.ir. M.C.M. van Loosdrecht	Delft University of Technology, promotor
Dr. W.M. van Gulik	Delft University of Technology, copromotor

Independent members

Prof.dr. J.G. Daran	Delft University of Technology
Prof.dr. G. Eggink	Wageningen University
Prof.dr.ir. M. De Mey	University Ghent
Dr. M. Jansen	DSM
Prof.dr. P. Osseweijer	Delft University of Technology

Other member

Dr. L. Domingues	University of Minho

The Road Not Taken
by Robert Frost

Two roads diverged in a yellow wood,
And sorry I could not travel both
And be one traveler, long I stood
And looked down one as far as I could
To where it bent in the undergrowth;

Then took the other, as just as fair,
And having perhaps the better claim,
Because it was grassy and wanted wear;
Though as for that the passing there
Had worn them really about the same,

And both that morning equally lay
In leaves no step had trodden black.
Oh, I kept the first for another day!
Yet knowing how way leads on to way,
I doubted if I should ever come back.

I shall be telling this with a sigh
Somewhere ages and ages hence:
Two roads diverged in a wood, and I—
I took the one less travelled by,
And that has made all the difference.

Contents

Summary

Saccharomyces yeasts are common workhorses for the production of alcoholic beverage and bio-ethanol. In these production processes, temperature is one of the predominant factors determining the operational costs of the industrial fermentation processes and the quality of the products (alcoholic beverage) because it influences the functioning of cellular activities in yeast cells. *Saccharomyces* yeasts in natural habitats have a wide range of difference in temperature optimal due to the geographic difference of habitats. *Saccharomyces* yeasts in an artificial environment, such as industrial fermentation processes, adapt to the conditions and have a temperature optimal close to the condition of the production process. In **chapter 2**, various *Saccharomyces* yeasts were compared for their growth performance between 12°C and 40°C wherein we selected two industrial strains which grew the fastest at sub- (12-27°C) and supra-optimal (33-40°C) temperatures. A top-down holistic approach was used to evaluate the temperature impact on cell growth, meaning the substrate uptake rates, (by)products production rates, as well as cellular protein and storage carbohydrates accumulations were measured. To do so, the two selected industrial strains and a laboratory strain were grown in anaerobic chemostat cultures at 12, 30, and 39°C to separate the growth rate effect from temperature effect. Significant differences in biomass and ethanol yields on glucose, total biomass protein, storage carbohydrates contents were observed between strains and cultivation temperatures.

In order to elucidate the possible temperature tolerance mechanisms in the two selected industrial strains, the proteomic profiles of the anaerobic chemostat cultures for the two selected industrial strains together with a laboratory strain were performed by SWITH-MS (sequential window acquisition of all theoretical fragment ion spectra mass spectrometry) and analysed in **chapter 3**.

The proteomic profile of these three strains at three different cultivation temperatures resulted in the quantification of 997 proteins and indicated temperature responses differ between different strains. The common responsive proteins and the strain-specific responsive proteins were detected via PCA (principal component analysis) which is a linear dimension reduction approach and is beneficial for the analysis of data set consists of more than one variable (Temperatures and genetic heterogeneity). Overall, the sub-optimal temperature conditions involved a higher proteome readjustment than that in the supra-optimal temperature conditions. The proteomic data evidenced that the cold response involves strong repression of translation related proteins as well as induction of amino acid metabolism, together with components related to protein folding and degradation. The high temperature response mainly recruits amino acid metabolism.

Different yeast strains showed various responses to sub- and supra-optimal temperature from **chapter 2** and **chapter 3**. To minimize strain to strain differences, an adaptive laboratory evolution of CEN.PK113-7D was performed via the cultivation in an anaerobic SBR (sequential batch reactor) whereby the cultivation temperature was increased stepwise until 39.8°C (**chapter 4**). After 475 generations an evolved strain was obtained. **Chapter 4** outlines the comparison between the unevolved and the evolved strains based on their whole genome sequencing and physiological characteristic in anaerobic sequential batch reactor cultures at 39.8°C, as well as in anaerobic chemostat cultures at 30.0°C and 39.0°C. The evolved strain showed to be better adapted to growth at high temperature compared to the non-evolved strain; the death rate was significantly reduced, and there were fewer cells with membrane rupture at 39.8°C. Deprived of the growth rate effect, both strains had different storage carbohydrate contents and lipid compositions at the supra-optimal temperature. The selection pressure under prolonged high temperature cultivation and anaerobic conditions provoked several mutations, such as single nucleotide polymorphisms as well as small insertions and deletions, in the genome of CEN.PK113-7D. The enrichment gene ontology terms associated with those high impact single nucleotide variants were analysed to identify the related specific biological processes from those mutations which may be responsible for the enhanced thermotolerance and the physiology of the evolved strain at the supra-optimal temperature.

The proteome and metabolome differences between the chemostat cultures of CEN.PK113-7D and the evolved CEN.PK113-7D were investigated in **chapter 5**. The untargeted analysis of the anaerobic chemostat cultures of both strains by shotgun proteomics revealed the responses to supra-optimal temperature involves general (common between both strains) and strain-specific mechanisms. Overall, the general stress response to supra-optimal temperature involves a strong repression of proteins in central carbon metabolism and translation, as well as upregulation of protein involved protein folding. The strain-specific responses of the evolved strain at supra-optimal temperature involves upregulation of ribosome proteins, downregulation of aminoacul-tRNA biosynthesis and proteasome. The multi-omics analysis (**chapter 4** and **chapter 5**) generated new hypotheses on the cellular regulatory mechanisms of the evolved CEN.PK113-7D at the supra-optimal temperature. The enzymatic activities of the glycolytic enzymes in the anaerobic chemostat cultures of both strains were measured under in vivo like

condition at 30.0°C and 39.0°C, in order to investigate the impact of elevated cultivation temperature on the capacities of the glycolytic enzymes of both strains. Overall, the glycolytic enzymes of both strains showed similar temperature dependency. Although no mutation was found within the protein sequence of the glycolytic enzymes in the evolved strain, some glycolytic enzymes showed difference in quantity and capacity at evaluated cultivation temperature compared to that of the unevolved strain.

4

Samenvatting

Saccharomyces-gisten zijn veelvoorkomende werkpaarden in de productieprocessen van alcoholische dranken en bio-ethanol. Bij deze processen is het constant houden van de temperatuur één van de belangrijkste factoren die de operationele kosten bepalen, zoals voor koeling. De fermentatietemperatuur heeft een directe invloed op de (bio)chemische processen in en buiten de cellen en daarbij, in het geval van productie van alcoholische dranken, op de productkwaliteit en het aroma. *Saccharomyces*-gisten die groeien in hun natuurlijke omgeving ervaren een breed scala van verschillende temperaturen, vanwege de geografische verschillen van hun habitats, en hebben zich dienovereenkomstig aangepast. *Saccharomyces*-gisten in een kunstmatige omgeving, zoals een industrieel fermentatieproces, kunnen zich ook aan deze toestand aanpassen en een temperatuuroptimum bereiken dat dicht bij die van het productieproces ligt. In **hoofdstuk 2** zijn een aantal *Saccharomyces*-giststammen die worden toegepast in industriële fermentatieprocessen vergeleken aan de hand van hun groeiprestaties bij kweektemperaturen tussen 12°C en 40°C. We selecteerden twee industriële stammen, één die het snelst groeide bij sub optimale (12-27°C) en één bij supra-optimale (33-40°C) temperaturen. Een top-down benadering werd gebruikt om de temperatuurimpact op de kwantitatieve fysiologie van de stammen te evalueren, dat wil zeggen de opnamesnelheden van het substraat, de vorming van (bij)producten, evenals het gehalte aan cellulair eiwit en opslagkoolhydraat. Om dit te doen, werden de twee geselecteerde industriële stammen en een laboratoriumstam gekweekt in anaërobe chemostaatculturen bij 12,0, 30,0 en 39,0°C bij een constante groeisnelheid om temperatuur effecten op de groeisnelheid te elimineren. We namen hierbij significante verschillen in biomassa- en ethanolopbrengsten op glucose, totaal biomassa-eiwit en opslagkoolhydraatgehaltes waar tussen de verschillende stammen en kweektemperaturen.

Om de mogelijke temperatuurtolerantiemechanismen in de twee geselecteerde industriële stammen op te helderen, werden de proteoom profielen van de anaërobe chemostaatculturen voor de twee geselecteerde industriële stammen samen met een laboratoriumstam uitgevoerd met behulp van SWATH-MS (sequentiële vensteracquisitie van alle theoretische fragment-ionspectramassa's) spectrometrie) en geanalyseerd in **hoofdstuk 3**. Het proteoom profiel van deze drie stammen bij drie verschillende kweektemperaturen resulteerde in de kwantificering van 997 eiwitten en gaf aan dat temperatuur respons verschilde tussen de verschillende stammen. De gemeenschappelijke en stamspecifieke responsieve eiwitten werden gedetecteerd via PCA (principal component analysis), wat een benadering is voor lineaire dimensiereductie en gunstig is voor de analyse van gegevenssets die meer dan één variabele bevatten (in dit geval temperatuur en genetische heterogeniteit). Over het algemeen hebben we vastgesteld dat de suboptimale temperatuuromstandigheden een hogere aanpassing van het proteoom met zich meebrachten in vergelijking met de supra-optimale temperatuuromstandigheden. De proteoom gegevens toonden aan dat de koude respons een sterke onderdrukking van translatie-gerelateerde eiwitten omvat, evenals inductie van aminozuur metabolisme, samen met componenten die verband houden met eiwitvouwing en -afbraak. De reactie op hoge temperatuur bleek voornamelijk het aminozuurmetabolisme te beinvloeden.

Uit het werk beschreven in **hoofdstuk 2** en **hoofdstuk 3** hebben we gevonden dat verschillende giststammen een verschillende respons vertoonden op sub- en supra-optimale temperaturen. Om stam tot stam verschillen te minimaliseren, werd een adaptieve laboratoriumevolutie (ALE) met de goed gekarakteriseerde laboratoriumstam CEN.PK113-7D uitgevoerd, door middel van langdurige kweek in een anaërobe SBR (sequentiële batchreactor) waarbij de kweektemperatuur stapsgewijs werd verhoogd tot 39,8 (**hoofdstuk 4**). Na 475 generaties werd een geëvolueerde stam verkregen. Hoofdstuk 4 schetst de vergelijking tussen de niet-geëvolueerde en de geëvolueerde stam, gebaseerd op hun volledige genoomsequencing en fysiologische karakterisering in anaërobe sequentiële batchreactorculturen bij 39.8°C alsmede anaërobe chemostaatculturen bij 30,0°C en 39.0°C . De geëvolueerde stam bleek beter aangepast te zijn aan groei bij hoge temperaturen in vergelijking met de niet-geëvolueerde stam; het sterftecijfer was aanzienlijk verminderd en er waren minder cellen met gescheurde membranen bij 39,8. Na eliminatie van het groeisnelheidseffect op het opslagkoolhydraat metabolisme, hadden beide stammen verschillende opslagkoolhydraatgehalten en lipidesamenstellingen bij de supra-optimale temperatuur. De selectiedruk onder langdurige kweek bij hoge temperatuur en anaërobe omstandigheden veroorzaakte verschillende mutaties, zoals polymorfismen van één nucleotide en kleine inserties en deleties in het genoom van CEN.PK113-7D. De ontologietermen geassocieerd met die enkele hoge impact nucleotidevarianten werden geanalyseerd, om de gerelateerde specifieke biologische processen van die mutaties te identificeren die verantwoordelijk kunnen zijn voor de verhoogde thermotolerantie en de fysiologie van de geëvolueerde stam bij supra-optimale temperaturen.

Naast de genomics karakterisering werd ook proteoom- en metaboloomanalyse uitgevoerd van de CEN.PK113-7D en de geëvolueerde CEN.PK113-7D stammen die onder goed gedefinieerde omstandigheden in anaërobe chemostaatculturen bij 30,0 en 39,0 °C waren gekweekt

(**hoofdstuk 5**). De ongerichte analyse van de anaërobe chemostaatculturen van beide stammen door shotgun-proteomics onthulde dat de reacties op supra-optimale temperatuur algemene (gemeenschappelijk bij beide stammen) en stamspecifieke mechanismen omvatten. Over het algemeen hebben we waargenomen dat de algemene stressrespons op supra-optimale temperaturen een sterke neerwaartse regulatie van eiwitten in het centrale koolstofmetabolisme en -translatie omvat, evenals opwaartse regulatie van eiwitten die betrokken zijn bij eiwitvouwing. De stamspecifieke reacties van de geëvolueerde stam bij supra-optimale temperaturen omvatten opwaartse regulatie van ribosoomeiwitten, neerwaartse regulatie van aminoacyl-tRNA-biosynthese en proteasoom. De multi-omics-analyse (**hoofdstuk 4** en **hoofdstuk 5**) genereerde nieuwe hypothesen over de cellulaire regulatiemechanismen van de geëvolueerde CEN.PK113-7D als aanpassing aan supra-optimale temperaturen. De activiteiten van de glycolytische enzymen in de anaërobe chemostaatculturen van beide stammen werden gemeten onder in vivo-achtige omstandigheden bij 30,0°C en 39,0°C, om de impact van verhoogde kweektemperatuur op de capaciteiten van de glycolytische enzymen van beide stammen te onderzoeken. Over het algemeen vertoonden de glycolytische enzymen van beide stammen vergelijkbare temperatuurafhankelijkheden. Hoewel er geen mutaties werden gevonden in de coderende gebieden voor de glycolytische enzymen in de geëvolueerde stam, vertoonden verschillende glycolytische enzymen significante verschillen in hoeveelheid en capaciteit bij verhoogde kweektemperaturen in vergelijking met die van de niet-geëvolueerde stam, wat aangeeft dat veranderingen in genetische controlemechanismen moeten hebben plaatsgevonden tijdens de evolutie.

Chapter 1
Introduction

Wine,
beer,
and biofuel

The alcoholic beverage and bio-energy industry uses *Saccharomyces* yeasts to produce various commercial products, such as wine, cider, beer, and biofuel. *Saccharomyces* yeast is one of the common microorganisms used in this industry because of its ability to grow both aerobically and anaerobically [1], high ethanol tolerance (> 40.0 $g \cdot L^{-1}$), high ethanol productivity (> 1.0 $g \cdot L^{-1} \cdot h^{-1}$), high ethanol yield (90% of the theoretical yield), and the ability to ferment different sugars [2]. In wine making processes, the yeast ferments grape must and converts its sugars (mainly glucose and fructose) into alcohol and carbon dioxide. The traditional fermentation processes for alcoholic beverages are carried out within specific temperature ranges for optimal production of aroma compounds (lager beer, 6-14°C; ales, 15-25°C; red wine, 20-30°C; white and rosé wine, 10-18°C[3–5]). In many cases, these are below the optimum growth temperatures of the yeast strains used. Yeasts in general grow best in the temperature range between 30°C and 33°C [6–8]. Second generation biofuel production can be achieved through simultaneous saccharification of agricultural feedstocks (wood chips or sugarcane leaves) and fermentation by yeast. The temperature optima of the enzymes (40-50°C) applied for the saccharification are typically higher than the optimum growth temperature of the yeast strain, and therefore, these processes are carried out at supra-optimal temperatures [9,10].

Temperature is one of the predominant factors determining the cost of the industrial fermentation processes. The alcoholic beverage and bio-energy industries in Europe spend around 30-60% of the total energy requirement in the production process on controlling the operation temperatures where the yeast strains can still survive and operate [11]. The dilemma is that the optimum growth temperature of yeasts in general is different from the operation temperatures which favour the quantity and quality of the product [12]. However, the optimum growth temperature

of yeasts in general does not benefit the alcoholic beverage and bio-energy production processes in industry. The low working temperatures applied there result in prolonged fermentation process duration and cause high risk of halted or sluggish fermentation [13]. Conversely, biofuel production processes perform best at ≥40°C in order to minimise contamination risk and to cut cost from cooling [14], but this temperature can be fatal to yeasts [15].

Improving temperature tolerance of yeast strains outside the optimum range can be an opportunity to make the production process more economical and eco-efficient. Cryo-/thermo-tolerance is a complicated quantitative trait which is determined by multiple genes [16,17]. The knowledge about the mechanisms behind the cryo-/thermo-tolerance of yeast is still not fully understood. Tolerance of yeast strains to non-optimal growth conditions can be developed naturally through prolonged cultivation under clearly defined stress conditions [18–21]. The selection of improved phenotypes is driven by evolutionary biology which leads to diversification and adaptation over time. According to Europe's (EU-28) annual beer and biofuels production report and statistics, the substitution of the production processes with yeast strains with improved tolerance to sub-optimal growth temperatures can help the production industry in Europe saving 263 million euro annually on energy expenses [22]. Understanding the mechanisms behind temperature tolerance to tailor yeast strains for industrial application can be an opportunity to improve productivity and to lower energy expense in process operation.

Opportunities and challenges

9

Many efforts have been made to investigate the cellular properties of yeast beneficial to growth under non-optimal temperatures. at aerobic conditions [23–29]. Many of these studies were based on investigating the effects of abrupt temperature shocks. Fermentation processes for production of alcoholic beverages and biofuels are respectively operated at sub- and supra-optimal temperatures. The selected workhorses for these bioprocesses have some resilient properties to cope with these non-optimal growth conditions, for example with respect to membrane composition [30–32], trehalose accumulation [33–35], the expression of heat shock or chaperon proteins [36,37], transcription and translation processes [23,38], and oxidative stress defence systems [39,40].

Yeast strain properties coping with high and low temperatures

The fluidity of the lipid bilayer of the cell membrane depends on the temperature, which influences the molecular order of the membrane lipids. The membrane fluidity has a positive relation with an increase in temperature. Therefore, low temperature causes membrane rigidification, whereas high temperature causes membrane fluidization [41]. In order to cope with temperature stress on cell membranes, yeast cells have mechanisms to modulate the ratio of lipid types within the lipid layers. It has been shown that yeast cell membranes are predominated by unsaturated fatty acids at low temperatures [15,42,43] and by saturated acids/branched sterols at high temperatures [32,44]. Compared to saturated fatty acids, unsaturated fatty acids have a lower melting point which benefits cell membranes to maintain fluidity at low temperature and prevents rigidification. These adaptations involve the action of several desaturases to introduce double bonds in the lipid chains linked to the glycerol backbone of the glycolipids, which has also been found to occur in cells exposed to osmotic or ethanol stress [45,46].

Trehalose is one of the carbohydrates shown to accumulate in yeast cells at both high and low temperatures. Trehalose synthesis is catalysed by trehalose-6-phosphate synthetase and trehalose-6-phosphatase, which convert glucose-6-phosphate to trehalose in two steps [47]. Several studies indicated that under temperature stress conditions trehalose acts as a structural stabilizer for cell membranes and proteins [48,35,49–51]. The degradation of trehalose by neutral and acidic trehalases also accelerated yeast cells to resume growth after heat shock [52]. During heat shock, trehalose and the heat shock protein HSP104 together assist in the repair of damaged proteins in the cytosol and in the endoplasmic reticulum [53,33]. There are also several heat shock proteins in the cytoplasm, mainly HSP12, small HSPs, HSP70, and HSP90 which assist cells to cope with high and low temperatures [36].

Either decreased or increased temperatures are known to influence the stability of the RNA structure [54,55] and obstruct the transcription and translation processes in return. The expression of genes encoding the components of the transcription and translation machinery of the cells were different during temperature shock [56,23] and adaptation to heat/cold environment [26,57]. Temperature stress induced the expression of RNA helicases (DBP2 and DED1), RNA polymerases (RPA and RPB), and RNA-binding/processing proteins (NSR1,

PRP5, PRP11) to ensure the efficiency of the transcription and translation processes. Several studies showed that cells with defects in these genes displayed increased temperature sensitivity [58,59,6,60].

There is a positive correlation between temperature (low and high) and reactive oxygen species (ROS) under aerobic conditions [61–63]. Oxygen solubility increases at low temperature, thereby increasing the production of ROS [64,65]. High temperature causes damage to the integrity of mitochondrial membranes and increases ROS production in return [39]. ROS include hydrogen peroxide (H_2O_2), hydroxyl radicals ($OH^{\bullet}$), and superoxide anions ($O2^{\bullet-}$). These molecules can compromise cell viability by damaging proteins, lipids, and nucleic acids due to their highly reactive nature [66].

Fermentation processes for the production of alcoholic beverages and biofuels are commonly performed under anaerobic conditions. The yeast strains used in the fermentation processes for the production of these compounds experience prolonged temperature stress instead of abrupt temperature shocks. There are limited studies focusing on the effects of prolonged temperature stress under anaerobic conditions [57,67]. Therefore, the aim of this thesis is to understand the mechanisms which benefit *S. cerevisiae* to grow at sub-and supra-optimal temperatures under anaerobic conditions.

Cells are composed of various (macro)molecules, such as nucleic acids, proteins, carbohydrates, lipids, etc. which work synergistically as a whole in response to the environmental conditions. In order to understand how the cellular system responds to temperature stress under anaerobic conditions, it is important to study the entire system, from the level of the genes to the metabolic pathways (top-down holistic approach). Especially, temperature tolerance of yeasts is a complicated quantitative trait. It is therefore difficult to study the separate effect of an individual gene from the effects of other genes. Compared to a reductionistic approach, a holistic approach is based upon quantitative measurements and realistic models of the complete system, thereby allowing robust and versatile assessments.

Strain improvements through random approaches

Evolution of *Saccharomyces* yeasts has commonly been observed in industrial settings as a result of long-term exposure to stressful conditions [68,69]. These practices have commonly been used in industrial applications to generate yeast strains with stable characteristic improvements for specific operational conditions [70,71]. Adaptive laboratory evolution (ALE) and interspecific hybridization are genetic improvement methods which are generally accepted for food applications because the food industry in Europe rejects the use of GMOs [72]. During ALE genetic changes are induced as a result of prolonged exposure of the cells to a specific selective pressure [73]. The imposed selection pressure, for example temperatures below/above optimal growth temperatures in this case, results in the selection of mutants with better growth characteristics which outgrow the entire population [74]. Hybridization between species (Interspecific hybridization) can induce extensive genome reorganisation which leads to partial loss of heterozygosity and chromosomal rearrangement [75,76]. The genetic events during hybridization can improve the polygenicity of cryo/thermo-tolerance in return. Compared to interspecific hybridization, ALE requires a much simpler experimental set up and less prior knowledge of the genes contributed to desirable phenotypes.

Figure 1
Methods for ALE.
a) Batch cultivation where cell culture was cultivated by serial of batches.
b) continuous cultivation where cell culture was cultivated at a fixed growth rate and a well-defined condition by bioreactor.
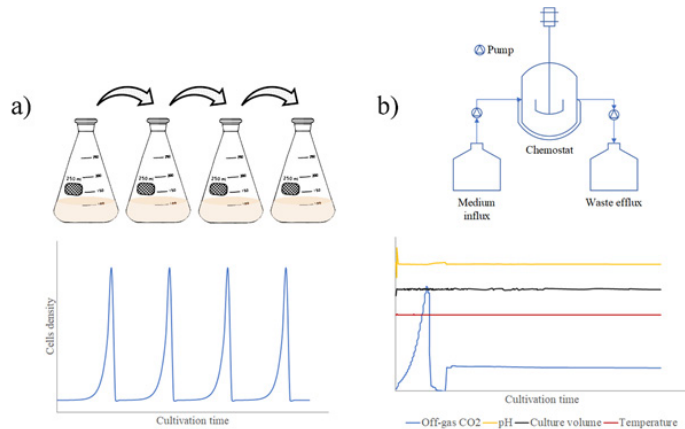
There are two common methods to perform ALE, which are serial batch cultivations and continuous cultivations (Figure 1). In case of the serial batch cultivations, the culture is maintained by transferring an aliquot of the culture to fresh medium in a new shake flask. This easy and cheap experimental set-up can benefit in massive parallel culture cultivations, but the disadvantages of it are the fluctuating environment conditions resulting in the variation of population density and growth rate in each culture. For the ALE in continuous culture, cells are cultivated at a constant growth rate in a chemostat system which ensures a constant cellular environment in terms of concentrations of dissolved compounds and cell density. When an ALE experiment is aimed at improving the growth rate of the cells under a certain selective pressure, unlimited growth in batch cultivation is a better approach than continuous cultivation. This can be achieved by carrying out sequential batch cultivations in shake flasks, but this has the disadvantage that the transfer to the next flask is a manual process. If the cultivations are carried out in a sequential batch reactor (SBR), the transfer to the next batch can be fully automated. SBR system have been commonly used for activated sludge processes for wastewater treatment [77]. Sequential batches can be operated under well-defined conditions in a controlled bioreactor, thereby avoiding the fluctuating environmental conditions commonly observed in shake flask cultivations and thus give a better reproducibility.

To identify specific genotypic and phenotypic changes which have occurred as a result of ALE under a certain selective pressure, the evolved strain(s) should be compared with the parental strain using a multi-level quantitative physiology and omics approach. To do so, the unevolved and evolved strains should be cultivated under tightly controlled identical conditions at a constant growth rate. Steady state chemostat cultivation allows cultivation of cell cultures at a fixed specific growth rate, thereby separating the effect of specific growth rate from temperature on cells because the specific growth rate affect transcriptions [78].

Omics technologies

Omics technologies focus on the detection of genes (genomics), mRNA (transcriptomics), proteins (proteomics), metabolites (metabolomics) and fluxes (fluxomics) in a biological system [79]. These technologies have a broad range of applications and allow to understand a biological system as a whole (holistic view) as they provide information on all levels of cellular regulation.

13

Omics studies generate enormous amounts of data but are not necessarily driven by hypotheses and can be a way to generate hypotheses for scientific discovery instead [80]. Therefore, data generated from hypothesis-poor omics studies rely on robust data-handling procedures and statistical analysis, in order to evaluate the reliability of enormous data and to convey hypotheses for scientific studies [81,82].

Figure 2
Workflow for omics
data analysis
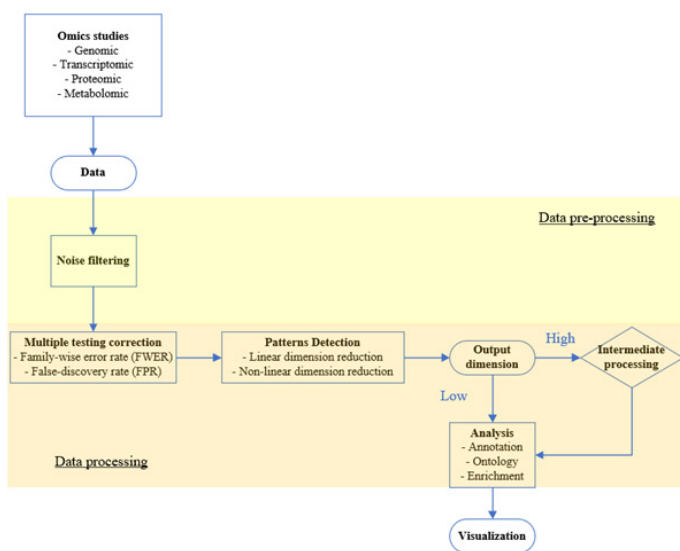
The general workflow of omics data analysis is illustrated in Figure 2. The output of omics studies (genomics, transcriptomics, proteomics, and metabolomics) first has to be processed to remove noise. In order to avoid bias, the noise filtering can be done by statistical methods, such as binning and regression [83,84]. Filtering data with this coverage value could significantly eliminate the data generated by inaccurate measurements and give confidence to the obtained data set.

After data smoothing (noise filtering), the data has to be evaluated by the measurement confidence for identification of genes, transcript, proteins, and metabolites in the biological process (study objective). The interpretation of experimental

outputs depend on study objectives, and therefore, the data analysis methods vary with the size of the samples [82]; the statistical significance of measurements based on the number of tests performed is controlled by multiple testing correction. Family-wise error rate (FWER) and false-discovery rate (FDR) are the methods for multiple testing correction [85]. On the other hand, FDR allows multiple dataset comparisons with an increasing number of hypothesis tests [86]. A confidence interval of 95% (p-value ≤ 0.05) is commonly used in FDR, meaning that the obtained data would have 5% chance of false positive.

In order to identify patterns/informative components from the dataset with significant correlations to study objectives, the resulting data set can be analysed by an approach of dimension reduction. Sample clustering with expression profiles and principle component analysis (PCA) are the examples of linear methods for dimension reduction [87]. PCA projects each data point onto the investigated component axis, resulting in a scatter plot which shows correlations between different variables. There are also non-linear methods for dimension reduction, such as t-distributed stochastic neighbour embedding (t-SNE) and uniform manifold approximation and projection (UMAP) [88].

With the advance of bioinformatics, the reduced output data can be translated into biological information via annotation and ontology. These processes allow identifying the detected components (genes, transcripts, proteins, and metabolites) in the location of the related genomes and provides biological relations associated with these components [89]. The databases used in annotation and ontology are curated based on scientific literature and facilitates the omics data analysis from a very large database. When the output dimension is too high, further processing is required to simplify the complicated dataset (reduce the dimension to fewer components). Apart from annotation and ontology, enrichment analysis is a method to examine the data sets for the enriched functional terms in a subset of a dataset, such as the components involved in the biological events, in order to identify the significant difference of the detect components among the total dataset [90–93]. It should be kept in mind that these analyses are based on statistical tests, but still relay on our critical thinking to come to an interpretation of these analyses.

Aim and outline
of the thesis

The goal of this thesis is to use a top-down holistic approach to identify the mechanisms of *S. cerevisiae* coping with temperature stresses under anaerobic conditions. As a result, the generated knowledge can give insight into the industry of alcoholic beverages and biofuel to generate tailored cryo/thermo-tolerant yeasts for industrial applications.

Chapter 2 addresses a phenotypic evaluation of industrial and laboratory *Saccharomyces* yeasts, in terms of their capacity to grow at different temperatures. An initial phenotypic screening was carried out using microtiter plates to select target strains for in depth physiological characterization of temperature tolerance for the related industrial applications. Not only industrial strains but also a well-characterized laboratory strain of *S. cerevisiae* (CEN.PK113-7D) was used as a reference next to the industrial strains which are less well characterized. Each selected candidate strain was characterized within its intrinsic temperature region for growth by using microbial growth models. We carried out a quantitative physiology study with the selected industrial strains together with CEN.PK113-7D through steady state chemostat cultivation at sub-optimal, optimal and supra-optimal temperatures. The chemostat cultures were carried out at a fixed dilution rate to separate the effects of the specific growth rate from the temperature effects.

Chapter 3 describes a global proteomics approach to identify possible mechanisms of the three strains to adapt to different cultivation temperatures by using SWATH-MS (sequential window acquisition of all theoretical fragment ion spectra mass spectrometry).

The research performed in **chapter 2** and **chapter 3** indicated that different strains within the same species had various mechanisms to cope with cold and heat stresses. With the aim to minimize the genetic differences between strains for the research of thermal tolerance, we designed an experimental set-up to perform adaptive laboratory evolution to CEN.PK113-7D to improve its thermotolerance in **chapter 4**. A well-defined experimental set-up gave a clear indication for the occurrence of evolution. We performed whole genome sequencing of the unevolved and the evolved strain to find out the genomic differences which may attribute to the improved thermotolerance observed in the evolved strain. The single nucleotide polymorphisms (SNPs)

identified in the evolved CEN.PK113-7D were analysed and annotated with their gene ontology terms in order to understand the associated biological processes or functional terms attributed to the species.

To further understand the mechanisms of the evolved strain to cope with thermal stress and the impact of the genomic changes found after evolution, we performed a shotgun proteomic analysis of chemostat grown cells of both the unevolved and evolved CEN.PK113-7D strains in **chapter 5**. Moreover, we also analysed the activities of the glycolytic enzymes in the anaerobic chemostat cultures of both strains under in vivo like conditions at different temperatures. These enzymatic analyses were carried out to study possible differences in enzyme capacity, enzyme quantity, and temperature dependency between the unevolved and evolved stains. Integrating different omics analysis (**chapter 4** and **chapter 5**), we generated new hypotheses on the possible strategies/mechanisms acquired by the evolved strain responsible for its better growth at supra-optimal temperatures compared to the unevolved strain.

References

[1]   J.P. van Dijken, R.A. Weusthuis, J.T. Pronk, Kinetics of growth and sugar consumption in yeasts, Antonie Van Leeuwenhoek 63 343-352. (1993). http://repository.tudelft.nl/islandora/object/uuid%3Ae9618b7b-5227-4b9f-b0d8-a8b703346a71 (accessed January 16, 2017).

[2]   S.H. Mohd Azhar, R. Abdulla, S.A. Jambo, H. Marbawi, J.A. Gansau, A.A. Mohd Faik, K.F. Rodrigues, Yeasts in sustainable bioethanol production: A review, Biochem. Biophys. Rep. 10 (2017) 52–61. https://doi.org/10.1016/j.bbrep.2017.03.003.

[3]   R.E. Kunkee, Selection and modification of yeasts and lactic acid bacteria for wine fermentation, Food Microbiol. 1 (1984) 315–332. https://doi.org/10.1016/0740-0020(84)90065-0.

[4]   A. Reynolds, M. Cliff, B. Girard, T.G. Kopp, Influence of Fermentation Temperature on Composition and Sensory Properties of Semillon and Shiraz Wines, Am. J. Enol. Vitic. 52 (2001) 235–240.

[5]   V. Vidgren, J.-P. Multanen, L. Ruohonen, J. Londesborough, The temperature dependence of maltose transport in ale and lager strains of brewer's yeast, Fems Yeast Res. 10 (2010) 402–411. https://doi.org/10.1111/j.1567-1364.2010.00627.x.

[6]   G.-W. Choi, H.-J. Um, Y. Kim, H.-W. Kang, M. Kim, B.-W. Chung, Y.-H. Kim, Isolation and characterization of two soil derived yeasts for bioethanol production on Cassava starch, Biomass Bioenergy. 34 (2010) 1223–1231. https://doi.org/10.1016/j.biombioe.2010.03.019.

[7]   Z. Salvadó, F.N. Arroyo-López, J.M. Guillamón, G. Salazar, A. Querol, E. Barrio, Temperature Adaptation Markedly Determines Evolution within the Genus *Saccharomyces*, Appl. Environ. Microbiol. 77 (2011) 2292–2302. https://doi.org/10.1128/AEM.01861-10.

[8]   J. Yu, XuZhang, T. Tan, Ethanol production by solid state fermentation of sweet sorghum using thermotolerant yeast strain, Fuel Process. Technol. 89 (2008) 1056–1059. https://doi.org/10.1016/j.fuproc.2008.04.008.

[9]   L. Olsson, B. Hahn-Hägerdal, Fermentation of lignocellulosic hydrolysates for ethanol production, Enzyme Microb. Technol. 18 (1996) 312–331. https://doi.org/10.1016/0141-0229(95)00157-3.

[10]   S.N. Naik, V.V. Goud, P.K. Rout, A.K. Dalai, Production of first and second generation biofuels: A comprehensive review, Renew. Sustain. Energy Rev. 14 (2010) 578–597. https://doi.org/10.1016/j.rser.2009.10.003.

[11]   Y. Chan, R. Kantamaneni, Study on energy efficiency and energy saving potential in industry and on possible policy mechanisms, ICF Consulting Limited, 2016. https://ec.europa.eu/energy/studies/study-energy-efficiency-and-energy-saving-potential-industry-and-possible-policy-mechanisms_en?redir=1.

[12]   J. Samoticha, A. Wojdyło, J. Chmielewska, J. Nofer, Effect of Different Yeast Strains and Temperature of Fermentation on Basic Enological Parameters, Polyphenols and Volatile Compounds of Aurore White Wine, Foods Basel Switz. 8 (2019). https://doi.org/10.3390/foods8120599.

[13]   L.F. Bisson, Stuck and Sluggish Fermentations, Am. J. Enol. Vitic. 50 (1999) 107–119.

19

[14]   B.M.A. Abdel-Banat, H. Hoshida, A. Ano, S. Nonklang, R. Akada, High-temperature fermentation: how can processes for ethanol production at high temperatures become superior to the traditional process using mesophilic yeast?, Appl. Microbiol. Biotechnol. 85 (2010) 861–867. https://doi.org/10.1007/s00253-009-2248-5.

[15]   M. Redón, J.M. Guillamón, A. Mas, N. Rozès, Effect of growth temperature on yeast lipid composition and alcoholic fermentation at low temperature, Eur. Food Res. Technol. 232 (2011) 517–527. https://doi.org/10.1007/s00217-010-1415-3.

[16]   Y. Yang, M.R. Foulquié-Moreno, L. Clement, É. Erdei, A. Tanghe, K. Schaerlaekens, F. Dumortier, J.M. Thevelein, QTL Analysis of High Thermotolerance with Superior and Downgraded Parental Yeast Strains Reveals New Minor QTLs and Converges on Novel Causative Alleles Involved in RNA Processing, PLoS Genet. 9 (2013). https://doi.org/10.1371/journal.pgen.1003693.

[17]   Z. Wang, Q. Qi, Y. Lin, Y. Guo, Y. Liu, Q. Wang, QTL analysis reveals genomic variants linked to high-temperature fermentation performance in the industrial yeast, Biotechnol. Biofuels. 12 (2019) 59. https://doi.org/10.1186/s13068-019-1398-7.

[18]   L. Caspeta, J. Nielsen, Thermotolerant Yeast Strains Adapted by Laboratory Evolution Show Trade-Off at Ancestral Temperatures and Preadaptation to Other Stresses, MBio. 6 (2015) e00431-15. https://doi.org/10.1128/mBio.00431-15.

[19]   V.J. Higgins, P.J.L. Bell, I.W. Dawes, P.V. Attfield, Generation of a Novel *Saccharomyces* cerevisiae Strain That Exhibits Strong Maltose Utilization and Hyperosmotic Resistance Using Nonrecombinant Techniques, Appl. Environ. Microbiol. 67 (2001) 4346–4348. https://doi.org/10.1128/AEM.67.9.4346-4348.2001.

[20]   I.-S. Kim, Y.-S. Kim, H. Kim, H. Jin, H.-S. Yoon, *Saccharomyces* cerevisiae KNU5377 stress response during high-temperature ethanol fermentation, Mol. Cells. 35 (2013) 210–218. https://doi.org/10.1007/s10059-013-2258-0.

[21]   M. López-Malo, E. García-Rios, B. Melgar, M.R. Sanchez, M.J. Dunham, J.M. Guillamón, Evolutionary engineering of a wine yeast strain revealed a key role of inositol and mannoprotein metabolism during low-temperature fermentation, BMC Genomics. 16 (2015) 537. https://doi.org/10.1186/s12864-015-1755-2.

[22]   O. Bettini, EU-28, Wine Annual, Wine Annual Report and Statistics 2014, (2014).

[23]   L. Castells-Roca, J. García-Martínez, J. Moreno, E. Herrero, G. Bellí, J.E. Pérez-Ortín, Heat Shock Response in Yeast Involves Changes in Both Transcription Rates and mRNA Stabilities, PLOS ONE. 6 (2011) e17272. https://doi.org/10.1371/journal.pone.0017272.

[24]   M.B. Al-Fageeh, C.M. Smales, Control and regulation of the cellular responses to cold shock: the responses in yeast and mammalian systems, Biochem. J. 397 (2006) 247–259. https://doi.org/10.1042/BJ20060166.

[25]   Y. Murata, T. Homma, E. Kitagawa, Y. Momose, M.S. Sato, M. Odani, H. Shimizu, M. Hasegawa-Mizusawa, R. Matsumoto, S. Mizukami, K. Fujita, M. Parveen, Y. Komatsu, H. Iwahashi, Genome-wide expression analysis of yeast response during exposure to 4 degrees C, Extrem. Life Extreme Cond. 10 (2006) 117–128. https://doi.org/10.1007/s00792-005-0480-1.

[26]   B. Schade, G. Jansen, M. Whiteway, K.D. Entian, D.Y. Thomas, Cold Adaptation in Budding Yeast, Mol. Biol. Cell. 15 (2004) 5492–5502. https://doi.org/10.1091/mbc.E04-03-0167.

[27]   M. Becerra, L.J. Lombardía, M.I. González-Siso, E. Rodríguez-Belmonte, N.C. Hauser, M.E. Cerdán, Genome-wide analysis of the yeast transcriptome upon heat and cold shock, Comp. Funct. Genomics. 4 (2003) 366–375. https://doi.org/10.1002/cfg.301.

[28]   T. Sahara, T. Goda, S. Ohgiya, Comprehensive expression analysis of time-dependent genetic responses in yeast cells to low temperature, J. Biol. Chem. 277 (2002) 50015–50021. https://doi.org/10.1074/jbc.M209258200.

[29]   E.G. Rikhvanov, N.N. Varakina, T.M. Rusaleva, E.I. Rachenko, V.A. Kiseleva, V.K. Voinikov, Heat Shock–Induced Changes in the Respiration of the Yeast *Saccharomyces* cerevisiae, Microbiology. 70 (2001) 462–465. https://doi.org/10.1023/A:1010442429489.

[30]   G. Beltran, M. Novo, J.M. Guillamón, A. Mas, N. Rozès, Effect of fermentation temperature and culture media on the yeast lipid composition and wine volatile compounds, Int. J. Food Microbiol. 121 (2008) 169–177. https://doi.org/10.1016/j.ijfoodmicro.2007.11.030.

[31]   G. Beltran, M. Novo, V. Leberre, S. Sokol, D. Labourdette, J.-M. Guillamon, A. Mas, J. François, N. Rozes, Integration of transcriptomic and metabolic analyses for understanding the global responses of low-temperature winemaking fermentations, FEMS Yeast Res. 6 (2006) 1167–1183. https://doi.org/10.1111/j.1567-1364.2006.00106.x.

[32]   H. Arthur, K. Watson, Thermal adaptation in yeast: growth temperatures, membrane lipid, and cytochrome composition of psychrophilic, mesophilic, and thermophilic yeasts., J. Bacteriol. 128 (1976) 56–68.

[33]   M. Simola, A.-L. Hänninen, S.-M. Stranius, M. Makarow, Trehalose is required for conformational repair of heat-denatured proteins in the yeast endoplasmic reticulum but not for maintenance of membrane traffic functions after severe heat stress, Mol. Microbiol. 37 (2000) 42–53. https://doi.org/10.1046/j.1365-2958.2000.01970.x.

[34]   M.A. Singer, S. Lindquist, Thermotolerance in *Saccharomyces* cerevisiae: the Yin and Yang of trehalose, Trends Biotechnol. 16 (1998) 460–468. https://doi.org/10.1016/S0167-7799(98)01251-7.

[35]   C. Coutinho, E. Bernardes, D. Félix, A.D. Panek, Trehalose as cryoprotectant for preservation of yeast strains, J. Biotechnol. 7 (1988) 23–32. https://doi.org/10.1016/0168-1656(88)90032-6.

[36]   J. Verghese, J. Abrams, Y. Wang, K.A. Morano, Biology of the heat shock response and protein chaperones: budding yeast (*Saccharomyces* cerevisiae) as a model system, Microbiol. Mol. Biol. Rev. MMBR. 76 (2012) 115–158. https://doi.org/10.1128/MMBR.05018-11.

[37]   M.A. Singer, S. Lindquist, Multiple Effects of Trehalose on Protein Folding In Vitro and In Vivo, Mol. Cell. 1 (1998) 639–648. https://doi.org/10.1016/S1097-2765(00)80064-7.

[38]   C.E. Barraza, C.A. Solari, I. Marcovich, C. Kershaw, F. Galello, S. Rossi, M.P. Ashe, P. Portela, The role of PKA in the translational response to heat stress in *Saccharomyces* cerevisiae, PLOS ONE. 12 (2017) e0185416. https://doi.org/10.1371/journal.pone.0185416.

[39]   A.V. Fedyaeva, A.V. Stepanov, I.V. Lyubushkina, T.P. Pobezhimova, E.G. Rikhvanov, Heat shock induces production of reactive oxygen species and increases inner mitochondrial membrane potential in winter wheat cells, Biochem. Biokhimiia. 79 (2014) 1202–1210. https://doi.org/10.1134/S0006297914110078.

[40]   J.F. Davidson, R.H. Schiestl, Cytotoxic and Genotoxic Consequences of Heat Stress Are Dependent on the Presence of Oxygen in *Saccharomyces* cerevisiae, J. Bacteriol. 183 (2001) 4580–4587. https://doi.org/10.1128/JB.183.15.4580-4587.2001.

[41]   D.A. Los, N. Murata, Membrane fluidity and its roles in the perception of environmental signals, Biochim. Biophys. Acta BBA - Biomembr. 1666 (2004) 142–157. https://doi.org/10.1016/j.bbamem.2004.08.002.

[42]   Y. Tasaka, Z. Gombos, Y. Nishiyama, P. Mohanty, T. Ohba, K. Ohki, N. Murata, Targeted mutagenesis of acyl-lipid desaturases in Synechocystis: evidence for the important roles of polyunsaturated membrane lipids in growth, respiration and photosynthesis., EMBO J. 15 (1996) 6416–6425.

[43]   J.E. Stukey, V.M. McDonough, C.E. Martin, The OLE1 gene of *Saccharomyces* cerevisiae encodes the delta 9 fatty acid desaturase and can be functionally replaced by the rat stearoyl-CoA desaturase gene, J. Biol. Chem. 265 (1990) 20144–20149.

[44]   L. Caspeta, Y. Chen, P. Ghiaci, A. Feizi, S. Buskov, B.M. Hallström, D. Petranovic, J. Nielsen, Altered sterol composition renders yeast thermotolerant, Science. 346 (2014) 75–78. https://doi.org/10.1126/science.1258137.

[45]   S. Rodríguez-Vargas, A. Sánchez-García, J.M. Martínez-Rivas, J.A. Prieto, F. Randez-Gil, Fluidization of Membrane Lipids Enhances the Tolerance of *Saccharomyces* cerevisiae to Freezing and Salt Stress, Appl. Environ. Microbiol. 73 (2007) 110–116. https://doi.org/10.1128/AEM.01360-06.

[46]   C.M. Henderson, D.E. Block, Examining the Role of Membrane Lipid Composition in Determining the Ethanol Tolerance of *Saccharomyces* cerevisiae, Appl. Environ. Microbiol. 80 (2014) 2966–2972. https://doi.org/10.1128/AEM.04151-13.

[47]   J. François, J.L. Parrou, Reserve carbohydrates metabolism in the yeast *Saccharomyces* cerevisiae, FEMS Microbiol. Rev. 25 (2001) 125–145. https://doi.org/10.1111/j.1574-6976.2001.tb00574.x.

[48]   J.H. Crowe, L.M. Crowe, D. Chapman, Preservation of Membranes in Anhydrobiotic Organisms: The Role of Trehalose, Science. 223 (1984) 701–703. https://doi.org/10.1126/science.223.4637.701.

[49]   M.J. Neves, J. François, On the mechanism by which a heat shock induces trehalose accumulation in *Saccharomyces* cerevisiae, Biochem. J. 288 (1992) 859–864. https://doi.org/10.1042/bj2880859.

[50]   T. Hottiger, C.D. Virgilio, M.N. Hall, T. Boller, A. Wiemken, The role of trehalose synthesis for the acquisition of thermotolerance in yeast, Eur. J. Biochem. 219 (1994) 187–193. https://doi.org/10.1111/j.1432-1033.1994.tb19929.x.

[51]   R.S.S. Magalhães, B. Popova, G.H. Braus, T.F. Outeiro, E.C.A. Eleutherio, The trehalose protective mechanism during thermal stress in *Saccharomyces* cerevisiae: the roles of Ath1 and Agt1, FEMS Yeast Res. 18 (2018). https://doi.org/10.1093/femsyr/foy066.

[52]   N. Avonce, A. Mendoza-Vargas, E. Morett, G. Iturriaga, Insights on the evolution of trehalose biosynthesis, BMC Evol. Biol. 6 (2006) 109. https://doi.org/10.1186/1471-2148-6-109.

[53]   S. Lindquist, G. Kim, Heat-shock protein 104 expression is sufficient for thermotolerance in yeast., Proc. Natl. Acad. Sci. U. S. A. 93 (1996) 5301–5306.

[54]   A. Chursov, S.J. Kopetzky, G. Bocharov, D. Frishman, A. Shneider, RNAtips: analysis of temperature-induced changes of RNA secondary structure, Nucleic Acids Res. 41 (2013) W486–W491. https://doi.org/10.1093/nar/gkt486.

[55]   F. Qi, D. Frishman, Melting temperature highlights functionally important RNA structure and sequence elements in yeast mRNA coding regions, Nucleic Acids Res. 45 (2017) 6109–6118. https://doi.org/10.1093/nar/gkx161.

[56]   B.A. Infanzon, K.M. Buckmelter, E.M. Liu, O.S. Sakhon, W.T. Citti, K.D. Dahlquist, *Saccharomyces* cerevisiae responds to cold shock by inducing the transcription of ribosome biogenesis genes, FASEB J. 24 (2010) 833.13-833.13. https://doi.org/10.1096/fasebj.24.1_supplement.833.13.

[57]   S.L. Tai, P. Daran-Lapujade, M.C. Walsh, J.T. Pronk, J.-M. Daran, Acclimation of *Saccharomyces* cerevisiae to Low Temperature: A Chemostat-based Transcriptome Analysis, Mol. Biol. Cell. 18 (2007) 5100–5112. https://doi.org/10.1091/mbc.E07-02-0131.

[58]   L. Minvielle-Sebastia, B. Winsor, N. Bonneaud, F. Lacroute, Mutations in the yeast RNA14 and RNA15 genes result in an abnormal mRNA decay rate; sequence analysis reveals an RNA-binding domain in the RNA15 protein., Mol. Cell. Biol. 11 (1991) 3075–3087. https://doi.org/10.1128/MCB.11.6.3075.

[59]   A.O. Noueiry, J. Chen, P. Ahlquist, A mutant allele of essential, general translation initiation factor DED1 selectively inhibits translation of a viral mRNA, Proc. Natl. Acad. Sci. U. S. A. 97 (2000) 12985–12990.

[60]   M.A. Hossain, T.L. Johnson, Using Yeast Genetics to Study Splicing Mechanisms, Methods Mol. Biol. Clifton NJ. 1126 (2014) 285–298. https://doi.org/10.1007/978-1-62703-980-2_21.

[61]   L. Zhang, K. Onda, R. Imai, R. Fukuda, H. Horiuchi, A. Ohta, Growth temperature downshift induces antioxidant response in *Saccharomyces* cerevisiae, Biochem. Biophys. Res. Commun. 307 (2003) 308–314. https://doi.org/10.1016/s0006-291x(03)01168-9.

[62]   R.-T. Ju, H.-P. Wei, F. Wang, X.-H. Zhou, B. Li, Anaerobic respiration and antioxidant responses of Corythucha ciliata (Say) adults to heat-induced oxidative stress under laboratory and field conditions, Cell Stress Chaperones. 19 (2014) 255–262. https://doi.org/10.1007/s12192-013-0451-x.

[63]   E. García-Ríos, L. Ramos-Alonso, J.M. Guillamón, Correlation between Low Temperature Adaptation and Oxidative Stress in *Saccharomyces* cerevisiae, Front. Microbiol. 7 (2016). https://doi.org/10.3389/fmicb.2016.01199.

[64]   D. Abele, S. Puntarulo, Formation of reactive species and induction of antioxidant defence systems in polar and temperate marine invertebrates and fish, Comp. Biochem. Physiol. A. Mol. Integr. Physiol. 138 (2004) 405–415. https://doi.org/10.1016/j.cbpb.2004.05.013.

[65]   C. Vinagre, D. Madeira, V. Mendonça, M. Dias, J. Roma, M.S. Diniz, Effect of temperature in multiple biomarkers of oxidative stress in coastal shrimp, J. Therm. Biol. 41 (2014) 38–42. https://doi.org/10.1016/j.jtherbio.2014.02.005.

[66]   E. Herrero, J. Ros, G. Bellí, E. Cabiscol, Redox control and oxidative stress in yeast cells, Biochim. Biophys. Acta. 1780 (2008) 1217–1235. https://doi.org/10.1016/j.bbagen.2007.12.004.

[67]   S.L. Tai, P. Daran-Lapujade, M.A.H. Luttik, M.C. Walsh, J.A. Diderich, G.C. Krijger, W.M. van Gulik, J.T. Pronk, J.-M. Daran, Control of the Glycolytic Flux in *Saccharomyces* cerevisiae Grown at Low Temperature A MULTI-LEVEL ANALYSIS IN ANAEROBIC CHEMOSTAT CULTURES, J. Biol. Chem. 282 (2007) 10243–10251. https://doi.org/10.1074/jbc.M610845200.

[68]   K. Giannakou, M. Cotterrell, D. Delneri, Genomic Adaptation of *Saccharomyces* Species to Industrial Environments, Front. Genet. 11 (2020). https://doi.org/10.3389/fgene.2020.00916.

[69]   M. Dragosits, D. Mattanovich, Adaptive laboratory evolution – principles and applications for biotechnology, Microb. Cell Factories. 12 (2013) 64. https://doi.org/10.1186/1475-2859-12-64.

[70]   E. Valero, B. Cambon, D. Schuller, M. Casal, S. Dequin, Biodiversity of *Saccharomyces* yeast strains from grape berries of wine-producing areas using starter commercial yeasts, FEMS Yeast Res. 7 (2007) 317–329. https://doi.org/10.1111/j.1567-1364.2006.00161.x.

[71]   D. Peris, R.V. Moriarty, W.G. Alexander, E. Baker, K. Sylvester, M. Sardi, Q.K. Langdon, D. Libkind, Q.-M. Wang, F.-Y. Bai, J.-B. Leducq, G. Charron, C.R. Landry, J.P. Sampaio, P. Gonçalves, K.E. Hyma, J.C. Fay, T.K. Sato, C.T. Hittinger, Hybridization and adaptive evolution of diverse *Saccharomyces* species for cellulosic biofuel production, Biotechnol. Biofuels. 10 (2017) 78. https://doi.org/10.1186/s13068-017-0763-7.

[72]   White Paper on Food Safety. COM (99) 719 final, 12 January 2000, (1999) 52. http://aei.pitt.edu/1141/ (accessed May 30, 2021).

[73]   C. McBryde, J.M. Gardner, M. de B. Lopes, V. Jiranek, Generation of Novel Wine Yeast Strains by Adaptive Evolution, Am. J. Enol. Vitic. 57 (2006) 423–430.

[74]   C.F. Olson-Manning, M.R. Wagner, T. Mitchell-Olds, Adaptive evolution: evaluating empirical support for theoretical predictions, Nat. Rev. Genet. 13 (2012) 867–877. https://doi.org/10.1038/nrg3322.

[75]   Y. Nakao, T. Kanamori, T. Itoh, Y. Kodama, S. Rainieri, N. Nakamura, T. Shimonaga, M. Hattori, T. Ashikari, Genome Sequence of the Lager Brewing Yeast, an Interspecies Hybrid, DNA Res. 16 (2009) 115–129. https://doi.org/10.1093/dnares/dsp003.

[76]   T. Walther, F. Létisse, L. Peyriga, C. Alkim, Y. Liu, A. Lardenois, H. Martin-Yken, J.-C. Portais, M. Primig, J.M. François\, Developmental stage-dependent metabolic regulation during meiotic differentiation in budding yeast, BMC Biol. 12 (2014) 60. https://doi.org/10.1186/s12915-014-0060-x.

[77]   R.L. Irvine, A.W. Busch, Sequencing Batch Biological Reactors: An Overview, J. Water Pollut. Control Fed. 51 (1979) 235–243.

[78]   B. Regenberg, T. Grotkjær, O. Winther, A. Fausbøll, M. Åkesson, C. Bro, L.K. Hansen, S. Brunak, J. Nielsen, Growth-rate regulated genes have profound impact on interpretation of transcriptome profiling in *Saccharomyces* cerevisiae, Genome Biol. 7 (2006) R107. https://doi.org/10.1186/gb-2006-7-11-r107.

[79]   S. Brul, J. Bassett, P. Cook, S. Kathariou, P. McClure, P.R. Jasti, R. Betts, 'Omics' technologies in quantitative microbial risk assessment, Trends Food Sci. Technol. 27 (2012) 12–24. https://doi.org/10.1016/j.tifs.2012.04.004.

[80]   D.B. Kell, S.G. Oliver, Here is the evidence, now what is the hypothesis? The complementary roles of inductive and hypothesis-driven science in the post-genomic era, BioEssays News Rev. Mol. Cell. Dev. Biol. 26 (2004) 99–105. https://doi.org/10.1002/bies.10385.

[81]   R. Yamada, D. Okada, J. Wang, T. Basak, S. Koyama, Interpretation of omics data analyses, J. Hum. Genet. 66 (2021) 93–102. https://doi.org/10.1038/s10038-020-0763-5.

[82]   D. Dunkler, F. Sánchez-Cabo, G. Heinze, Statistical analysis principles for Omics data, Methods Mol. Biol. Clifton NJ. 719 (2011) 113–131. https://doi.org/10.1007/978-1-61779-027-0_5.

[83]   H. Xiong, G. Pandey, M. Steinbach, V. Kumar, Enhancing data analysis with noise removal, IEEE Trans. Knowl. Data Eng. 18 (2006) 304–319. https://doi.org/10.1109/TKDE.2006.46.

[84]   Data Mining: Concepts and Techniques - 3rd Edition, (n.d.). https://www.elsevier.com/books/data-mining-concepts-and-techniques/han/978-0-12-381479-1 (accessed May 18, 2021).

[85]   W.S. Noble, How does multiple testing correction work?, Nat. Biotechnol. 27 (2009) 1135–1137. https://doi.org/10.1038/nbt1209-1135.

[86]   J.J. Chen, P.K. Robeson, M.J. Schell, The False Discovery Rate: A Key Concept in Large-Scale Genetic Studies, Cancer Control. 17 (2010) 58–62. https://doi.org/10.1177/107327481001700108.

[87]   I.T. Jolliffe, J. Cadima, Principal component analysis: a review and recent developments, Philos. Trans. R. Soc. Math. Phys. Eng. Sci. 374 (2016) 20150202. https://doi.org/10.1098/rsta.2015.0202.

[88]   S. Sakaue, J. Hirata, M. Kanai, K. Suzuki, M. Akiyama, C. Lai Too, T. Arayssi, M. Hammoudeh, S. Al Emadi, B.K. Masri, H. Halabi, H. Badsha, I.W. Uthman, R. Saxena, L. Padyukov, M. Hirata, K. Matsuda, Y. Murakami, Y. Kamatani, Y. Okada, Dimensionality reduction reveals fine-scale structure in the Japanese population with consequences for polygenic risk prediction, Nat. Commun. 11 (2020) 1569. https://doi.org/10.1038/s41467-020-15194-z.

[89]   D.P. Hill, B. Smith, M.S. McAndrews-Hill, J.A. Blake, Gene Ontology annotations: what they mean and where they come from, BMC Bioinformatics. 9 (2008) S2. https://doi.org/10.1186/1471-2105-9-S5-S2.

[90]   A. Subramanian, P. Tamayo, V.K. Mootha, S. Mukherjee, B.L. Ebert, M.A. Gillette, A. Paulovich, S.L. Pomeroy, T.R. Golub, E.S. Lander, J.P. Mesirov, Gene set enrichment analysis: A knowledge-based approach for interpreting genome-wide expression profiles, Proc. Natl. Acad. Sci. 102 (2005) 15545–15550. https://doi.org/10.1073/pnas.0506580102.

[91]   J. Xia, D.S. Wishart, MSEA: a web-based tool to identify biologically meaningful patterns in quantitative metabolomic data, Nucleic Acids Res. 38 (2010) W71-77. https://doi.org/10.1093/nar/gkq329.

[92]   J. Reimand, R. Isserlin, V. Voisin, M. Kucera, C. Tannus-Lopes, A. Rostamianfar, L. Wadi, M. Meyer, J. Wong, C. Xu, D. Merico, G.D. Bader, Pathway enrichment analysis and visualization of omics data using g:Profiler, GSEA, Cytoscape and EnrichmentMap, Nat. Protoc. 14 (2019) 482–517. https://doi.org/10.1038/s41596-018-0103-9.

[93]   M. Paczkowska, J. Barenboim, N. Sintupisut, N.S. Fox, H. Zhu, D. Abd-Rabbo, M.W. Mee, P.C. Boutros, J. Reimand, Integrative pathway enrichment analysis of multivariate omics data, Nat. Commun. 11 (2020) 735. https://doi.org/10.1038/s41467-019-13983-9.

Chapter 2

Selection and subsequent
physiological characterisation
of industrial *Saccharomyces*
cerevisiae strains during
continuous growth at sub- and
supra-optimal temperatures

A phenotypic screening of 12 industrial yeast strains and the well-studied laboratory strain CEN.PK113-7D at cultivation temperatures between 12°C and 40°C revealed significant differences in maximum growth rates and temperature tolerance. From those twelve, two strains, one performing best at 12°C and the other at 40°C, plus the laboratory strain, were selected for further physiological characterization in well-controlled bioreactors. The strains were grown in anaerobic chemostats, at a fixed specific growth rate of 0.03 h^{-1} and sequential batch cultures at 12, 30, and 39°C. We observed significant differences in biomass and ethanol yields on glucose, biomass protein and storage carbohydrate contents, and biomass yields on ATP between strains and cultivation temperatures. Increased temperature tolerance coincided with higher energetic efficiency of cell growth, indicating that temperature intolerance is a result of energy wasting processes, such as increased turnover of cellular components (e.g. proteins) due to temperature induced damage.

1

Introduction

The alcoholic beverage and bio-ethanol industries mainly use *Saccharomyces* yeasts as their workhorses, because of their robustness to low pH and high ethanol tolerance. The ethanol yield and productivity of fermentation processes highly depend on the performance of the yeast strains used at the temperatures applied in these processes. Large differences in performance and adaptation to working temperatures exist between individual yeast strains [1].

Temperature is one of the predominant factors determining the operational costs of industrial fermentation processes. According to an energy study of the European Commission, the alcoholic beverage and bio-energy industries spend around 30-60 % of their total energy requirement of the whole production process to control the cultivation temperature [2]. In general, the optimum growth temperature of *Saccharomyces* yeasts lies between 28°C to 33°C [3]. However, this temperature range is not applicable for both the alcoholic beverage and bio-ethanol production processes in industry. In particular, cider, beer, white and rosé wine fermentation processes are commonly operated at sub optimal temperatures [4,5], range from 10°C to 25°C, to enhance and retain their flavour volatiles [6]. These low working temperatures result in prolonged fermentation process duration and cause high risk of halted or sluggish fermentation [7]. Conversely, biofuel production processes are preferably performed at temperatures ≥40°C especially for fermentation processes with simultaneous saccharification of lignocellulosic feedstocks [8,9]. Therefore, the adaptation of yeast strains to temperatures outside the optimum range for growth provides an opportunity to make the production process more economical and eco-efficient.

Temperature tolerance is a polygenic trait which is influenced by a group of non-epistatic genes [10,11]. Several studies

have been performed to increase the understanding of the impact of the cultivation temperature on the physiology of *Saccharomyces* yeasts and to elucidate the mechanisms which contribute to differences in temperature tolerance [5,12–23].

In the majority of these studies, temperature shocks were applied rather than prolonged temperature stress, while the latter is much more relevant for industrial processes. To understand the cellular response and adaptation to temperature, the chosen research methodology is crucial to separate transient stress responses and adaptation. This work aims at addressing the long term impacts of different cultivation temperatures on *Saccharomyces* strains with better growth performance at sub- and supra-optimal temperatures. We first characterized a collection of industrial *Saccharomyces* strains in terms of their capabilities to grow at sub-and supra-optimal temperatures ranging from 12°C to 40°C. This allowed us to select one strain which performed best at sub-optimal and another strain which performed best at supra-optimal temperatures. Subsequently, the physiological responses of these strains, together with a well-characterized laboratory strain, CEN.PK113-7D, to sub-optimal, optimal and supra-optimal temperatures were investigated in well-defined chemostat cultures at a constant growth rate.

2
Methods and materials

2.1
Yeast strains, growth conditions, and storage

A total of 13 *Saccharomyces* strains used in this study of which one S. uvarum, one *S. cerevisiae* x *S. cerevisiae* hybrid and the others were *S. cerevisiae* species (Table 1). Inocula were prepared by introducing a single colony of a pure culture of each strain into 5 mL sterilized synthetic medium [24] with 15 g·L⁻¹ $C_6H_{12}O_6 \cdot H_2O$ in a 30°C incubator shaker at 220 rpm. Biomass stocks were prepared by the addition of sterilized glycerol to the exponentially growing cultures of all 13 strains, resulting the final concentration of 30% (v/v). The biomass stocks were stored aseptically at -80°C. These frozen stocks were used to inoculate the different experiments described as below.

Table 1
Yeast strains used in this study.

Strains	Commercial name	Species	Origin	Source
ADY1	Lalvin® QA23	*S. cerevisiae*	Portugal	Lallemand Inc., France
ADY2	Lalvin® ICV GRE	*S. cerevisiae*	France	Lallemand Inc., France
ADY3	Lalvin® T73	*S. cerevisiae*	Spain	Lallemand Inc., France
ADY5	CROSS EVOLUTION®	*S. cerevisiae x S. cerevisiae*	South Africa	Lallemand Inc., France
ADY6	Velluto BMV58 ™	*S. uvarum*	Spain	Lallemand Inc., France
ADY7	Lalvin® ICV OKAY	*S. cerevisiae*	France	Lallemand Inc., France
ADY8	Lalvin® Rhône 2056	*S. cerevisiae*	France	Lallemand Inc., France
ADY20	Uvaferm® WAM	*S. cerevisiae*	Spain	Lallemand Inc., France
ADY21	Lalvin® Rhône 2226	*S. cerevisiae*	France	Lallemand Inc., France
ADY22	Uvaferm® CEG	*S. cerevisiae*	Germany	Lallemand Inc., France
ADH30	-	S. cerevisiae	Spain	Lallemand Inc., France
CEN.PK113-7D	-	*S. cerevisiae*	Unknown	Fungal Biodiversity Centre, Utrecht, The Netherlands
Ethanol Red	Ethanol Red	*S. cerevisiae*	Unknown	Fermentis, S.I. Lesaffre

(-) Lab strain or non-marketed strain

The growth profile can be obtained by growing the yeast strains on a microtiter plate at different temperatures ranging from 12°C to 40°C under aerobic condition. Pre-culture was grown at 30°C and 220 rpm in sterilized synthetic medium [24] with 7.5 g·L^{-1} $C_6H_{12}O_6$·H_2O. the pre-culture was transferred to the microtiter plate (24 wells) with fresh synthetic medium resulted in an initial optical density at 600nm of approximately 0.1 and grown at the temperature ranged from 12°C to 40°C with continuous shaking (300 rpm, 1-inch amplitude). Growth was monitored via the optical density at 600 nm in a Synergy HTX Multi-Mode reader (BioTek, USA), and measurement was taken every 15 minutes for 18 hours. For the cultivation at temperature below 30°C, microtiter plates were cultivated in an incubator (New Brunswick Innova 44, Eppendorf) with continuous shaking (300 rpm, 1-inch amplitude) and measured the OD600 by the Synergy HTX Multi-Mode reader every 8 hours for 4 days. The growth profile of each strain at different temperatures was obtained by triplicate measurements and was fit to two models.

The maximum specific growth rates of each strain at different temperatures were obtained by fitting the experimental OD$_{600}$ to the corrected modified Gompertz model equation modified from the original version [25].

2.2
Primary model

$$\ln\left(\frac{ODt}{OD0}\right) = a * \exp\left\{-\exp\left[\left(\mu_{max} * \frac{\exp(1)}{a}\right) * (\lambda - t) + 1\right]\right\}$$

$$-a * \exp\left\{-\exp\left[\left(\mu_{max} * \frac{\exp(1)}{a}\right) * (\lambda) + 1\right]\right\}$$

Where OD$_0$ is the initial OD$_{600}$ and OD$_t$ is that at time t; *a* is the asymptotic maximum of ln (ODtODo) ; μ_{max} is the maximum specific growth rate with a unit of h^{-1}, and λ is the lag phase period. All the parameters of time have a unit of hour.

2.3
Secondary model

The CTMI model was used to fit with the obtained μ_{max} of each strain at different temperatures. The CTMI has the following expression;

$$\mu = 0\,, \qquad if\ T \leq T_{min}\ or\ T \geq T_{max}$$

$$\mu = \mu_{opt}\left(\frac{D}{E}\right), \qquad if\ T_{min}\ < T < T_{max}$$

$$D = (T - T_{max})(T - T_{min})^2$$

$$E = (T_{opt} - T_{min})[(T_{opt} - T_{min})(T - T_{opt}) - (T_{opt} - T_{max})(T_{opt} + T_{min} - 2T)]$$

2.4
Fermentation set-up

Where T_{max} is the temperature above which no growth occurs, T_{min} is the temperature below which no growth is observed, and T_{opt} is the temperature at which μ_{max} is equal to µopt. Both the primary and secondary models were fitted by minimizing the residual sum of squares (RSS) with respect to the experimental data.

All pre-cultures were grown aerobically at 220 rpm and at 30°C in the sterilized medium containing 5 g·L^{-1} $(NH_4)_2SO_4$, 3 g·L^{-1} KH_2PO_4, 0.5 g·L^{-1} $MgSO_4$·$7H_2O$, 22 g·L^{-1} $C_6H_{12}O_6$·H_2O, 1.0 mL·L^{-1} of trace element solution, and 1.0 mL·L^{-1} vitamin solution [24]. The sterilization of the medium was performed using a 0.2 µm Sartopore 2 filter unit (Sartorius Stedim, Goettingen, Germany).

All bioreactors (described in detail below) were equipped with norprene tubing, to minimize the diffusion of oxygen into the vessels and were sterilized by autoclaving at 121°C. The exhaust gas from all fermentations was passed through a condenser kept at 4.0°C and then through a Perma Pure Dryer (Inacom Instruments, Overberg, The Netherlands) to remove all water vapour and subsequently entered a Rosemount NGA 2000 gas analyser (Minnesota, USA) for measurement of the CO_2 concentration. The medium of all fermentations was continuously sparged with nitrogen gas prior and was contained 5.0 g·L^{-1} $(NH_4)_2SO_4$, 3.0 g·L^{-1} KH_2PO_4, 0.5 g·L^{-1} $MgSO_4$·$7H_2O$, 22.0 g·L^{-1} $C_6H_{12}O6$·H_2O, 0.4 g·L^{-1} Tween80, 10 mg·L^{-1} ergosterol, 0.26 g·L^{-1} antifoam C (Sigma-Aldrich, Missouri, USA), 1.0 mL·L^{-1} trace element solution, and 1.0 mL·L^{-1} vitamin solution [24]. The cultivations were carried out at temperatures of either 12.0 ± 0.1°C, 30.0 ± 0.1°C or 39.0 ± 0.1°C, by pumping cooled or heated water through the stainless-steel jacket surrounding the bottom part of the reactor vessel using a cryothermostat (Lauda

RE630, Lauda-Königshofen, Germany). The water temperature of the cryothermostat was controlled by using the signal of a Pt 100 temperature sensor inside the reactor, for accurate measurement and control of the cultivation temperature. Anaerobic conditions were maintained by continuously gassing of the reactor with nitrogen gas at a flowrate of 1.00 ± 0.01 SLM (standard liter per minute) using a mass flow controller (Brooks, Hatfield, USA). Also, the feed medium was kept anaerobic by sparging with nitrogen gas. The nitrogen gas was sterilized by passing through hydrophobic plate filters with a pore size of 0.2 μm (Millex, Millipore, Billerica, USA). The culture broth in the reactor was mixed using one 6-bladed Rushton turbine (diameter 80 mm) operated at a rotation speed of 450 rpm. The pH was controlled at 5.00 ± 0.05 by automatic titration with 2.0 M KOH.

The progression of all batch fermentations was monitored by the CO_2 measurement in the exhaust gas from the off-gas analyser and the base addition into the culture broth. The base bottle was placed on a load cell (Mettler Toledo, Tiel, The Netherlands), and thus the amount of base addition was measured by the weight decreased from the base bottle and by a totalizer of a feed pump. When there was no based addition for a defined amount of time, the culture broth was automatically drained from the bottom of the bioreactor by the effluent pump until there was 0.20 kg left which was regulated by using the weight balance of the bioreactor (Mettler Toledo, Tiel, The Netherlands). Fresh medium was subsequently added to fill the reactor until the total volume was 4.0 kg. The volume of the broth in the bioreactor was regulated by the weight balance of the bioreactor (Mettler Toledo, Tiel, The Netherlands) which was placed underneath the bioreactor. Six sequential batches were carried out in the above-mentioned cycle at each temperature set point (12°C, 30°C, and 39°C). The temperature set point was changed after every 6 sequential batches. The maximum specific growth rate of each strain at each cultivation temperature was calculated and averaged from the CO2 off-gas profiles of the last three sequential batches.

2.5
Sequential
batch
cultivations

2.6
Chemostat
Fermentation

All chemostat cultivations were carried out at a dilution rate of 0.030 ± 0.002 h⁻¹ in 7 L bioreactors (Applikon, Delft, The Netherlands) equipped with a DCU3 control system and MFCS data acquisition and control software (Sartorius Stedim Biotech, Goettingen, Germany).

All chemostat fermentations were initially operated in anaerobic batch cultivation with 4 L biomass culture broth in a 7 L bioreactor (Applikon, Delft, The Netherlands) to achieve enough biomass at the start of the chemostat phase. Four hundred mL of pre-culture was inoculated in each batch cultivation. When the off-gas CO_2 level from the batch cultivation dropped significantly close to the level after the pre-culture inoculation, this indicated the end of the batch phase. The fermentation was switched to a chemostat phase by switching on the continuous feed of the sterilized medium to the bioreactor, of which the sterile feed medium was pumped into the reactor vessel at a constant flowrate using a peristaltic pump (Masterflex, Barrington, USA), such that the outflow rate of the culture broth was 120 ± 1 g·h⁻¹. The effluent vessel was placed on a load cell of which the signal was continuously logged for accurate determination of the dilution rate of the chemostat and manual adjustment of the medium feed rate if needed. The working volume was kept constant at 4.00 ± 0.05 kg using the weight balance of the bioreactor (Mettler Toledo, Tiel, The Netherlands) which controlled the effluent pump. All chemostat cultures reached a steady-state after 5 volume changes, which was apparent from stable CO_2 levels in the exhaust gas and the biomass dry weight concentration were obtained. After reaching steady-state, triplicate samples at four sampling time points were withdrawn during another period of 4 to 5 volume changes, for quantification of the concentrations of biomass, residual glucose and extracellular metabolites.

2.7
Analytical
methods

Optical density was monitored using a Libra Su spectrophotometer (Biochrom Libra, Cambridge, UK) at a wavelength of 600 nm. Biomass dry weight was determined using the filtration of sample broth over a dry nitrocellulose filter (0.45 µm pore size, Gelman laboratory, Ann Arbor, USA) which was dried in a 70°C oven overnight. After the filtration of the sample broth, two sample volume of demineralized water was used to wash the filters which were subsequently dried in the oven at 70°C for two days. Prior and after sample filtration the filters were measured after cooling down in a desiccator for two hours. Extracellular metabolite of

the sample broth was obtained using cold stainless-steel beads [26]. The resulting supernatant broth was immediately frozen by liquid nitrogen and followed by the storage at -80°C. The supernatant broth was defrosted and analysed in duplicate using high-performance liquid chromatography (HPLC) with a Bio-Rad Aminex column (Bio-Rad Laboratories, California, USA) at 60°C. The column was eluted with 5.0 mM phosphoric acid at a flow rate of 0.6 mL·min^{-1}. Ethanol and glycerol were detected with a Waters 2414 refractive index detector (Waters Corporation, Massachusetts, USA), while a Waters 1489 UV-Vis detector (Waters Corporation, Massachusetts, USA) was used to detect acetate, lactate, malate, and succinate. Residual glucose was measured by ion chromatography using Dionex-ICS 5000+ (Thermo Fisher Scientific, Massachusettts, USA).

The metabolic flux distributions as well as the best estimates of the biomass specific net conversion rates of the chemostat experiments were obtained via metabolic flux analysis using a stoichiometric model for anaerobic growth of *S. cerevisiae* [21]. With sufficient available conversion rates as input variables an overdetermined system was obtained, we could calculate the best estimates of the biomass specific net conversion rates within their error margins as well as the metabolic flux distributions under the constraint that the elemental and compound balances were satisfied [27,28].

2.8
Metabolic
Flux Analysis
and Data
Reconciliation

The total organic carbon (TOC) of the chemostat total broth and the chemostat supernatant broth was calculated from the subtraction between the total carbon (TC) and the total inorganic carbon (TIC) which were both measured by a total organic carbon analyser (TOC-L CSH, Shimadzu, Kyoto, Japan).

2.9
Total organic
carbon and
total nitrogen
measurement

The total nitrogen (TN) of the freeze-dried biomass (10 mL culture broth) from the chemostat culture was measured by a total nitrogen unit (TNM-L, Shimadzu, Kyoto, Japan). The TN contents of a sample were in the form of ammonium, nitrite, nitrate, as well as organic compounds.

The injection of the samples for both TOC and TN measurement was carried out by an auto-sampler (ASI-L, Shimadzu, Kyoto, Japan).

2.10
Cellular protein measurement

Thirty millilitres chemostat cultural broth was drawn from the reactor and subsequently centrifuged at 4°C and at 5000 rpm for 5 minutes. The supernatant was discarded, and the biomass pellet was immediately frozen in liquid nitrogen and stored in -80°C prior freeze-drying. The cellular protein of the freeze-dried biomass was determined using Biuret method as described in [29] at which freeze-dried BSA was used as standard.

2.11
Cellular glycogen measurement

Approximately 2 mg of biomass was quenched into 100% methanol, which was chilled in -40°C prior, using a rapid sampling setup [30]. The quenching volume ratio of sample broth and methanol was 1 to 6. The quenching sample in 100% methanol was centrifuged at -19°C and at 5000 rpm for 5 minutes. The supernatant was discarded, and the biomass pellet was immediately frozen in liquid nitrogen and stored in -80°C.

The biomass pellet was washed twice with 1.5 mL cold Mi-Q water in an Eppendorf tube and followed by centrifugation at 4°C and at 8000 rpm for 2 minutes. The supernatant was discarded. The pellet was dissolved in 250µL of 0.25 M sodium carbonate solution and subsequently incubated at 95°C for 3 hours with continuous shaking. After the incubation, 600 µL of 0.2M sodium acetate was added into the mixture, the pH of which was adjusted to 5.3 with 1M acetate acid afterwards. The hydrolysis of the glycogen was performed by adding α-amyloglucosidase dissolved in 0.2 M sodium acetate to the mixture to have the final concentration of 1.2 U/mL. The reaction of the hydrolysis was carried out at 57°C overnight with continuously shaking. The equivalent glucose released from the glycogen digestion was determined in triplicate using the UV bioanalysis kit (R-Biopharm/Roche, Darmstadt, Germany). The resulting assay was measured at the wavelength 340 nm by a spectrophotometer.

2.12
Cellular trehalose measurement

Approximately 2 mg of biomass was quenched into 100% methanol, which was chilled at -40°C prior, using a rapid sampling setup [30]. Sample filtrate was washed twice with 20 mL 80% (v/v) methanol, which was chilled at -40°C prior, and was extracted with boiling ethanol as described in [30]. Cellular trehalose of the chemostat culture was measured by GC-MS analysis as described in [31]. C13 labelled cell extract was added into the extracted sample as internal standard [32].

3
Results

The growth capacities of 13 *Saccharomyces* yeasts were determined at temperatures between 12°C and 40°C in aerobic microtiter plate cultivations. For all cultivations the purity of the strains was verified through analysis of DNA delta sequences after PCR amplification as described previously [33] (data not shown). Via this growth phenotypic screening, an inventory was made of the tolerance of these strains to the sub-optimal temperatures used in the alcoholic beverage industry and the supra-optimal temperatures used in the bio-fuel production industry. Due to the Crabtree effect [34], all strains showed diauxic growth in the presence of oxygen. Only the initial parts of the growth curves, representing growth on glucose with concurrent production of ethanol, were used. The obtained growth profiles of the strains at the different temperatures were fitted to the corrected modified Gompertz model as proposed by Zwietering et al. [25] which was modified from Salvado et al. [3]. The fit of this model to the experimental data yielded two parameters, a maximum specific growth rate (μ_{max}) and a lag time (λ). The obtained lag times of the strains at the different cultivation temperatures were not correlated with the μ_{max} (data not shown). The fit of the model to the data was satisfactory for all strains at all cultivation temperatures with R-squared values (R^2) ranging from 0.92 to 0.99.

A hierarchical cluster analysis (HCL) of the relation between μ_{max} and cultivation temperature was performed using Euclidean distance to further analyse the growth performance between different strains within the temperature range from 12°C to 40°C (Figure 3). The colours in the heat map represent the values of μ_{max}. Based on the growth performance of all strains, the HCL seperated the applied temperature ranges into a range with sluggish growth (blue) and with facilitated growth (black or yellow). At 12°C, 15°C, and 40°C, the growth rates of all strains were below the median (0.25 h^{-1}).

3.1
Growth phenotypic comparison of industrial Saccharomyces strains at different temperatures (12°C to 40°C)

The growth capacities of 13 *Saccharomyces* yeasts were determined at temperatures between 12°C and 40°C in aerobic microtiter plate cultivations. For all cultivations the purity of the strains was verified through analysis of DNA delta sequences after PCR amplification as described previously [33] (data not shown). Via this growth phenotypic screening, an inventory was made of the tolerance of these strains to the sub-optimal temperatures used in the alcoholic beverage industry and the supra-optimal temperatures used in the bio-fuel production industry. Due to the Crabtree effect [34], all strains showed diauxic growth in the presence of oxygen. Only the initial parts of the growth curves, representing growth on glucose with concurrent production of ethanol, were used. The obtained growth profiles of the strains at the different temperatures were fitted to the corrected modified Gompertz model as proposed by Zwietering et al. [25] which was modified from Salvado et al. [3]. The fit of this model to the experimental data yielded two parameters, a maximum specific growth rate (μ_{max}) and a lag time (λ). The obtained lag times of the strains at the different cultivation temperatures were not correlated with the μ_{max} (data not shown). The fit of the model to the data was satisfactory for all strains at all cultivation temperatures with R-squared values (R2) ranging from 0.92 to 0.99.

A hierarchical cluster analysis (HCL) of the relation between μ_{max} and cultivation temperature was performed using Euclidean distance to further analyse the growth performance between different strains within the temperature range from 12°C to 40°C (Figure 3). The colours in the heat map represent the values of μ_{max}. Based on the growth performance of all strains, the HCL separated the applied temperature ranges into a range with sluggish growth (blue) and with facilitated growth (black or yellow). At 12°C, 15°C, and 40°C, the growth rates of all strains were below the median (0.25 h^{-1}). The cluster facilitated growth occurred could be divided into two subgroups (optimal and sub- or supra-optimal growth). The optimal growth temperatures of all strains were observed at 28°C and 33°C, at which the heat map at this area mostly shows a yellow colour. The sub- and-supra-optimal growth occurred at 25°C and below and 37°C and above, respectively, at which the heat map mostly shows a black colour. Regarding the sluggish and facilitated growth conditions, the HCL separated all strains into two major groups (1 and 2). Strains in group 1 had poor growth performance at all growth conditions, whereas strains in group 2 had a comparatively better growth performance.

To obtain relations for the μ_{max} as a function of the cultivation temperature for all strains tested, the growth rates obtained for the different strains at the different cultivation temperatures were used to fit the cardinal temperature model with inflection point (CTMI) [3]. The goodness of fit of the CTMI model to the μ_{max} data was satisfactory in all cases, with p-values between 0.97 and 0.99. The CTMI fits of μ_{max} vs growth temperature for the different strains are shown in Figure 4. ADY5 clearly showed the fastest growth in the temperature range from 12°C to 27°C. At temperatures between 27°C and 33°C, ADY2 had the highest μmax, while between 33°C and 40°C Ethanol Red grew faster than all other strains. Ethanol Red and ADY5 showed the best thermo- and cryo-tolerance, respectively, and were selected for further investigation of the underlying molecular and metabolic mechanisms. ADY5 is a *S. cerevisiae* hybrid strain which is particularly used for the production of aromatic white and rosé wines in the industry at low fermentation temperatures and low nitrogen levels. Ethanol Red is an industrial yeast strain with high ethanol tolerance and is commonly used for the production of industrial ethanol at fermentation temperatures up to 40°C.

Figure 4
CTMI fit of the
maximum specific
growth rate as
a function of
the cultivation
temperature (from
12°C to 40°C) to all of
the 13 *Saccharomyces*
yeasts.
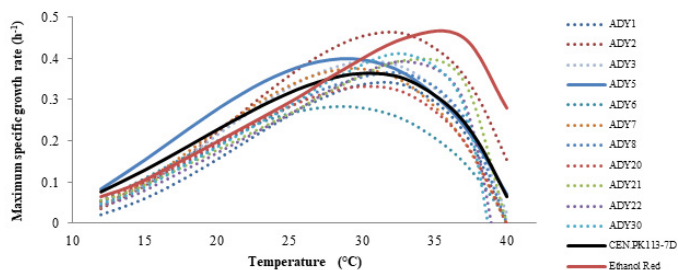
Table 2
Estimated parameters
with standard
deviation from the
CTMI fit for all the
13 strains. Standard
deviations for each
parameter were
obtained from three
independent non-
linear fits.

Strains	μ_{opt} (h^{-1})	T_{max} (°C)	T_{min} (°C)	T_{opt} (°C)
ADY1	0.343 ± 0.008	39.97 ± 0.01	7.78 ± 0.45	31.45 ± 0.02
ADY2	0.464 ± 0.011	41.58 ± 0.56	7.36 ± 0.79	31.86 ± 0.25
ADY3	0.381 ± 0.009	41.02 ± 0.41	7.29 ± 0.09	29.61 ± 0.39
ADY5	0.409 ± 0.002	40.61 ± 0.02	4.06 ± 0.39	29.17 ± 0.65
ADY6	0.297 ± 0.002	40.12 ± 0.02	4.14 ± 0.00	29.38 ± 0.09
ADY7	0.375 ± 0.004	39.98 ± 0.01	7.34 ± 0.90	29.47 ± 0.51
ADY8	0.367 ± 0.008	40.01 ± 0.00	3.93 ± 0.00	31.94 ± 0.59
ADY20	0.330 ± 0.006	39.97 ± 0.01	4.79 ± 0.84	30.43 ± 0.12
ADY21	0.302 ± 0.010	40.00 ± 0.00	2.11 ± 0.75	35.00 ± 0.17
ADY22	0.370 ± 0.027	39.98 ± 0.02	1.79 ± 0.93	32.50 ± 0.13
ADH30	0.236 ± 0.004	40.00 ± 0.00	4.00 ± 0.10	31.77 ± 0.64
CEN.PK113-7D	0.368 ± 0.018	41.21 ± 0.81	3.08 ± 0.92	30.03 ± 0.85
Ethanol Red	0.467 ± 0.004	41.48 ± 0.05	1.45 ± 0.09	35.26 ± 0.18

The CTMI fit also provided the cardinal growth parameters of each strain (T_{max}, T_{opt}, T_{min}, and μ_{opt}). The average values of the estimated parameters for all strains were obtained from three independent experiments and are summarized in Table 2. The T_{min} of all strains ranged from 1°C to 8°C, whereas the T_{max} of all strains ranged from 39°C to 41°C. For all 13 strains, the optimum growth temperatures, T_{opt}, were in the range between 29°C and 35°C wherein the corresponding specific growth rates ranged from 0.30 h^{-1} to 0.46 h^{-1}.

To validate the phenotypic screening results and the maximum growth rate estimations from the CTMI at the different temperatures for the selected strains (ADY5 and Ethanol Red) and the reference strain (CEN.PK113-7D), we performed sequential batch reactor (SBR) cultivations of the three strains. SBR instead of single batch cultures were chosen because these were shown to give a better reproducibility and more consistent results [35] as the effect of carryover from the inoculum, which might play a role during the first batch, vanishes after a few repetitive batch cultivations. Within ten repetitive batches, we did not observe adaptation/evolution of cell cultures because no increase of the maximum specific growth rate occurred. The carbon dioxide production profiles during the exponential phases of these SBR cultivations were used to calculate the μ_{max} of the selected strains at the three different cultivation temperatures (Table 3). Ethanol Red grew the fastest at 39°C, while ADY5 grew the fastest at 12°C, thereby confirming the results from the screening experiments in microtiter plates. Compared to these strains, CEN.PK113-7D showed the lowest maximum specific growth rate at the supra-optimal temperature, which was roughly 50% lower than that of the cold tolerant strain ADY5.

43

3.2.1
Maximum specific growth rate determination of the selected strains in anaerobic sequential batches cultures

Strains	12°C	30°C	39°C
ADY5	0.059 ± 0.001	0.416 ± 0.004	0.236 ± 0.003
CEN.PK113-7D	0.051 ± 0.001	0.361 ± 0.001	0.121 ± 0.009
Ethanol Red	0.045 ± 0.001	0.358 ± 0.001	0.392 ± 0.002

Table 3
Maximum specific growth rates (h^{-1}) in anaerobic SBR cultivations at 12°C, 30°C, and 39°C. Standard errors for each strain and for each growth temperature were obtained from three independent batches.

of these SBR cultivations were used to calculate the μ_{max} of the selected strains at the three different cultivation temperatures (Table 3). Ethanol Red grew the fastest at 39°C, while ADY5 grew the fastest at 12°C, thereby confirming the results from the screening experiments in microtiter plates. Compared to these strains, CEN.PK113-7D showed the lowest maximum specific growth rate at the supra-optimal temperature, which was roughly 50% lower than that of the cold tolerant strain ADY5.

3.2.2 Further physiological characterization of the strains in anaerobic chemostat cultures

To identify possible underlying mechanisms for the superior growth performances of ADY5 and Ethanol Red at respectively sub- and supra-optimal temperatures, we compared their physiology at 12°C, 30°C, and 39°C with the well-studied laboratory strain CEN.PK113-7D under well-defined conditions at a constant specific growth rate. To this end the strains were grown at these three temperatures in anaerobic steady-state chemostat cultures at a dilution rate of 0.03 h^{-1}. This dilution rate was slightly below the μ_{max} of the selected strains as well as CEN.PK113-7D at 12°C under anaerobic conditions (Table 3). During all steady-states the measured residual glucose concentration was below 0.50 mmol L^{-1}, confirming glucose limited conditions. Chemostat instead of batch cultivation was chosen as this allowed us to separate the temperature effects from the effects of the specific growth rate. It is well known that differences in growth rate result in physiological changes in yeast, such as transcript levels [6]. Fully anaerobic instead of micro-aerobic conditions were chosen to rule out effects of differences in dissolved oxygen levels at different cultivation temperatures. Besides, alcoholic beverage and bio-fuel production is mainly performed in the absence of oxygen [36,37].

3.2.3 Large differences between strains in the effect of temperature on net conversion rates

The biomass specific conversion rates (q_i, mmol·g_{DW}^{-1}·h^{-1}) were calculated for all steady-state chemostat cultivations at the three different temperatures. The first order evaporation constants for culture broth and ethanol during chemostat cultivations at different temperatures were experimentally determined (Table S3, supplementary) and used for a proper calculation of the specific ethanol production rate. Simultaneous metabolic flux analysis and data reconciliation was applied (see materials and methods) and yielded the best estimations of the conversion rates within their error margins (Table 4 and Table 5). The reconciled data for the nine chemostat conditions fitted well with the experimental data as the p-values of the reconciled conversion rates were all greater than the significance level of 0.05 (data not shown).

	q_s (mmol·gDW^{-1}·h^{-1})	q_{CO_2}(mmol·gDW^{-1}·h^{-1})	q_{eth} (mmol·gDW^{-1}·h^{-1})	q_{gly} (mmol·gDW^{-1}·h^{-1})
ADY5				
12°C	-1.804 ± 0.092	3.055 ± 0.183	2.899 ± 0.183	0.298 ± 0.008
30°C	-1.761 ± 0.067	2.955 ± 0.134	2.794 ± 0.134	0.306 ± 0.008
39°C	-2.158 ± 0.049	3.558 ± 0.096	3.464 ± 0.097	0.27 ± 0.012
CEN.PK113-7D				
12°C	-2.749 ± 0.100	4.56 ± 0.201	4.339 ± 0.201	0.428 ± 0.011
30°C	-2.078 ± 0.052	3.568 ± 0.104	3.399 ± 0.105	0.299 ± 0.011
39°C	-3.411 ± 0.007	4.805 ± 0.014	4.658 ± 0.014	0.309 ± 0.005
Ethanol Red				
12°C	-1.594 ± 0.092	2.599 ± 0.184	2.418 ± 0.184	0.334 ± 0.006
30°C	-1.837 ± 0.048	3.03 ± 0.096	2.855 ± 0.096	0.326 ± 0.013
39°C	-2.069 ± 0.069	3.404 ± 0.138	3.242 ± 0.138	0.365 ± 0.009

Table 4
Reconciled specific conversion rates of the three strains with their standard errors during anaerobic chemostat cultivation at 12°C, 30 °C, and 39 °C at a dilution rate of 0.03 h^{-1}. The nomenclature of s, eth, and gly represents as substrate (glucose), ethanol, and glycerol, respectively.

	q_{mal} (mmol·gDW^{-1}·h^{-1})	q_{suc} (mmol·gDW^{-1}·h^{-1})	q_{ace} (mmol·gDW^{-1}·h^{-1})	q_{lac} (mmol·gDW^{-1}·h^{-1})
ADY5				
12°C	0.006 ± 0.000	0.013 ± 0.000	0.000 ± 0.000	0.000 ± 0.000
30°C	0.006 ± 0.006	0.013 ± 0.000	0.000 ± 0.000	0.000 ± 0.000
39°C	0.014 ± 0.014	0.094 ± 0.000	0.021 ± 0.004	0.021 ± 0.004
CEN.PK113-7D				
12°C	0.008 ± 0.000	0.008 ± 0.000	0.067 ± 0.004	0.030 ± 0.004
30°C	0.000 ± 0.000	0.000 ± 0.000	0.000 ± 0.000	0.080 ± 0.000
39°C	0.007 ± 0.001	0.042 ± 0.003	0.016 ± 0.002	0.029 ± 0.002
Ethanol Red				
12°C	0.000 ± 0.000	0.013 ± 0.0000	0.018 ± 0.001	0.018 ± 0.001
30°C	0.000 ± 0.000	0.017 ± 0.0000	0.012 ± 0.004	0.012 ± 0.004
39°C	0.040 ± 0.040	0.001 ± 0.0000	0.025 ± 0.001	0.025 ± 0.001

Table 5
Reconciled specific conversion rates of the three strains with their standard errors during anaerobic chemostat cultivation at 12°C, 30°C, and 39°C at a dilution rate of 0.03 h^{-1}. The nomenclature of mal, suc, ace, and lac represents as malate, succinate, acetate, and lactate, respectively.

As expected from the stoichiometry of ethanol fermentation from glucose, the ratios (mol·mol^{-1}) of the CO_2 production rate (qco2) and ethanol production rate (qeth) were close to one for each strain and each temperature condition (Table 4). Although the dilution rate, and thus the specific growth rate, of all cultivations was the same, significant differences in the obtained qi values were observed for different strains and at different cultivation temperatures. As an example, the highest (absolute) value of the specific glucose uptake rate (qs), obtained for the CEN.PK113-7D cultivated at the supra-optimal temperature (39°C), was more than a factor of two higher than the lowest (absolute) value which was obtained for the Ethanol Red strain cultivated at the sub-optimal temperature (12°C). Comparable differences were observed for the ethanol and carbon dioxide production rates. For all the strains, the glucose consumption as well as ethanol and CO2 production rates were highest at the highest cultivation temperature. However, the differences between the individual strains were large thereof CEN.PK113-7D showed the highest values.

With respect to the sub-optimal temperature, the responses of the three strains were all different. For CEN.PK113-7D the qs, qeth, and qCO2 values were all significantly higher at 12°C compared to the control temperature; ADY5 showed no significant differences while for Ethanol Red these specific conversion rates were all significantly lower at 12°C compared to the control temperature (30°C). These results clearly indicate large differences in cellular energetics between the distinct strains cultivated at different temperatures.

There were also differences in the production rates of glycerol (Table 4) and acidic by-products (Table 5) between the individual strains, but there appeared to be no clear correlation with the cultivation temperature. Glycerol production rates were similar for the different strains and temperatures, except for CEN.PK113-7D, which had a significantly increased glycerol production rate at the sub-optimal temperature, which was accompanied with an increased acetate production rate. Nevertheless, all three strains produced very small amounts of acids, with production rates up to 0.09 mmol·g_{dw}^{-1}·h^{-1} (Table S1, supplementary).

3.2.4
*Large
differences
between strains
in the effect of
temperature on
yields*

	$Y_{biomass}$ (mol·mol⁻¹)	Y_{CO2} (mol·mol⁻¹)	$Y_{ethanol}$ (mol·mol⁻¹)	$Y_{glycerol}$ (mol·mol⁻¹)
ADY5				
12°C	0.595 ± 0.017	1.161 ± 0.046	1.607 ± 0.065	0.165 ± 0.005
30°C	0.625 ± 0.014	1.422 ± 0.042	1.587 ± 0.049	0.174 ± 0.004
39°C	0.514 ± 0.01	1.649 ± 0.096	1.605 ± 0.029	0.125 ± 0.003
CEN.PK113-7D				
12°C	0.396 ± 0.009	1.733 ± 0.05	1.649 ± 0.049	0.162 ± 0.005
30°C	0.498 ± 0.011	1.717 ± 0.033	1.636 ± 0.032	0.144 ± 0.003
39°C	0.404 ± 0.001	1.758 ± 0.003	1.704 ± 0.003	0.113 ± 0.001
Ethanol Red				
12°C	0.675 ± 0.02	1.63 ± 0.074	1.517 ± 0.072	0.210 ± 0.006
30°C	0.601 ± 0.013	1.649 ± 0.034	1.554 ± 0.033	0.178 ± 0.004
39°C	0.528 ± 0.011	1.645 ± 0.043	1.567 ± 0.042	0.176 ± 0.004

Table 6
Table 6 Yields of
biomass and main
products on glucose of
the three strains with
their standard errors,
calculated from the
specific net conversion
rates shown in Table 3.

	Y_{malate} (mol·mol⁻¹)	$Y_{sucinnate}$ (mol·mol⁻¹)	$Y_{acetate}$ (mol·mol⁻¹)	$Y_{lactate}$ (mol·mol⁻¹)
ADY5				
12°C	0.003 ± 0.000	0.007 ± 0.000	0.000 ± 0.000	0.000 ± 0.000
30°C	0.004 ± 0.000	0.007 ± 0.000	0.000 ± 0.000	0.000 ± 0.000
39°C	0.007 ± 0.000	0.044 ± 0.000	0.010 ± 0.001	0.021 ± 0.000
CEN.PK113-7D				
12°C	0.003 ± 0.000	0.003 ± 0.000	0.025 ± 0.001	0.011 ± 0.000
30°C	0.000 ± 0.000	0.000 ± 0.000	0.000 ± 0.000	0.038 ± 0.001
39°C	0.003 ± 0.000	0.016 ± 0.000	0.006 ± 0.000	0.011 ± 0.000
Ethanol Red				
12°C	0.000 ± 0.000	0.008 ± 0.000	0.011 ± 0.000	0.007 ± 0.000
30°C	0.000 ± 0.000	0.009 ± 0.000	0.006 ± 0.001	0.033 ± 0.003
39°C	0.019 ± 0.004	0.000 ± 0.000	0.012 ± 0.000	0.032 ± 0.001

Table 7
Yields of by-products
on glucose for the
three strains with
their standard errors,
calculated from the
specific net conversion
rates shown in Table 4.

A further analysis of the physiological differences between the strains grown at different temperatures was performed by comparing the yields of biomass and (by)products on glucose for the different cultivations (Table 6 and Table 7). Also, here, significant differences between strains and cultivation temperatures were observed. For all three strains the biomass yields on glucose were significantly lower at 39°C compared to 30°C wherein CEN.PK113-7D had the lowest biomass yield. Likewise, at 12°C CEN.PK113-7D had the lowest biomass yield. For ADY5 the biomass yields were the same at 12°C and 30°C, while for Ethanol Red the biomass yield was highest at 12°C. The ethanol yields on glucose for the three strains at the different cultivation temperatures varied between 1.52 (Ethanol Red, 12°C)

and 1.70 (CEN.PK113-7D, 39°C) mol ethanol per mol glucose, whereby each individual strain showed a slightly different ethanol yield on glucose in general (Table 6). Although Ethanol Red and ADY5 were designated, respectively, as hosts for the production of bioethanol and alcoholic beverages, they both had a lower ethanol yield on glucose than the laboratory strain CEN.PK113-7D, regardless of the cultivation temperature. CEN.PK113-7D showed the highest ethanol yield on glucose at 39°C, which was accompanied with a corresponding low biomass yield on glucose, as a larger part of the consumed glucose was converted to ethanol. As the fermentation of glucose to ethanol is directly coupled to cellular energy generation in the form of ATP, this clearly indicated that CEN.PK113-7D was negatively affected by the supra-optimal temperature which increased the cellular energy demand.

*3.2.5
Temperature
effect on
metabolic
efficiency
of biomass
formation*

Metabolic flux analysis was performed for each individual strain at each cultivation temperature using a stoichiometric model for anaerobic growth of *S. cerevisiae* on glucose. Hereby the metabolic flux distributions were calculated using the biomass specific conversion rates obtained from the steady-state chemostat cultivations as input. This allowed us to calculate the energetic efficiency of growth of each individual strain as a function of the cultivation temperature. For each condition, we calculated the net biomass specific rate of catabolic ATP production by summing up the hexokinase, glycerol-3-phosphase, phosphofructokinase, phosphoglycerate kinase, and pyruvate kinase fluxes. The ratios of the biomass specific growth rates and net biomass specific ATP production rates provided the biomass yields with respect to the produced ATP (Yx/ATP) at the different cultivation temperatures for each strain (Table 8). In spite of the fixed dilution rate, and thus identical specific growth rates, we observed large differences between the individual strains at the different cultivation temperatures. Ethanol Red cultivated at 12°C produced three times more biomass per mole of ATP than CEN.PK113-7D cultivated at 39°C. For each cultivation temperature, the Yx/ATP values for Ethanol Red and ADY5 were significantly higher than for CEN.PK113-7D. Ethanol Red grew most efficiently at both 12°C and 39°C. A possible reason for the differences in growth efficiencies might be differences in biochemical composition, e.g., protein contents of the cells among distinct strains. Therefore, for all chemostat cultivations the cellular contents of protein and storage carbohydrates were quantified for each strain and cultivation temperature.

	12°C	30°C	39°C
ADY5	11.79 ± 0.23	12.75 ± 0.18	9.17 ± 0.27
CEN.PK113-7D	7.64 ± 0.17	9.45 ± 0.12	5.35 ± 0.22
Ethanol Red	15.24 ± 0.30	12.27 ± 0.13	10.69 ± 0.16

Table 8
Yields of by-products on glucose for the three strains with their standard errors, calculated from the specific net conversion rates shown in Table 4.

3.3
Cellular protein, glycogen and trehalose contents

49

	12°C	30°C	39°C
ADY5	0.316 ± 0.004	0.334 ± 0.008	0.274 ± 0.030
CEN.PK113-7D	0.332 ± 0.010	0.376 ± 0.007	0.246 ± 0.002
Ethanol Red	0.325 ± 0.006	0.342 ± 0.005	0.284 ± 0.008

Table 9
Total protein contents of biomass ($g_{protein} \cdot g_{DW}^{-1}$) for the three strains with their standard deviations during anaerobic chemostat cultivation at different temperatures.

During chemostat cultivation at 12°C, the total cellular protein content was very similar for the three strains (Table 9), with an average value of about 0.32 $g_{protein} \cdot g_{DW}^{-1}$. At a cultivation temperature of 30°C, the protein contents of ADY5 and Ethanol Red were slightly higher, while there was a significant increase for CEN.PK113-7D compared to the 12°C cultivations. Remarkably, the total protein contents at the supra-optimal cultivation temperature of 39°C were significantly lower for all strains. These results were confirmed by quantification of the total cellular nitrogen contents (Table S2, supplementary) which indeed showed the same trends.

Figure 5
Glycogen accumulation of the three strains in anaerobic chemostat at 12°C, 30°C, and 39°C. Error bars represent standard deviations of average values of measurements in biomass samples from identical chemostat cultures at four different time points in steady-state.
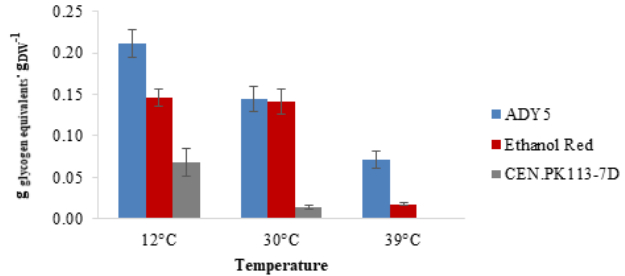
Figure 6
Trehalose accumulation of the three strains in anaerobic chemostat at 12°C, 30°C, and 39°C. Error bars represent standard deviations of average values of measurements in biomass samples obtained from identical chemostat cultures collected at four different time points in steady-state.
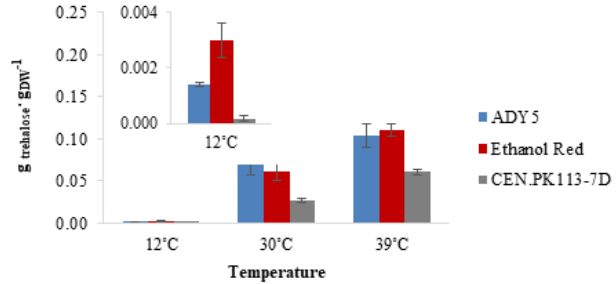
We observed large differences for the cellular contents of glycogen and trehalose between different strains and cultivation temperatures (Figure 5 and Figure 6). For all cultivation temperatures, both Ethanol Red and ADY5 had higher glycogen and trehalose accumulations than CEN.PK113-7D. The accumulations of glycogen and trehalose for all three strains showed opposite patterns with respect to the cultivation temperature. All three strains had higher glycogen but lower trehalose accumulations at 12°C, and vice versa at 39°C. At 12°C, the trehalose contents of all three strains were extremely low (below 1 %). We observed significant differences in glycogen accumulation between various strains at the sub-optimal temperature wherein ADY5 had the highest value of about 20 %. At 39°C, the trehalose accumulations of ADY5 and Ethanol Red were particularly high with values around 10 %. The glycogen accumulations at this temperature were also significantly different between strains. ADY5 had the highest value, more than 5 %, whereas CEN.PK113-7D had the lowest value, below 1 %.

4
Discussion

The growth performance of the three selected strains at 12°C, 30°C and 39°C in the anaerobic SBR cultures aligned well with the description of the CTMI model (Table 2) derived from the microtiter plate data. The μ_{max} values obtained from the anaerobic SBR cultivations (Table 3) showed that ADY5 and Ethanol Red clearly performed better at 12°C and 39°C, respectively, compared to CEN.PK113-7D. The μ_{max} values of ADY5 and CEN.PK113-7D at 30°C were very similar to the estimated optimal μ_{max} obtained from the CTMI. The estimated optimum temperature of Ethanol Red from the CTMI was five degrees higher than that of the other two strains, highlighting its temperature tolerance, and was close to the value reported in the literature [38]. Therefore, the CTMI model was useful and reliable in our study to describe the growth profile of the selected strains over the temperature range.

Further physiological characterization of the three strains in anaerobic glucose limited chemostat cultures at a fixed dilution rate revealed very large differences in the biomass yields on glucose between the different strains, but also between the different cultivation temperatures for the same strain (Table 6). Generally, lower biomass yields correlated with higher ethanol and CO_2 yields, suggesting differences in energy requirements for growth and maintenance for the different strains and temperatures. Also, the formation of increased amounts of by-products (glycerol and acids) will result in decreased biomass yields. However, the total yield of by-products on glucose was very similar for all chemostat cultivations and was on average 0.100 ± 0.005 mol of carbon produced per mol of carbon consumed as glucose. Notably, CEN.PK113-7D, of which the biomass yields at the different temperatures were the lowest, also showed the lowest average by-product yields, indicating that by-product formation was not the cause of the low biomass yields. The observed large differences in biomass yields must therefore

have been caused by large differences in cellular energy demands, which were quantified by calculating the biomass yields on ATP (Y_{ATP}) (Table 8). The Y_{ATP} of anaerobically grown *S. cerevisiae* (CBS8066) has been determined previously from glucose limited chemostat experiments at a cultivation temperature of 30°C [39] in which the maximum value was 16 $g_{DW} \cdot mol_{ATP}^{-1}$.

From retentostat experiments it was found that the ATP dissipation rate for maintenance (mATP) of CEN.PK113-7D under anaerobic conditions equals 1 $mmolATP \cdot g_{DW}^{-1} \cdot h^{-1}$ at 30°C [40]. From these figures it can be calculated that Y_{ATP} should be around 14 $g_{DW} \cdot mol_{ATP}^{-1}$ at a growth rate of 0.1 h^{-1}, which was indeed observed experimentally [39] and due to an increased contribution of maintenance energy requirements, around 10.5 $g_{DW} \cdot mol_{ATP}^{-1}$ at the growth rate of 0.03 h^{-1} used in our chemostat cultivations. The Y_{ATP} values we observed for the three strains at 30°C (between 9.5 and 12.8 $g_{DW} \cdot mol_{ATP}^{-1}$) are close to this value, whereby differences in biomass composition, especially protein content of which the biosynthesis is the most energy demanding, could be responsible for the differences in Y_{ATP} values between the strains at the same cultivation temperature. Quantification of the total protein contents revealed, however, that there were minor differences in protein contents between the three strains at the same temperature, thus ruling out that the observed differences in Y_{ATP} between the strains were caused by differences in protein content. The cultivation temperature itself had more effect, especially at 39°C the protein contents of all three strains were significantly lower than at 30°C and 12°C. This could be a strategy of the cells to decrease their ATP expenses to cope with the stress during growth at supra-optimal temperatures.

It is well known that maintenance energy requirements of microorganisms increase with increasing cultivation temperature [41]. Using the correlation proposed by these authors, an increase of the cultivation temperature from 30°C to 39°C would result in a 2.2-fold increase of the maintenance coefficient, which would result in a decrease of Y_{ATP} with 30 % to 7.4 $g_{DW} \cdot mol_{ATP}^{-1}$ at a growth rate of 0.03 h^{-1}. The decrease of Y_{ATP} of the ADY5 strain at 39°C is indeed very close to 30% value while for CEN.PK113-7D the decrease is more than 40 %. Ethanol Red appeared clearly better adapted to higher cultivation temperatures as the Y_{ATP} decreased with only 13 %. Conversely, a decrease of the

cultivation temperature from 30°C to 12°C would, according to the correlation of Tijhuis et al. [41], result in a decrease of the maintenance energy requirements with more than a factor of 5 and, consequently, an increase of Y_{ATP} with almost 40 % at a growth rate of 0.03 h^{-1}. Such an increase was not observed in our chemostat cultures, on the contrary, for two strains (CEN.PK113-7D and ADY5) Y_{ATP} was lower at 12°C than at 30°C. Nevertheless, for Ethanol Red Y_{ATP} was 24 % higher at 12°C compared to 30°C.

Another factor which can lead to differences in Y_{ATP} between different strains and/or cultivation temperatures is differences in the concentrations of weak acids [38]. Passive diffusion of the undissociated form into the cells and subsequent active export results in an ATP dissipating futile cycle leading to increased non-growth associated energy requirements. Of the acidic by products excreted, acetic acid (pKa = 4.76) would have the most significant influence on the maintenance energy requirements because at the cultivation pH of 5, 37 % of the acid is present in the undissociated form. The maximum residual acetic acid concentration of the chemostat cultures was 2.84 mmol·L^{-1} for CEN.PK113-7D cultivated at 12 ºC (Table S1). At this residual acetic acid concentration, the maintenance energy requirements would be approximately 2.3 mmolATP·g$_{DW}$$^{-1}$·h^{-1} at pH 5, and 30°C [39] and would result in an Y_{ATP} of 7.2 g$_{DW}$·mol$_{ATP}$$^{-1}$, which is close to the observed value of 7.64 (Table 8). For all the other strains and temperatures, the residual acetic acid concentrations were around 1 mM or lower and thus the effect on the maintenance energy requirements were assumed to be small. Interestingly, ADY5 did not produce acetic acid at 12°C and 30 ºC. Possible uncoupling of acetic acid seems not to attribute significantly to the Y_{ATP} of Ethanol Red at 12°C where the residual acetic acid concentration was 2 times higher than that at 30ºC.

Another cause of the effect of temperature on Y_{ATP} could be protein misfolding at high temperatures and aggregation at low temperatures. Remarkably the proteome analysis of the identical chemostat cultured strains revealed that for both CEN. PK113-7D and ADY5 the proteins related to protein folding and degradation processes were upregulated at 12°C, in contrast to Ethanol Red [42]. This could indicate that protein aggregation and/or misfolding and subsequent degradation and re-synthesismight have occurred in these strains at 12°C, resulting in an increased energy demand and thus a decreased Y_{ATP}.

In Ethanol Red Erg13, one of the first and rate controlling enzymes in the ergosterol biosynthesis pathway was upregulated at both 12°C and 39°C [42]. Although ergosterol was one of the anaerobic growth factors supplemented to the chemostat medium as its synthesis requires oxygen, this upregulation could indicate increased incorporation of ergosterol in the cell membrane of Ethanol Red. Several studies have reported that the activation of the ergosterol pathways makes yeast cells more resistant/tolerant to a variety of stresses, including low temperature, low-sugar conditions, oxidative stress and ethanol [43–46].

All three strains showed upregulation of proteins involved in transport and metabolism of carbohydrates as well as energy and amino acid metabolism at 12°C compared to 30°C [42]. This shows that maintaining the same specific growth rate of 0.03 h^{-1} in the chemostat at 12°C, where maximum enzyme capacities have decreased, requires upregulation of proteins in central metabolism.

It is well-known that the accumulation of the storage carbohydrates glycogen and trehalose in *S. cerevisiae* strongly depends on the growth rate [47] and that in particular trehalose was shown to protect cells during stress conditions [48–50]. As in this work all cultivations were carried out at a fixed dilution rate, differences in storage carbohydrate accumulation can only be attributed to the particular strain used and/or the cultivation temperature. During glucose limited chemostat cultivation all three strains accumulated both trehalose and glycogen, whereby the differences in total accumulations (glycogen and trehalose) between strains were more significant than between cultivation temperatures for the same strain. It is well known that *S. cerevisiae* accumulates these carbohydrates at growth rates below 0.1 h^{-1} whereby the contents are related to the duration of the G1 phase [51]. Under carbon limited conditions trehalose and glycogen serve as carbon and energy reserves to enable the survival during starvation but are also mobilized to facilitate a transient increase in the ATP flux for progression through the cell cycle [52]. For all three strains the accumulations of trehalose and glycogen were strongly dependent on the cultivation temperature, with highest glycogen accumulation at 12°C and highest trehalose accumulation at 39°C. Increased trehalose accumulation at high cultivation temperatures have been observed before and were caused by a stimulation of trehalose synthase and inhibition

of trehalose [53]. Because of the α-1,1-glycosidic bond linkage within the structure, trehalose has stronger resistance to heat and acid and was shown to be a preferable energy reserve over glycogen during stress conditions [48,54], although the synthesis of trehalose requires more ATP per glucose than that of glycogen [47]. Besides, the degradation of trehalose releases two glucoses, whereas one glucose is released after the degradation of the α-1,4-glycosidic bond within glycogen. Apart from its role as a reserve carbohydrate, trehalose also has a protective function during stress conditions e.g. thermal stress, whereby it acts as the protector of membranes and proteins [55–57]. Therefore, the significantly higher trehalose accumulation of ADY5 and Ethanol Red might have contributed to the better growth performance at 39°C compared with CEN.PK113-7D.

The superior growth performance of ADY5 during SBR cultivation at 12°C coincided with a high capacity to accumulate glycogen. Increased carbohydrate accumulation, in particular glycogen, as a response to prolonged exposure of yeast to cold (10°C) has been observed before [58]. Furthermore, a positive correlation between cell wall bound glycogen and viability under glucose deprived conditions was reported [59]. Although the precise function of this glycogen pool remains unclear, it might play a role in membrane stabilization which may improve the resistance to cold [60].

5
Conclusion

From a growth phenotypic screening of 12 industrial *Saccharomyces* strains for their temperature tolerance, we selected ADY5, Ethanol Red, and CEN.PK113-7D to further elucidate the possible underlying mechanisms for temperature tolerance. The chemostat results revealed significant differences in the metabolic response and cellular energetics between strains and among different growth temperatures. Despite a fixed growth rate, different growth temperatures resulted in large differences between the three strains in terms of net conversion rates, substrate yields and energetic efficiency of biomass formation. All strains showed a decrease of protein content at supra-optimal temperatures which was nevertheless accompanied with a decrease of Y_{ATP}, thus implying an increase of non-growth associated energy demands. Increased temperature tolerance coincided with higher energetic efficiency of cell growth, indicating that temperature intolerance is a result of energy wasting processes, such as increased turnover of cellular components due to temperature induced damage, e.g. protein misfolding. Further research is required to deepen our comprehension on the underlying mechanisms. With this knowledge, we can develop and apply strategies to obtain tailored cryo- and-thermo tolerant yeasts for industrial applications.

Author Contributions

All authors have been involved in the conceptualization and the methodology of the experiments. JMG provided information about the industrial strains. CEC, EGR, and KYFL performed the growth phenotypic screenings in microtiter plates. EGR and KYFL performed the computational simulations. EGR performed the HCL analysis. KYFL performed the measurements of total proteins, total nitrogen, and storage carbohydrates of the chemostat cultures. KYFL and WMVG performed the fermentations in bioreactors, analysis of the results, and wrote the original draft of the paper. CEC and LD made the graphic abstract. All authors reviewed, edited, and approved the final manuscript.

Conflict of Interest

The authors declare that they have no known competing financial interests or personal relationships that could have appeared to affect the work reported in this paper.

References

[1]   Amparo. Querol, G.H. Fleet, Yeasts in food and beverages, Springer, Berlin, 2006.

[2]   Y. Chan, R. Kantamaneni, Study on energy efficiency and energy saving potential in industry and on possible policy mechanisms, ICF Consulting Limited, 2016. https://ec.europa.eu/energy/studies/study-energy-efficiency-and-energy-saving-potential-industry-and-possible-policy-mechanisms_en?redir=1.

[3]   Z. Salvadó, F.N. Arroyo-López, J.M. Guillamón, G. Salazar, A. Querol, E. Barrio, Temperature Adaptation Markedly Determines Evolution within the Genus Saccharomyces, Appl. Environ. Microbiol. 77 (2011) 2292–2302. https://doi.org/10.1128/AEM.01861-10.

[4]   R.E. Kunkee, Selection and modification of yeasts and lactic acid bacteria for wine fermentation, Food Microbiology. 1 (1984) 315–332. https://doi.org/10.1016/0740-0020(84)90065-0.

[5]   M.J. Torija, G. Beltran, M. Novo, M. Poblet, J.M. Guillamón, A. Mas, N. Rozès, Effects of fermentation temperature and Saccharomyces species on the cell fatty acid composition and presence of volatile compounds in wine, International Journal of Food Microbiology. 85 (2003) 127–136. https://doi.org/10.1016/S0168-1605(02)00506-8.

[6]   G. Beltran, M. Novo, V. Leberre, S. Sokol, D. Labourdette, J.-M. Guillamon, A. Mas, J. François, N. Rozes, Integration of transcriptomic and metabolic analyses for understanding the global responses of low-temperature winemaking fermentations, FEMS Yeast Res. 6 (2006) 1167–1183. https://doi.org/10.1111/j.1567-1364.2006.00106.x.

[7]   L.F. Bisson, Stuck and Sluggish Fermentations, Am J Enol Vitic. 50 (1999) 107–119.

[8]   M. Kelbert, A. Romaní, E. Coelho, L. Pereira, J.A. Teixeira, L. Domingues, Simultaneous saccharification and fermentation of hydrothermal pretreated lignocellulosic biomass: evaluation of process performance under multiple stress conditions, Bioenerg. Res. 9 (2016) 750–762. https://doi.org/10.1007/s12155-016-9722-6.

[9]   U. Breuer, Yeast Biotechnology: Diversity and applications. By T. Satyanarayana and Gotthard Kunze (Eds.), Biotechnology Journal. 5 (2010) 427–428. https://doi.org/10.1002/biot.201000029.

[10]   Y. Yang, M.R. Foulquié-Moreno, L. Clement, É. Erdei, A. Tanghe, K. Schaerlaekens, F. Dumortier, J.M. Thevelein, QTL Analysis of High Thermotolerance with Superior and Downgraded Parental Yeast Strains Reveals New Minor QTLs and Converges on Novel Causative Alleles Involved in RNA Processing, PLoS Genet. 9 (2013). https://doi.org/10.1371/journal.pgen.1003693.

[11]   Z. Wang, Q. Qi, Y. Lin, Y. Guo, Y. Liu, Q. Wang, QTL analysis reveals genomic variants linked to high-temperature fermentation performance in the industrial yeast, Biotechnology for Biofuels. 12 (2019) 59. https://doi.org/10.1186/s13068-019-1398-7.

[12]   J. Verghese, J. Abrams, Y. Wang, K.A. Morano, Biology of the heat shock response and protein chaperones: budding yeast (Saccharomyces cerevisiae) as a model system, Microbiol. Mol. Biol. Rev. 76 (2012) 115–158. https://doi.org/10.1128/MMBR.05018-11.

[13]   V.A. Kalyuzhin, Heat resistance in Saccharomyces cerevisiae yeast, Biol Bull Rev. 1 (2011) 207–213. https://doi.org/10.1134/S2079086411030042.

[14]   L. Castells-Roca, J. García-Martínez, J. Moreno, E. Herrero, G. Bellí, J.E. Pérez-Ortín, Heat Shock Response in Yeast Involves Changes in Both Transcription Rates and mRNA Stabilities, PLOS ONE. 6 (2011) e17272. https://doi.org/10.1371/journal.pone.0017272.

[15]   E.G. Rikhvanov, N.N. Varakina, T.M. Rusaleva, E.I. Rachenko, V.A. Kiseleva, V.K. Voinikov, Heat Shock–Induced Changes in the Respiration of the Yeast Saccharomyces cerevisiae, Microbiology. 70 (2001) 462–465. https://doi.org/10.1023/A:1010442429489.

[16]   D.A. Costa, C.J.A. de Souza, P.S. Costa, M.Q.R.B. Rodrigues, A.F. dos Santos, M.R. Lopes, H.L.A. Genier, W.B. Silveira, L.G. Fietto, Physiological characterization of thermotolerant yeast for cellulosic ethanol production, Appl Microbiol Biotechnol. 98 (2014) 3829–3840. https://doi.org/10.1007/s00253-014-5580-3.

[17]   J. Postmus, A.B. Canelas, J. Bouwman, B.M. Bakker, W. van Gulik, M.J.T. de Mattos, S. Brul, G.J. Smits, Quantitative Analysis of the High Temperature-induced Glycolytic Flux Increase in Saccharomyces cerevisiae Reveals Dominant Metabolic Regulation, J. Biol. Chem. 283 (2008) 23524–23532. https://doi.org/10.1074/jbc.M802908200.

[18]   K.A. Morano, C.M. Grant, W.S. Moye-Rowley, The Response to Heat Shock and Oxidative Stress in Saccharomyces cerevisiae, Genetics. 190 (2012) 1157–1195. https://doi.org/10.1534/genetics.111.128033.

[19]   L. Caspeta, J. Nielsen, Thermotolerant Yeast Strains Adapted by Laboratory Evolution Show Trade-Off at Ancestral Temperatures and Preadaptation to Other Stresses, MBio. 6 (2015) e00431-15. https://doi.org/10.1128/mBio.00431-15.

[20]   L. Caspeta, Y. Chen, J. Nielsen, Thermotolerant yeasts selected by adaptive evolution express heat stress response at 30°C, Scientific Reports. 6 (2016) 27003. https://doi.org/10.1038/srep27003.

[21]   S.L. Tai, P. Daran-Lapujade, M.A.H. Luttik, M.C. Walsh, J.A. Diderich, G.C. Krijger, W.M. van Gulik, J.T. Pronk, J.-M. Daran, Control of the Glycolytic Flux in Saccharomyces cerevisiae Grown at Low Temperature A MULTI-LEVEL ANALYSIS IN ANAEROBIC CHEMOSTAT CULTURES, J. Biol. Chem. 282 (2007) 10243–10251. https://doi.org/10.1074/jbc.M610845200.

[22]   S.L. Tai, P. Daran-Lapujade, M.C. Walsh, J.T. Pronk, J.-M. Daran, Acclimation of Saccharomyces cerevisiae to Low Temperature: A Chemostat-based Transcriptome Analysis, Mol Biol Cell. 18 (2007) 5100–5112. https://doi.org/10.1091/mbc.E07-02-0131.

[23]   E. García-Ríos, M. Morard, L. Parts, G. Liti, J.M. Guillamón, The genetic architecture of low-temperature adaptation in the wine yeast Saccharomyces cerevisiae, BMC Genomics. 18 (2017) 159. https://doi.org/10.1186/s12864-017-3572-2.

[24]   C. Verduyn, E. Postma, W.A. Scheffers, J.P. van Dijken, Physiology of Saccharomyces Cerevisiae in Anaerobic Glucose-Limited Chemostat Culturesx, Microbiology. 136 (1990) 395–403. https://doi.org/10.1099/00221287-136-3-395.

[25]   M.H. Zwietering, I. Jongenburger, F.M. Rombouts, K. van 't Riet, Modeling of the Bacterial Growth Curve, Appl Environ Microbiol. 56 (1990) 1875–1881.

[26]   M.R. Mashego, W.M. van Gulik, J.L. Vinke, J.J. Heijnen, Critical evaluation of sampling techniques for residual glucose determination in carbon-limited chemostat culture of Saccharomyces cerevisiae, Biotechnol. Bioeng. 83 (2003) 395–399. https://doi.org/10.1002/bit.10683.

[27]   R.T.J.M. van der Heijden, J.J. Heijnen, C. Hellinga, B. Romein, K.C.A.M. Luyben, Linear constraint relations in biochemical reaction systems: I. Classification of the calculability and the balanceability of conversion rates, Biotechnology and Bioengineering. 43 (1994) 3–10. https://doi.org/10.1002/bit.260430103.

[28]   R.T.J.M. van der Heijden, B. Romein, J.J. Heijnen, C. Hellinga, K.C.A.M. Luyben, Linear constraint relations in biochemical reaction systems: II. Diagnosis and estimation of gross errors, Biotechnology and Bioengineering. 43 (1994) 11–20. https://doi.org/10.1002/bit.260430104.

[29]   H.C. Lange, J.J. Heijnen, Statistical reconciliation of the elemental and molecular biomass composition of Saccharomyces cerevisiae, Biotechnol. Bioeng. 75 (2001) 334–344. https://doi.org/10.1002/bit.10054.

[30]   A.B. Canelas, A. ten Pierick, C. Ras, R.M. Seifar, J.C. van Dam, W.M. van Gulik, J.J. Heijnen, Quantitative Evaluation of Intracellular Metabolite Extraction Techniques for Yeast Metabolomics, Anal. Chem. 81 (2009) 7379–7389. https://doi.org/10.1021/ac900999t.

[31]   D. Visser, G.A. van Zuylen, J.C. van Dam, A. Oudshoorn, M.R. Eman, C. Ras, W.M. van Gulik, J. Frank, G.W.K. van Dedem, J.J. Heijnen, Rapid sampling for analysis of in vivo kinetics using the BioScope: A system for continuous-pulse experiments, Biotechnology and Bioengineering. 79 (2002) 674–681. https://doi.org/10.1002/bit.10328.

[32]   L. Wu, M.R. Mashego, J.C. van Dam, A.M. Proell, J.L. Vinke, C. Ras, W.A. van Winden, W.M. van Gulik, J.J. Heijnen, Quantitative analysis of the microbial metabolome by isotope dilution mass spectrometry using uniformly 13C-labeled cell extracts as internal standards, Analytical Biochemistry. 336 (2005) 164–171. https://doi.org/10.1016/j.ab.2004.09.001.

[33]   A. Xufre, H. Albergaria, F. Gírio, I. Spencer-Martins, Use of interdelta polymorphisms of Saccharomyces cerevisiae strains to monitor population evolution during wine fermentation, J Ind Microbiol Biotechnol. 38 (2010) 127–132. https://doi.org/10.1007/s10295-010-0837-z.

[34]   De Deken RH, The Crabtree effect: a regulatory system in yeast., Journal of General Microbiology. 44 (1966) 149–56.

[35]   A. l. b. Cruz, A. j. Verbon, L. j. Geurink, P. j. t. Verheijen, J. j. Heijnen, W.M. van Gulik, Use of sequential-batch fermentations to characterize the impact of mild hypothermic temperatures on the anaerobic stoichiometry and kinetics of Saccharomyces cerevisiae, Biotechnol. Bioeng. 109 (2012) 1735–1744. https://doi.org/10.1002/bit.24454.

[36]   P. Saranraj, P. Sivasakthivelan, M. Naveen, Fermentation of fruit wine and its quality analysis: A review, Australian Journal of Science and Technology. 1 (2017) 85–97.

[37]   S.H. Mohd Azhar, R. Abdulla, S.A. Jambo, H. Marbawi, J.A. Gansau, A.A. Mohd Faik, K.F. Rodrigues, Yeasts in sustainable bioethanol production: A review, Biochemistry and Biophysics Reports. 10 (2017) 52–61. https://doi.org/10.1016/j.bbrep.2017.03.003.

[38]   A. Ullah, R. Orij, S. Brul, G.J. Smits, Quantitative Analysis of the Modes of Growth Inhibition by Weak Organic Acids in Saccharomyces cerevisiae, Appl. Environ. Microbiol. 78 (2012) 8377–8387. https://doi.org/10.1128/AEM.02126-12.

[39]   C. Verduyn, E. Postma, W.A. Scheffers, J.P. Van Dijken, Energetics of Saccharomyces cerevisiae in Anaerobic Glucose-Limited Chemostat Cultures, Microbiology. 136 (1990) 405–412. https://doi.org/10.1099/00221287-136-3-405.

[40]   L.G.M. Boender, E.A.F. de Hulster, A.J.A. van Maris, P.A.S. Daran-Lapujade, J.T. Pronk, Quantitative Physiology of Saccharomyces cerevisiae at Near-Zero Specific Growth Rates, Appl. Environ. Microbiol. 75 (2009) 7578. https://doi.org/10.1128/AEM.02344-09.

[41]   L. Tijhuis, M.C. Van Loosdrecht, J.J. Heijnen, A thermodynamically based correlation for maintenance gibbs energy requirements in aerobic and anaerobic chemotrophic growth, Biotechnol. Bioeng. 42 (1993) 509–519. https://doi.org/10.1002/bit.260420415.

[42]   T. Pinheiro, K.Y.F. Lip, E. Garcia-Rios, A. Querol, J.A. Teixeira, W. van Gulik, J.M. Guillamon, L. Domingues, Differential proteomic analysis by SWATH-MS unravels the most dominant mechanisms underlying yeast adaptation to non-optimal temperatures under anaerobic conditions, BioRxiv. (2020) 2020.01.06.895581. https://doi.org/10.1101/2020.01.06.895581.

[43]   F. Aguilera, R.A. Peinado, C. Millán, J.M. Ortega, J.C. Mauricio, Relationship between ethanol tolerance, H+-ATPase activity and the lipid composition of the plasma membrane in different wine yeast strains, International Journal of Food Microbiology. 110 (2006) 34–42. https://doi.org/10.1016/j.ijfoodmicro.2006.02.002.

[44]   J. Ding, X. Huang, L. Zhang, N. Zhao, D. Yang, K. Zhang, Tolerance and stress response to ethanol in the yeast Saccharomyces cerevisiae, Appl Microbiol Biotechnol. 85 (2009) 253. https://doi.org/10.1007/s00253-009-2223-1.

[45]   C.A. Suarez-Mendez, M. Hanemaaijer, A. ten Pierick, J.C. Wolters, J.J. Heijnen, S.A. Wahl, Interaction of storage carbohydrates and other cyclic fluxes with central metabolism: A quantitative approach by non-stationary 13C metabolic flux analysis, Metabolic Engineering Communications. 3 (2016) 52–63. https://doi.org/10.1016/j.meteno.2016.01.001.

[46]   T. Higashiyama, Novel functions and applications of trehalose, Pure and Applied Chemistry. 74 (2002) 1263–1269. https://doi.org/10.1351/pac200274071263.

[47]   M.A. Singer, S. Lindquist, Multiple Effects of Trehalose on Protein Folding In Vitro and In Vivo, Molecular Cell. 1 (1998) 639–648. https://doi.org/10.1016/S1097-2765(00)80064-7.

[48]   M.B. França, A.D. Panek, E.C.A. Eleutherio, Oxidative stress and its effects during dehydration, Comparative Biochemistry and Physiology Part A: Molecular & Integrative Physiology. 146 (2007) 621–631. https://doi.org/10.1016/j.cbpa.2006.02.030.

[49]   J.W.G. Paalman, R. Verwaal, S.H. Slofstra, A.J. Verkleij, J. Boonstra, C.T. Verrips, Trehalose and glycogen accumulation is related to the duration of the G1 phase of Saccharomyces cerevisiae, FEMS Yeast Research. 3 (2003) 261–268. https://doi.org/10.1111/j.1567-1364.2003.tb00168.x.

[50]   H.H.W. Silljé, J.W.G. Paalman, E.G. ter Schure, S.Q.B. Olsthoorn, A.J. Verkleij, J. Boonstra, C.T. Verrips, Function of Trehalose and Glycogen in Cell Cycle Progression and Cell Viability in Saccharomyces cerevisiae, J Bacteriol. 181 (1999) 396–400.

[51]   J.L. Parrou, M.-A. Teste, J. François, Effects of various types of stress on the metabolism of reserve carbohydrates in Saccharomyces cerevisiae: genetic evidence for a stress-induced recycling of glycogen and trehalose, Microbiology. 143 (1997) 1891–1900. https://doi.org/10.1099/00221287-143-6-1891.

[52]   B.M.A. Abdel-Banat, H. Hoshida, A. Ano, S. Nonklang, R. Akada, High-temperature fermentation: how can processes for ethanol production at high temperatures become superior to the traditional process using mesophilic yeast?, Appl Microbiol Biotechnol. 85 (2010) 861–867. https://doi.org/10.1007/s00253-009-2248-5.

[53]   E. Eleutherio, A. Panek, J.F.D. Mesquita, E. Trevisol, R. Magalhães, Revisiting yeast trehalose metabolism, Curr Genet. 61 (2015) 263–274. https://doi.org/10.1007/s00294-014-0450-1.

[54]   P.A. Gibney, A. Schieler, J.C. Chen, J.D. Rabinowitz, D. Botstein, Characterizing the in vivo role of trehalose in Saccharomyces cerevisiae using the AGT1 transporter, Proc Natl Acad Sci U S A. 112 (2015) 6116–6121. https://doi.org/10.1073/pnas.1506289112.

[55]   C. Coutinho, E. Bernardes, D. Félix, A.D. Panek, Trehalose as cryoprotectant for preservation of yeast strains, Journal of Biotechnology. 7 (1988) 23–32. https://doi.org/10.1016/0168-1656(88)90032-6.

[56]   B. Schade, G. Jansen, M. Whiteway, K.D. Entian, D.Y. Thomas, Cold Adaptation in Budding Yeast, Mol Biol Cell. 15 (2004) 5492–5502. https://doi.org/10.1091/mbc.E04-03-0167.

[57]   R. Pérez-Torrado, J.V. Gimeno-Alcañiz, E. Matallana, Wine Yeast Strains Engineered for Glycogen Overproduction Display Enhanced Viability under Glucose Deprivation Conditions, Appl Environ Microbiol. 68 (2002) 3339–3344. https://doi.org/10.1128/AEM.68.7.3339-3344.2002.

[58]   S. Rodríguez-Vargas, A. Sánchez-García, J.M. Martínez-Rivas, J.A. Prieto, F. Randez-Gil, Fluidization of Membrane Lipids Enhances the Tolerance of Saccharomyces cerevisiae to Freezing and Salt Stress, Appl. Environ. Microbiol. 73 (2007) 110–116. https://doi.org/10.1128/AEM.01360-06.

Supplementary Materials

Table S1
Average acetic acid concentrations (mmol·L⁻¹) in the extracellular broth during steady-state of chemostat cultivation of the three strains at 12°C, 30°C, and 39°C. Standard errors were obtained from four measurements at different time points during the steady-states.

	12°C	30°C	39°C
ADY5	0.00 ± 0.00	0.00 ± 0.00	1.06 ± 0.10
CEN.PK113-7D	2.84 ± 0.10	0.52 ± 0.04	0.54 ± 0.09
Ethanol Red	1.16 ± 0.03	0.67 ± 0.12	1.19 ± 0.03

Table S2
Average cellular nitrogen contents (g total N·g$_{DW}$⁻¹) of the three strains during anaerobic steady state chemostat cultivation at 12°C, 30°C, and 39°C. Standard errors were obtained from four measurements at different time points during the steady-states.

	12°C	30°C	39°C
ADY5	0.060 ± 0.004	0.046 ± 0.004	0.044 ± 0.002
CEN.PK113-7D	0.054 ± 0.003	0.051 ± 0.002	0.044 ± 0.003
Ethanol Red	0.061 ± 0.005	0.067 ± 0.001	0.046 ± 0.001

Appendix

Determination of the ethanol
evaporation constant in a 7-litres
bio-reactor at different operation
temperatures

The off-gas from the fermentor is passed through a condenser to minimize the evaporation of water and ethanol. The efficiency of the condenser was, however, is not expected to be 100%, especially at the highest cultivation temperature (39°C), and thus needs to be verified. If significant, the evaporation of the cultural broth and ethanol from the cultural broth should be taken into account for a proper calculation of the ethanol production rate. In order to verify the efficiency of the condenser at various cultivation temperatures, batch experiments with synthetic broth, containing a known initial ethanol concentration, were carried out at three different cultivation temperatures (12°C, 30°C, and 39°C) and a constant nitrogen gassing rate.

The decrease of the total broth mass in the reactor and the total ethanol content of the broth follows from their respective mass and mole balances:

equation A1

$$\frac{d(M)}{dt} = M * (-k_{broth})$$

equation A2

$$\frac{d(M * C_{eth})}{dt} = M * (-k_{eth}) * C_{eth}$$

Herein M is the mass of broth with a unit of kg, and k_{broth} is the broth evaporation constant with a unit of $g_{waterevaporated}$ / ($k_{gbroth\ in\ bioreactor}$·h).

C_{eth} is the concentration of ethanol in broth which has a unit of mmol·kg^{-1}, and k_{eth} is the ethanol evaporation constant with a unit of mmol$_{ethanol\ evaporated}$ / (mol$_{ethanol\ in\ broth\ in\ bioreactor}$·h).

These two differential equations can be solved to give the ethanol concentration as a function of time:

equation A3

$$C_{eth}(t) = C_{eth}(0)e^{(-k_{broth} - k_{eth})*t}$$

The broth mass as a function of time is obtained by the integration of eq.A1:

$$M(t) = M(0)e^{-k_{broth}*t}$$

The k_{broth} at different temperatures were determined by plotting the synthetic broth mass as a function of time, which is expected to follow an exponential profile (equation A4). From eq. A3, the exponential function of the ethanol concentration in the synthetic broth with time is dependent on two evaporation constants, which are k_{broth} and k_{eth}.

Methods and Materials

Batch fermentation

Batch experiments were performed in a 7L fermenter (Applikon, Schiedam, the Netherlands) with 4L synthetic broth containing 5.0 g·L^{-1} (NH$_4$)SO$_4$, 3.0 g·L^{-1} KH$_2$PO$_4$, 0.5 g·L^{-1} MgSO$_4$·7H$_2$O, 0.27 g·L^{-1} antifoam (Antifoam C, Sigma Aldrich, Saint Louis, USA), 18.43 g·L^{-1} ethanol, and 0.42 g·L^{-1} Tween 80. The pH of the synthetic broth was set at pH 5 by the addition of 2.0M potassium hydroxide or 2.0M sulfuric acid. The batch experiments were performed at 12°C, 30°C, and 39°C. The temperature of the synthetic broth in the bioreactor was measured continuously by a temperature sensor and was maintained by the water bath jacket of the bioreactor at which the temperature was regulated by a thermocirculator (Biostat B plus). Nitrogen gas (1L·min^{-1}) was continuously sparged in the fermenter to maintain fully anaerobic conditions. The batch fermentations were performed at a stirrer speed of 450 *rpm*. The weight of synthetic broth was continuously measured by a load cell which was placed underneath the bioreactor.

Analytical method

The ethanol concentration of the synthetic broth in the samples was analysed using high performance liquid chromatography (HPLC) with a proton exchange column at 60°C (Bio-Rad HPX-87H 300*7.8mm). The mobile phase of the column employed 1.5 mM phosphoric acid in Milli-Q water at 70°C. The quantification of the analysis was performed by UV detection (Waters 2489; 210 mM).

Results

Each batch experiment was carried out for 14 days, and samples of the synthetic broth were taken from the bioreactor twice a day at which the amount of the broth withdrawn was measured by a weight balance. The broth mass in the bioreactor was recorded continuously online and was compensated with the sample volume. The ethanol concentration in the broth sample was measured by HPLC. The total broth evaporation constants

at different temperatures were determined by plotting the exponential relations of the synthetic broth mass as a function of time (equation A4, Figure S1). The ethanol evaporation constants for different temperatures were obtained through fitting the exponential function given by equation A3 (Figure S 2). The values of the parameters were estimated by minimizing the weighted sum of the squared errors. The obtained evaporation constants are summarized in Table S3.

Temperatures °C	k_{broth} $\dfrac{g_{broth\ evaporated}}{(kg_{broth\ in\ bioreactor} \cdot h)}$	k_{eth} $\dfrac{mmol_{ethanol\ evaporated}}{(mol_{ethanol\ in\ broth\ in\ bioreactor} \cdot h)}$	p-value
12	-0.075 ± 0.009	-1.62 ± 0.20	0.260
30	-0.332 ± 0.010	-4.44 ± 0.31	0.228
39	-0.359 ± 0.013	-7.71 ± 0.22	0.293

Table S3
First order evaporation constants for broth (water + ethanol) and ethanol determined from measured broth and ethanol disappearance of an ethanol water mixture during fermentation conditions at 12˚C, 30˚C, and 39˚C.

Broth Mass

R² = 0.8923
R² = 0.9934
R² = 0.9801

Weight (kg)
Time (h)

12℃
30℃
39℃
Expon. (12℃)
Expon. (30℃)
Expon. (39℃)
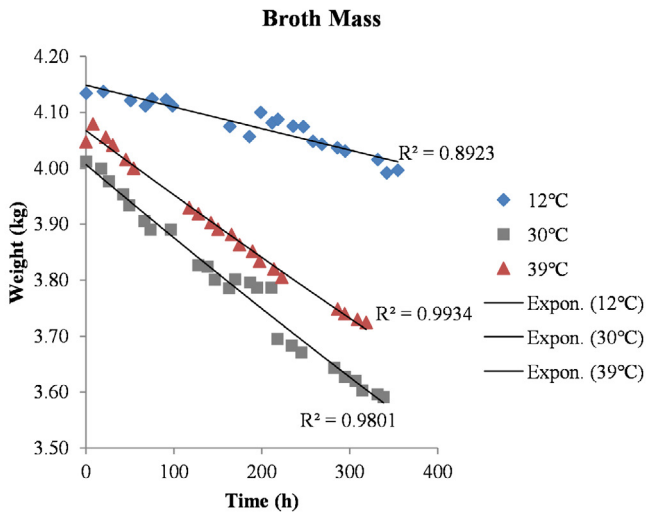
Figure S 1
Synthetic mass in batch at 12°C, 30°C, and 39°C.

Figure S 2
Ethanol concentration
in synthetic broth at
12°C, 30°C, and 39°C
batches.

Ethanol Concentration in Broth
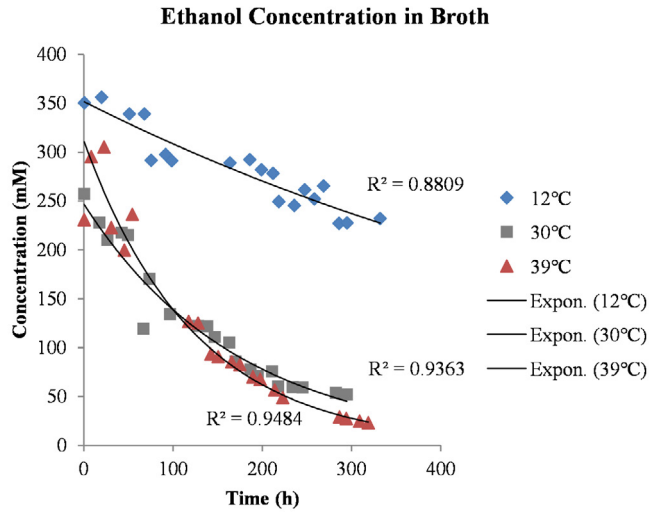
Nomenclature

t Time [hours]

M Weight of broth mass [kg]

C_{eth} Ethanol concentration in synthetic broth [mM]

k_{broth} Total broth evaporation [$g_{waterevaporated}$ / ($k_{gbroth\ in\ bioreactor}$·h)]

k_{eth} Ethanol evaporation constant
[$mmol_{ethanol\ evaporated}$ / ($mol_{ethanol\ in\ broth\ in\ bioreactor}$·h)]

Chapter 3

Differential proteomic analysis by SWATH-MS unravels the most dominant mechanisms underlying yeast adaptation to non-optimal temperatures under anaerobic conditions

Elucidation of temperature tolerance mechanisms in yeast is essential for enhancing cellular robustness of strains, providing more economically and sustainable processes. We investigated the differential responses of three distinct *Saccharomyces* cerevisiae strains, an industrial wine strain, ADY5, a laboratory strain, CEN.PK113-7D and an industrial bioethanol strain, Ethanol Red, grown at sub- and supra-optimal temperatures under chemostat conditions. We employed anaerobic conditions, mimicking the industrial processes. The proteomic profile of these strains was performed by SWATH-MS, allowing the quantification of 997 proteins, data available via ProteomeXchange (PXD016567). Our analysis demonstrated that temperature responses differ between the strains; however, we also found some common responsive proteins, revealing that the response to temperature involves general stress and specific mechanisms. Overall, sub-optimal temperature conditions involved a higher remodeling of the proteome. The proteomic data evidenced that the cold response involves strong repression of translation-related proteins as well as induction of amino acid metabolism, together with components related to protein folding and degradation while, the high temperature response mainly recruits amino acid metabolism. Our study provides a global and thorough insight into how growth temperature affects the yeast proteome, which can be a step forward in the comprehension and improvement of yeast thermotolerance.

1
Introduction

The yeast *Saccharomyces* cerevisiae is used as a microbial cell factory in a wide range of industrial applications, from the production of beer, wine, cider and bread to biofuels and pharmaceuticals [1]. However, these industrial processes impose severe stresses that impact the efficiency of this cell factory. Among these factors, temperature is one of the most relevant variables, with a direct influence on yeast growth and fermentation performance, representing a major economic concern in the biotechnology industry. In fact, the industry spends large amounts of energy in heating or cooling and, in many cases, the optimum growth temperature is sacrificed [2]. Hence, a significant cost reduction and productivity increase would be achieved in fermentations with better-adapted yeast to ferment at non-optimal temperatures. For these reasons, there is a clear interest in identifying the mechanisms that underlie yeast adaptation at high and low temperatures, as this would make it possible to improve or engineer yeast strains with enhanced robustness.

In past years, some attempts have been made to elucidate the thermal response of *S. cerevisiae* [3–11]. Much of the current knowledge has been derived from studies on the effects of abrupt temperature shocks rather than prolonged thermal stress. However, the magnitude of the stress response is highly influenced by the rate of change of environmental conditions, which is why it is crucial to distinguish between transient stress responses and stress adaptation [12]. Studies on transient stress responses are typically conducted in batch cultures, whereby stress in the form of a shock is applied, so that cells are more prone to triggering fast and highly dynamic stress response phenomena [13]. This type of studies is carried out in continuous culture experiments, such as chemostats, and has the advantage of discriminating the effects of the growth rate and the applied stressor [14]. Moreover,

most of these approaches have used genome-wide transcriptomic data [3,7,9,15]. An inspection of the transcriptome provides accurate identification of the genes which are active in cells. Nevertheless, strong gene expression and high mRNA levels, does not necessarily mean that the corresponding protein is also abundant or indeed active in the cell. Although proteomic analysis techniques are not as straightforward as those used in transcriptomics, they offer the advantage of studying proteins, which represent the actual functional molecules in the cell [16]. To our knowledge, there are only two proteomic studies that examine the tolerance mechanisms of yeast grown at high temperature [4,5], and one at low temperature [17]. However, only the study performed by García-Ríos et al. (2016) was conducted under adapted stress conditions such as chemostats [17].

Yeast thermotolerance is recognized to be a complicated quantitative trait. In addition, the heterogeneity among *S. cerevisiae* strains is significant, with laboratory strains presenting lower thermotolerance than robust industrial and natural yeast strains [18,19]. Still, studies are generally focused on only one background strain, which is not enough to elucidate the intricate mechanism of thermotolerance.

The goal of the present study is to make significant advances in our understanding of yeast response to sub- and supra-optimal temperatures. To this end, we used SWATH-MS (sequential window acquisition of all theoretical spectra-mass spectrometry), a highly accurate quantification technique, to characterize the proteome remodeling of three phenotypically distinct *S. cerevisiae* strains – Ethanol Red (bioethanol strain), a previously selected high temperature tolerant strain, ADY5 (wine strain) a previously selected low temperature tolerant strain, and CEN.PK113-7D (laboratory reference strain) [20]. To eliminate interference by specific growth rate, the strains were grown at 12°C, 30°C and 39°C, in anaerobic chemostat cultures, at a fixed specific growth rate of 0.03 h^{-1}, enabling an accurate investigation of the impact of temperature. Anaerobic conditions were chosen to mimic the process of industrial fermentation of alcoholic beverages and bioethanol production. Furthermore, it also prevents the possible effect of temperature-dependent oxygen solubility and of temperature dependent distribution of sugar metabolism over respiration and alcoholic fermentation [13]. Using independent culture replicates and stringent statistical

filtering, we defined a robust dataset of 259 differential quantified proteins. Beyond uncovering the most dominant mechanisms underlying temperature adaptation, the use of three strains with different degrees of thermotolerance represents a comprehensive strategy that will allow the identification of key strain-dependent and temperature-dependent physiological differences, providing the necessary knowledge for the further production of tailored thermotolerant yeasts.

2
Methods and materials

The yeast strains used in this work were *S. cerevisiae* ADY5 (Lallemand Inc., Canada), a commercial wine strain, *S. cerevisiae* Ethanol Red® (Fermentis, S.I. Lesaffre, France), a commercial bioethanol strain, and the haploid laboratory strain *S. cerevisiae* CEN.PK113-7D (Fungal Biodiversity Centre, Utrecht, The Netherlands). The ADY5 amd Ethanol Red were selected from a screening involving 12 industrial strains, as the most tolerant to 12°C and 39°C, respectively [20].

Working stocks were prepared by cultivation in YPD medium, containing per L: 10 g Bacto yeast extract, 20 g Bacto peptone and 20 g D-glucose. After addition of 30 % (v/v) glycerol, culture aliquots were stored in sterilized Eppendorf tubes at -80°C.

Inocula for the chemostat cultivations were grown aerobically at 220 rpm at 30°C in 2 L Erlenmeyer flasks containing 400 mL of filter sterilized medium containing per L: 5 g $(NH_4)_2SO_4$, 3 g KH_2PO_4, 0.5 g $MgSO_4 \cdot 7H_2O$, 15 g glucose.H_2O, 1.0 mL of trace element solution, and 1.0 mL vitamin solution. Trace element and vitamin solutions were prepared as described by Verduyn et al. (1992) [21]. The preculture medium was filter sterilized using a 0.2 μm membrane filter (Supor AcroPak 20, Pall, Port Washington, USA).

The medium for anaerobic chemostat cultivation as well as the preceding batch cultivations contained per L: 5.0 g $(NH_4)_2SO_4$, 3.0 g KH_2PO_4, 0.5 g·$MgSO_4 \cdot 7H_2O$, 22.0 g D-glucose·H_2O, 0.4 g Tween80, 10 mg ergosterol, 0.26 g antifoam C (Sigma-Aldrich, Missouri, USA), 1.0 mL trace element solution, and 1.0 mL vitamin solution. The medium was filter sterilized using a 0.2 μm Sartopore 2 filter unit (Sartorius Stedim, Goettingen, Germany).

2.1
Yeast strains, cultivation media and inoculum preparation

77

2.2
Chemostat cultivations

All chemostat cultivations were carried out at a dilution rate of 0.030 ± 0.002 h^{-1} in 7 L bioreactors (Applikon, Delft, The Netherlands) equipped with a DCU3 control system and MFCS data acquisition and control software (Sartorius Stedim Biotech, Goettingen, Germany).

The reactor vessels were equipped with norprene tubing, to minimize the diffusion of oxygen into the vessels, and were sterilized by autoclaving at 121°C.

During chemostat operation, the sterile feed medium was pumped into the reactor vessel at a constant flowrate using a peristaltic pump (Masterflex, Barrington, USA), such that the outflow rate of the culture broth was 120 ± 1 $g \cdot h^{-1}$. The broth mass in the reactor was maintained at 4.00 ± 0.05 kg, by discontinuous removal of culture into a sterile effluent vessel, via a pneumatically operated valve in the bottom of the reactor and a peristaltic pump, which were operated by weight control. Therefore, the complete reactor was placed on a load cell (Mettler Toledo, Tiel, The Netherlands). Also, the effluent vessel was placed on a load cell of which the signal was continuously logged for accurate determination of the dilution rate of the chemostat and manual adjustment of the medium feed rate if needed.

The cultivations were carried out at temperatures of either 12.0 ± 0.1°C, 30.0 ± 0.1°C or 39.0 ± 0.1°C, by pumping cooled or heated water through the stainless-steel jacket surrounding the bottom part of the reactor vessel, using a cryothermostat (Lauda RE630, Lauda-Königshofen, Germany). The water temperature of the cryothermostat was controlled by using the signal of a Pt 100 temperature sensor inside the reactor, for accurate measurement and control of the cultivation temperature. Anaerobic conditions were maintained by continuously gassing of the reactor with nitrogen gas at a flowrate of 1 SLM (standard liter per minute) using a mass flow controller (Brooks, Hatfield, USA). Also, the feed medium was kept anaerobic by sparging with nitrogen gas. The nitrogen gas was sterilized by passing through sterile hydrophobic plate filters with a pore size of 0.2 μm (Millex, Millipore, Billerica, USA). The culture broth in the reactor was mixed using one 6-bladed Rushton turbine (diameter 80 mm) operated at a rotation speed of 450 rpm. The pH was controlled at 5.00 ± 0.05 by automatic titration with 4M KOH. The bioreactor was inoculated with 400 mL of pre-culture and

subsequently operated in batch-mode, allowing the cells to grow at the same temperature as the chemostat culture and to achieve enough biomass at the start of the chemostat phase. The exhaust gas from the chemostat was passed through a condenser kept at 4°C and then through a Perma Pure Dryer (Inacom Instruments, Overberg, The Netherlands) to remove all water vapor and subsequently entered a Rosemount NGA 2000 gas analyser (Minnesota, USA) for measurement of the CO_2 concentration. When the CO_2 level of the exhaust gas during the batch cultivation dropped significantly, close to the level after the pre-culture inoculation, this indicated the end of the batch phase. Thereafter the culture was switched to chemostat mode. Sampling was carried out during steady state conditions, after stable values of the CO_2 level in the exhaust gas and the biomass dry weight concentration were obtained. Triplicate samples were taken from each chemostat cultivation approximately every 48 h during the steady state for measurement of cell dry weight and proteomics analysis. The steady-state of the chemostat cultures was confirmed by the stable CO_2 offgas profile and steady dry-weight measurements [20].

Biomass dry weight was determined by filtration of 5 g of chemostat broth over pre-dried nitrocellulose filters (0.45 μm pore size, Gelman laboratory, Ann Arbor, USA), which were wetted with 1 mL demineralized water before filtration. After filtration of the broth, 10 mL of demineralized water was used to wash the cells on the filters, which were subsequently dried in an oven at 70°C for two days. Before weighing, the filters were allowed to cool down in a desiccator for two hours.

For proteomics analysis 3 x 10 g of chemostat broth was immediately cooled down to around 4°C after sampling by pouring into a tube containing cold steel beads. After cold centrifugation the cell pellets were snap frozen in liquid nitrogen and stored at -80°C until analysis.

2.3
Protein extraction and digestion

Cell pellets were then resuspended in 500 μL of UTC lysis buffer, containing 8 M urea, 2 M thiourea and 4% 3-[(3- cholamidopropyl) dimethylammonio]-1-propanesulfonate, (CHAPS), followed by vigorous stirring at 5°C during 1 h. After, the samples were treated with 10 % (final concentration) of trichloroacetic acid (TCA) and incubated at 4°C overnight. Protein extracts from total cell were clarified by centrifugation at 15000g during 10 min and precipitated according to the TCA/Acetone protocol. Briefly, the treated samples were diluted (equal volume of the initial sample) in cold acetone solution, stirred and stored at 4°C during 10 min. Then, the samples were subjected to centrifugation 15000g for 15min and the supernatants were discarded. The total of the precipitated proteins was taken for one dimensional sodium dodecyl sulfate-polyacrylamide gel electrophoresis (1D SDS-PAGE). The samples were loaded but not resolved.

The protein samples were digested with 500 ng of sequencing grade trypsin (V511, Promega Co., Madison, WI, USA) and incubated at 37°C following the protocol described by Shevchenko et al. [22]. The trypsin digestion was stopped by the addition of 10 % trifuoroacetic (TFA) and the supernatant, containing the non-extracted digests, was removed, leaving behind the sliced gels in the Eppendorf tube, which were dehydrate with pure acetonitrile (ACN). The new peptide solutions were carefully combined with the corresponding supernatant and dried in a speed vacuum. Next, they were re-suspended in 2 % ACN and 0.1 % TFA prior to liquid chromatography and tandem mass spectrometry (LC-MS/MS) analyses. The volume was adjusted according to the intensity of the staining.

2.4
LC-MS/MS analyses

2.4.1
Spectral library building

Liquid chromatography and tandem mass spectrometry (LC–MS/MS): 5 μL of a pool of all the digested samples were loaded into a trap column (Nano LC Column, 3μ C18-CL, 75 μm x 15 cm; Eksigent Technologies, Dublin, CA, USA) and desalted with 0.1% TFA at 3μL/min during 5 min. The peptides were loaded into an analytical column (LC Column, 3 μm particles size C18-CL, 75 μm ×12cm, Nikkyo Technos Co®, Tokyo, Japan), equilibrated in 5 % ACN and 0.1 % formic acid (FA). The peptide elution was carried out with a linear gradient of 5 % to 35 % buffer B (B: ACN, 0.1 % FA) in A (A: 0.1 % FA) at a constant flow rate of 300 nL/min over 240 min. The eluted peptides were analysed in a mass spectrometer nanoESI-qQTOF (5600 TripleTOF, AB SCIEX). The TripleTOF was operated in information-dependent

acquisition mode, in which a 250-ms TOF MS scan from 350–1250 m/z, was performed, followed by 150-ms product ion scans from 350–1500 m/z on the 25 most intense 2-5 charged ions. The rolling collision energies equations were set for all ions as for 2+ ions according to the equation |CE|=(slope) × (m/z) + (intercept), with Slope = 0.0575 and Intercept = 9.

The digested peptides recovered were examined by LC using a NanoLC Ultra 1-D plus Eksigent (Eksigent Technologies, Dublin, CA, USA) connected to a TripleTOF 5600 mass spectrometer (AB SCIEX, Framingham, MA, USA). Briefly, 5 μL of each digested sample were loaded onto a trap Nano LC pre-column (3 μm particles size C18-CL, 0.5 mm × 300 μm, Eksigent Technologies) and desalted with 0.1 % TFA at 3μL/min during 5 min. Then, the digested peptides present in the samples were separated using an analytical column (LC Column, 3 μm particles size C18-CL, 75 μm ×12cm, Nikkyo Technos Co®, Tokyo, Japan), equilibrated in 5 % ACN and 0.1 % FA. The peptide elution was carried out with a linear gradient of 5% to 35% of ACN containing 0.1% FA at a constant flow rate of 300 nL/min over 90 min. The eluted peptides were thereafter analysed with a spectrometer nanoESI-qQTOF (5600 TripleTOF, AB SCIEX) coupled to the NanoLC sysntem. The TripleTOF was operated in SWATH mode, in which a 0.050s TOF MS scan from 350 to 1250m/z was performed, followed by 0.080s product ion scans from 350 to 1250 m/z in the 32 defined windows (3.05 sec/cycle). The rolling collision energies equations were set for all ions as for 2+ ions according to the equation |CE|=(slope) × (m/z) + (intercept), with Charge = 2; Slope = 0.0575 and Intercept = 9.

2.4.2
SWATH
acquisition

For spectral library building after LC-MS/MS analysis, the generated 5600 TripleTof.wiff data-files were processed using ProteinPilot search engine (version 5.0, AB SCIEX). The Paragon algorithm of ProteinPilot [23] was used to search against the Uniprot database (SwissProt-032018.fasta, 556819 proteins in database) with the following parameters: trypsin specificity, cys-alkylation (IAM), no taxonomy restricted, and the search effort set to through and FDR correction for proteins. The proteins identified were grouped through the Protein-Pilot Pro ™ group algorithm exclusively from observed peptides and based on MS / MS spectra. Then, unobserved regions of protein sequence play no role for explaining the data.

2.5
Protein
identification
and
quantification

The resulting Protein-Pilot group file was used by PeakView® (version 2.1, AB SCIEX) to quantify proteins, by chromatographic area, in SWATH runs. For every protein, in the spectral library a maximum of 50 peptides were quantified among those with a confidence threshold of 95 % and a false discovery rate (FDR) lower than 1 %. Shared peptides were also excluded.

For every peptide a maximum of 6 transitions (fragment ions) were quantified. The peptide retention times were normalized among samples using high confident peptides of main proteins.

2.6
Statistical
analysis

The identified and quantified peak intensities of all the conditions (temperature and strains) were first transformed by the logarithm with base 2. Further, in order to filter the most differentiable proteins, an elastic-net penalized logistic regression (ENLR) model was performed to obtain the estimation of the coefficients. We use the glmnet package of R software to adjust the regression model [24] and with the train function of the caret package to obtain a possible value for α and λ. The train function of the caret package was used to obtain the values for parameters needed for the regression model with Elastic net penalty. Train function sets up a grid of adjustment parameters for a number of classification and regression routines, adjusts to each model and calculates an efficiency measurement based on resampling. Within this function, tuneGrid parameter was used with an array of data with possible adjustment values. This matrix has a range of values that goes from the parameters that the glmnet function takes when alpha = 0 to alpha = 1. In this way the train function gives us a possible value for alpha and another for lambda. For each of the comparisons, we have applied a regression model with Elastic Net penalty, so we have had different parameters for each case.

The explanatory capacity of resulting selected proteins was shown using heatmaps after z-score normalization. To validate this methodology, multiple comparisons were performed by applying a False Discovery Rate (FDR). We also performed a PLS-DA classification of the proteins by using the mixOmics packet of R software. VIP function shows the importance of each of the explanatory variables in the projection which allow us to determine which of the variables is more important to predict the response variable. When vip value is greater than 1.5, the influence of the explanatory variable on the response variable is very high. We have checked that the proteins obtained with the

Elastic Net regression model presented vip greater than 1.

Venn diagrams of the proteins with different concentrations at low temperature and high temperature were created using Venny online software (Venny, http://bioinfogp.cnb.csic.es/tools/venny/index.html), to select the common proteins from among the analyses. Principal component analysis (PCA) was performed using StatSoft, Inc. (2004) STATISTICA, version 7.0 (www.statsoft.com).

To explore whether certain biological processes are enriched among the proteins that were found significantly changed with the temperature, a gene enrichment analysis was manually performed using the comprehensive bioinformatics tool for functional annotation Swiss-Prot/TrEMBL (http://www.uniprot.org/uniprot) and evolutionary genealogy of genes: NOGs (http://eggnog.embl.de) databases.

2.7
Functional annotation and enrichment analysis

83

3
Results and Discussion

*3.1
Overview of
quantitative
proteomic
analysis*

Our study presents the first proteomic characterization of three *Saccharomyces* strains grown at optimal temperature (i.e., 30°C) versus low (i.e., 12°C) and high temperature (i.e., 39°C). This strategy allowed us to assess both the extent of the changes in protein expression levels in response to temperature and the degree of variance in the proteome expression profiles in yeasts from different ecological niches.

Quantitative proteomic data were obtained using the SWATH mass spectrometry (SWATH-MS) technology and resulted in the quantification of 997 unique proteins for all the samples, that is, the three strains cultivated at three temperatures with three biological replicates for each condition (27 samples in total). The full set of protein quantification data is provided in supplemental Table S1. To uncover the proteins significantly associated with temperature response, we employed elastic net regression analysis [25], which is a method that allows the selection of highly correlated groups of variables. From the 997 proteins detected, the elastic net was able to significantly reduce the dataset in all the conditions, as can be seen in Table 1. Only these 259 selected proteins were considered in the following analysis.

To obtain an overview of the proteomic variability between the three strains, a Principal Component Analysis (PCA) was carried out (Figure 1).

The PCA score plot of the first three principal components accounted for 64.8 % of the total variance. The use of these components in a 2D representation mainly allowed the effective separation of the samples based on the strain and growth temperature. The first principal component (PC1) captured the largest variance of the data (31.7 %) and evidenced inter-strain differences, with a clear differentiation of the laboratory

strain CEN.PK from the two industrial strains under study. The second PCA axis (PC2) accounted for 19.9 % of the total variance and clearly separated the strains according to the growth temperature. Thus, our preliminary proteome comparisons reveal that there are substantial differences at the molecular level in how the three strains respond to temperature changes and that the response to high and low temperature is quite distinct. Still, the third component (PC3) suggest that there are some general mechanisms of temperature response in each yeast strain, which probably corresponds to general stress response proteins.
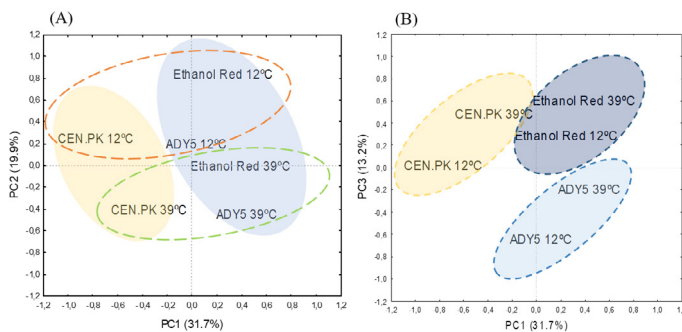
Figure 1
Principal component analysis (PCA) score plot from fold-change values of the differential expressed proteins in Ethanol Red, ADY5 and CEN.PK at 12°C and 39°C. (A) PCA Loadings of the second and first principal components (PC1 vs PC2); (B) PCA Loadings of the third and first principal components (PC1 vs PC3). The explained variances are shown in brackets. To make clear the hidden patterns in the data set, the different groups discriminated by each of the components (PC1, PC2 and PC3) were highlighted using coloured elllipses and dashed lines.

The ability to adapt to non-optimal temperatures is potentially accompanied by changes in protein expression. To examine these changes, we evaluated the differentially expressed proteins of CEN.PK, Ethanol Red and ADY5 at 12°C and 39°C, compared to the respective control temperature (30°C). Gene ontology analysis was performed to determine the main functional categories arising from the up- and down- regulated proteins. A total of 19 enriched GO terms (Table 1) were identified revealing the complexity of the cell's response to temperature changes. A significant amount of proteins with unknown function were also identified.

The distribution of the differentially regulated proteins in functional categories differed considerably between the two temperature conditions. In fact, in all strains the number of differentially expressed proteins during cultivation at low temperature was much higher than at high temperature, indicating greater remodeling of the proteome. More specifically, in the ADY5 strain, the number of differentially regulated proteins at 12°C was 85, whereas at 39°C was 54; in the case of

85

3.2
Biological mechanisms that govern cellular response to sub- and supra-physiological temperatures

Ethanol Red, we identified 54 proteins at low temperature and 37 at high temperature; in CEN.PK, the discrepancy was even higher, with 104 differentially regulated proteins at low temperature, and only 24 at high temperature.

Table 1
Functional classification of differentially regulated protein expressed in ADY5, CEN.PK and Ethanol Red at 12°C and 39°C.

Functional category	12°C						39°C					
	A-D[a]	A-U[a]	C-D[a]	C-U[a]	E-D[a]	E-U[a]	A-D[a]	A-U[a]	C-D[a]	C-U[a]	E-D[a]	E-U[a]
Protein folding and degradation	6	10	4	8	4	2	2	14	2	4	1	5
Amino acid metabolism	2	3	1	8	2	9	5	2	4	1	4	2
Coenzyme metabolism	2	0	1	2	1	0	0	0	1	0	0	0
Inorganic ion metabolism	2	0	0	2	0	0	0	0	1	0	0	0
Signal transduction	1	0	1	0	1	0	0	0	1	0	0	1
Energy metabolism	2	5	1	7	0	5	2	0	1	0	0	1
Translation	12	1	17	2	5	0	0	3	0	4	0	4
Intracellular trafficking, secretion, and vesicular transport	2	1	0	2	0	0	0	2	0	1	0	0
Nucleotide metabolism	2	1	2	4	0	1	2	3	0	1	1	4
Carbohydrate metabolism	0	6	2	8	3	3	1	2	0	0	2	1
Cell cycle control, cell division, chromosome partitioning	0	1	0	1	0	0	0	0	0	0	0	0
Transcription	3	0	1	2	1	1	0	2	0	0	0	2
Replication, recombination and repair	2	0	1	1	1	0	0	0	0	0	0	0
Lipid metabolism	0	0	2	1	5	1	0	0	0	0	0	1
Secondary metabolites metabolism	0	0	0	1	0	0	0	0	0	0	0	0
Cytoskeleton	1	0	0	0	0	0	0	1	0	0	0	0
Chromatin structure and dynamics	1	0	0	0	0	0	0	0	0	0	0	0
RNA processing and modification	3	0	0	0	0	0	0	1	0	0	0	1
Cell wall biogenesis	0	0	0	0	2	0	0	0	0	0	0	1
Unknown Function	8	8	2	20	4	3	1	11	1	2	2	3
Total	49	36	35	69	29	25	13	41	11	13	10	27

Scale bar: 1-5   6-10   11-15   16-20

[a] The number of up (U) – or down (D)- regulated proteins in ADY5 (A), CEN.PK (C) and Ethanol Red (E) strains.

Regarding the overall response to high and low temperatures, we found some resemblances because similar functions are induced or repressed under both experimental settings. The most remarkable groups of regulated proteins fell into the translation category, along with protein folding and degradation, and amino acid metabolism. In addition, at 12°C, the transport and metabolism of carbohydrates as well as the production and conversion of energy also seem to be important categories. It is worth mentioning that at 12°C there was a strong downregulation of proteins related to protein synthesis (translation process), particularly in the ADY5 and CEN.PK strains. Furthermore, the low temperature response of these two strains was also characterized by an increase in the levels of several proteins related to folding and degradation processes. The specific role of these functions and respective proteins will be explored in the next sections.

We further compared the proteome profile of the same strain but at different temperatures (12/30°C versus 39/30°C) to evaluate a possible stress-specific response. Regarding CEN.PK the comparison between the two temperature conditions showed that 92 and 12 proteins were uniquely differentially expressed at low and high temperature, respectively, whereby 12 proteins were differentially expressed at both conditions (Figure 2A). The shared proteins are mostly associated with translation, amino acid transport and protein folding and degradation.

3.3
Strain-specific responses to sub- and supra-optimal temperature

87
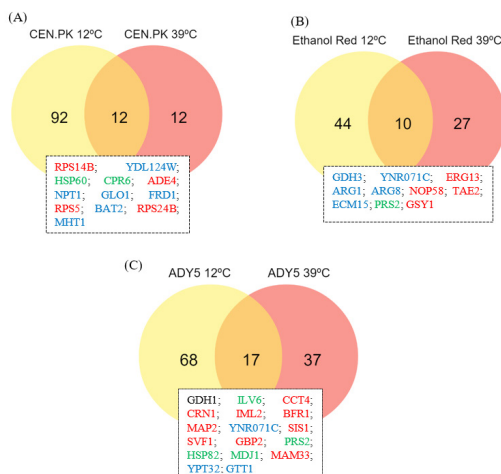
Figure 2
Venn diagram indicating the overlap of differentially expressed proteins between 12°C and 39°C conditions, compared to the respective control temperature (30°C), in CEN.PK (A), Ethanol Red (B) and ADY5 (C). The standard name of the proteins common to both temperature settings are provided in the text boxes. Proteins are coloured according to significant change as follows: red (increased at 39°C and decreased at 12°C), blue (decreased at 39°C and increased at 12°C), green (increased at both temperatures), or black (decreased at both temperatures).

(A) CEN.PK 12°C   CEN.PK 39°C

92   12   12

RPS14B;   YDL124W;
HSP60;   CPR6;   ADE4;
NPT1;   GLO1;   FRD1;
RPS5;   BAT2;   RPS24B;
MHT1

(B) Ethanol Red 12°C   Ethanol Red 39°C

44   10   27

GDH3;   YNR071C;   ERG13;
ARG1;   ARG8;   NOP58;   TAE2;
ECM15;   PRS2;   GSY1

(C) ADY5 12°C   ADY5 39°C

68   17   37

GDH1;   ILV6;   CCT4;
CRN1;   IML2;   BFR1;
MAP2;   YNR071C;   SIS1;
SVF1;   GBP2;   PRS2;
HSP82;   MDJ1;   MAM3;
YPT32;   GTT1

In the case of Ethanol Red, it was observed that of the 81 identified proteins, 44 were unique to the cold response, 27 were unique to the heat response, and 10 were common to both (Figure 2B). Among the group of common proteins, we found proteins that have widespread functions in amino acid metabolism, carbohydrate metabolism, lipid metabolism, transcription, nucleotide metabolism and cell wall biogenesis.

In the ADY5 experiments we detected a similar behavior, with 17 proteins being involved in both high and low temperature response (Figure 2C). This group comprises proteins involved in several cellular functions such as amino acid metabolism (Gdh1, Ilv6), protein folding and degradation (Cct4, Sis1, Hsp82, Mdj1, Gtt1), RNA processing and modification (Svf1), translation (Map2), carbohydrate metabolism (Ynr071c), nucleotide metabolism (Prs2) and proteins with unknown functions (Crn1, Iml2, Bfr1, Gbp2, Mam33, Ypt32).

It should be noted that the proteins identified as common between low and high temperature response in most cases displayed opposite trends, which means that the proteins induced at 12°C were repressed at 39°C and vice versa. In a previous study on the molecular response to temperature, Strassburg et al. (2010) noticed that high and low temperatures cause distinct changes at both the metabolic and the transcript level [3]. They proposed that the yeast's response to temperature involves two phases. First, there is the general stress response, which, through the perception of a stress-induced signal, allows the system to cope with cell damage and death; and second, there are specific adaptive responses to prolonged high and low temperature stress. Comparing the profile of some genes obtained at heat and cold conditions, they observed an opposite trend of regulation, in agreement with our results. Notwithstanding, a minor group of proteins was found to be induced or repressed in both temperature regimes. Specifically, for CEN.PK, Hsp60 and Cpr6 are upregulated at 12°C and 39°C, compare to the control temperature. These results evidenced that, in this strain, non-optimal temperature conditions impair protein folding processes.

In relation to Ethanol Red, of the proteins described above, Prs2 was the only one that presented the same regulation patterns in the two temperature regimes. Prs2 is a member of the ribose-phosphate pyrophosphokinase family and is required

for nucleotide, histidine and tryptophan synthesis. The ability to synthetize tryptophan is vital for yeast survival under several environmental stresses. Previous studies have reported that tryptophan uptake at low temperature is a rate-limiting step for *S. cerevisiae* growth. Low temperature increases the rigidity of the plasma membrane, which results in the slower lateral diffusion of membrane proteins, less active membrane-associated enzymes, and a major reduction in membrane transport [26]. Sensitivity of tryptophan uptake at low temperature has been related to a dramatic conformational change in Tat2p [27]. Disorders that affect the stability of the membrane have strong auxotrophic requirements for tryptophan [28,29]. It has been proposed that tryptophan itself provides protection against membrane interruptions. Besides these cell wall/membrane related stresses, it has also been described that tryptophan levels can influence growth recovery after DNA damage [29]. We then speculate that the overexpression of Prs2, in Ethanol Red strain, is mainly related to the requirement of tryptophan and the maintenance of a robust cell membrane to endure thermal stress.

Finally, in the ADY5 experiment, the set of proteins with an identical regulation pattern includes the Hsp82, Mdj1, Ilv6 and Prs2, whose levels were increased, and Gdh1 whose level was diminished. Hsp82 is one of the most highly preserved and synthesized heat shock proteins of eukaryotic cells; while Mdj1 is a mitochondrial Hsp40 involved in many key functions including folding of nascent peptides and cooperation with mt-Hsp70 in mediating the degradation of misfolded proteins [30]. Hsp82 and Mdj1 proteins have a well-known role in heat-response, and their increment has been reported previously by Shui et al. 2015 [4]. On the other hand, nothing is known about the role of these two proteins in the cold-response. Furthermore, the presence of two proteins involved in amino-acid metabolism (Ilv6 and Gdh1), in the set of proteins with an identical regulation at sub- and supra-optimal temperatures, was also detected. The first enzyme is an acetolactate synthase, which catalyzes the first step of branched-chain amino acid biosynthesis; and the second is a glutamate dehydrogenase, which participates in the synthesis of glutamate from ammonia and alpha-ketoglutarate [31]. The branched-chain amino acids, such as isoleucine, have already been related to temperature response. Indeed, it has been demonstrated for *Bacillus subtilis* that isoleucine-deficient strains show a cold-sensitive phenotype [31]. In addition, isoleucine has

been described as part of a set of amino acids typically abundant in thermophilic organisms, contributing to a high thermal stability of proteins [32]. Likewise, Mara and co-authors observed that overexpression of Gdh1 had detrimental effects on yeast growth at 15°C [33]. The GDH pathway is involved in the recycling of NADH-NAD by controlling the levels of α-ketoglutarate. The downregulation of Gdh1 may be a strategy to assure NADH-NAD homeostasis, which is essential to ensure an appropriate cellular response to environmental changes.

Taken together, these findings suggest that, in addition to a general thermal response, the strains elicit different protein sets in order to respond to each environmental condition - high or low temperature.

3.4 Comparative analysis of differentially expressed proteins at supra-optimal temperature in the three Saccharomyces strains

As in the comparison made of each strain at both temperatures, significant differentially expressed proteins were plotted in a Venn diagram to identify common expression changes in the three strains at 39°C (Figure 3). The 259 proteins were detected in all strains, however there are not always significant differences in the pattern of expression compared to the respective control temperature (30°C). Only cases where there is a significant increase or decrease will be discussed.

Only three proteins were commonly over-represented in the three *Saccharomyces* strains - Hsp60, Cpr6 and Ydj1 - all belonging to the heat shock proteins-family. This result reinforces the view that protein folding is critical for high temperature adaptation and wide-spread among different yeast backgrounds [34].

Figure 3
Venn diagram representing the differentially expressed proteins identified in the three *Saccharomyces* strains cultivated at 39°C, in anaerobic chemostat cultures. Proteins are coloured according to significant change as follows: green (increased in both strains), or black (decreased in both strains).
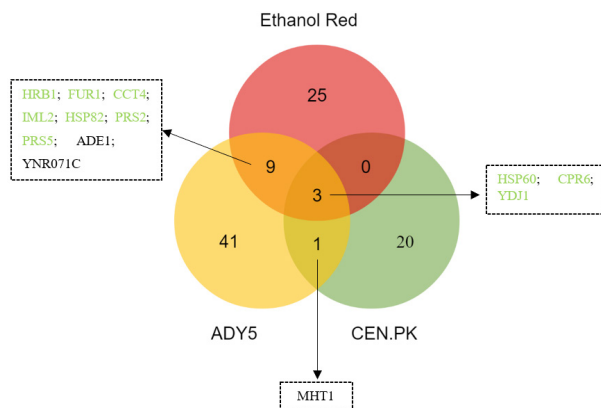
In relation to Ethanol Red/CEN.PK, the disparity between the two strains is evident since they do not share any proteins other than those mentioned above. Likewise, ADY5/CEN.PK only have one common protein (Mht1), downregulated in both strains. This homocysteine S-methyltransferase catalyzes the conversion of S-adenosylmethionine (AdoMet) to methionine, regulating the methionine/AdoMet ratio [35]. The repression of this protein allows to keep the amount of methionine reduced, which is essential since methionine suppresses the synthesis of adenylyl sulfate (APS). APS plays an important role in yeast thermotolerance, increasing tolerance to high temperatures [36].

In contrast, the overlap observed between Ethanol Red and ADY5 was larger, with 9 shared proteins (Figure 3). Most of these proteins are related with nucleotide metabolism. Of particular interest is the downregulation of Ade1 and upregulation of Fur1. These two proteins are involved in distinct pathways of nucleotide biosynthesis: the de novo pathway and the salvage pathway, respectively. The de novo pathway synthesizes nucleotides from amino acids, carbon dioxide and ammonia; whereas the salvage pathway uses preformed nucleosides and nucleobases that are imported or present inside the cell [37]. Our data suggest that at supra-optimal temperatures, nucleotide biosynthesis may shift to use the salvage pathway. The de novo pathway has a high requirement for energy compared to the salvage pathway [38]. As the cell would be in state of low energy and NADH reserves during temperature adaptation, a reduced demand of these resources could be beneficial. Moreover, the overexpression of Prs2 and Prs5 is also expected since they are key enzymes of 5-phosphoribosyl-1-pyrophosphate (PRPP) synthesis – a compound required for the both de novo and salvage synthesis of nucleotides as well as for the synthesis of histidine, tryptophan and NAD [38]. Besides that, both strains show increased expression of proteins related to cellular quality control pathways, namely Hrb1, Cct4 and Iml2 [39–41]. The downregulation of a putative epimerase-1 (Ynr071c) was also a common feature between the industrial strains. However, little is known about this protein.

3.4.1 Detailed analysis of differential proteins at supra-optimal temperature for the Ethanol Red Saccharomyces strain

Ethanol Red is a strain commercially available that has been developed for the industrial ethanol production. Most of the large-scale production of bioethanol is typically carried out at high temperatures (above 35°C) [42]. Thus, of the three *Saccharomyces* strains under study, Ethanol Red is the most accustomed to being exposed to high temperatures for long periods [20]. Given that, we decided to analyse more deeply the proteomic alterations of this strain in response to the high temperature.

Our study uncovered some significant elements of the Ethanol Red response to high temperature (Figure 4). The first component involves proteins from the amino acid metabolism. Indeed, we observed repression of proteins involved in arginine biosynthesis, such as Arg1, Arg5, Arg6 and Arg8, and induction of a protein that catalyze the degradation of arginine - ornithine transaminase (Car2). Interestingly, a similar change was recently reported for the thermotolerant yeast Kluveromyces marxianus grown at 45°C in chemostat culture, and therefore could represent an acquired thermotolerance strategy [43]. The reduction of arginine biosynthesis and the acceleration of the conversion of ornithine to proline - catalyzed by the enzyme Car2 ensures both glutamate conservation and proline production. In fact, proline is the main metabolite of arginine metabolism. Under anaerobic conditions, the degradation of arginine leads to intracellular proline accumulation. This increase in proline has been connected with stress protection, being involved in protein and membrane stabilization, lowering the Tm of DNA and scavenging of reactive oxygen species [44]. Moreover, glutamate and proline are precursor metabolites required for the tricarboxylic acid pathway (TCA). It is worth noting that the TCA has been shown not to function completely as a cycle under oxygen deprivation but to be restricted to an oxidative branch leading to 2-oxoglutarate and a reductive branch leading to oxaloacetate [45,46]. Furthermore, the Ethanol Red also increases the expression of several proteins belonging to the nucleotide metabolism.

This strain also exhibited a modest downregulation of 6-phosphoglucogalactonase (Sol3) enzyme, which is involved in the so-called oxidative phase in the pentose phosphate pathway (ox-PPP). This downregulation at the second step of the pentose phosphate pathway is a key to shifting the glucose metabolism in favor of glycolysis over pentose phosphate pathway. Many of the adaptive responses of yeast to high temperature put a

significant additional energy burden on the cells. The increase in temperature causes an increase in the demand for ATP, which can also exert control over the glycolytic flux [47].

Another notable feature of this strain in relation to the supra-optimal temperature response mechanisms was the overexpression of Erg13 – a protein involved in early ergosterol biosynthesis – and the Gsy1 – a glycogen synthetase. Both proteins were also upregulated at sub-optimal temperature. It has been found that the ability of yeast to tolerate stress is closely related to ergosterol levels. In fact, an increase in the ergosterol content of cell membrane helps to minimize the deleterious effects and maintain a normal membrane permeability [48]. Several studies have reported that the activation of the ergosterol pathways makes yeast cells more resistant/tolerant to a variety of stresses, including low temperature, low-sugar conditions, oxidative stress and ethanol [49,50]. The importance of ergosterol in yeast temperature tolerance has also been demonstrated. It was observed that the compromise of the ergosterol synthesis by mutation in the biosynthesis genes – erg10, erg11, erg19 and erg24 – makes *S. cerevisiae* more sensitive to low temperature [48]. Moreover, Caspeta et al. (2014) also identified Erg3, a desaturase in late biosynthesis of ergosterol, as an efficient target to increase the thermotolerance capacity of yeast [51]. Ergosterol requires molecular oxygen for production and hence it was one of the anaerobic growth factors supplemented to the chemostat medium as it is well known that *S. cerevisiae* has to import sterols under anaerobic conditions [52]. Interestingly, one of the functions attributed to mitochondria under anaerobic conditions is related with sterol uptake [53]. Still, Krantz et al. (2004) also detected upregulation of ERG13 under anaerobic conditions and concluded that this gene is exquisitely sensitive to addition of even trace amounts of oxygen and that the upregulation could be provoked by addition of water only [54].

Regarding the increased expression of Gsy1, glycogen has also been reported to be involved with tolerance toward several stresses, such as heat, osmotic and oxidative stress, entry into stationary phase and starvation[55]. The precise role of glycogen in the yeast response to high temperature remains unknown.

In addition, this industrial strain has increased the expression of proteins involved in different translation stages: Ded81 and Ses1

(elongation) and Sup35 (termination), and of proteins related to rRNA processing components (Nop58 and Rix1), which can be a strategy to make the translation process more efficient.
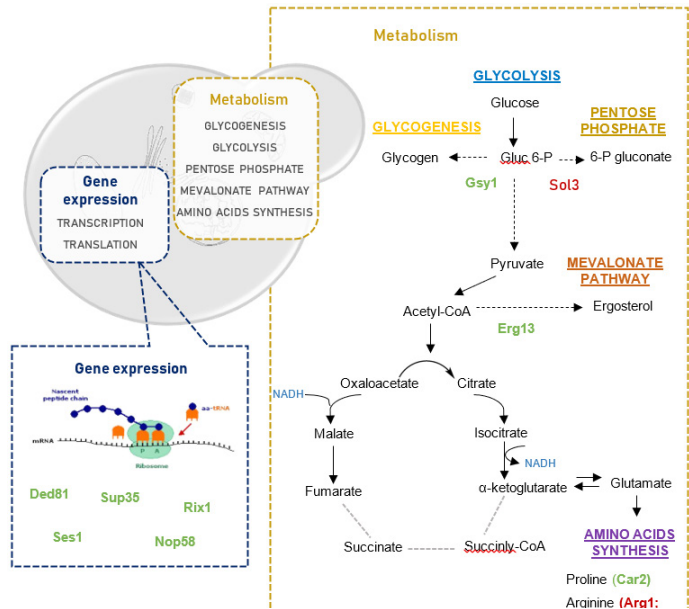
Figure 4

A schematic illustration of the major pathways involved in the unique response of Ethanol Red to supra-optimal growth temperature (39°C). Under anaerobic conditions, the TCA pathway operates as an oxidative branch and a reductive branch. Broken grey lines represent the point at which the cycle may be interrupted. The precise step of interruption in yeast cells is not yet identified. The proteins are highlighted in green (upregulated) or red (downregulated), indicating their enhancement or repression compared to the levels observed at control temperature (30°C). In this figure only the proteins are shown which were significantly altered exclusively in the Ethanol Red strain. Altered proteins common to other strains are not shown.

Likewise, the proteomic response of the three *Saccharomyces* strains grown at low temperature was compared (Figure 5). Contrary to that observed at high temperature, no common proteins were found among the three strains, which seems to suggest that a higher disparity between these strains exists in relation to cold-response. However, when directly comparing one strain to another, the number of common proteins is higher than that observed with high temperature.
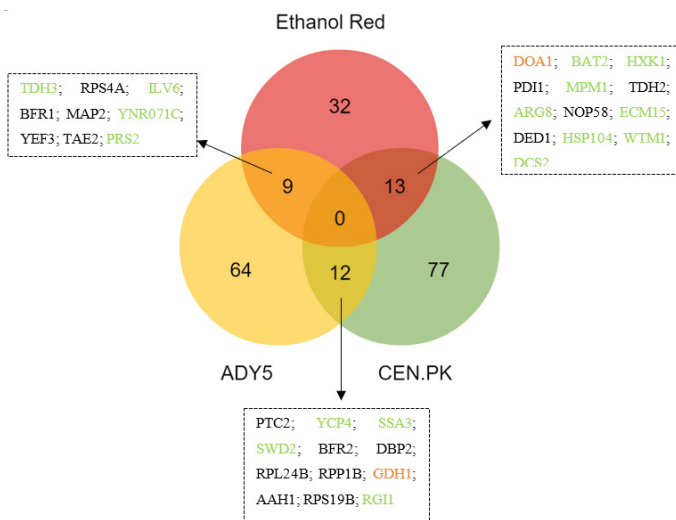
95

CEN.PK and Ethanol Red shared 13 proteins, belonging to different functional categories such as protein folding, amino acid and carbohydrate metabolism, transcription and replication, recombination and repair. Although most of these common proteins showed a consistent up- or- downregulation in both strains, differences in the expression levels were observed. Surprisingly, two of these proteins – Ecm15 and Doa1 – exhibited opposite patterns of expression in the two strains. Ecm15 is a non-essential protein of unknown function and is believed to play a role in the biogenesis of the yeast cell wall; while Doa1 is a protein involved in the ubiquitin recycling process, vacuolar degradation pathway and DNA damage repair [56]. Ubiquitin homeostasis is required for the maintenance and growth of the cell. In the case of DNA damage, ubiquitin should be readily available for post-translational modification of proteins involved in the detection,

3.5.1
Response of CEN.PK versus Ethanol Red

repair and/or tolerance of damage [57]. Therefore, the increased expression of the Doa1 protein in CEN.PK and consequent increase in ubiquitin levels reflects the need for a higher protein turnover, typical of stressed cells. In contrast, the Ethanol Red strain reduces the expression of this ubiquitin protein. Thus, we can interpret that this opposite expression pattern of both strains is related to their different tolerance at low temperatures.

Another key metabolic change common to both laboratory and bioethanol strain lays on carbohydrate metabolism. Both strains increased the expression of hexokinase 1 (Hxk1), which catalyzes the primary step in the glycolytic pathway and reduced the expression of glyceraldehyde-3-phosphate dehydrogenase (Tdh2), which catalyzes the sixth step of glycolysis. Despite being the first step of glycolysis, hexokinase is not the major point of regulation. Glucose 6-phosphate is a branch point between glycolysis, glycogen synthesis and the oxidative arm of the pentose phosphate pathway [58]. The ox-PPP is the main producer of cellular NADPH and is thus critical for the antioxidant defense of cells. It is described that in the presence of oxidants, glucose is channeled towards the ox-PPP through a rearrangement of the carbon distribution. More specifically, the redirection of glycolytic flux through the ox-PPP can be achieved by targeting glycolytic enzymes downstream of Pfk1, such is the case of Tdh2, in which it has already been demonstrated that inhibition leads to a rerouted flux to the PPP, by allowing the accumulation of metabolites upstream of the inhibition point [59].

Both strains increased the expression of the acetylornithine aminotransferase (Arg8) - a protein involved in the synthesis of arginine. This amino acid is known to have a significant cryoprotective activity, increasing freezing tolerance in yeast cells. The mechanisms underlying this protective property of Arg are not yet known, but it is possible that it acts as an ion coating on the surface of membrane components, avoiding denaturation by the NH_2 group in the molecules [60]. Besides, arginine has been shown to reduce cellular oxidative stress, being considered as an effective protectant for proteins, DNA and phospholipids, contributing to maintain intracellular homeostasis [61].

It is also worth mentioning that CEN.PK had a significant increase in Hsp104 protein at 12°C although the fold-change was lower in relation to that observed with Ethanol Red. The Hsp104

is considered one of the most crucial thermotolerance-related protein of *S. cerevisiae*, increasing the chances of survival after exposure to extreme heat or high concentrations of ethanol [62,63]. In addition, Hsp104 induction was also observed during late cold response by Schade and his collaborators [9]. It acts as an ATP dependent chaperone that has the distinct ability to solubilize and refold proteins that are already aggregated, allowing other chaperones to have access to otherwise inaccessible surface of the aggregates [64].

Likewise, a set of twelve proteins, mainly associated with translation related processes, cell cycle control, nucleotide and amino acid metabolism, were found to be commonly changed in CEN.PK and ADY5 in response to the sub-physiological temperature condition.

3.5.2
Response of CEN.PK strain versus ADY5 strain

To go further, we looked more closely at the common proteins and found three aspects of great interest. First, inspection of the regulation pattern of this set of proteins showed that a glutamate dehydrogenase (Gdh1) exhibited significant changes in both strains, but in opposite directions. Low temperature diminished the concentrations in the wine strain but increased it in the laboratory strain. As mentioned earlier, overexpression of this protein may be detrimental at low temperatures due to a NADH–NAD imbalance [33]. However, a downward shift in the growth temperature also induced an oxidative stress response. It is typically assumed that under anaerobic conditions organisms are spared of the toxic effects of oxidative stress; nevertheless, it has been noted that there are other factors besides oxygen that may induce an oxidative stress response. Gibson et al. (2008) detected an increase in transcription of several antioxidant-encoding genes during small-scale fermentation with *S. cerevisiae* in anaerobic conditions [65]. These authors suggested that the response to oxidative stress may have been triggered by a catabolite repression or the influence of other stresses such as ethanol toxicity. Likewise, we observed an increase in the expression of antioxidant proteins implicated in glutathione synthesis. Gdh1 is involved in glutamate synthesis, which is thought to be part of the defense against oxidative stress through the glutathione system, preventing cold-induced reactive oxygen species (ROS) accumulation [33]. This double and apparently contradictory role of Gdh1 in the cold growth of yeast strains has already been observed by Ballester-Tomás et

al. (2015) [66] and emphasizes the complexity of its responses.

The downregulation of the concentration of Bfr2, which is known for its cold-shock response, was also striking. Bfr2 is involved in protein trafficking to the Golgi and previous studies have demonstrated that its mRNA levels increase rapidly over 5-fold in response to cold shock (when the temperature is changed from 30°C to 10°C) [67]. However, this protein may be involved in the recovery from cold shock and the transition back to higher temperatures rather than in survival or adaptation to lower temperatures. This finding underlines that the adaptation to the growth environment and response to shock are distinct mechanisms and straightforward conclusions from one to the other are not always possible.

Another interesting feature is the downregulation of Ptc2 in the CEN.PK strain compared to ADY5, a phosphatase protein known to negatively regulate the high-osmolarity glycerol (HOG) pathway, along with Ptc1 and Ptc3 [68]. The HOG pathway is a preserved MAPK cascade in *S. cerevisiae*, which among other functions, is critical for tolerance to different stresses, such as osmotic, citric acid stress and heat stress [69]. Additionally, Panadero et al. (2005) showed that the HOG pathway is clearly activated in response to a downshift in temperature from 30°C to 12°C, participating in the transmission of the cold signal and on the regulation of the expression of a subset of cold-induced genes [70]. So, the downregulation of Ptc2, which directly dephosphorylates Hog1 MAPK and limits the maximal activation of the HOG pathway [69], may be related to this need to activate this pathway.

3.5.3
Response of
ADY5 strain
versus Ethanol
Red strain

Finally, the comparison of the proteomic profile of the two industrial strains revealed an overlap of 9 proteins, related to the functional categories of carbohydrate metabolism, translation, amino acid and nucleotide metabolism.

One of the most interesting features that has emerged from this comparison is the induction of Prs2. It should be noted that this protein was also identified as significantly altered in the response to supra-optimal temperatures of both strains, Ethanol Red and ADY5 (Figure 3). Therefore, these results suggest that this phosphoribosyl-pyrophosphate synthetase is vital for cellular response to either sub- and supra-physiological temperatures,

being essential for the thermotolerance capacity of these two industrial strains.

Apart from this, we found an enzyme of the lower part of glycolysis, Tdh3, which is one of three isoforms of glyceraldehyde-3-phosphate dehydrogenase protein (GAPDH). However, the yeast response does not seem to be so straightforward. For instance, the Ethanol Red strain increased Tdh3 expression, but reduced Tdh2 expression. Likewise, García-Rios et al. (2014) [11] observed an overexpression of the Tdh3 protein in two wine yeast strains of the genus *Saccharomyces* cultivated at 15°C. The yeast Tdh2 and Tdh3 GAPDH isoenzymes share extensive sequence homology but appear to have distinct roles in regulating glycolytic flux under oxidative stress conditions [71].

The ability to ferment at low temperatures (between 10–15°C) is of paramount importance in the wine industry, since it increases production and retains flavor volatiles, improving the sensory qualities of the wine. As ADY5 strain was previously selected as the best low temperature adapted strain [20] the main responses observed exclusively in this strain at sub-optimal growth temperature were analysed and represented in Figure 6.

99

*3.6
Comprehensive
proteome
analysis of the
wine strain at
sub-optimal
temperature*

The response of ADY5 to suboptimal temperatures was characterized by a downregulation of several translation-related proteins. For instance, several protein components of the 40S and 60S ribosomal subunit were strongly downregulated [72]. Furthermore, we also noticed the downregulation of translation initiation factors, which influence the translation rate. Yeast adaptation to temperature downshift is dependent of the duration and magnitude of the temperature change [7]. Although several studies have shown an increase in translation-related proteins [7,17,73], this only happens in the initial and mid phases of cold adaptation. Sahara et al. (2002) observed that after 8 h of exposure to 10°C, this machinery is significantly downregulated [7]. Similarly, Murata et al. (2005) noticed repression of key genes involved in protein synthesis in yeast cells exposed at 4°C for 6 to 48 hours [10]. Notwithstanding, this strain presents some interesting molecular mechanisms to overcome the stressors and cell modifications caused by low temperature.

It is worth mentioning the previously reported correlation between low temperature robustness and resistance to oxidative

stress in *S. cerevisiae*. Indeed, the fitter strains to fight against oxidative stress were found to display better growth and fermentation performance at low temperature [19]. In the present work, the ADY5 strain increased the expression of a set of proteins belonging to the ROS detoxification systems, including Gtt1 (glutathione transferase), Trx2 (thioredoxin) and Tsa1 (thioredoxin peroxidase). Of these, cytoplasmic thioredoxin 2 is considered one of the most important redox controls together with the glutathione/glutaredoxin system [74]. Considering that these three proteins have only been identified as significantly altered in the ADY5 strain, it can be assumed that they may represent a specific response of the wine strain.

In the category of cell rescue and defense, it is also notable that heat shock proteins are induced, such as Hsp12, Hsp82 and Sse2, which play an equally important role in the response to low temperature in *S. cerevisiae* [75]. Of particular interest was the expression of Hsp12, which has been reported as massively induced in yeast cells under several stress conditions (e.g. heat shock, osmotic stress, oxidative stress or high concentrations of alcohol) [76]. Moreover, Hsp12 is also induced when the cells are exposed to 0°C [77] and 4°C [10]. Hsp12 seems to play a role in cryotolerance of *S. cerevisiae*, presenting similarities with trehalose activity [78]. In fact, Hsp12 acts at the plasma membrane level, protecting it against desiccation and maintaining the integrity of the yeast cells in the freezing stage [75].

In addition, we also found a remarkable proteomic reprograming in proteins implicated in carbohydrate metabolism and energy production. Of particular interest was the upregulation of two alcohol dehydrogenases, involved in the last step of ethanol synthesis – Adh1 and Adh3. This may represent a strategy of *S. cerevisiae* ADY5 to deal with the redox imbalance produced due to the slower kinetics of alcohol dehydrogenases at low temperature [17]. By increasing the concentration of the main alcohol dehydrogenases, Adh1 and Adh3, the strain overcomes the slower conversion of acetaldehyde into ethanol, avoiding the accumulation of NADH and the blockage of glycolytic flux. Besides, it has been reported that cells of *S. cerevisiae* lacking the Adh3 gene have decreased fitness at low temperature, while its overexpression enhanced cold growth [79]. This may be related with the fact that this protein is part of ethanol-acetaldehyde redox shuttle, being involved in the transfer of redox equivalents from

the mitochondria to the cytosol. It is known that low temperatures can compromise the oxidation of mitochondrial NADH, having a strong impact on the intracellular compartmentalization of NAD pools [80]. Therefore, increased expression of proteins like Adh3 may be critical for growth at low temperatures as it helps maintain the optimal balance between the reduced and oxidized forms of nicotinamide adenine dinucleotides.

Furthermore, three proteins from the TCA pathway – Lpd1, Kgd2 and Sdh3 – were also found among the upregulated proteins of this strain. The lipoamide dehydrogenase (Lpd1) is a common component of the multienzyme complexes pyruvate dehydrogenase (PDH), α-ketoglutarate dehydrogenase (OGDH) and glycine decarboxylase (GCV) [81]. Among the several functions of this enzymatic complex, its involvement in one-carbon metabolism is particularly interesting since it is a key pathway that provides single carbon units for the biosynthesis of purines, thymidylates, serine, methionine and N-formylmethionyl tRNA [82], and part of these components are involved in the cold response. Kgd2 proteins is also a component of OGDH; while Sdh3 is a subunit of succinate dehydrogenase complex, which is supposed to be inactive under anaerobic conditions [46]. Binai et al. (2014) also observed an upregulation of this mitochondrial protein under anaerobic calorie restriction conditions [83]. The upregulation of Sdh3 can be related with the dual function of this protein in the respiratory chain and as a translocase of the TIM22 complex, which is responsible for the insertion of large hydrophobic proteins, typically transporters (carrier proteins), into the inner membrane [84]. The involvement of this complex in yeast response to sub-optimal temperatures has been previously reported by the mutation in Tim18p, a component of the TIM22 complex, which caused a cold-sensitive phenotype [85].
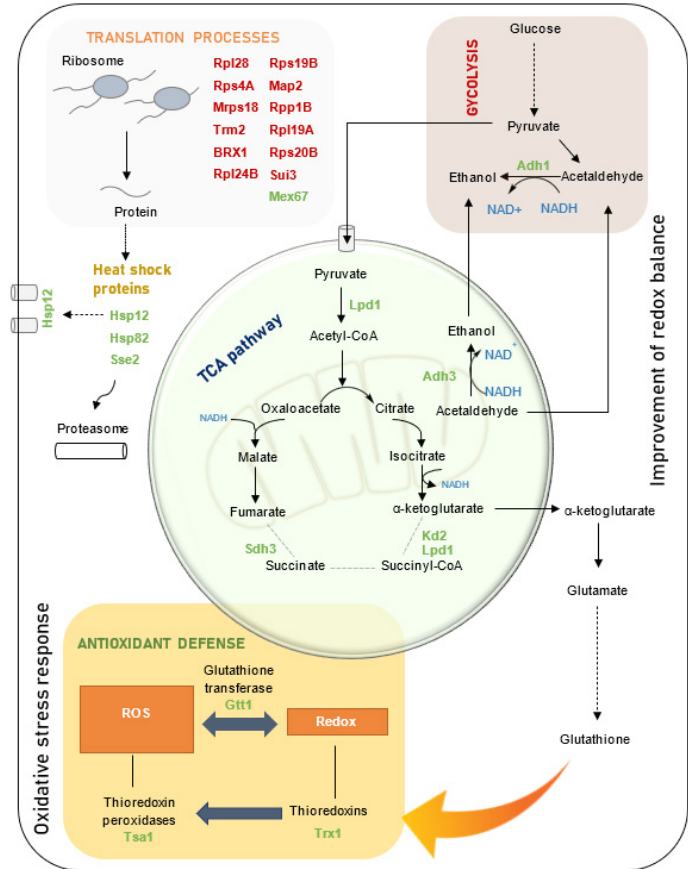
Figure 6

A schematic illustration of the major pathways involved in the unique response of ADY5 to sub-optimal growth temperature (12°C). Under anaerobic conditions, the TCA pathway operates as an oxidative branch and a reductive branch. Broken grey lines represent the point at which the cycle may be interrupted. The precise step of interruption in yeast cells is not yet identified. The proteins are highlighted in green (upregulated) or red (downregulated), indicating their enhancement or repression compared to the levels observed at control temperature (30°C). In this figure are represented only the proteins significantly altered exclusively in ADY5 strain. The proteins common to other strains were not represented.

4
Conclusions

Adaptation and tolerance of yeast strains to temperatures beyond an optimum range is crucial for economic and eco-efficient production processes of new and traditional fermentations.

Our broad approach highlights the complexity of the proteome remodeling associated with growth temperature perturbation, as well the importance of studying different strains to come to meaningful biological conclusions. The variability of responses of the three strains examined shows that no general rules can be assumed for different *S. cerevisiae* strains, and that the temperature-response is highly dependent of their genetic and environmental background. Overall, proteomic data evidenced that the cold response involves a strong repression of translation-related proteins as well as induction of amino acid metabolism, along with components involved in protein folding and degradation. On the other hand, at high-temperature, the amino acid biosynthetic pathways and metabolism represent the main function recruited. Although the changes in the biological processes are, in some cases, similar among strains, differences in the number, type and even in the expression patterns of the proteins were observed and are probably behind the differences in thermotolerance of the strains. Regarding sub-optimal temperature response, the ADY5 strain exhibited a strong activation of antioxidant proteins revealing its importance for low temperature tolerance even under anaerobic conditions. Conversely, at supra-optimal temperatures, Ethanol Red increased the expression of proteins involved in ergosterol and glycogen synthesis, along with Hsp104p, which are known to play a crucial role in heat adaptation.

Our approach and results evidenced the advantages of carrying out a proteomic-wide expression analysis in industrial strains and in an experimental context similar to industrial

conditions since it will be valuable for later application in the productive sector. Thus, this study identifies potential proteins involved in yeast thermotolerance that can be useful for the biotechnological industry either through the selection of proper strains or through the development of yeast strains with improved performance at sub- and supra-optimal temperatures.

Associated content

The mass spectrometry proteomics data have been deposited to the ProteomeXchange Consortium via the PRIDE84 partner repository with the dataset identifier PXD016567.

Supporting Information

Table S1: Summary of differential proteins found in Ethanol Red, ADY5 and CEN.PK113-7D during sub-optimal or supra-optimal growth temperature experiments.

Acknowledgments

Author Contributions

All authors have been involved in the design of the experiments. K.Y.F.L. and W.V.G. run the chemostats and took samples for proteomic analysis. K.Y.F.L. and E.G.R. prepared the samples for protein extraction and digestion. J.T., A.Q. and J.M.G. supervised the proteomic service. T.P. and L.D. analysed the proteomic results and wrote the draft of the paper. All authors read, edited, and approved the final manuscript.

References

[1]   D. Schuller, M. Casal, The use of genetically modified Saccharomyces cerevisiae strains in the wine industry, Applied Microbiology and Biotechnology. 68 (2005) 292–304.

[2]   Q. Deparis, A. Claes, M.R. Foulquié-Moreno, J.M. Thevelein, Engineering tolerance to industrially relevant stress factors in yeast cell factories, FEMS Yeast Research. 17 (2017).

[3]   K. Strassburg, D. Walther, H. Takahashi, S. Kanaya, J. Kopka, Dynamic transcriptional and metabolic responses in yeast adapting to temperature stress, Omics: A Journal of Integrative Biology. 14 (2010) 249–259.

[4]   W. Shui, Y. Xiong, W. Xiao, X. Qi, Y. Zhang, Y. Lin, Y. Guo, Z. Zhang, Q. Wang, Y. Ma, Understanding the Mechanism of Thermotolerance Distinct From Heat Shock Response Through Proteomic Analysis of Industrial Strains of Saccharomyces cerevisiae, 2015. https://doi.org/10.1074/mcp.M114.045781.

[5]   W. Xiao, X. Duan, Y. Lin, Q. Cao, S. Li, Y. Guo, Y. Gan, X. Qi, Y. Zhou, L. Guo, Distinct proteome remodeling of industrial Saccharomyces cerevisiae in response to prolonged thermal stress or transient heat shock, Journal of Proteome Research. 17 (2018) 1812–1825.

[6]   M. Becerra, L.J. Lombardia, M.I. Gonzalez-Siso, E. Rodriguez-Belmonte, N.C. Hauser, M.E. Cerdán, Genome-wide analysis of the yeast transcriptome upon heat and cold shock, International Journal of Genomics. 4 (2003) 366–375.

[7]   T. Sahara, T. Goda, S. Ohgiya, Comprehensive expression analysis of time-dependent genetic responses in yeast cells to low temperature, Journal of Biological Chemistry. 277 (2002) 50015–50021.

[8]   J. Aguilera, F. Randez-Gil, J.A. Prieto, Cold response in Saccharomyces cerevisiae: new functions for old mechanisms, FEMS Microbiology Reviews. 31 (2007) 327–341.

[9]   B. Schade, G. Jansen, M. Whiteway, K.D. Entian, D.Y. Thomas, Cold adaptation in budding yeast, Molecular Biology of the Cell. 15 (2004) 5492–5502.

[10]   Y. Murata, T. Homma, E. Kitagawa, Y. Momose, M.S. Sato, M. Odani, H. Shimizu, M. Hasegawa-Mizusawa, R. Matsumoto, S. Mizukami, Genome-wide expression analysis of yeast response during exposure to 4 C, Extremophiles. 10 (2006) 117–128.

105

References

[11]   E. García-Ríos, M. López-Malo, J.M. Guillamón, Global phenotypic and genomic comparison of two Saccharomyces cerevisiae wine strains reveals a novel role of the sulfur assimilation pathway in adaptation at low temperature fermentations, BMC Genomics. 15 (2014) 1059.

[12]   I. Nisamedtinov, G.G. Lindsey, R. Karreman, K. Orumets, M. Koplimaa, K. Kevvai, T. Paalme, The response of the yeast Saccharomyces cerevisiae to sudden vs. gradual changes in environmental stress monitored by expression of the stress response protein Hsp12p, FEMS Yeast Research. 8 (2008) 829–838.

[13]   S.L. Tai, P. Daran-Lapujade, M.C. Walsh, J.T. Pronk, J.-M. Daran, Acclimation of Saccharomyces cerevisiae to low temperature: a chemostat-based transcriptome analysis, Molecular Biology of the Cell. 18 (2007) 5100–5112.

[14]   P.-J. Lahtvee, R. Kumar, B.M. Hallström, J. Nielsen, Adaptation to different types of stress converge on mitochondrial metabolism, Molecular Biology of the Cell. 27 (2016) 2505–2514.

[15]   L. Caspeta, J. Nielsen, Thermotolerant yeast strains adapted by laboratory evolution show trade-off at ancestral temperatures and preadaptation to other stresses, MBio. 6 (2015) e00431-15.

[16]   P. Jamnik, P. Raspor, Methods for monitoring oxidative stress response in yeasts, Journal of Biochemical and Molecular Toxicology. 19 (2005) 195–203.

[17]   E. García-Ríos, A. Querol, J.M. Guillamón, iTRAQ-based proteome profiling of Saccharomyces cerevisiae and cryotolerant species Saccharomyces uvarum and Saccharomyces kudriavzevii during low-temperature wine fermentation, Journal of Proteomics. 146 (2016) 70–79.

[18]   Z. Wang, Q. Qi, Y. Lin, Y. Guo, Y. Liu, Q. Wang, QTL analysis reveals genomic variants linked to high-temperature fermentation performance in the industrial yeast, Biotechnology for Biofuels. 12 (2019) 59.

[19]   E. García-Ríos, L. Ramos-Alonso, J.M. Guillamón, Correlation between low temperature adaptation and oxidative stress in Saccharomyces cerevisiae, Frontiers in Microbiology. 7 (2016) 1199.

[20]   K.Y.F. Lip, E. García-Ríos, C.E. Costa, J.M. Guillamón, L. Domingues, J. Teixeira, W.M. van Gulik, Selection and subsequent physiological characterization of industrial Saccharomyces cerevisiae strains during continuous growth at sub- and supra-optimal temperatures, Biotechnology Reports. 26 (2020) e00462. https://doi.org/10.1016/j.btre.2020.e00462.

[21]   C. Verduyn, E. Postma, W.A. Scheffers, J.P. Van Dijken, Effect of benzoic acid on metabolic fluxes in yeasts: a continuous-culture study on the regulation of respiration and alcoholic fermentation, Yeast. 8 (1992) 501–517.

[22]   A. Shevchenko, O.N. Jensen, A. V Podtelejnikov, F. S. A. Ghisailiocco, M. Wilm, O. Vorm, P. Mortensen, A. Shevchenko, H. Boucherie, M. Mann, Linking genome and proteome by mass spectrometry: large-scale identification of yeast proteins from two dimensional gels, Proceedings of the National Academy of Sciences. 93 (1996) 14440–14445.

[23]   I. V Shilov, S.L. Seymour, A.A. Patel, A. Loboda, W.H. Tang, S.P. Keating, C.L. Hunter, L.M. Nuwaysir, D.A. Schaeffer, The Paragon Algorithm, a next generation search engine that uses sequence temperature values and feature probabilities to identify peptides from tandem mass spectra, Molecular & Cellular Proteomics. 6 (2007) 1638–1655.

[24]   J. Friedman, T. Hastie, R. Tibshirani, Regularization Paths for Generalized Linear Models via Coordinate Descent, J Stat Softw. 33 (2010) 1–22.

[25]   H. Zou, T. Hastie, Regularization and variable selection via the elastic net, Journal of the Royal Statistical Society: Series B (Statistical Methodology). 67 (2005) 301–320.

[26]   M. Tokai, H. Kawasaki, Y. Kikuchi, K. Ouchi, Cloning and Characterization of the CSF1 Gene ofSaccharomyces cerevisiae, Which Is Required for Nutrient Uptake at Low Temperature, Journal of Bacteriology. 182 (2000) 2865–2868.

[27]   F. Abe, K. Horikoshi, Tryptophan permease gene TAT2 confers high-pressure growth in Saccharomyces cerevisiae, Molecular and Cellular Biology. 20 (2000) 8093–8102.

[28]   B.E. Bauer, D. Rossington, M. Mollapour, Y. Mamnun, K. Kuchler, P.W. Piper, Weak organic acid stress inhibits aromatic amino acid uptake by yeast, causing a strong influence of amino acid auxotrophies on the phenotypes of membrane transporter mutants, European Journal of Biochemistry. 270 (2003) 3189–3195.

[29]   S.K. Godin, A.G. Lee, J.M. Baird, B.W. Herken, K.A. Bernstein, Tryptophan biosynthesis is important for resistance to replicative stress in Saccharomyces cerevisiae, Yeast. 33 (2016) 183–189.

[30]   B. Westermann, B. Gaume, J.M. Herrmann, W. Neupert, E. Schwarz, Role of the mitochondrial DnaJ homolog Mdj1p as a chaperone for mitochondrially synthesized and imported proteins., Molecular and Cellular Biology. 16 (1996) 7063–7071.

[31]   W. Klein, M.H.W. Weber, M.A. Marahiel, Cold shock response of Bacillus subtilis: isoleucine-dependent switch in the fatty acid branching pattern for membrane adaptation to low temperatures, Journal of Bacteriology. 181 (1999) 5341–5349.

[32]   L. Gao, Y. Liu, H. Sun, C. Li, Z. Zhao, G. Liu, Advances in mechanisms and modifications for rendering yeast thermotolerance, Journal of Bioscience and Bioengineering. 121 (2016) 599–606.

[33]   P. Mara, G.S. Fragiadakis, F. Gkountromichos, D. Alexandraki, The pleiotropic effects of the glutamate dehydrogenase (GDH) pathway in Saccharomyces cerevisiae, Microbial Cell Factories. 17 (2018) 170.

[34]   J.-S. Hahn, Z. Hu, D.J. Thiele, V.R. Iyer, Genome-wide analysis of the biology of stress responses through heat shock transcription factor, Molecular and Cellular Biology. 24 (2004) 5249–5256.

References

[35] O. Tehlivets, N. Malanovic, M. Visram, T. Pavkov-Keller, W. Keller, S-adenosyl-L-homocysteine hydrolase and methylation disorders: yeast as a model system, Biochimica et Biophysica Acta (BBA)-Molecular Basis of Disease. 1832 (2013) 204–215.

[36] D. Thomas, Y. Surdin-Kerjan, Metabolism of sulfur amino acids in Saccharomyces cerevisiae., Microbiol. Mol. Biol. Rev. 61 (1997) 503–532.

[37] D. Kowalski, L. Pendyala, B. Daignan-Fornier, S.B. Howell, R.-Y. Huang, Dysregulation of purine nucleotide biosynthesis pathways modulates cisplatin cytotoxicity in Saccharomyces cerevisiae, Molecular Pharmacology. 74 (2008) 1092–1100.

[38] B.A. Moffatt, H. Ashihara, Purine and pyrimidine nucleotide synthesis and metabolism, The Arabidopsis Book/American Society of Plant Biologists. 1 (2002).

[39] A. Hackmann, H. Wu, U.-M. Schneider, K. Meyer, K. Jung, H. Krebber, Quality control of spliced mRNAs requires the shuttling SR proteins Gbp2 and Hrb1, Nature Communications. 5 (2014) 3123.

[40] J. Verghese, J. Abrams, Y. Wang, K.A. Morano, Biology of the heat shock response and protein chaperones: budding yeast (Saccharomyces cerevisiae) as a model system, Microbiol. Mol. Biol. Rev. 76 (2012) 115–158.

[41] O. Moldavski, T. Amen, S. Levin-Zaidman, M. Eisenstein, I. Rogachev, A. Brandis, D. Kaganovich, M. Schuldiner, Lipid droplets are essential for efficient clearance of cytosolic inclusion bodies, Developmental Cell. 33 (2015) 603–610.

[42] S.H.M. Azhar, R. Abdulla, S.A. Jambo, H. Marbawi, J.A. Gansau, A.A.M. Faik, K.F. Rodrigues, Yeasts in sustainable bioethanol production: A review, Biochemistry and Biophysics Reports. 10 (2017) 52–61.

[43] S. Marcišauskas, B. Ji, J. Nielsen, Reconstruction and Analysis of a Kluyveromyces marxianus Genome-scale Metabolic Model, BioRxiv. (2019) 581587.

[44] H. Takagi, Proline as a stress protectant in yeast: physiological functions, metabolic regulations, and biotechnological applications, Applied Microbiology and Biotechnology. 81 (2008) 211.

[45] M.J.L. de Groot, P. Daran-Lapujade, B. van Breukelen, T.A. Knijnenburg, E.A.F. de Hulster, M.J.T. Reinders, J.T. Pronk, A.J.R. Heck, M. Slijper, Quantitative proteomics and transcriptomics of anaerobic and aerobic yeast cultures reveals post-transcriptional regulation of key cellular processes, Microbiology. 153 (2007) 3864–3878.

[46] C. Camarasa, J.-P. Grivet, S. Dequin, Investigation by 13C-NMR and tricarboxylic acid (TCA) deletion mutant analysis of pathways for succinate formation in Saccharomyces cerevisiae during anaerobic fermentation, Microbiology. 149 (2003) 2669–2678.

[47]   J. Postmus, A.B. Canelas, J. Bouwman, B.M. Bakker, W. van Gulik, M.J.T. de Mattos, S. Brul, G.J. Smits, Quantitative analysis of the high temperature-induced glycolytic flux increase in Saccharomyces cerevisiae reveals dominant metabolic regulation, Journal of Biological Chemistry. 283 (2008) 23524–23532.

[48]   Z. Hu, B. He, L. Ma, Y. Sun, Y. Niu, B. Zeng, Recent advances in ergosterol biosynthesis and regulation mechanisms in Saccharomyces cerevisiae, Indian Journal of Microbiology. 57 (2017) 270–277.

[49]   F. Aguilera, R.A. Peinado, C. Millan, J.M. Ortega, J.C. Mauricio, Relationship between ethanol tolerance, H+-ATPase activity and the lipid composition of the plasma membrane in different wine yeast strains, International Journal of Food Microbiology. 110 (2006) 34–42.

[50]   J. Ding, X. Huang, L. Zhang, N. Zhao, D. Yang, K. Zhang, Tolerance and stress response to ethanol in the yeast Saccharomyces cerevisiae, Applied Microbiology and Biotechnology. 85 (2009) 253.

[51]   L. Caspeta, Y. Chen, P. Ghiaci, A. Feizi, S. Buskov, B.M. Hallström, D. Petranovic, J. Nielsen, Altered sterol composition renders yeast thermotolerant, Science. 346 (2014) 75–78.

[52]   M. Zavrel, S.J. Hoot, T.C. White, Comparison of sterol import under aerobic and anaerobic conditions in three fungal species, Candida albicans, Candida glabrata, and Saccharomyces cerevisiae, Eukaryotic Cell. 12 (2013) 725–738.

[53]   S. Reiner, D. Micolod, G. Zellnig, R. Schneiter, A genomewide screen reveals a role of mitochondria in anaerobic uptake of sterols in yeast, Molecular Biology of the Cell. 17 (2006) 90–103.

[54]   M. Krantz, B. Nordlander, H. Valadi, M. Johansson, L. Gustafsson, S. Hohmann, Anaerobicity prepares Saccharomyces cerevisiae cells for faster adaptation to osmotic shock, Eukaryotic Cell. 3 (2004) 1381–1390.

[55]   I. Unnikrishnan, S. Miller, M. Meinke, D.C. LaPorte, Multiple positive and negative elements involved in the regulation of expression of GSY1 in Saccharomyces cerevisiae, Journal of Biological Chemistry. 278 (2003) 26450–26457.

[56]   A. Huseinovic, M. van Dijk, N.P.E. Vermeulen, F. van Leeuwen, J.M. Kooter, J.C. Vos, Drug toxicity profiling of a Saccharomyces cerevisiae deubiquitinase deletion panel shows that acetaminophen mimics tyrosine, Toxicology in Vitro. 47 (2018) 259–268.

[57]   E.T. Lis, F.E. Romesberg, Role of Doa1 in the Saccharomyces cerevisiae DNA damage response, Molecular and Cellular Biology. 26 (2006) 4122–4133.
[58]   E. Mullarky, L.C. Cantley, Diverting glycolysis to combat oxidative stress, in: Innovative Medicine, Springer, Tokyo, 2015: pp. 3–23.

[59]   M. Ralser, M.M. Wamelink, A. Kowald, B. Gerisch, G. Heeren, E.A. Struys, E. Klipp, C. Jakobs, M. Breitenbach, H. Lehrach, Dynamic rerouting of the carbohydrate flux is key to counteracting oxidative stress, Journal of Biology. 6 (2007) 10.

References

[60]   H. Takagi, Metabolic regulatory mechanisms and physiological roles of functional amino acids and their applications in yeast, Bioscience, Biotechnology, and Biochemistry. (2019) 1–14.

[61]   Y. Cheng, Z. Du, H. Zhu, X. Guo, X. He, Protective effects of arginine on Saccharomyces cerevisiae against ethanol stress, Scientific Reports. 6 (2016) 31311.

[62]   S. Lindquist, G. Kim, Heat-shock protein 104 expression is sufficient for thermotolerance in yeast, Proceedings of the National Academy of Sciences. 93 (1996) 5301–5306.

[63]   I. V Fedoseeva, E.G. Rikhvanov, N.N. Varakina, T.M. Rusaleva, D. V Pyatrikas, A. V Stepanov, A. V Fedyaeva, Induction of Hsp104 synthesis in Saccharomyces cerevisiae in the stationary growth phase is inhibited by the petite mutation, Russian Journal of Genetics. 50 (2014) 237–244.

[64]   R. Lum, J.M. Tkach, E. Vierling, J.R. Glover, Evidence for an unfolding/threading mechanism for protein diS. A. Ghisaigregation by Saccharomyces cerevisiae Hsp104, Journal of Biological Chemistry. 279 (2004) 29139–29146.

[65]   B.R. Gibson, S.J. Lawrence, C.A. Boulton, W.G. Box, N.S. Graham, R.S.T. Linforth, K.A. Smart, The oxidative stress response of a lager brewing yeast strain during industrial propagation and fermentation, FEMS Yeast Research. 8 (2008) 574–585. https://doi.org/10.1111/j.1567-1364.2008.00371.x.

[66]   L. Ballester-Tomás, F. Randez-Gil, R. Pérez-Torrado, J.A. Prieto, Redox engineering by ectopic expression of glutamate dehydrogenase genes links NADPH availability and NADH oxidation with cold growth in Saccharomyces cerevisiae, Microbial Cell Factories. 14 (2015) 100.

[67]   S. Chabane, F. Kepes, Expression of the yeast BFR2 gene is regulated at the transcriptional level and through degradation of its product, Molecular and General Genetics MGG. 258 (1998) 215–221.

[68]   C. Young, J. Mapes, J. Hanneman, S. Al-Zarban, I. Ota, Role of Ptc2 type 2C Ser/Thr phosphatase in yeast high-osmolarity glycerol pathway inactivation, Eukaryotic Cell. 1 (2002) 1032–1040.

[69]   D. Sharmin, Y. Sasano, M. Sugiyama, S. Harashima, Effects of deletion of different PP2C protein phosphatase genes on stress responses in Saccharomyces cerevisiae, Yeast. 31 (2014) 393–409.

[70]   J. Panadero, C. Pallotti, S. Rodríguez-Vargas, F. Randez-Gil, J.A. Prieto, A downshift in temperature activates the high osmolarity glycerol (HOG) pathway, which determines freeze tolerance in Saccharomyces cerevisiae, Journal of Biological Chemistry. 281 (2006) 4638–4645.

[71]   C.M. Grant, K.A. Quinn, I.W. Dawes, Differential protein S-thiolation of glyceraldehyde-3-phosphate dehydrogenase isoenzymes influences sensitivity to oxidative stress, Molecular and Cellular Biology. 19 (1999) 2650–2656.

[72]   P.B. Moore, T.A. Steitz, The structural basis of large ribosomal subunit function, Annual Review of Biochemistry. 72 (2003) 813–850.

[73]   J. Tronchoni, V. Medina, J.M. Guillamón, A. Querol, R. Pérez-Torrado, Transcriptomics of cryophilic Saccharomyces kudriavzevii reveals the key role of gene translation efficiency in cold stress adaptations, BMC Genomics. 15 (2014) 432.

[74]   C.M. Grant, Role of the glutathione/glutaredoxin and thioredoxin systems in yeast growth and response to stress conditions, Molecular Microbiology. 39 (2001) 533–541.

[75]   S. Tiwari, R. Thakur, J. Shankar, Role of heat-shock proteins in cellular function and in the biology of fungi, Biotechnology Research International. 2015 (2015).

[76]   A. Pacheco, C. Pereira, M.J. Almeida, M.J. Sousa, Small heat-shock protein Hsp12 contributes to yeast tolerance to freezing stress, Microbiology. 155 (2009) 2021–2028.

[77]   O. Kandror, N. Bretschneider, E. Kreydin, D. Cavalieri, A.L. Goldberg, Yeast adapt to near-freezing temperatures by STRE/Msn2, 4-dependent induction of trehalose synthesis and certain molecular chaperones, Molecular Cell. 13 (2004) 771–781.

[78]   K. Sales, W. Brandt, E. Rumbak, G. Lindsey, The LEA-like protein HSP 12 in Saccharomyces cerevisiae has a plasma membrane location and protects membranes against desiccation and ethanol-induced stress, Biochimica et Biophysica Acta (BBA)-Biomembranes. 1463 (2000) 267–278.

[79]   C.M. Paget, J. Schwartz, D. Delneri, Environmental systems biology of cold-tolerant phenotype in Saccharomyces species adapted to grow at different temperatures, Molecular Ecology. 23 (2014) 5241–5257.

[80]   M. Kato, S.-J. Lin, Regulation of NAD+ metabolism, signaling and compartmentalization in the yeast Saccharomyces cerevisiae, DNA Repair. 23 (2014) 49–58.

[81]   M. Heublein, M.A. Burguillos, F.N. Vögtle, P.F. Teixeira, A. Imhof, C. Meisinger, M. Ott, The novel component Kgd4 recruits the E3 subunit to the mitochondrial α-ketoglutarate dehydrogenase, Molecular Biology of the Cell. 25 (2014) 3342–3349.

[82]   J.T. Fox, P.J. Stover, Folate-mediated one-carbon metabolism, Vitamins & Hormones. 79 (2008) 1–44.

[83]   N.A. Binai, M.M.M. Bisschops, B. van Breukelen, S. Mohammed, L. Loeff, J.T. Pronk, A.J.R. Heck, P. Daran-Lapujade, M. Slijper, Proteome adaptation of Saccharomyces cerevisiae to severe calorie restriction in retentostat cultures, Journal of Proteome Research. 13 (2014) 3542–3553.

[84]   N. Gebert, M. Gebert, S. Oeljeklaus, K. von der Malsburg, D.A. Stroud, B. Kulawiak, C. Wirth, R.P. Zahedi, P. Dolezal, S. Wiese, Dual function of Sdh3 in the respiratory chain and TIM22 protein translocase of the mitochondrial inner membrane, Molecular Cell. 44 (2011) 811–818.

[85]   O. Kerscher, N.B. Sepuri, R.E. Jensen, Tim18p is a new component of the Tim54p-Tim22p translocon in the mitochondrial inner membrane, Molecular Biology of the Cell. 11 (2000) 103–116. https://doi.org/10.1091/mbc.11.1.103.

Chapter 4

Adaptive Evolution of *Saccharomyces cerevisiae* for High Temperature Tolerance under Anaerobic Conditions

Summary

Adaptive laboratory evolution of *Saccharomyces* cerevisiae CEN. PK113-7D was performed through cultivation in an anaerobic sequential batch reactor (SBR) whereby the cultivation temperature was increased stepwise until 39.8°C. After 475 generations an evolved strain was obtained which was better adapted to growth at high temperature, as the death rate was significantly reduced compared to the non-evolved strain. The selection pressure under prolonged high temperature cultivation and anaerobic conditions provoked several mutations, such as single nucleotide polymorphisms as well as small insertions and deletions, in the genome of CEN.PK113-7D. The enrichment gene ontology terms associated with those high impact single nucleotide variants indicated that they could have affected the TORC1 pathway, as well as the biosynthesis of phosphatidylethanolamine, phospholipid, and ribonucleotides. The mutations resulted in a stable isolate, CEN.PK-EVO, with 3.6 times lower death rate and in return improved biomass yield on glucose, as well as fewer cells with membrane rupture at 39.8°C. Comparison of both strains during anaerobic growth in chemostat cultures at a constant growth rate at 39°C revealed that the evolved strain had 37.7% increase in trehalose accumulation, a 25.9% decrease of the phosphatidylcholine to phosphatidylethanolamine ratio, and a 73.7% increase of the ergosterol content, compared to the unevolved strain.

1
Introduction

Saccharomyces cerevisiae is one of the common workhorses used in the first- and second-generation bio-ethanol industry due to its robustness and ethanol tolerance. The increasing demand for affordable bioethanol requires further process improvement and scale up of fermentation vessels. To reduce the cooling costs and risk of contamination, fermentation is preferably carried out at high temperatures ($\geq$ 40°C). High temperature fermentation will also benefit simultaneous saccharification of cellulosic feedstock, as the optimum temperature for the enzymes (e.g. fungal cellulases) used for the hydrolysis of substrate feedstock is around 50°C [1,2]. However, the optimum growth temperature of *S. cerevisiae* lies between 28°C and 33°C [3]. Thermotolerant yeasts are a promising subject for bio-ethanol production. Previous studies have shown that thermotolerance of yeasts was conferred by various causative genes, which are for example involved in RNA processing [4], trehalose accumulation [5–7], and lipid composition of the cell membrane [8–10]. However, most of these findings were obtained for different *S. cerevisiae* strains wherein the mechanisms induced by acute heat stress seems to vary by cultivation conditions. In a previous study, we compared industrial *S. cerevisiae* yeasts with the well-studied laboratory strain CEN.PK113-7D to identify the possible physiological properties contributing to low and high temperature tolerance under anaerobic conditions [11,12]. Hereby it was observed that increased high temperature tolerance coincided with higher energetic efficiency of cell growth and various strain-specific up and downregulations in the proteome. High-throughput sequencing has revealed large sequence variations between yeast strains [13] which could result in strain specific responses to sub- and supra-optimal cultivation temperatures. To minimize strain to strain differences, a comparison between a laboratory reference strain and a temperature adapted yeast strain both with an identical genetic origin would be beneficial to identify the mechanisms behind temperature tolerance.

There are random and rational strategies for breeding yeasts with desired phenotypes. Since thermotolerance is influenced by multiple genes [5], we used a random approach using adaptive laboratory evolution (ALE) to improve the thermotolerance of the well-studied laboratory strain CEN.PK113-7D. As improved thermotolerance is relevant for bioethanol production, which is carried out under anaerobic conditions, we used anaerobic conditions in our experiments as well. ALE induces phenotypic changes associated with a defined growth condition due to random mutations resulting in a stable trait selection. To ensure well-defined cultivation conditions with a minimal duration of the stationary phase, we used a fully-controlled automated sequential batch reactor (SBR) system. Prolonged SBR cultivation at increasing temperature resulted a stable isolate with improved thermotolerance at 39.8°C. The evolved strain was characterized to identify the genomic and phenotypic changes responsible for the enhanced thermotolerance. To this end, whole genome sequencing and physiological characterization in SBR and chemostat cultures at optimal (30.0°C) and supra-optimal (≥ 39.0°C) cultivation temperatures were performed. A summary of the study scheme can be found in Figure S3.

2
Methods and materials

2.1
Yeast strains and preparation of working stocks

The *S. cerevisiae* strains used in this study were the haploid laboratory strains CEN.PK113-7D (Fungal Biodiversity Centre, Utrecht, The Netherlands) and S288C, the diploid laboratory strain FY1679, as well as the high temperature evolved CEN.PK113-7D (CEN.PK-EVO) which was derived from the laboratory strain by in-vitro evolution as described in the results section. Inocula were prepared by introducing a single colony of a pure culture of each strain into 5 mL sterilized synthetic medium [14] supplemented with 15 g·L⁻¹ D-glucose monohydrate in a 30°C orbital shaker at 220 rpm. Working stocks were prepared by cultivation in minimal medium [14] supplemented with 15 g·L⁻¹ D-glucose monohydrate. After addition of sterile 30% (v/v) glycerol, culture aliquots were stored in sterilized Eppendorf tubes at -80°C.

2.2
Preparation of inocula and lab scale fermentations

All pre-cultures were initiated from the frozen working stocks and grown aerobically at 220 rpm and at 30°C in 1000 mL shake flasks with 200 mL defined medium containing 5 g·L⁻¹ (NH₄)₂SO₄, 3 g·L⁻¹ KH₂PO₄, 0.5 g·L⁻¹ MgSO₄·7H₂O, 22 g·L⁻¹ D-glucose monohydrate, 1.0 mL·L⁻¹ of trace element solution, and 1.0 mL·L⁻¹ vitamin solution [14]. The medium was filter sterilized using a 0.2 μm Sartopore 2 filter unit (Sartorius Stedim, Goettingen, Germany). All fermentations (described in detail below) were performed in 7 L bioreactors (Applikon, Delft, The Netherlands) equipped as described previously [11].

2.3
Adaptive evolution by sequential batch cultivations

The CEN.PK113-7D strain was evolved under anaerobic conditions in a 7 L sequential batch reactor (SBR) containing 4.00 ± 0.05 kg of culture broth. Anaerobic conditions were maintained by sparging both the medium vessel and the bioreactor with nitrogen gas (0.1 NL·min⁻¹ and 1.0 NL·min⁻¹, respectively). The set-up and computer control of the SBR set up has been described previously [11]. The cultivation was performed with using defined minimal medium [14] supplemented with 44.0 g·L⁻¹ D-glucose

monohydrate, 0.4 g·L⁻¹ Tween80, 10 mg·L⁻¹ ergosterol, 0.26 g·L⁻¹ antifoam C (Sigma-Aldrich, Missouri, USA). The progression of all sequential batch cultivations was monitored by the CO_2 content of the exhaust gas and the base addition for pH control. Each subsequent batch of the SBR was initiated with 1/10 of the culture broth of the previous batch. The effluent was drained at the bottom of the reactor at each subsequent batch, so it helps to remove the fast-sedimenting cells. Fresh medium was added from the top of the bioreactor (headspace) to prevent cells contamination in the medium vessel. During cultivation, the pH of the culture broth was controlled at 5.00 ± 0.05 by automatic titration with 2.0 M KOH. During the SBR cultivation, the temperature was initially increased from 30.0°C to 34.0°C and subsequently to 38.0°C in steps; of 4.0°C with an adaptation time of at least 4 cycles. From 38.0°C the temperature was increased in small steps of 0.2°C each 4 cycles until a temperature of 38.6°C was reached. Thereafter the temperature was further increased with steps of 0.2°C every 15 cycles until a temperature of 39.8°C was reached. The complete SBR cultivation was carried out for in total 143 cycles, corresponding to 475 generations (supplementary materials, equation 1). At the end of the evolution experiment, culture samples were taken and plated on YPD agar plates, containing 0.4 g·L⁻¹ Tween80 and 10 mg·L⁻¹ ergosterol, and subsequently incubated at 39.8°C in a desiccator which was sparged with nitrogen gas to maintain anaerobic conditions. After two subsequent restreaks on YPD agar plates, two single-cell isolates were obtained and grown in shake flasks as mentioned above in the preparation of working stocks.

The technical set up and control of the SBR fermentations was carried out in the same way as the SBR for adaptive evolution described above. The culture broth was maintained at pH 5.00 ±0.05 by automatic titration with 2.0 M KOH and the cultivation temperature was controlled at 39.8 ± 0.01°C. The stirring speed was set at 450 *rpm*. Eight sequential batches were carried out in total for the characterisation of each strain. After four sequential batches, triplicate samples were taken at 5 sampling time points during the exponential phase of each batch. In total, samples were collected from three sequential batches for the characterisation of each strain at 39.8°C.

*2.4
Physiological
characterisation
by SBR
fermentation*

2.5
Anaerobic chemostat cultivations

Chemostat cultivations were carried out at a dilution rate of 0.030 ± 0.002 h^{-1} and cultivation temperatures of 30.0°C and 39.0°C. The set-up, data acquisition and control of the chemostat cultures was carried out as described previously [11]. The defined minimal medium [14] for cultivation was supplemented with 22.0 g·L^{-1} D-glucose monohydrate, 0.4 g·L^{-1} Tween80, 10 mg·L^{-1} ergosterol, and 0.26 g·L^{-1} antifoam C (Sigma-Aldrich, Missouri, USA). Chemostat cultures were considered to have reached steady-state if after at least 5 volume changes, stable CO_2 levels in the exhaust gas and biomass dry mass concentrations were obtained. After a steady stat was reached, triplicate samples were withdrawn at four time points with intervals of one residence time.

2.6
Viability measurement

To measure the culture viability diluted broth samples were stained with propidium iodide (PI) and 5-carboxyfluorescein diacetate acetoxymethyl ester (5-CFDA,AM) (FungaLight 5-CFDA,AM/PI yeast viability kit; Invitrogen, USA) as described previously [15]. Counting of stained cells was performed with an Accuri flow cytometer (BD Bioscience, USA) as described in [15]. Dry weight concentrations were multiplied by the fraction viable cells to obtain the concentration of viable cells (Cxv) in gDM·L-1.

2.7
Analytical methods

Optical density was monitored using a Libra Su spectrophotometer (Biochrom Libra, Cambridge, UK) at a wavelength of 600 nm. Biomass dry mass was determined by the filtration of broth samples over dry nitrocellulose filters (0.45 µm pore size, Gelman laboratory, Ann Arbor, USA) which were pre-dried overnight in a 70°C oven. Two sample volumes of demineralized water were used to wash the cell cakes on the filters after filtration. The thus obtained washed biomass samples were subsequently dried in an oven at 70°C for two days. Before and after sample filtration the filters were weighted after cooling down in a desiccator for a period of two hours.

Samples for the quantification of extracellular metabolites were withdrawn using the cold stainless-steel beads method to immediately cool down the sample to 0°C and subsequent rapid filtration to remove the cells [16]. The resulting supernatant was immediately frozen in liquid nitrogen and stored at -80°C until analysis. The quantification of the metabolites is performed by HPLC whose details are described in supplementary materials.

A black box model was constructed to find the best estimates of the biomass specific conversion rates under the constraint that the four elemental conservation relations (carbon, hydrogen, oxygen, and nitrogen) were satisfied. The best estimates were obtained by a least squares method (LSM) [17] whose details are described in the supplementary materials. We used the quantification data of nine compounds (acetate, biomass, CO_2, ethanol, glucose, glycerol, lactate, malate, and succinate) to obtain all eleven net conversion rates by an optimization model which minimized the scaled squared residuals between the experimental data and the predicted data. To eliminate the effect of carryover from the inoculum [17], we allowed each SBR to run four initial fill-and-drain cycles where during the subsequent three batches measurements were performed for determination of the above-mentioned specific rates.

The metabolic flux distributions as well as the best estimates of the biomass specific net conversion rates of the chemostat experiments were obtained via metabolic flux analysis using a stoichiometric model for anaerobic growth of *S. cerevisiae* [18]. With sufficient available conversion rates as input variables an overdetermined system was obtained, allowing to find the best estimates of the biomass specific net conversion rates within their error margins as well as the metabolic flux distributions under the constraint that the elemental and compound balances were satisfied [19,20].

The total organic carbon (TOC) contents of the chemostat total broth and the culture supernatant were obtained from the difference between the total carbon (TC) contents and the total inorganic carbon (TIC) contents which were both measured by a total organic carbon analyser (TOC-L CSH, Shimadzu, Kyoto, Japan). The total nitrogen (TN) contents of the freeze-dried biomass samples from the chemostat cultures were quantified by a total nitrogen analyser (TNM-L, Shimadzu, Kyoto, Japan). The injection of the samples for both TOC and TN measurement was carried out by an auto-sampler (ASI-L, Shimadzu, Kyoto, Japan).

2.8
Data reconciliation for the best estimations of biomass specific conversion rates

2.8.1
Least squares method for SBR

2.8.2
Metabolic flux analysis for the chemostat steady-states

119

2.9
Total organic carbon and total nitrogen measurement

2.10
Cellular protein measurement

Thirty millilitres of chemostat broth were withdrawn from the reactor and subsequently centrifuged at 4°C and at 5000 x g for 5 minsutes. The supernatant was discarded, and the biomass pellet was immediately frozen in liquid nitrogen and stored at -80°C prior to freeze-drying. The cellular protein contents of the freeze-dried biomass were determined using the Biuret method as described in [21] using freeze-dried bovine serum albumin as standard.

2.11
Quantification of glycogen and trehalose

For quantification of glycogen, samples containing approximately 2 mg dry weight of cells were obtained by immediate quenching of 1.3 ± 0.2 mL of culture broth into 8.0 mL of 100% -40°C methanol using a rapid sampling setup [22]. The exact sample weights were determined by weighing each tube before and directly after sampling. The quenched samples were subsequently centrifuged at -19°C and at 5000 x g for 5 minutes. The supernatants were discarded, and the biomass pellets were immediately frozen in liquid nitrogen and stored at -80°C until analysis.

Before analysis, the biomass pellets were defrosted on ice and washed twice with 1.5 mL cold Mi-Q water in an Eppendorf tube and subsequently centrifuged at 4°C and at 8000 x g for 2 minutes. After discarding the supernatant, the pellet was resuspended in 250 μL of 0.25 M sodium carbonate solution and subsequently incubated at 95°C for 3 hours with continuous shaking. After the incubation, 600 μL of 0.2 M sodium acetate was added to the mixture, and the pH was adjusted to 5.3 with 1M acetic acid. Glycogen hydrolysis was performed by adding α-amyloglucosidase dissolved in 0.2 M sodium acetate to the mixture to a final concentration of 1.2 U·mL^{-1}. The hydrolysis was carried out at 57°C overnight with continuous shaking. The glucose released from the glycogen digestion was determined in triplicate using an enzymatic kit (UV bioanalysis kit, R-Biopharm/Roche, Darmstadt, Germany) thereby measuring the increase in NADPH which was quantified by means of light absorbance at 340 nm by a spectrophotometer.

For trehalose quantification, samples containing approximately 2 mg dry weight of cells were obtained by immediate quenching of 1.3 ± 0.2 mL of culture broth into 8.0 mL of 100% -40°C methanol using a rapid sampling setup [22]. Subsequently, the separation and washing of the cells were done by cold filtration with 80% (v/v) -40°C methanol. The intracellular metabolites extraction

was carried out with the boiling ethanol method as described previously [23]. At the beginning of the extraction process, C13 labelled cell extract was added as internal standard [24]. Cellular trehalose content from the extracted biomass was measured by GC-MS as described in [25].

Genomic DNA from CEN.PK113-7D and CEN.PK-EVO was extracted according to [26], wherein paired-end sequencing libraries with a mean insert size of 300 bp were prepared and run on an Illumina HiSeq2500 instrument. Raw reads were submitted to NCBI Sequence Read Archive (SRA) as SRR11697748 (CEN. PK113-7D) and SRR11697747 (CEN.PK-EVO). Reads were trimmed using Sickle v1.2 [27] with a minimum quality value per base of 28 at both ends and a minimum read length of 35 bp. The average sequencing coverage of CEN.PK113-7D and CEN. PK-EVO was 150X and 135X, respectively. To identify changes in the genome of the evolved strain, the obtained reads of both CEN.PK113-7D and CEN.PK-EVO strains were mapped against the S288c strain. The strategy employed to study both genomes was based on sequenced reads mapping against S288c reference genome.

Reads were mapped against *S. cerevisiae* genome reference (S288C, version R64-2-1) using bowtie2 v2.3.0 [28] with default parameters. We then used bedtools v2.17.0 [29] to obtain the read depth (RD) or coverage "per base" which was processed to have an average coverage value each 1000 positions which allowed a smoother chromosome representation based on coverage values. Freebayes (v1.1.0-60gc15b070) was used to find genetic variants, as Single Nucleotide Positions SNPs (options: -C 10, -F 0.25 and pool continuous), in the two mapped samples. We then used VCFtools (v0.1.13) [30] to filter variant positions with a minimum base quality of 200 and to compare changes between CEN.PK113-7D and CEN.PK-EVO. This minimum base quality is a phred-scaled quality score for the assertion made in calling a non-reference (alternative) position. The obtained file was then modified to keep only the variants present in CEN.PK-EVO with respect to CEN.PK113-7D. The variants were then analysed for their functional effect on *S. cerevisiae* S288c ORFs using the Ensembl Variant Effect [31]. Non-synonymous variants in coding positions were retrieved and were manually confirmed through visual inspection in the Integrative Genomics Viewer (IGV) [32]. We performed Gene Ontology (GO) and pathway enrichment

2.12
Whole genome sequencing

121

2.12.1
Variant calling, filtration, copy number variation and annotation

analysis with the list of genes with non-synonymous variants. We analysed this set of genes using YeastMine tools at SGD [33]. We considered that a term was statistically enriched when *p*-value < 0.05 (Benjamini Hochberg corrected). CNVnator was used for the copy number variation discovery [34]. We used the two mapped samples of CEN.PK113-7D and CEN.PK-EVO against S288c and used a bin size of 100 positions to detect duplications and deletions in CEN.PK113-7D and CEN.PK-EVO genomes in comparison to the S288c strain. Read depth was normalized to 1 and regions with unusual read depths after normalization were annotated. All sequencing data are available from the NCBI Sequence Read Archive: Bioproject, accession number PRJNA630580 (SRA number: SRR11697748 (CEN.PK113-7D); SRR11697747 (CEN.PK-EVO).

2.12.2
Ploidy estimation by flow cytometry

The DNA content of unevolved strain (CEN.PK113-7D) and evolved strain (CEN.PK-EVO) was assessed by flow cytometry in a Beckman Coulter FC 500 (Beckman Coulter Inc., Brea, CA, United States) by the SYTOX Green dye method described in [35]. The DNA content values were scored based on the fluorescence intensity compared with the haploid (S288c) and the diploid (FY1679) *S. cerevisiae* references strains. The DNA content value reported for each strain was the result of two independent measurements (Table S5).

2.13
Lipid composition measurements

The fatty acid methyl ester analysis was performed as described in [36]. Sterols and squalene were determined by GC/MS using the method as described in [37]. Prior to lipid extraction, a solution of 100 μL of cold methanol and 10 μL of EDTA 0.1 mM was added to the chemostat cultures (10–15 mg of dried weight) with 100 mg glass beads (0.5 mm, Biospec Products) in an Eppendorf tube and then mixed for 5 mins in a mini-bead-beater-8 (Biospec Products, Qiagen). glass beads (0.5 mm, Biospec Products) in an Eppendorf tube and then mixed for 5 mins in a mini-bead-beater-8 (Biospec Products, Qiagen). Lipid extraction was performed in four steps, two steps with 300 μL chloroform/methanol (2:1, v/v, for 30 mins), and one step with 300 μL of chloroform/methanol 1:1 (v/v) for 30 mins. Both organic phases were transferred to a 15 mL glass screw-cap tube and cleaned twice by adding KCl 0.88% (w/v), (1/4 of the total volume of the extract). After vortexing and cooling at 4°C for 10 mins, samples were centrifuged at 1300 g for 5 mins. The organic phase was collected and finally concentrated to dryness under a nitrogen stream. The residue was dissolved in

chloroform/methanol (1:1, v/v) and stored at -80°C until chromatography analysis whose details are described in supplementary materials.

The statistical significance of all measurements was evaluated by tailed student t-tests with a 95% confidence interval: the cellular protein measurements, storage carbohydrates measurements (glycogen and trehalose), as well as the measurements of total fatty acids, squalene, and sterols. The cytometry results were tested by a one-way ANOVA and a Tukey HSD test (α=0.05, n=2). In the enrichment analysis was considered that a term was statistically enriched when p-value < 0.05 (Benjamini-Hochberg corrected).

2.14
ribed in
supplementary
materials.
Statistical
analysis

123

3
Results

3.1
Adaptive evolution of CEN.PK113-7D at high temperature by prolonged SBR cultivation under anaerobic conditions

We imposed increasing heat stress on CEN.PK113-7D during prolonged anaerobic SBR cultivation under anaerobic conditions, to improve its thermotolerance via adaptive evolution. To avoid a fatal heat shock to the cells, we increased the cultivation temperature stepwise from the initial value of 30.0°C until a final value of 39.8°C (materials and methods). Because all specific production and consumption rates during unlimited exponential growth in batch culture are stoichiometrically coupled to the maximum specific growth rate at the applied temperature $\mu_{max(T)}$, we could calculate the $\mu_{max(T)}$ of each SBR batch from the on-line measurement of the CO_2 concentration in the exhaust gas (materials and methods). To this end, we performed regression of the CO_2 profile vs time with the corrected modified Gompertz model [11] for each single batch culture of the SBR. Figure 1 shows the $\mu_{max(T)}$ of the strain for the SBR batches between 30.0°C and 39.8°C. At a cultivation temperature of 34.0°C the highest specific growth rate was reached. When the temperature was increased from 34.0°C to 38.6°C, the growth rate decreased significantly. Further stepwise increase of the cultivation temperature above 38.6°C resulted each time in a decrease of the growth rate during the first SBR cycles, after the temperature was increased. However, after each initial decline the growth rate was observed to increase again in subsequent cycles, showing that the strain adapted to the increased temperature (indicated by the yellow areas in the graph). After approximately 475 generations of SBR cultivation a significant improvement in the thermotolerance was obtained. At this point the ALE experiment was terminated to yield the high temperature evolved strain (CEN.PK-EVO).

To investigate the performance of the evolved strain at high temperature, we compared the specific growth rates, consumption rates of glucose and ammonium, as well as production rates of CO_2, ethanol, glycerol and several by-products of the unevolved and the evolved strains during SBR cultivation at 39.8°C (Table 1). The culture viability of each batch culture during the exponential phase was measured by combined PI/CFDA staining to calculate the specific death rate (k_d) of the strains during cultivation at 39.8°C (Table 1). The average viable cell fractions for three SBR cycles were 0.36 ± 0.01 for the unevolved strain and 0.89 ± 0.00 for CEN.PK-EVO. The apparent specific growth rate of the evolved strain appeared more than three times higher than that of the unevolved strain (Table S1). However, taking the measured culture viabilities into account, the maximum specific growth rates of both strains at 39.8°C corrected for cell death (supplementary materials, equation 3) were similar (Table 1).
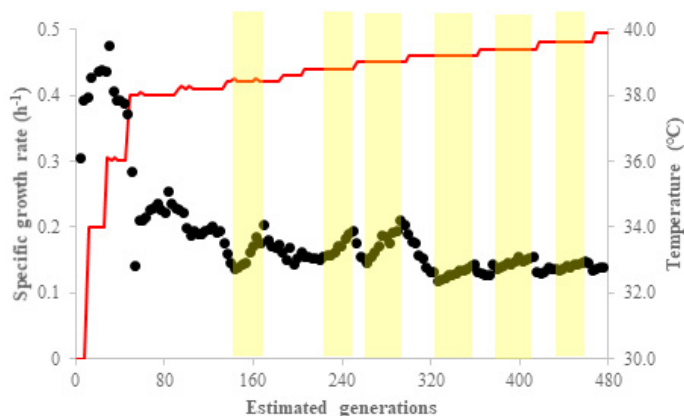
Figure 1
Adaptive evolution of CEN.PK113-7D by SBR in a bioreactor under anaerobic conditions between 30.0°C and 39.8°C. Red line indicates the cultivation temperature during SBR. Dots represent the maximal specific growth rates. The yellow area indicates the sign of evolution at the respective cultivation temperature.

Except for the production rates of acetate, glycerol, and succinate, most specific conversion rates of the two strains at 39.8°C were similar (Table 1). The unevolved strain produced two times more acetate and succinate than the evolved strain, thereby accompanied by an increased production rate of glycerol. Under anaerobic conditions, glycerol formation allows the re-oxidation of NADH whereby the unevolved strain produced more glycerol compared to the evolved strain due to the higher net production of NADH from acetate formation. The evolved strain had 67% higher viable biomass yield compared to the unevolved strain

(Table 1), showing the effect of the high death rate of the unevolved strain. Both strains showed similar specific CO_2 and ethanol production rates, therefore, both strains had a similar fermentative capacity during SBR cultivation at 39.8°C. The yields of ethanol on glucose of both strains were also similar (Table 1).

	CEN.PK113-7D			CEN.PK-EVO		
$\mu_{max(T),est}$ h^{-1}	0.17	±	0.050	0.23	±	0.027
$^{*}k_d$, h^{-1}	0.11	±	0.033	0.03	±	0.003
$^{*}q_{acetate.max}$	0.87	±	0.235	0.33	±	0.063
$q_{CO2.max}$	21.19	±	3.220	18.71	±	1.008
$q_{ethanol.max}$	19.77	±	3.047	18.12	±	0.944
$^{*}q_{glycerol.max}$	3.61	±	0.980	1.49	±	0.215
$^{*}q_{lactate.max}$	0.09	±	0.018	0.15	±	0.019
$q_{malate.max}$	0.02	±	0.008	0.02	±	0.008
$q_{NH3. max}$	-0.01	±	0.002	-0.03	±	0.003
$q_{s.max}$	-12.78	±	2.070	-10.32	±	0.618
$^{*}q_{succinate.max}$	0.74	±	0.197	0.28	±	0.020
$^{*}Y_{acetate}$	0.067	±	0.021	0.032	±	0.006
$^{*}Y_{biomass}$	0.50	±	0.17	0.83	±	0.12
Y_{CO2}	1.66	±	0.37	1.81	±	0.15
$Y_{ethanol}$	1.55	±	0.35	1.76	±	0.14
$^{*}Y_{glycerol}$	0.28	±	0.09	0.14	±	0.02
$^{*}Y_{lactate}$	0.007	±	0.002	0.015	±	0.002
Y_{malate}	0.002	±	0.001	0.002	±	0.001
$^{*}Y_{succinate}$	0.058	±	0.018	0.027	±	0.002

Table 1

Best estimated maximal specific growth rate, death rate, reconciled biomass specific conversion rates, and yields of biomass and main products on glucose at 39.8°C of the unevolved and evolved strains with their standard errors during anaerobic SBR. The reconciled biomass specific conversion rates have a unit of $mmol \cdot g_{viable\ DM}^{-1} \cdot h^{-1}$. The nomenclature of q_s represents as substrate (glucose) uptake rate. Yields of biomass and main products on glucose were calculated from the maximal biomass specific conversion rates and have a unit of $mol_i \cdot mol_{glucose}^{-1}$. * Indicates a significant difference with a p-value (paired T-test) of < 0.05.

We compared the morphology of the unevolved and evolved strains during the exponential growth phase of the SBR cultivations and found more cells with intact cell membranes in the SBR culture of the evolved strain than that of the unevolved strain (Figure 2). In the SBR culture of both strains, the cells attached to each other to form small clusters. Cells of both strains were similar in size.

3.2.2
Temperature influence on morphology

a)

b)
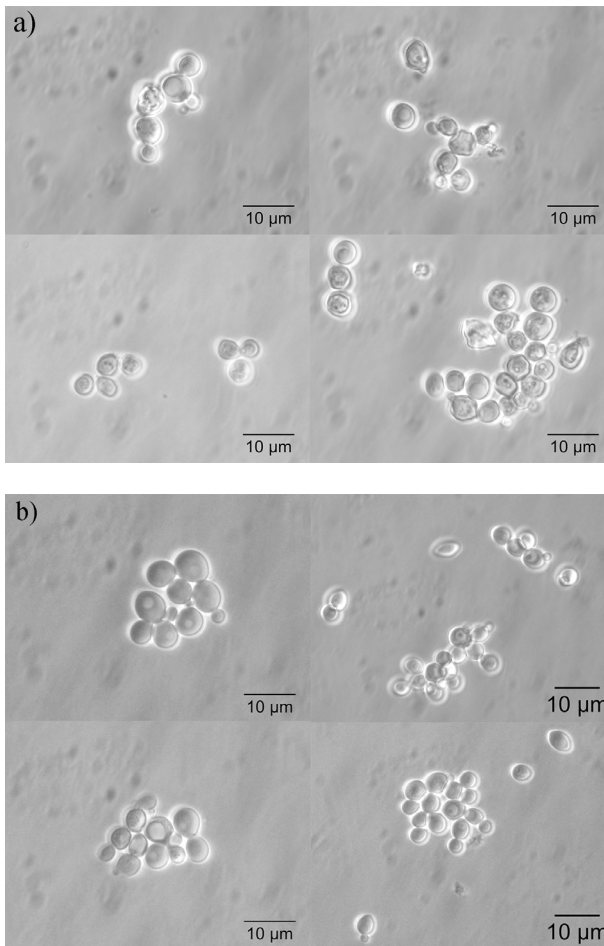
Figure 2
Microscopic observations during physiology characterisation by anaerobic SBR at 39.8°C. Biomass culture was taken during the exponential growth phase of multiple sequential batches; a): CEN.PK113-7D; b): CEN.PK-EVO. Biomass cultures were observed directly with a light microscope at magnification x1000

3.3
Physiological characterization of the evolved and unevolved strains during anaerobic chemostat cultivation at 30.0°C and 39.0°C

To separate the temperature effect from the effect of specific growth rates, we grew both strains at 30.0°C and 39.0°C in anaerobic steady-state chemostat cultures at a dilution rate of 0.03 h^{-1}. After five volume changes all chemostat cultures showed stable off-gas CO_2, biomass dry mass concentrations and by-product levels indicating steady-state conditions. During all steady-states, the residual glucose concentration was below 0.50 mmol·L^{-1} confirming glucose limited conditions. The specific conversion rates for all steady-state chemostats with their error margins can be found in the supplementary material (Table S2). From these rates, the corresponding yields of biomass and by-products on glucose were calculated (Table 2).

We observed very similar CO_2 and ethanol yields between both strains and between the two cultivation temperatures (Table 2). The yields of the acid by-products acetate, lactate, malate, and succinate were also similar between both strains for both cultivation temperatures, but were all significantly higher at 39.0°C. The glycerol yield showed an opposite trend and decreased at increased cultivation temperature, while no significant differences between both strains were observed. The biomass yields of both strains decreased at increased cultivation temperature whereby the decrease was more pronounced for the unevolved strain. The evolved strain showed a lower biomass yield at 30.0°C and a slightly higher biomass yield at 39.0°C than the unevolved strain. Without the influence of different specific growth rates, both strains responded similarly to the increased cultivation temperature of 39.0°C.

Table 2
Yield of biomass and main products on glucose of CEN.PK113-7D and CEN.PK-EVO during characterisation by chemostat with their standard errors, calculated from the biomass specific conversion rates shown in Table S2. Compared with the unevolved strain at the same temperature, * indicate a significant difference with a p-value (paired T-test) of < 0.05.

mol·mol$_{glucose}$$^{-1}$	CEN.PK113-7D		CEN.PK-EVO	
	30 °C	39 °C	30 °C	39 °C
$Y_{acetate}$	0.006 ± 0.001	0.016 ± 0.003	0.005 ± 0.001	0.012 ± 0.002
$Y_{biomass}$	0.559 ± 0.011	0.374* ± 0.013	0.509 ± 0.017	0.423* ± 0.013
Y_{CO2}	1.70 ± 0.02	1.74 ± 0.07	1.73 ± 0.06	1.71 ± 0.06
$Y_{ethanol}$	1.61 ± 0.02	1.69 ± 0.07	1.64 ± 0.06	1.67 ± 0.06
$Y_{glycerol}$	0.169 ± 0.004	0.115 ± 0.008	0.153 ± 0.006	0.114 ± 0.005
$Y_{lactate}$	0.005 ± 0.001	0.010 ± 0.001	0.007 ± 0.002	0.015 ± 0.001
Y_{malate}	0.002 ± 0.000	0.004 ± 0.000	0.001 ± 0.000	0.004 ± 0.000
$Y_{succinate}$	0.006 ± 0.001	0.025* ± 0.004	0.005 ± 0.001	0.033* ± 0.002

	CEN.PK113-7D	CEN.PK-EVO
30°C	10.44 ± 1.41	9.83 ± 0.83
39°C	5.66* ± 0.51	7.40* ± 1.41

Table 3
Yield of biomass on ATP ($g_{DM}\cdot mol_{ATP}^{-1}$) with their standard errors for the anaerobic chemostat cultures at different temperatures. Compared with the unevolved strain at the same temperature, * indicate a significant difference with a p-value (paired T-test) of < 0.05

From metabolic flux analysis, whereby all measured specific conversion rates were used as input [11], the net ATP consumption rate for growth could be obtained and used to calculate the biomass yield on ATP for all chemostat steady-states (Table 3). The biomass yields on ATP showed similar trends as the biomass yields on glucose; the increase of the cultivation temperature resulted in a decrease of the biomass yield on ATP for both strains whereby the decrease was most pronounced for the unevolved strain. At the same specific growth rate, the evolved strain showed slightly better energetic efficiency of growth than the unevolved strain at 39.0°C.

We also analysed the cellular protein content and the storage carbohydrates accumulation of the chemostat cultures at the different cultivation temperatures (Figure 3a and 3b) to investigate whether the strains had differences in biochemical composition. At the cultivation temperature of 39.0°C, the total protein content of both strains was lower than at 30.0°C. The protein content of the unevolved strain at 30.0°C was higher than that of the evolved strain, while both strains had similar total protein contents at 39.0°C (Figure 3a). Regardless of the cultivation temperatures, the evolved strain contained on average 30% more storage carbohydrates (glycogen + trehalose) than the unevolved strain (Figure 3b). Both strains accumulated more trehalose than glycogen at 39.0°C. However, the strains showed differences at 30.0°C, whereby the unevolved strain accumulated more trehalose than glycogen, whereas the evolved strain had the opposite behaviour.

Figure 3
 a) Total protein
content of chemostat
culture for CEN.PK113-
7D and CEN.PK-EVO
with their standard
deviations at different
temperatures.
b) Storage
carbohydrates
accumulation of
chemostat culture at
30°C and 39°C under
anaerobic condition.
Error bars represents
standard deviations
of average values of
measurements in
biomass sample from
chemostat culture at
four different time
points in steady-state.
Compared with the
unevolved strain at the
same temperature,
* indicate a significant
difference with a
p-value (paired T-test)
of < 0.05.
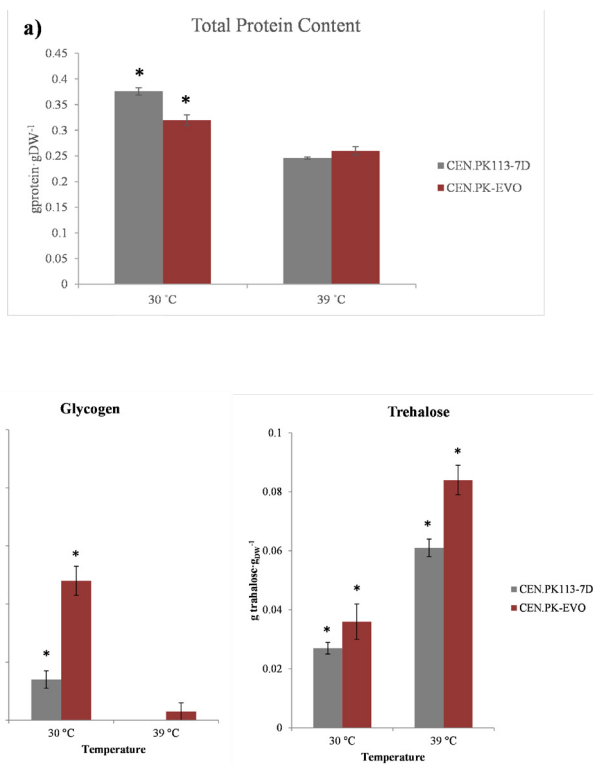
The membrane fluidity of cells is determined by the contents of fatty acids, phospholipids and sterols. These were quantified for both strains grown in steady state chemostat cultures at 30.0 and 39.0 °C (Figure 4a, 4b, 4d, and supplementary Figure S2). The fatty acids of both strains were dominated (>45%) by unsaturated fatty acids (UFA) ($C14:1 + C16:1 + C18:1$), (34 – 40%) saturated fatty acids (SFA) ($C14 + C16 + C18$), and 5 – 11% medium chain fatty acids (MCFA) ($C8-C12$). At increased cultivation temperature (39.0°C), the UFA content remained at a similar level as at 30.0°Cin the evolved strain, but was 9.1% higher than at 30.0°C in the unevolved strain. Compared with at 30.0°C, the SFA increased 15.9% at 39.0°C in the evolved strain, but decreased slightly (5.2%) at 39.0°C in the unevolved strain. In the absence of oxygen at a dilution rate of 0.03 h^{-1} and with glucose as a carbon source, the UFA/SFA ratio in the unevolved strain was 1.43 ± 0.14, whereas in the evolved strain it was 1.26 ± 0.15. The evolved strain showed significant lower ratios of C14:1 (myristoleic acid) /C14 (myrisitic

acid), C16:1 (palmitoleic acid) /C16 (palmitic acid), and C18:1(Oleic acid) / C18 (stearic acid) than the unevolved strain at 39.0°C (Table 4). For both cultivation temperatures, the evolved strain contained a 2-3-fold higher level of C14 than the unevolved strain (Figure 4b). Increased cultivation temperature had a direct effect on the production C16:1 for the evolved strain. The C16:1 composition changed differently between the strains when the cultivation temperature increased. There was a 36.7% increase of C16:1 in the unevolved strain but a 65.2% decrease in the evolved strain, wherein the evolved strain has significantly lower C16:1 than the unevolved strain at 39.0°C (p-value < 0.05) (Figure 4b). The MCFA content in both strains was slightly lower at 39.0°Cthan at 30.0°C; the evolved strain has comparatively higher MCFA content than the unevolved strain at both temperatures, wherein the MCFA in the evolved strain was 52.6% higher at 30.0°C and 32.3% higher at 39.0°C. As shown in Figure 4b, the evolved strain had significantly higher C12 (lauric acid) than the unevolved strain at both cultivation temperatures.

There are two most abundant phospholipids in plasma membranes; phosphatidylcholines (PC) and phosphatidylethanolamine (PE), predominantly distributed on the outer and inner leaflets of the plasma membranes. While the PC composition level remained steady in both strains regardless of cultivation temperatures, the PE composition level varied greatly in the evolved strain at 39.0°C(p-value < 0.05) (supplementary, Figure S2). The unevolved strain at 30.0°C and 39.0°C, as well as the evolved strain at 30.0°C had a PC/PE ratio between 3.0 and 3.3, but the evolved strain at 39.0°C had a ratio of 2.2 (Figure 4c). The increase of PE in the evolved strain at 39.0°C resulted in 25.9% decrease of PC/PE ratio.
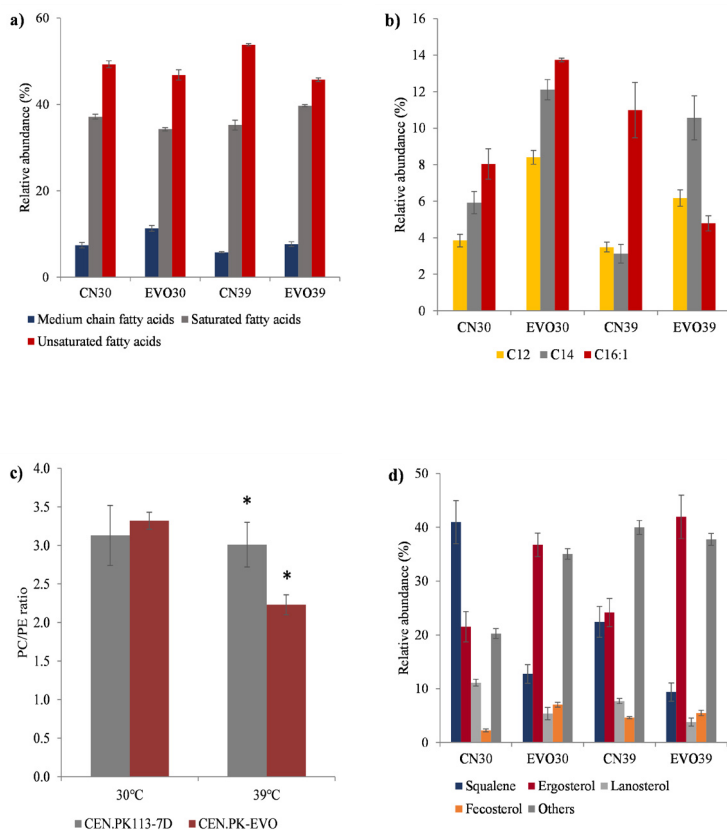
Figure 4

a) The total fatty acids of chemostat culture at 30.0°C and 39.0°C for both the unevolved and evolved strains, according to Table S9: the medium chain fatty acids (C8-C12), the saturated fatty acids (C14 + C16 + C18), and the unsaturated fatty acids (C14:1 + C16:1 + C18:1). The relative abundance (%) based on the total sum of the identified fatty acids in each strain which was normalized by the weight of the sample analysed.

b) Fatty acids composition (C12, C14, and C16:1) of the chemostat culture at 30.0°C and 39.0°C for both unevolved and the evolved strains, according to Table S9. The relative abundance based on the total sum of the identified fatty acids in each strain which was normalized by the weight of the sample analysed.

c) The phosphatidylcholines (PC) / phosphatidylethanolamine (PE) ratio of chemostat culture at 30.0°C and 39.0°C for both unevolved and the evolved strains. The ratio was calculated from the measurements of phospholipids shown in Figure S2.

d) The sterols compositions of chemostat culture at 30.0°C and 39.0°C for both the unevolved and evolved strains. The standard deviation of all graphs based on three independent samples collected at three different time points during the steady state chemostat. Compared with the unevolved strain at the same temperature, *indicate a significant difference with a p-value (ANOVA and Tukey HSD test, α=0.05, n=3) of < 0.05.

From the sterol's composition measurements shown in Figure 4d, significant differences in sterols composition were observed between the unevolved and the evolved strain. The evolved strain had significantly higher ergosterol and fecosterol levels than the unevolved strain (p-value < 0.05). The evolved strain had 1.7-fold higher ergosterol level than the unevolved strain at both cultivation temperatures. The evolved strain had 3.1-fold higher fecosterol level at 30.0°C and 1.2-fold higher at 39.0°C than the unevolved strain. There were also significantly lower levels of lanosterol and squalene observed in the evolved strain. Compared to the unevolved strain, the evolved strain had 2-fold lower lanosterol level at both cultivation temperatures, whereas 3.2-fold lower squalene level at 30.0°C and 2.4-fold lower at 39.0°C.

	CEN 30	EVO 30	CEN 39	EVO 39
C14:1/C14	0.029 ± 0.08	0.199 ± 0.06	0.053 ± 0.10	0.022 ± 0.17
C16:1/C16	0.27 ± 0.06	0.07 ± 0.03	0.35 ± 0.08	0.17 ± 0.06
C18:1/C18	25.7 ± 0.09	12.2 ± 0.06	97.9 ± 0.06	27.9 ± 0.08

Table 4
The ratio of UFA (C14:1, and C16:1, and C18:1) and SFA (C14, C16, and C18) for the chemostat culture of the unevolved and evolved strains at 30.0°C and 39.0°C. The standard deviation based on three independent samples collected at three different time points during the steady state chemostat. CN30 and CN39 indicated as the chemostat culture of CEN.PK113-7D at 30.0°C and 39.0°C, respectively. EVO30 and EVO39 indicated as the chemostat culture of CEN.PK-EVO at 30.0°C and 39.0°C, respectively. Compared with the unevolved strain at the same temperature, all fatty acids indicate a significant difference with a p-value (ANOVA and Tukey HSD test, α=0.05, n=3) of < 0.05.

3.4 Genomic analysis of CEN.PK-EVO

The genomes comparison approximation between the unevolved and evolved strains against S288c reference genome is useful for SNPs, duplications and deletions detection, but assumes that the genomes of the analysed strains are collinear with S288c reference, thus the possible variations in genome structure (translocations, inversions) would not be detected. We first processed the coverage files obtained for the two strains and represented chromosome coverage for each of the 16 chromosomes of both strains (supplementary, Figure S1). This first analysis showed that chromosomes I, III, and IV had increase of their coverage, but no significant differences were observed in the coverage of the rest of the chromosomes. In addition, no copy number variation nor big aneuploidies were observed among the unevolved and

evolved strain. A very low coverage of the mitochondrial genome was detected in the evolved strain (data not shown). We then identified the SNPs present in the genomes of both strains. We annotated the number of positions in the genome with only one allele variant (homozygous alternative positions) and with two allele variants (heterozygous) by using VCFtools. In both strains, the ratio of homozygous and total positions (heterozygous + homozygous) was high (99.18% and 99.33% for CEN.PK113-7D and CEN.PK-EVO. SNVs frequency analysis from the genome sequencing results compared with the S288c reference strain indicated that both strains are highly homozygous. This result is congruent with the results of the DNA quantification by flow cytometry (supplementary, Table S5), indicating that both CEN.PK113-7D and CEN.PK-EVO are haploid strains. The low level of heterozygous position indicated by VCFtools is most probably caused by read sequencing or mapping errors. Furthermore, the evolved strain seemed to be free of big genomic rearrangements or chromosomic aneuploidies (Figure 5), but it contains changes in its genome in terms of single nucleotide variants (SNVs) and small insertions and deletions (InDels). Figure 5 shows the distribution of SNVs along the genome of the evolved strain compared with the unevolved strain, wherein different colours indicate their genomic consequence. There were in total 440 positions with a quality higher than 200 which is our minimum base quality in the phred-scaled quality score. These positions were analysed by using Variant Effect Predictor (Ensembl). This tool showed that the SNPs can be associated with 390 variants. The analysis of the SNVs of the evolved strain which are located in coding regions gave as a result a total of 286 SNVs (supplementary, Table S6). Of 286 SNVs 13 correspond to stop codons (red) and 199 to non-synonymous variants (orange), respectively. To validate these variants, we used IGV to perform a visual inspection and confirmed 13/13 stop codons and 178/199 non-synonymous variants, thus resulting in 191 SNV's with possible high and moderate phenotypic consequences. We annotated these positions and displayed the exact position of each one of the SNPs present in coding positions in supplementary Table S6. They were spread over all the 16 chromosomes.
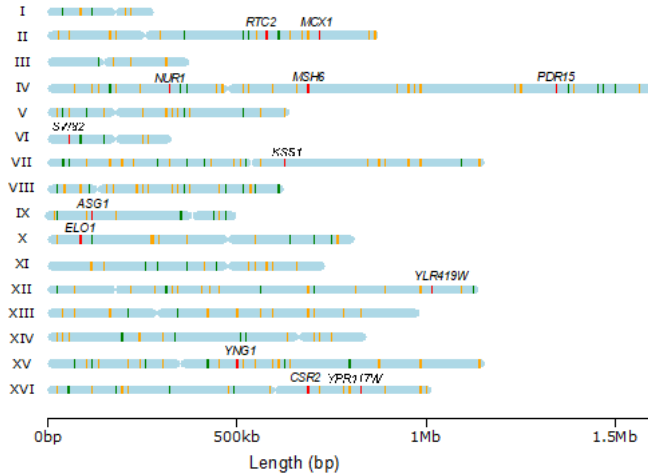
Figure 5
Genome-wide
representation of the 16
chromosomes of CEN.
PK-EVO strain by using
R package chromoMap.
Using the reference
genome (*S. cerevisiae*
S288c) for the length of
the chromosomes, SNPs
positions with coding
consequences which
present in CEN.PK-EVO
strain but not in CEN.
PK113-7D are marked in
different colours; green
indicates synonymous
variants; orange indicates
missense variants; red
indicates stop gains in
gene, of which with a stop
gain the name of the 13
genes are indicated.

With the 191 SNVs associated with high or moderate effects, we performed Gene Ontology (GO) enrichment analysis to identify enriched groups of genes related to specific biological processes. The analysis resulted in a large number of significant (p-value < 0.05) functional categories associated with biological processes involving the signalling and regulation of the target of rapamycin complex 1 (TORC1) processes, chromosome organisation and telomere maintenance and processes related to DNA repair and cell cycle (Figure 6a). Among these categories, it is noteworthy to mention the mutations in six genes (*GCN1*, *NPR2*, *PMA1*, *PSR2*, *SEA4*, and *WHI2*) involved in TORC1 processes (supplementary, Table S7). *NPR2*, *PSR2*, *SEA4*, and *WHI2* regulate the inhibition of TORC1 in response to limited amino acid availability [38–40]. *GCN1* encodes a trans-acting positive effector which is required for the phosphorylation of the alpha subunit of initiation factor 2 (eIF2) by protein kinase GCN2P for down-regulation of protein synthesis under stress and nutrient limited conditions [41,42]. *PMA1* encodes the major plasma membrane H+-ATPase which pumps protons out of the membrane to maintain the cytoplasmic pH and to facilitate the import of nutrients into cells, and its expression was positively correlated to activation of TORC1 signalling in response to glucose availability [43]. All these genes contribute to the regulation of cell growth.

*3.4.1
Enrichment
analysis for the
SNVs with high
or moderate
consequences*

Figure 6
Gene Ontology
biological process
terms enrichment
(a) and pathway
enrichment
(b) retrieved from
the list of genes
with SNVs (Single
nucleotide variants)
which cause moderate
or high impact. The
numbers of genes with
SNVs that belong to
each GO term were
indicated in a, based
on Table S7). The name
of the genes included
in each enriched
pathway is shown in
b, based on Table S8).
Enriched GO and
pathways shown in
the bar graph have
their adjusted p.values
(Benjamini Hochberg)
lower than 0.05.

Pathway enrichment analysis of the 191 SNV's (Figure 6b) revealed some biological pathways related with fatty acids (FAS1) and phospholipids biosynthesis (CHO1 and PSD2), phosphatidylethanolamine biosynthesis (CHO1 and PSD2), de novo biosynthesis of pyrimidines (URA7 and URA6), and urea degradation (DUR1,2). We used ammonia as a main nitrogen in the cultivation medium of this study and thus do not consider the mutations in genes DUR1 and DUR2 contributed significantly to improve the growth performance of the evolved strain at supra-optimum temperatures.

Thirteen genes of the evolved strain were considered high impact variants, as each of them acquired a mutation which resulted in a stop codon in their sequence making them non-functional (supplementary, Table S6). One of these genes was *ELO1*, elongase I, which catalyses the elongation of unsaturated C12-C16 fatty acil-CoA to C16-C18 fatty acids [44]. Another gene which acquired a stop codon was *ASG1* which encodes a zinc cluster protein proposed to be a transcriptional regulator involved in stress response [45]. There were also two genes, *KSS1* and *MSH6*, involved in cell cycle regulation. The gene *KSS1* encodes the mitogen-activated kinase (MAPK) which activates the invasive response of haploid yeast cells under nutrient limiting conditions [46]. The gene *MSH6* is involved in the DNA mismatch repair system during mitosis and meiosis of budding yeast.

3.4.2
Stop codon as a consequence of the SNVs

We found multiple missense changes in three genes in the evolved strain namely, *GLT1*, *YTA7* and *ACE2* (supplementary, Table S6). The GLT1 gene is a glutamate synthase (GOGAT) which synthesizes glutamate from glutamine and alpha-ketoglutarate. Its expression is controlled by the nitrogen source. *ACE2* is a transcription factor required for septum destruction after cytokinesis and *YTA7* has a role in regulation of histone gene expression.

3.4.3
Genes with more than one mutation in the evolved strain

137

The possible InDels of different chromosome regions that were obtained by comparing coverage values of the evolved strain with the unevolved strain using CNVnator. CNVnator normalizes the coverage values to 1, if the resulting number of coverages has deviated from these values, there is a putative deletion or duplication in the region. In this sense, we found 3 duplicated regions in the evolved strain's genome, all of them corresponding to sub-telomeric regions in chromosomes V, X and XVI. There is limited information about the genes in the sub-telomeric regions because they contain repeat sequences and are genomic hot spots of recombination which increase the challenge for sequence mapping and annotation [47]. The region located in the right arm of chromosome XVI presented a size of 55800 bp and a CNVnator coverage value of 4.11729 (supplementary, Figure S1). This region includes some interesting genes associated with thermotolerance such as AQY1 and OPT2. AQY1 is an aquaporin involved in the transport of water across cell membranes [48,49], while OPT2 is an oligopeptide transporter that affects glutathione redox homeostasis and has a role in maintenance of lipid asymmetry

3.4.4
Segmental duplication events in the evolved strain

between the inner and outer leaflets of the plasma membrane. The duplicated regions in chromosome V and X are smaller, 17600 and 35200 bp, respectively, but their coverage values are 6.6 and 5.1 times higher than the mean coverage obtained in chromosome V and X, respectively. It is noteworthy to mention the gene OPT1, a proton-coupled oligopeptide transporter of the plasma membrane involved in the glutathione and phytochelatin transport.

4
Discussion

Adaptive laboratory evolution (ALE) of *S. cerevisiae* CEN.PK113-D in an automated anaerobic SBR at increasing cultivation temperature resulted in a stable isolate, CEN.PK-EVO, better adapted to unlimited growth in batch culture at a supra-optimal temperature of almost 40°C. An important aspect in the design of ALE experiments is to make sure that, in addition to the intended selection pressure, no additional unintended selection pressures are applied. Compared to manual daily transfers as e.g. performed during ALE in shake flasks, the advantage of an automated SBR system is that the stationary phase is kept as short as possible because a new batch is started immediately after the previous one has ended, thus avoiding the specific selection of mutants surviving better during glucose starvation instead of faster growing cells. To avoid selection of aggregate forming, fast-sedimenting mutants, as was observed by Oud et al. [50], draining of the culture broth at the end of each cycle was performed from the bottom, at the lowest point of SBR vessel. This successfully avoided the development of a fast-sedimenting phenotype because aggregates were preferentially removed during draining of the SBR after each batch. Nevertheless, the whole genome sequencing of our evolved strain revealed two missense mutations in ACE2 (supplementary, Table S6). Oud et. al showed that mutations in ACE2 in the CEN.PK113-7D strains evolved on galactose as a sole carbon source resulted in premature stop codons in ACE2 which, in combination with whole genome duplication, attributed to a fast-sedimenting phenotype. Whole genome duplication did not occur in our evolved strain, although genome duplication is claimed to be one of the strategies for rapid adaptation during evolution [51]. We did not isolate and sequence the intermediate population during adaptive evolution, so we cannot confirm how the mutation events of the evolved strain accumulated, but probably some intermediate states presented aneuploidies which could have led to the SNVs we found [52].

Although higher coverage numbers above the mean coverage value of the genome were observed in chromosomes I, III, and VI in the evolved strain (Figure S1), it is difficult to conclude whether the evolved strain suffered some aneuploidy in its genome. Regarding the ploidy estimation by flow cytometry (Table S5), the evolved strain showed the same DNA content as the S288c strain (haploid reference strain). In this sense, and taking into account the ploidy estimation chromosomes I, III, and VI are the smallest in S. cerevisiae (≤450kb) compared to the other chromosomes (Figure 5). Their smaller size could lead to an overrepresentation of their reads during the Illumina sequencing. Together with the comparatively higher GC content, these three chromosomes would also cause better fragmentation during the library preparation [53]. Both facts could cause higher coverage numbers compared to the rest of the chromosomes and causing artefacts during the library preparation and sequencing process. Similar observations were also found in the study of Morard et al. 2019 who observed that diploid *S. cerevisiae* strain T73 showed higher coverages in chromosomes I, III, and VI, but the SNPs frequency data clearly indicated that T73 was a diploid strain [54]. If the T73 strain would have been a triploid strain, the SNPs frequency of all chromosomes would have been either 0.33 or 0.66 instead of 0.5. As CEN.PK113-7D is a haploid strain, in the plausible scenario of a diploidization with additional copy of these three chromosomes, no SNPs could be used to verify the ploidy of the evolved strain. However, due to the possibility of both situations explaining the increased coverage, the sporulation capacity of the evolved strain together with the confirmation of the ploidy value could give insights into the genome of the evolved strain. Furthermore, a very low coverage of the mitochondrial genome detected in the evolved strain could indicate the loss of the mitochondria, which may lead to a trade-off growing in aerobic conditions due to the petite phenotype which cannot grow in non-fermentable carbon source (e.g., glycerol) [55].

Further physiological characterization of our evolved and unevolved strains in glucose limited chemostat cultures at 30.0°C and 39.0°C showed a very similar behaviour. For both strains the yields of biomass on glucose and ATP were lower during chemostat cultivation at 39.0°C compared to 30.0°C. However, for the unevolved strain the decrease of the ATP yield (46%) was more pronounced than for the unevolved strain (25%), most probably caused by the severe cell damage and resulting

high death rate of the unevolved strain at 39 °C. As a comparison to the previous study, the high temperature tolerant strain Ethanol Red which was grown in identical chemostat cultures, only showed a 13% decrease in the biomass yield on ATP when grown at 39.0°C instead of 30.0°C [11]. Therefore, this strain appears better adapted to cultivation at supra-optimal temperatures than CEN.PK-EVO.

The biomass yields of both strains during chemostat cultivation were significantly lower than during SBR cultivation at high temperature. The main reason for this is that the growth rate during chemostat cultivation was much lower than during SBR cultivation (7.7-fold for the evolved strain), resulting in a higher impact of maintenance energy requirements on the biomass yield during chemostat cultivation (calculations for the evolved strain in supplementary material).

Both strains produced acids during anaerobic SBR cultivation, wherein the main acids by-products were acetate and succinate. It is known that the presence of weak acids results in additional ATP dissipation because the undissociated species diffuse into the cells at the cultivation pH of 5, whereafter the dissociation of acids occurs at the near neutral pH in the cytosol. To avoid acidification of the cytosol, the anion plus the corresponding proton(s) are exported at the expense of ATP resulting in an ATP dissipating futile cycle. For concentrations up to 5 mM the additional ATP dissipation caused by diffusion into and active export from the cells of acetate is very limited in yeast, while for succinate this is even negligible [14]. Therefore, weak acid uncoupling was considered not to have played a major role in the behaviour of both strains during chemostat cultivation at elevated temperatures as in that case the acid concentrations were lower (supplementary, Table S5). We did not measure the final concentrations of the acid products in SBR cultivation of both strains, but the acetate concentrations of both strains during the late exponential phase of the SBR cultivation were below 5mM (data not shown).

To identify possible mechanisms behind high temperature tolerance, the evolved and unevolved CEN.PK113-7D strains were sequenced. Genomic analysis revealed that around 75% (133) of the 178 SNVs found in the evolved strain were caused by a nucleotide change to either guanine or thymine (supplementary,

Table S6). We hypothesize that the acquired mutation *MSH6-2559G>C*, which resulted in a stop codon at position 853 of the native protein and resulted in inactivation of *MSH6*, may have contributed to an increment of the mutation rate. *MSH6* encodes a protein required for mismatch repair in mitosis and meiosis [53,54]. The early termination of the protein resulted in the loss of the ATP binding domain located between position 982 and 989 of the native *MSH6*. This ATP binding domain is essential for the formation of the ternary complex where the interaction between the MutS alpha complex and the mismatch DNA takes place for the DNA mismatch repair system [54,55]. As a result, the malfunction of *MSH6* could possibly have increased the mismatch binding of either guanine or thymine during ALE and thus could have facilitated the occurrence of more than half of the SNV's identified.

The evolved strain had a significantly lower death rate (Table 1) than the unevolved strain during SBR cultivation at 39.8°C, which contributed to its improved thermo-tolerance. Regulation of cell death in yeast can occur in various ways [56], such as apoptosis and autophagy. From the enrichment analysis for the SNVs of the evolved strain (Figure 6), the mutations which possibly have attributed to lower cell death might be involved in modulating TORC1 processes. Active TORC1 stimulates anabolic processes and thus promotes cell growth and antagonizes processes involved in stress response [57]. TORC1 is inhibited by a wide range of environmental stresses, such as heat shock. Four genes containing mutations (*NPR2*, *PSR2*, *SEA4*, *WHI2*) regulate TORC1 activity in nutrient uptake under poor nutrient conditions. The translated proteins *NPR2* and *SEA4* are part of the SEA complex which regulates TORC1 in response to nitrogen starvation [58,59]. The SEA complex consists of two subcomplexes, named the SEA subcomplex inhibiting TORC1 (SEACIT) and the SEA subcomplex activating TORC1 (SEACAT) [59]; *NPR2* is a subunit of the SEACIT subcomplex, whereas *SEA2* is of the SEACAT subcomplex. *NPR2* is also identified as GTPase activating complex localized at the vacuolar membrane and controls the activation of MEP2 activity and thus facilitates ammonium transport activity [60]. Phosphorylated *NPR2* (inactive) triggers the endocytosis/degradation of non-preferable amino acid permeases in the plasma membrane under the condition that more preferred nitrogen sources are available [61]. *NPR2* is one of the upstream regulators of TORC1 kinase

and inhibits TORC1 and activates autophagy, whereas *SEA4* is localized in the cytoplasm and might be required in the autophagy pathway. However, the exact mechanism is still not clear [62]. One of the consequences of nitrogen starvation is autophagy, a process when cytoplasmic components are sequestered into autophagosomes and delivered into the vacuole/lysosome for degradation, thereby recycling nutrients for cell growth [63]. WHI1 binds to PSR1 and *PSR2* to inhibit TORC1 activity and activates the plasma membrane ammonium permease [38]. Besides, *WHI2* and *PSR1* work together to activate the STRE-mediated gene expression which was shown essential to suppress heat shock sensitivity [64]. Although the direct consequences of the mutations found at the four genes towards TORC1 activity cannot be proven yet, it is very likely that they take part in the regulation of TORC1 under thermal stress conditions for cell death and in return for the very significant reduction of the death rate of the evolved strain during SBR cultivation at 39.8°C.

The evolved strain showed significantly less cells with visible membrane damage (Figure 2) than the unevolved strain during the SBR cultivation at 39.8°C, contributing to the deceased death rate. Genes *URA6* and *URA7*, involved in the de novo biosynthesis of pyrimidine ribonucleotides, contained missense mutations in the evolved strain. Pyrimidine and purine nucleotides are the essential components required in metabolic pathways for cell growth [65]. *URA6* encodes uridine-monophosphate kinase which catalyses the conversion of uridine/cytidine monophosphate to uridine/cytidine diphosphate, whereas URA7 encodes cytidine triphosphate synthetase which catalyses the conversion of around 78% of total uridine triphosphate (UTP) to cytidine triphosphate (CTP) [66]. CTP is not only a precursor for nucleic acids formation but also for phospholipid synthesis in *S. cerevisiae* [67,68].

While protein synthesis is an energy expensive process, the better energy efficiency of growth of the evolved strain at 39.0°C (Table 3) was not caused by a lower total protein content of the biomass. Although there were two missense mutations in *GLT1* of the evolved strain (supplementary, Table S6) which catalyses the formation of the universal donor (glutamate) for amino acids biosynthesis, these did not lead to changes in the total protein content of the evolved strain compared to the unevolved strain at 39.0°C (Figure 3a). At an identical growth rate during steady

state chemostat cultivation, the evolved strain had a 37.7% higher trehalose content than the unevolved strain during growth at 39.0°C (Figure 3b). It has been reported that there is a strong correlation between the cellular trehalose content and tolerance to temperature stress due to the multiple roles of trehalose in heat-denatured protein repair [7,69] and cell-membrane protection under temperature stress conditions [70–72]. The mechanism through which trehalose assists heat shock proteins (*HSP104*) to restore protein refolding in the endoplasmic reticulum is still not well understood. The higher cellular trehalose content in the evolved strain plausibly protects the structure of the cell membrane by lowering the water activity at the lipid bilayer during temperature stress [73], which could explain the lower death rate and higher biomass yield of the evolved strain at 39.0°C (Table 2). Besides, the copy number variation of *AQY2* found in the evolved strain in chromosome XVI could possibly increase the efflux of water in cells which may also be beneficial in lowing the water activity in cells. Higher levels of aquaporins (AQY2) in the plasma membrane could reduce ice crystal formation upon freezing by lowering the water activity within yeast cells [74]. Exposure to high temperatures results in increasing water mobility within cells, while the permeability of the cell membrane is also enhanced due to increased membrane fluidity. Since trehalose is an effective osmoprotectant[75], the interaction of trehalose with the phospholipids within the cell membrane can maintain the integrity of the cell membrane during heating.

Multiple genes with mutations found in the evolved strain may contribute to the better cell membrane integrity, lower cell death and in return improved cell growth at the high temperature cultivation. Genes CHO1 and PSD2 present in phosphatidylethanolamine (PE) biosynthetic process had mutations in the evolved strain. PE is one of the most abundant phospholipids in biological membranes, concretely the second most abundant phospholipid in yeast membranes [76]. The significantly increased level of PE, resulting a lower PC/PE ratio, observed in the chemostat culture of the evolved strain at 39.0°C (Figure 4c) could benefit in maintaining the intrinsic membrane curvature and facilitate membrane fusion and fission at high temperature because PE can form nonbilayer structure to counteract the negative curvature due to the low bilayer-to-hexagonal phase transition temperature (TH) which indicates the high bilayer compatible [77,78]. The increase of PE is in

agreement with the significant increase of cells in the evolved strain at 39.9°C with intact membranes (Figure 2). PE also serves multiple important cellular functions as autophagy, cell division and protein folding [79,80]. On the other hand, PE is required for the delivery of cytoplasmic proteins to vacuole by autophagy by the formation of autophagosomes [81]. PE also represents a precursor for the synthesis of several protein modifications and it is an intermediate in the synthesis of other glycerophospholipid classes [82].

Another gene that had a mutation and that is annotated in the fatty acids biosynthesis is FAS1. FAS1 is a beta subunit of fatty acid synthetase; this complex catalyses the synthesis of long-chain saturated fatty acids. Fatty acids are essential components of yeast cells for membrane synthesis, energy storage and protein modification [83]. It has been stated that growth at high temperatures is correlated with increased saturation of the lipids of yeast cell membranes [9,84] and increased degree of fatty acids saturation with a decreased length of the fatty acyl chain [85]. The significant increase of SFA and decrease of UFA resulted in a lower UFA/SFA ratio in the evolved strain at 39.0°C (Figure 4a) allowing the maintenance of the membrane fluidity at high temperature. It has been shown that anaerobic growth promotes the production of MCFA [86]. At hight temperature the acyl chain disorder increases and caused the decrease of the bilayer thickness [78]. The membrane comprise of UFA is slightly thinner than that comprise of SFA because SFA is more ordered and compact in a high fluidity phase at high temperature. The significant increase of SFA in the evolved strain (Figure 4a) rigidified the plasma membrane and maintained the membrane fluidity at high temperature. The mutation in *ELO1136G>A* of the evolved strain resulted in a stop codon at position 46 of the protein ELO1 which could have resulted in a commensurate reduction of C16:1 at 30.0°C and 39.0°C (Figure 4b). The difference of sterol composition in the evolved strain also revealed the difference in cytoskeleton organisation compared to the unevolved strain. Caspeta et al showed a significantly increased level of fecosterol in a *S. cerevisiae* evolved strain due to an alternation from ergosterol attributed to improve thermotolerance [10]. We also observed an increased level of fecosterol in the evolved strain, but the relative abundance was below 10% and the increase of the fecosterol level in the evolved strain was more pronounced at 30.0°C than at 39.0°C compared to the unevolved strain. On the other hand, at

145

39.0°C a 1.7-fold higher ergosterol content was observed in the evolved strain, which was 42% of the total sterol composition and seems to bestow better thermotolerance of the evolved strain. It should be noted that ergosterol and tween 80 were supplemented to the media as a source of sterol and UFA for anaerobic growth, because their synthesis reactions are oxygen dependent [87,88]. However, it has been shown recently that the anaerobic growth of *S. cerevisiae* did not depend on the supplementation of UFA [89]. It is not clear if the increased level of ergosterol was caused by increased uptake from medium or by a yet unknown pathway under anaerobic conditions. Since the evolution experiment was not carried out multiple times, we could not identify mutations without phenotypic consequences. Therefore, the results of the whole genome sequencing provided only suggestions for possible mechanisms attributing to the enhanced thermotolerance of the evolved strain.

5
Conclusion

We have obtained CEN.PK-EVO with improved growth performance at 39.8°C after 475 generations in the anaerobic SBR with stepwise increasing cultivation temperatures. The whole genome sequencing indicated that the unevolved and evolved strain had similar copies of chromosome and aneuploidies, but there were mutations, such as SNVs and INDELS, in the genome of the evolved strain. Several SNVs found in the evolved strain were associated with the TORC1 pathway and the biosynthesis of the components of the cell membrane, such as phospholipids and fatty acids. These mutations plausibly modulate the regulation of cell death and benefit the evolved strain to maintain membrane integrity during growth at supra-optimal temperatures. Therefore, these could possibly explain the lower death rate and in return higher biomass yield on glucose, as well as fewer cells with membrane rupture during the SBR cultivation of the evolved strain at 39.8°C. Without the influence of the specific growth rate, the chemostat culture of the evolved strain at 39.0°C also showed a slightly higher biomass yield than the unevolved strain, possibly caused by the 37.7% increase of trehalose accumulation. The cell membrane is the first barrier for physical contact to temperature changes, and therefore, it is a well-known target for improving thermotolerance of yeast cells. Elucidating the mechanism of cell death caused by thermal stress can help identifying other potential targets. In order to unravel the impacts of the genomic changes and the cause of the lower cell death in the evolved strain, we need to further analyse the changes on the proteomic level. This knowledge will allow us to pinpoint the genomic and metabolic changes which benefit CEN.PK-EVO to cope with the heat stress under anaerobic conditions.

148

References

[1]   A. Tesfaw, F. Assefa, Current Trends in Bioethanol Production by Saccharomyces cerevisiae: Substrate, Inhibitor Reduction, Growth Variables, Coculture, and Immobilization, International Scholarly Research Notices. 2014 (2014) e532852. https://doi.org/10.1155/2014/532852.

[2]   A. Kumar, R. Deb, J. Singh, Bioethanol Production from Renewable Biomass by Yeast, in: P. Gehlot, J. Singh (Eds.), Fungi and Their Role in Sustainable Development: Current Perspectives, Springer, Singapore, 2018: pp. 427–448. https://doi.org/10.1007/978-981-13-0393-7_24.

[3]   Z. Salvadó, F.N. Arroyo-López, J.M. Guillamón, G. Salazar, A. Querol, E. Barrio, Temperature Adaptation Markedly Determines Evolution within the Genus Saccharomyces, Appl. Environ. Microbiol. 77 (2011) 2292–2302. https://doi.org/10.1128/AEM.01861-10.

[4]   Y. Yang, M.R. Foulquié-Moreno, L. Clement, É. Erdei, A. Tanghe, K. Schaerlaekens, F. Dumortier, J.M. Thevelein, QTL Analysis of High Thermotolerance with Superior and Downgraded Parental Yeast Strains Reveals New Minor QTLs and Converges on Novel Causative Alleles Involved in RNA Processing, PLoS Genet. 9 (2013). https://doi.org/10.1371/journal.pgen.1003693.

[5]   Z. Wang, Q. Qi, Y. Lin, Y. Guo, Y. Liu, Q. Wang, QTL analysis reveals genomic variants linked to high-temperature fermentation performance in the industrial yeast, Biotechnology for Biofuels. 12 (2019) 59. https://doi.org/10.1186/s13068-019-1398-7.

[6]   M.A. Singer, S. Lindquist, Thermotolerance in Saccharomyces cerevisiae: the Yin and Yang of trehalose, Trends in Biotechnology. 16 (1998) 460–468. https://doi.org/10.1016/S0167-7799(98)01251-7.

[7]   M. Simola, A.-L. Hänninen, S.-M. Stranius, M. Makarow, Trehalose is required for conformational repair of heat-denatured proteins in the yeast endoplasmic reticulum but not for maintenance of membrane traffic functions after severe heat stress, Molecular Microbiology. 37 (2000) 42–53. https://doi.org/10.1046/j.1365-2958.2000.01970.x.

[8]   A. Satomura, N. Miura, K. Kuroda, M. Ueda, Reconstruction of thermotolerant yeast by one-point mutation identified through whole-genome analyses of adaptively-evolved strains, Sci Rep. 6 (2016). https://doi.org/10.1038/srep23157.

[9]   E.L. Steels, R.P. Learmonth, K. Watson, Stress tolerance and membrane lipid unsaturation in Saccharomyces cerevisiae grown aerobically or anaerobically, Microbiology,. 140 (1994) 569–576. https://doi.org/10.1099/00221287-140-3-569.

[10]   L. Caspeta, Y. Chen, P. Ghiaci, A. Feizi, S. Buskov, B.M. Hallström, D. Petranovic, J. Nielsen, Altered sterol composition renders yeast thermotolerant, Science. 346 (2014) 75–78. https://doi.org/10.1126/science.1258137.

[11]   K.Y.F. Lip, E. García-Ríos, C.E. Costa, J.M. Guillamón, L. Domingues, J. Teixeira, W.M. van Gulik, Selection and subsequent physiological characterization of industrial Saccharomyces cerevisiae strains during continuous growth at sub- and- supra-optimal temperatures, Biotechnology Reports. 26 (2020) e00462. https://doi.org/10.1016/j.btre.2020.e00462.

[12]   T. Pinheiro, K.Y.F. Lip, E. García-Ríos, A. Querol, J. Teixeira, W. van Gulik, J.M. Guillamón, L. Domingues, Differential proteomic analysis by SWATH-MS unravels the most dominant mechanisms underlying yeast adaptation to non-optimal temperatures under anaerobic conditions, Scientific Reports. 10 (2020) 22329. https://doi.org/10.1038/s41598-020-77846-w.

[13]   D.A. Skelly, P.M. Magwene, Population perspectives on functional genomic variation in yeast, Brief Funct Genomics. 15 (2016) 138–146. https://doi.org/10.1093/bfgp/elv044.

[14]   C. Verduyn, E. Postma, W.A. Scheffers, J.P. van Dijken, Physiology of Saccharomyces Cerevisiae in Anaerobic Glucose-Limited Chemostat Culturesx, Microbiology. 136 (1990) 395–403. https://doi.org/10.1099/00221287-136-3-395.

[15]   X. Hakkaart, Y. Liu, M. Hulst, A. el Masoudi, E. Peuscher, J. Pronk, W. van Gulik, P. Daran-Lapujade, Physiological responses of Saccharomyces cerevisiae to industrially relevant conditions: Slow growth, low pH, and high CO_2 levels, Biotechnol Bioeng. 117 (2020) 721–735. https://doi.org/10.1002/bit.27210.

[16]   M.R. Mashego, W.M. van Gulik, J.L. Vinke, J.J. Heijnen, Critical evaluation of sampling techniques for residual glucose determination in carbon-limited chemostat culture of Saccharomyces cerevisiae, Biotechnol. Bioeng. 83 (2003) 395–399. https://doi.org/10.1002/bit.10683.

[17]   A. l. b. Cruz, A. j. Verbon, L. j. Geurink, P. j. t. Verheijen, J. j. Heijnen, W.M. van Gulik, Use of sequential-batch fermentations to characterize the impact of mild hypothermic temperatures on the anaerobic stoichiometry and kinetics of Saccharomyces cerevisiae, Biotechnol. Bioeng. 109 (2012) 1735–1744. https://doi.org/10.1002/bit.24454.

[18]   S.L. Tai, P. Daran-Lapujade, M.A.H. Luttik, M.C. Walsh, J.A. Diderich, G.C. Krijger, W.M. van Gulik, J.T. Pronk, J.-M. Daran, Control of the Glycolytic Flux in Saccharomyces cerevisiae Grown at Low Temperature A MULTI-LEVEL ANALYSIS IN ANAEROBIC CHEMOSTAT CULTURES, J. Biol. Chem. 282 (2007) 10243–10251. https://doi.org/10.1074/jbc.M610845200.

[19]   R.T.J.M. van der Heijden, J.J. Heijnen, C. Hellinga, B. Romein, K.C.A.M. Luyben, Linear constraint relations in biochemical reaction systems: I. Classification of the calculability and the balanceability of conversion rates, Biotechnology and Bioengineering. 43 (1994) 3–10. https://doi.org/10.1002/bit.260430103.

[20]   R.T.J.M. van der Heijden, B. Romein, J.J. Heijnen, C. Hellinga, K.C.A.M. Luyben, Linear constraint relations in biochemical reaction systems: II. Diagnosis and estimation of gross errors, Biotechnology and Bioengineering. 43 (1994) 11–20. https://doi.org/10.1002/bit.260430104.

[21]   H.C. Lange, J.J. Heijnen, Statistical reconciliation of the elemental and molecular biomass composition of Saccharomyces cerevisiae, Biotechnol. Bioeng. 75 (2001) 334–344. https://doi.org/10.1002/bit.10054.

[22]   A.B. Canelas, A. ten Pierick, C. Ras, R.M. Seifar, J.C. van Dam, W.M. van Gulik, J.J. Heijnen, Quantitative Evaluation of Intracellular Metabolite Extraction Techniques for Yeast Metabolomics, Anal. Chem. 81 (2009) 7379–7389. https://doi.org/10.1021/ac900999t.

[23]   H.C. Lange, M. Eman, G. van Zuijlen, D. Visser, J.C. van Dam, J. Frank, M.J. de Mattos, J.J. Heijnen, Improved rapid sampling for in vivo kinetics of intracellular metabolites in Saccharomyces cerevisiae, Biotechnol. Bioeng. 75 (2001) 406–415. https://doi.org/10.1002/bit.10048.

[24]   L. Wu, M.R. Mashego, J.C. van Dam, A.M. Proell, J.L. Vinke, C. Ras, W.A. van Winden, W.M. van Gulik, J.J. Heijnen, Quantitative analysis of the microbial metabolome by isotope dilution mass spectrometry using uniformly 13C-labeled cell extracts as internal standards, Analytical Biochemistry. 336 (2005) 164–171. https://doi.org/10.1016/j.ab.2004.09.001.

[25]   D. Visser, G.A. van Zuylen, J.C. van Dam, A. Oudshoorn, M.R. Eman, C. Ras, W.M. van Gulik, J. Frank, G.W.K. van Dedem, J.J. Heijnen, Rapid sampling for analysis of in vivo kinetics using the BioScope: A system for continuous-pulse experiments, Biotechnology and Bioengineering. 79 (2002) 674–681. https://doi.org/10.1002/bit.10328.

[26]   A. Querol, E. Barrio, T. Huerta, D. Ramón, Molecular Monitoring of Wine Fermentations Conducted by Active Dry Yeast Strains, Appl Environ Microbiol. 58 (1992) 2948–2953.

[27]   N. Joshi, J. Fass, Sickle: A sliding-window, adaptive, quality-based trimming tool for FastQ files (Version 1.33) [Software]., 2011. https://github.com/najoshi/sickle.

[28]   B. Langmead, S.L. Salzberg, Fast gapped-read alignment with Bowtie 2, Nature Methods. 9 (2012) 357–359. https://doi.org/10.1038/nmeth.1923.

[29]   A.R. Quinlan, I.M. Hall, BEDTools: a flexible suite of utilities for comparing genomic features, Bioinformatics. 26 (2010) 841–842. https://doi.org/10.1093/bioinformatics/btq033.

[30]   P. Danecek, A. Auton, G. Abecasis, C.A. Albers, E. Banks, M.A. DePristo, R.E. Handsaker, G. Lunter, G.T. Marth, S.T. Sherry, G. McVean, R. Durbin, The variant call format and VCFtools, Bioinformatics. 27 (2011) 2156–2158. https://doi.org/10.1093/bioinformatics/btr330.

[31]   W. McLaren, L. Gil, S.E. Hunt, H.S. Riat, G.R.S. Ritchie, A. Thormann, P. Flicek, F. Cunningham, The Ensembl Variant Effect Predictor, Genome Biology. 17 (2016) 122. https://doi.org/10.1186/s13059-016-0974-4.

[32]   J.T. Robinson, H. Thorvaldsdóttir, W. Winckler, M. Guttman, E.S. Lander, G. Getz, J.P. Mesirov, Integrative Genomics Viewer, Nat Biotechnol. 29 (2011) 24–26. https://doi.org/10.1038/nbt.1754.

[33]   R. Balakrishnan, J. Park, K. Karra, B.C. Hitz, G. Binkley, E.L. Hong, J. Sullivan, G. Micklem, J. Michael Cherry, YeastMine—an integrated data warehouse for Saccharomyces cerevisiae data as a multipurpose tool-kit, Database (Oxford). 2012 (2012). https://doi.org/10.1093/database/bar062.

[34]   A. Abyzov, A.E. Urban, M. Snyder, M. Gerstein, CNVnator: An approach to discover, genotype, and characterize typical and atypical CNVs from family and population genome sequencing, Genome Res. 21 (2011) 974–984. https://doi.org/10.1101/gr.114876.110.

[35]   S.B. Haase, S.I. Reed, Improved flow cytometric analysis of the budding yeast cell cycle, Cell Cycle. 1 (2002) 132–136.

[36]   A. Borrull, M. Poblet, N. Rozès, New insights into the capacity of commercial wine yeasts to grow on sparkling wine media. Factor screening for improving wine yeast selection, Food Microbiology. 48 (2015) 41–48. https://doi.org/10.1016/j.fm.2014.12.006.

[37]   M.A. Quail, S.L. Kelly, The extraction and analysis of sterols from yeast, Methods Mol Biol. 53 (1996) 123–131. https://doi.org/10.1385/0-89603-319-8:123.

[38]   X. Chen, G. Wang, Y. Zhang, M. Dayhoff-Brannigan, N.L. Diny, M. Zhao, G. He, C.N. Sing, K.A. Metz, Z.D. Stolp, A. Aouacheria, W.-C. Cheng, J.M. Hardwick, X. Teng, Whi2 is a conserved negative regulator of TORC1 in response to low amino acids, PLOS Genetics. 14 (2018) e1007592. https://doi.org/10.1371/journal.pgen.1007592.

[39]   S. Laxman, B.M. Sutter, L. Shi, B.P. Tu, Npr2 inhibits TORC1 to prevent inappropriate utilization of glutamine for biosynthesis of nitrogen-containing metabolites, Sci. Signal. 7 (2014) ra120–ra120. https://doi.org/10.1126/scisignal.2005948.

[40]   N. Panchaud, M.-P. Péli-Gulli, C.D. Virgilio, Amino Acid Deprivation Inhibits TORC1 Through a GTPase-Activating Protein Complex for the Rag Family GTPase Gtr1, Sci. Signal. 6 (2013) ra42–ra42. https://doi.org/10.1126/scisignal.2004112.

[41]   M. Garcia-Barrio, J. Dong, S. Ufano, A.G. Hinnebusch, Association of GCN1-GCN20 regulatory complex with the N-terminus of eIF2alpha kinase GCN2 is required for GCN2 activation, The EMBO Journal. 19 (2000) 1887–1899. https://doi.org/10.1093/emboj/19.8.1887.

[42]   H. Kubota, K. Ota, Y. Sakaki, T. Ito, Budding yeast GCN1 binds the GI domain to activate the eIF2alpha kinase GCN2, The Journal of Biological Chemistry. 276 (2001) 17591–17596. https://doi.org/10.1074/jbc.M011793200.

[43]   M.N. Devare, Y.H. Kim, J. Jung, W.K. Kang, K.-S. Kwon, J.-Y. Kim, TORC1 signaling regulates cytoplasmic pH through Sir2 in yeast, Aging Cell. 19 (2020) e13151. https://doi.org/10.1111/acel.13151.

[44]   H. Rössler, C. Rieck, T. Delong, U. Hoja, E. Schweizer, Functional differentiation and selective inactivation of multiple Saccharomyces cerevisiae genes involved in very-long-chain fatty acid synthesis, Mol Gen Genomics. 269 (2003) 290–298. https://doi.org/10.1007/s00438-003-0836-0.

[45]   B. Akache, B. Turcotte, New Regulators of Drug Sensitivity in the Family of Yeast Zinc Cluster Proteins, J. Biol. Chem. 277 (2002) 21254–21260. https://doi.org/10.1074/jbc.M202566200.

[46]   C. Widmann, S. Gibson, M.B. Jarpe, G.L. Johnson, Mitogen-Activated Protein Kinase: Conservation of a Three-Kinase Module From Yeast to Human, Physiological Reviews. 79 (1999) 143–180. https://doi.org/10.1152/physrev.1999.79.1.143.

[47]   E.J. Louis, A.V. Vershinin, Chromosome ends: different sequences may provide conserved functions, BioEssays. 27 (2005) 685–697. https://doi.org/10.1002/bies.20259.

[48]   A. Tanghe, P.V. Dijck, F. Dumortier, A. Teunissen, S. Hohmann, J.M. Thevelein, Aquaporin Expression Correlates with Freeze Tolerance in Baker's Yeast, and Overexpression Improves Freeze Tolerance in Industrial Strains, Appl. Environ. Microbiol. 68 (2002) 5981–5989. https://doi.org/10.1128/AEM.68.12.5981-5989.2002.

[49]   E. García-Ríos, M. Morard, L. Parts, G. Liti, J.M. Guillamón, The genetic architecture of low-temperature adaptation in the wine yeast Saccharomyces cerevisiae, BMC Genomics. 18 (2017) 159. https://doi.org/10.1186/s12864-017-3572-2.

[50]   B. Oud, V. Guadalupe-Medina, J.F. Nijkamp, D. de Ridder, J.T. Pronk, A.J.A. van Maris, J.-M. Daran, Genome duplication and mutations in ACE2 cause multicellular, fast-sedimenting phenotypes in evolved Saccharomyces cerevisiae, PNAS. 110 (2013) E4223–E4231. https://doi.org/10.1073/pnas.1305949110.

[51]   J. Adams, S. Puskas-Rozsa, J. Simlar, C.M. Wilke, Adaptation and major chromosomal changes in populations of Saccharomyces cerevisiae, Curr Genet. 22 (1992) 13–19. https://doi.org/10.1007/BF00351736.

[52]   E. García-Ríos, M. Lairón-Peris, S. Muñiz-Calvo, J.M. Heras, A. Ortiz-Julien, P. Poirot, N. Rozès, A. Querol, J.M. Guillamón, Thermo-adaptive evolution to generate improved Saccharomyces cerevisiae strains for cocoa pulp fermentations, International Journal of Food Microbiology. 342 (2021) 109077. https://doi.org/10.1016/j.ijfoodmicro.2021.109077.

[53]   K.R. Bradnam, C. Seoighe, P.M. Sharp, K.H. Wolfe, G+C content variation along and among Saccharomyces cerevisiae chromosomes, Mol Biol Evol. 16 (1999) 666–675. https://doi.org/10.1093/oxfordjournals.molbev.a026149.

[54]   M. Morard, L.G. Macías, A.C. Adam, M. Lairón-Peris, R. Pérez-Torrado, C. Toft, E. Barrio, Aneuploidy and Ethanol Tolerance in Saccharomyces cerevisiae, Frontiers in Genetics. 10 (2019). https://www.frontiersin.org/article/10.3389/fgene.2019.00082.

153

[55]   M. Day, Yeast petites and small colony variants: for everything there is a season, Adv Appl Microbiol. 85 (2013) 1–41. https://doi.org/10.1016/B978-0-12-407672-3.00001-0.

[56]   E. Antony, S. Khubchandani, S. Chen, M.M. Hingorani, Contribution of Msh2 and Msh6 subunits to the asymmetric ATPase and DNA mismatch binding activities of Saccharomyces cerevisiae Msh2-Msh6 mismatch repair protein, DNA Repair (Amst). 5 (2006) 153–162. https://doi.org/10.1016/j.dnarep.2005.08.016.

[57]   S.D. Lee, J.A. Surtees, E. Alani, Saccharomyces cerevisiae MSH2-MSH3 and MSH2-MSH6 complexes display distinct requirements for DNA binding Domain I in mismatch recognition., J Mol Biol. 366 (2007) 53–66. https://doi.org/10.1016/j.jmb.2006.10.09.

[58]   Y. Habraken, P. Sung, L. Prakash, S. Prakash, ATP-dependent assembly of a ternary complex consisting of a DNA mismatch and the yeast MSH2-MSH6 and MLH1-PMS1 protein complexes, J. Biol. Chem. 273 (1998) 9837–9841. https://doi.org/10.1074/jbc.273.16.9837.

[59]   C. Falcone, C. Mazzoni, External and internal triggers of cell death in yeast, Cell Mol Life Sci. 73 (2016) 2237–2250. https://doi.org/10.1007/s00018-016-2197-y.

[60]   R. Loewith, 9 - TORC1 Signaling in Budding Yeast, in: The Enzymes, Academic Press, 2010: pp. 147–175. https://doi.org/10.1016/S1874-6047(10)27009-9.

[61]   S. Dokudovskaya, M.P. Rout, A novel coatomer-related SEA complex dynamically associates with the vacuole in yeast and is implicated in the response to nitrogen starvation, Autophagy. 7 (2011) 1392. https://doi.org/10.4161/auto.7.11.17347.

[62]   R. Algret, J. Fernandez-Martinez, Y. Shi, S.J. Kim, R. Pellarin, P. Cimermancic, E. Cochet, A. Sali, B.T. Chait, M.P. Rout, S. Dokudovskaya, Molecular Architecture and Function of the SEA Complex, a Modulator of the TORC1 Pathway, Mol Cell Proteomics. 13 (2014) 2855–2870. https://doi.org/10.1074/mcp.M114.039388.

[63]   M. Boeckstaens, E. Llinares, P. Van Vooren, A.M. Marini, The TORC1 effector kinase Npr1 fine tunes the inherent activity of the Mep2 ammonium transport protein, Nature Communications. 5 (2014) 3101. https://doi.org/10.1038/ncomms4101.

[64]   M. Boeckstaens, A. Merhi, E. Llinares, P. Van Vooren, J.-Y. Springael, R. Wintjens, A.M. Marini, Identification of a Novel Regulatory Mechanism of Nutrient Transport Controlled by TORC1-Npr1-Amu1/Par32, PLoS Genet. 11 (2015) e1005382–e1005382. https://doi.org/10.1371/journal.pgen.1005382.

[65]   S. Dokudovskaya, F. Waharte, A. Schlessinger, U. Pieper, D.P. Devos, I.M. Cristea, R. Williams, J. Salamero, B.T. Chait, A. Sali, M.C. Field, M.P. Rout, C. Dargemont, A Conserved Coatomer-related Complex Containing Sec13 and Seh1 Dynamically Associates With the Vacuole in Saccharomyces cerevisiae, Mol Cell Proteomics. 10 (2011). https://doi.org/10.1074/mcp.M110.006478.

[66]   Z. Yang, D.J. Klionsky, An Overview of the Molecular Mechanism of Autophagy, Curr Top Microbiol Immunol. 335 (2009) 1–32. https://doi.org/10.1007/978-3-642-00302-8_1.

[67]   D. Kaida, H. Yashiroda, A. Toh-e, Y. Kikuchi, Yeast Whi2 and Psr1-phosphatase form a complex and regulate STRE-mediated gene expression, Genes to Cells. 7 (2002) 543–552. https://doi.org/10.1046/j.1365-2443.2002.00538.x.

[68]   J.E. Kurtz, F. Exinger, P. Erbs, R. Jund, New insights into the pyrimidine salvage pathway of Saccharomyces cerevisiae: requirement of six genes for cytidine metabolism, Curr Genet. 36 (1999) 130–136. https://doi.org/10.1007/s002940050482.

[69]   O. Ozier-Kalogeropoulos, M.T. Adeline, W.L. Yang, G.M. Carman, F. Lacroute, Use of synthetic lethal mutants to clone and characterize a novel CTP synthetase gene in Saccharomyces cerevisiae, Mol. Gen. Genet. 242 (1994) 431–439. https://doi.org/10.1007/BF00281793.

[70]   D.B. Ostrander, D.J. O'Brien, J.A. Gorman, G.M. Carman, Effect of CTP synthetase regulation by CTP on phospholipid synthesis in Saccharomyces cerevisiae, J. Biol. Chem. 273 (1998) 18992–19001. https://doi.org/10.1074/jbc.273.30.18992.

[71]   Y.-F. Chang, G.M. Carman, CTP synthetase and its role in phospholipid synthesis in the yeast Saccharomyces cerevisiae, Prog Lipid Res. 47 (2008) 333–339. https://doi.org/10.1016/j.plipres.2008.03.004.

[72]   T. Hottiger, C.D. Virgilio, M.N. Hall, T. Boller, A. Wiemken, The role of trehalose synthesis for the acquisition of thermotolerance in yeast, European Journal of Biochemistry. 219 (1994) 187–193. https://doi.org/10.1111/j.1432-1033.1994.tb19929.x.

[73]   R.S.S. Magalhães, B. Popova, G.H. Braus, T.F. Outeiro, E.C.A. Eleutherio, The trehalose protective mechanism during thermal stress in Saccharomyces cerevisiae: the roles of Ath1 and Agt1, FEMS Yeast Res. 18 (2018). https://doi.org/10.1093/femsyr/foy066.

[74]   C. Coutinho, E. Bernardes, D. Félix, A.D. Panek, Trehalose as cryoprotectant for preservation of yeast strains, Journal of Biotechnology. 7 (1988) 23–32. https://doi.org/10.1016/0168-1656(88)90032-6.

[75]   A. Wiemken, Trehalose in yeast, stress protectant rather than reserve carbohydrate, Antonie van Leeuwenhoek. 58 (1990) 209–217. https://doi.org/10.1007/BF00548935.

[76]   J.H. Crowe, L.M. Crowe, D. Chapman, Preservation of Membranes in Anhydrobiotic Organisms: The Role of Trehalose, Science. 223 (1984) 701–703. https://doi.org/10.1126/science.223.4637.701.

[77]   P. Mazur, Cryobiology: The Freezing of Biological Systems, Science. 168 (1970) 939–949. https://doi.org/10.1126/science.168.3934.939.

[78]   M.B. França, A.D. Panek, E.C.A. Eleutherio, Oxidative stress and its effects during dehydration, Comparative Biochemistry and Physiology Part A: Molecular & Integrative Physiology. 146 (2007) 621–631. https://doi.org/10.1016/j.cbpa.2006.02.030.

[79]   J.E. Vance, G. Tasseva, Formation and function of phosphatidylserine and phosphatidylethanolamine in mammalian cells, Biochimica et Biophysica Acta (BBA) - Molecular and Cell Biology of Lipids. 1831 (2013) 543–554. https://doi.org/10.1016/j.bbalip.2012.08.016.

[80]   H.A. Boumann, J. Gubbens, M.C. Koorengevel, C.-S. Oh, C.E. Martin, A.J.R. Heck, J. Patton-Vogt, S.A. Henry, B. de Kruijff, A.I.P.M. de Kroon, Depletion of Phosphatidylcholine in Yeast Induces Shortening and Increased Saturation of the Lipid Acyl Chains: Evidence for Regulation of Intrinsic Membrane Curvature in a Eukaryote, Mol Biol Cell. 17 (2006) 1006–1017. https://doi.org/10.1091/mbc.E05-04-0344.

[81]   M.F. Renne, A.I.P.M. de Kroon, The role of phospholipid molecular species in determining the physical properties of yeast membranes, FEBS Letters. 592 (2018) 1330–1345. https://doi.org/10.1002/1873-3468.12944.

[82]   P. Rockenfeller, M. Koska, F. Pietrocola, N. Minois, O. Knittelfelder, V. Sica, J. Franz, D. Carmona-Gutierrez, G. Kroemer, F. Madeo, Phosphatidylethanolamine positively regulates autophagy and longevity, Cell Death & Differentiation. 22 (2015) 499–508. https://doi.org/10.1038/cdd.2014.219.

[83]   M. Bogdanov, W. Dowhan, Lipid-assisted Protein Folding, J. Biol. Chem. 274 (1999) 36827–36830. https://doi.org/10.1074/jbc.274.52.36827.

[84]   Y. Ichimura, T. Kirisako, T. Takao, Y. Satomi, Y. Shimonishi, N. Ishihara, N. Mizushima, I. Tanida, E. Kominami, M. Ohsumi, T. Noda, Y. Ohsumi, A ubiquitin-like system mediates protein lipidation, Nature. 408 (2000) 488–492. https://doi.org/10.1038/35044114.

[85]   L. Farine, M. Niemann, A. Schneider, P. Bütikofer, Phosphatidylethanolamine and phosphatidylcholine biosynthesis by the Kennedy pathway occurs at different sites in Trypanosoma brucei, Scientific Reports. 5 (2015) 16787. https://doi.org/10.1038/srep16787.

[86]   O. Tehlivets, K. Scheuringer, S.D. Kohlwein, Fatty acid synthesis and elongation in yeast, Biochimica et Biophysica Acta (BBA) - Molecular and Cell Biology of Lipids. 1771 (2007) 255–270. https://doi.org/10.1016/j.bbalip.2006.07.004.

[87]   P.W. Piper, The heat shock and ethanol stress responses of yeast exhibit extensive similarity and functional overlap, FEMS Microbiology Letters. 134 (1995) 121–127. https://doi.org/10.1016/0378-1097(95)00431-9.

[88]   F. Randez-Gil, J.A. Prieto, A. Rodríguez-Puchades, J. Casas, V. Sentandreu, F. Estruch, Myriocin-induced adaptive laboratory evolution of an industrial strain of Saccharomyces cerevisiae reveals its potential to remodel lipid composition and heat tolerance, Microbial Biotechnology. 13 (2020) 1066–1081. https://doi.org/10.1111/1751-7915.13555.

[89]   L. Bardi, C. Cocito, M. Marzona, Saccharomyces cerevisiae cell fatty acid composition and release during fermentation without aeration and in absence of exogenous lipids, International Journal of Food Microbiology. 47 (1999) 133–140. https://doi.org/10.1016/S0168-1605(98)00203-7.

[90]   C.E. Martin, C.-S. Oh, Y. Jiang, Regulation of long chain unsaturated fatty acid synthesis in yeast, Biochimica et Biophysica Acta (BBA) - Molecular and Cell Biology of Lipids. 1771 (2007) 271–285. https://doi.org/10.1016/j.bbalip.2006.06.010.

[91]   C. Panozzo, M. Nawara, C. Suski, R. Kucharczyka, M. Skoneczny, A.-M. Bécam, J. Rytka, C.J. Herbert, Aerobic and anaerobic NAD+ metabolism in Saccharomyces cerevisiae, FEBS Letters. 517 (2002) 97–102. https://doi.org/10.1016/S0014-5793(02)02585-1.

[92]   W.J.C. Dekker, S.J. Wiersma, J. Bouwknegt, C. Mooiman, J.T. Pronk, Anaerobic growth of Saccharomyces cerevisiae CEN.PK113-7D does not depend on synthesis or supplementation of unsaturated fatty acids, FEMS Yeast Res. 19 (2019). https://doi.org/10.1093/femsyr/foz060.

[93]   K.Y.F. Lip, E. García-Ríos, C.E. Costa, J.M. Guillamón, L. Domingues, J. Teixeira, W.M. van Gulik, Selection and subsequent physiological characterization of industrial Saccharomyces cerevisiae strains during continuous growth at sub- and- supra-optimal temperatures, Biotechnol Rep (Amst). 26 (2020). https://doi.org/10.1016/j.btre.2020.e00462.

[94]   L.G.M. Boender, E.A.F. de Hulster, A.J.A. van Maris, P.A.S. Daran-Lapujade, J.T. Pronk, Quantitative Physiology of Saccharomyces cerevisiae at Near-Zero Specific Growth Rates, Appl. Environ. Microbiol. 75 (2009) 7578. https://doi.org/10.1128/AEM.02344-09.

[95]   L. Tijhuis, M.C. Van Loosdrecht, J.J. Heijnen, A thermodynamically based correlation for maintenance gibbs energy requirements in aerobic and anaerobic chemotrophic growth, Biotechnol. Bioeng. 42 (1993) 509–519. https://doi.org/10.1002/bit.260420415.

Supplementary materials

Metabolite's quantification

For quantification of extracellular metabolites, the supernatant sample was defrosted on ice and analysed in duplicate using high-performance liquid chromatography (HPLC) using a Bio-Rad Aminex column (Bio-Rad Laboratories, California, USA) at 60°C. The column was eluted with 5.0 mM phosphoric acid at a flow rate of 0.6 mL·min^{-1}. Ethanol and glycerol were detected with a Waters 2414 refractive index detector (Waters Corporation, Massachusetts, USA), while a Waters 1489 UV-Vis detector (Waters Corporation, Massachusetts, USA) was used to detect acetate, lactate, malate, and succinate. Residual glucose was measured by ion chromatography using a Dionex-ICS 5000+ (Thermo Fisher Scientific, Massachusettts, USA).

Total fatty acids measurements

A yeast pellet of around 2·10⁸ cells, 1 mL of HCl 1.25N in methanol and 10 µL heptanoic acid (C7, 1 g L^{-1}) and heptadecanoic acid (C17, 4 g L^{-1}) were added to the glass tubes containing the cells (ca 5-8 mg $_{DW}$$^{-1}$). Samples were heated to 90°C for 60 min and then cooled to room temperature. After cooling, 1 mL of NaCl 0.9% (w/v) in water and 300 µL hexane were added. The extraction was repeated twice. Between each extraction phase, tubes were centrifuged at 3000 g for 5 min to allow the best phase separation. Analytical GC was carried out using an Agilent 5890 connected to an HP Vectra computer with the ChemStation software (Agilent Technologies). The extract (2 µL) was injected (splitless, 0.75 min) into a DB-5HT column (30 m x 0.25 mm x 0.1 µm, Agilent Technologies) with an automatic injector (Agilent). Relative amounts of the given fatty acids were calculated from their respective chromatographic peak areas after normalization with internal standards (C17).

Around 5-8 mg $_{DW}^{-1}$ of cells were re-suspended in 1.5 mL methanol (MeOH), 1 mL of pyrogallol (0.5% (w/v) in MeOH), 1 mL KOH solution (60% (w/v) KOH in distilled water) and 10 μL of α-cholestane (internal standard (IS), 1 mg /mL in hexane) into a glass tube and saponified at 90°C during 2 hours. Finally, sterols and squalene were extracted twice with 500 μL hexane and the extract was dried in a speed vacuum system SC110 (Savant Instruments, USA). The dried residue was dissolved in 100 μL of hexane. From the collected organic phase, 2 μL was injected in pulsed splitless mode (70 psi, 0.10 min) onto a DB-5HT column (30 m x 0.25 mm x 0.1 μm, Agilent Technologies) with an automatic injector (7683B, Agilent Technologies). The identification of each compound was carried out by using a 6890N Agilent (Agilent Technologies) instrument fitted with a mass spectrometry detector (5975 Agilent Tecnologies) and comparing the mass fragmentation patterns of the peaks with those of the available standard in the method. The relative abundance of each identified compound was calculated according to the respective chromatographic peak areas corrected with respect to the IS peak area. The results are expressed as individual percentage of total sum of identified sterols and squalene.

Total sterol composition measurements by GC/MS

159

Samples were applied as narrow bands (8 mm) to a TLC plate at 5 mm from the edge using the CAMAG linomat V (CAMAG, Switzerland) under nitrogen. The yeast extract PL were separated by one-dimensional TLC on silica gel 60F254 plates (10 x 20 cm, 250 μm) (Merck, Germany) which was pretreated (8.5 cm) in a CAMAG vertical Automatic Development Chamber (ADC2, CAMAG) to remove impurities by methanol: ethyl acetate (6:4). Then after activation for 10 min at 130°C, the plate was developed in two steps with (1) chloroform:acetone:methanol:glacial acetic acid: water (5:1.5:1:1:0.4, v/v/v/v/v) to 7 cm and (2) with hexane to 8.5 cm. Then the plate was dried during 5 min under an air stream. After that, TLC lipids were charred with 10 % (w/v) of CuSO4 in 8 % (v/v) of H3PO4 in a CAMAG chromatogram immersion device, heated at 60°C during 15 min and then to160°C for 10 minutes on a TLC Plate Heater (CAMAG).

Phospholipid analysis

After cooling down the plate, the image was acquired in visible light with Gel Capture (version 5, DNR Bio-Imaging Systems Ltd, Jerusalem, Israel). Each density spot of the image was quantified as integrated Optical densities (IOD) with ImageJ software (a

public domain, Java-based image processing program developed at the National Institute of Health). Relative amounts of the given PLs were calculated from their respective chromatographic areas (Individual PL area/sum of total PL areas). The elution order (down to up) of PL on the plate was phosphatidylinositol (PI), phosphatidylserine (PS), phosphatidylcholine (PC), phosphatidylethanolamine (PE), cardiolipin (CL) and phosphatidic acid (PA).

Estimation of generations during adaptive evolution by SBR

Every cycle was begun with 1/10 of the total culture broth from the previous batch, so we used volumetric ratio for the biomass concentration (Cx) during the SBR cultivation. The Cx at t = 0 was 1/10 and at the end of the batch was 1.

$$n_{generations} = n_{SBR\ batches} * \frac{log_{10}(Cx_{end}) - log_{10}(Cx_0)}{log2} \qquad (1)$$

Estimation of the maximum biomass-specific growth rate and death rate during SBR

During exponential growth of SBR, the change in viable biomass (C_{xv}) can be expressed as equation (2). A fraction of the produced biomass contains non-viable biomass from which the rate is described as the specific death rate (k_d). This term was subtracted from the mass-balance to prevent underestimation of the actual growth rate ($\mu_{max(T),est}$) which can be calculated by dividing the observed $\mu_{max(T)}$ with the viable fraction of the biomass ($X_{viability}$). The $X_{viability}$ during SBR was measured at the exponential phase of the biomass culture by fluorescence dyes and flow cytometry.

$$C_{xv}(t) = C_{xv(0)}e^{\frac{(\mu_{max(T)}-k_d)obs}{X_{viability}}*t} \qquad (2)$$

$$\mu_{max(T),est} = \frac{\left(\mu_{max(T)} - k_d\right)_{obs}}{X_{viability}} \qquad (3)$$

Throughout the exponential phase of SBR cultivation, yeast cells produce and consume compounds at the maximum biomass specific rate ($q_{i,max}$). The mass-balance expressing the change in time of a compound i reads as following:

$$\frac{d(C_i * V_L)}{dt} = q_{i,max} V_L C_{xv}(t) \qquad (4)$$

Although batch cultivations were performed, the inlet flow consisted of an alkaline solution to maintain pH=5. However, part of the fermentation broth evaporated through the condenser. The difference between the inlet and outlet flow of the fermenter accounted for a volume variation of less than 1% of the total volume of the fermenter. Therefore, it was assumed that the concentrations of the compounds were not affected by this and that the volume only changed due to sample withdrawal. The mass-balance was further simplified by this assumption:

$$\frac{d(C_i)}{dt} = q_{i,max} C_{xv}(t) \qquad (5)$$

The volumetric CO_2 production rate was calculated from the CO_2 concentration in the off-gas, N_2 gassing rate (1.0 L·min-1) and the volume of the fermenter. From this result, the equation for exponential CO_2 production was obtained and substituted with the exponential growth equation (5):

$$\frac{F_{CO2}}{V_L} = q_{CO2,max} C_{xv} e^{\mu_{max,est} * t} \qquad (6)$$

The concentrations of glycerol, glucose, malate, succinate, acetate and lactate were expressed by substituting (4) and (5) with subsequent integration:

$$C_i(t) = C_i(0) + q_{i,max} \frac{C_{xv}(0)}{\mu_{max,est}} (e^{\mu_{max,est}*t} - 1) \qquad (7)$$

A significant amount of ethanol will be lost during fermentation caused by evaporation of ethanol through the off-gas. This leads to underestimation of the concentration ethanol in the fermentation broth. Therefore, the broth evaporation constant (, -0.359 g_{broth} $_{evaporated}$·L_{broth}^{-1}·h^{-1}) at 39°C was used to correct for the evaporated ethanol [90]. We made an assumption that the difference of the evaporation at 39°C and at 39.8°C was negligible. Integration of k_{broth} in the combined expression of (4) and (5), resulted in the formula expressing the concentration of ethanol during SBR at 39.8°C:

$$C_{eth}(t) = \left(C_{eth}(0) - q_{eth,max} \frac{C_{xv}(0)}{\mu_{max,est} + k_{broth}} \right) * e^{-k_{broth}*t}$$
$$+ q_{eth,max} \frac{C_{xv}(0)}{\mu_{max,est} + k_{broth}} e^{\mu_{max,est}*t} \qquad (8)$$

Elaboration on the difference in the biomass yields between chemostat and SBR

The growth rate during the batch cultivation of the evolved strain in the SBR was 0.23 ± 0.03 h^{-1}, while during chemostat cultivation the growth rate was 7.7 times lower, namely 0.03 h^{-1}. This implies that the impact of maintenance energy requirements on the yield during the chemostat cultivation was much higher than during the batch cultivation. The anaerobic maintenance coefficient for this strain at 30°C has been experimentally determined to be 0.5 mmol glucose•g CDM^{-1}•h^{-1} [91] ($\approx$ 13.2 mmol glucose•mol CDM-^{1}•h^{-1}). It is well known that maintenance energy requirements of microorganisms increase with increasing cultivation temperature [92]. Using the correlation proposed by these authors, an increase of the cultivation temperature from 30.0°C to 39.0°C would result in a 2.2-fold increase of the maintenance coefficient, so in

this case 2.2 x 13.2 = 29 mmol glucose•mol CDM^{-1}•h^{-1}. Using the Pirt equation ($q_s = \mu/Y_{xs,max}$ + ms) the biomass yield ($Y_{xs} = \mu/q_s$) can be calculated as a function of the growth rate, $Y_{xs} = \mu/(\mu/Y_{xs,max}$ + ms), with Yxs,max = 0.1 g CDM^1• g glucose-1 [91] ≈ 0.7 mol CDM^1• mol glucose^{-1}. Using this equation, the biomass yield for μ = 0.03 h^{-1} (chemostat) is calculated to be 0.42 mol CDM·mol glucose^{-1}, which is the same as the experimental value. For μ = 0.23 h^{-1} (SBR) the calculated yield is 0.64 mol CDM^1•mol glucose^{-1} which is somewhat lower than the experimental value (0.83 ± 0.12). This difference could be explained by a difference in biomass composition and thus Y_{xs},max between glucose limited (chemostat) and glucose excess (batch) grown cells.

During the exponential phase of SBR cultivation, the following parameters were obtained for the nine compounds (acetate, biomass, CO$_2$, ethanol, glucose, glycerol, lactate, malate, and succinate) from expressions (2), (3), and (4). The term $C_{i, t=0}$ represents the concentration of the metabolites (acetate, CO$_2$, ethanol, glucose, glycerol, lactate, malate, and succinate) at the start of each cycle of the SBR, whereas $C_{x,t=0}$ represents the initial concentration of biomass.

Data reconciliation by LSM

$$\mu_{max}$$
$$q_{i, max}$$
$$C_{i, t=0}$$
$$C_{x,t=0}$$

The considered metabolites are assumed to contain only the four main elements in microbial processes. The complexity of the metabolic processes for these metabolites were simplified by a black box model where the amount of an element produced should be equal to the amount consumed. Consequently, the rate at which the consumed and produced elements are converted should also be equal. The eleven main compounds involved in the fermentation process were: acetate, ammonia, biomass, CO$_2$, ethanol, glucose, glycerol, lactate, malate, succinate, water. The conservation law can be expressed in the following form:

$$\sum_{i=1}^{11} q_{i,max} * n_i = 0 \qquad (9)$$

The term n_i expresses the stoichiometric coefficient of the metabolites. The conservation law enables the determination of seven rates of these components, minimum, with eleven measured compounds. With a degree of freedom of two, we used the experimental data from nine of the compounds (acetate, biomass, CO2, ethanol, glucose, glycerol, lactate, malate, and succinate) to calculate all eleven rates by an optimization model which minimized the scaled squared residuals between the experimental data and the predicted data.

LSM is one of the regression analyses to approximate the solutions of an overestimated system. The method allows to minimize the sum of squares (SS) of the residuals by successive iterations with the parameter estimations of the model, which has the following expression:

$$ SS = \sum_{i=1}^{11} (\frac{c_{i,observed} \; - \; c_{i,estimated}}{\sigma_{i,observed}}) \quad (10) $$

Each residual was calculated by dividing the difference between the estimated ($c_{i,estimated}$) and the observed ($c_{i,observed}$) concentration of the measured compound over the influence of the measurement error to the observed value ($\sigma_{i,observed}$) which is the multiplication between the $c_{i,observed}$ with its measurement error. To this end, the measurement errors had a confidence interval between 80 to 95%.

The iterative cycle was performed under the constraint that the conservation law of the four elemental compounds was satisfied. The four elemental compounds with the elemental composition of the eleven compounds (acetate, ammonia, biomass, CO_2, ethanol, glucose, glycerol, lactate, malate, succinate, water) are listed in matrix A. The biomass composition was given for one mole of carbon [21]. The rate estimations were indicated in vector $\hat{x}$, with 11 variables and the corresponding rates were expressed as x_n. The elemental conservation law was satisfied when the product of vector $\hat{x}$ with each element in matrix A, equalled zero. Analogous to (9), this constraint can be presented as (11)

$$A = \begin{bmatrix} 1 & 1 & 6 & 2 & 2 & 3 & 4 & 4 & 3 & 0 & 0 \\ 1.748 & 0 & 12 & 6 & 4 & 6 & 6 & 6 & 8 & 2 & 3 \\ 0.596 & 2 & 6 & 1 & 2 & 3 & 4 & 5 & 3 & 1 & 0 \\ 0.148 & 0 & 0 & 0 & 0 & 0 & 0 & 0 & 0 & 0 & 1 \end{bmatrix}$$

$$\hat{x} = \begin{bmatrix} \mu_{max} - k_d & x_1 \\ q_{CO2,max} & x_2 \\ q_{glucose,max} & x_3 \\ q_{ethanol,max} & x_4 \\ q_{acetate,max} & x_5 \\ q_{lactate,max} & x_6 \\ q_{succinate,max} & x_7 \\ q_{malate,max} & x_8 \\ q_{glycerol,max} & x_9 \\ q_{H_2O,max} & x_{10} \\ q_{NH_3,max} & x_{11} \end{bmatrix}$$

$$A\hat{x} = 0 \qquad (11)$$
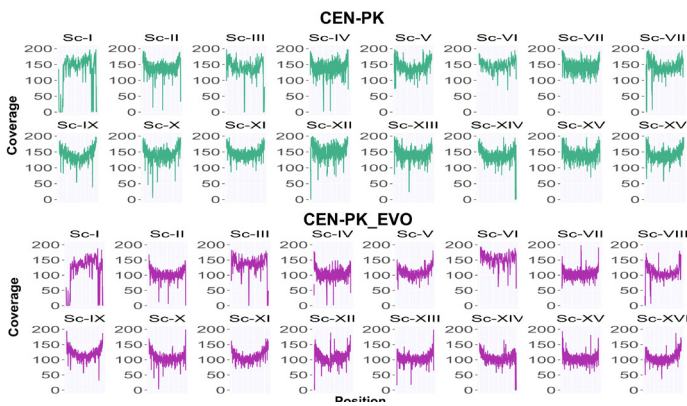
Figure S 1
Chromosome representation for each one of the 16 chromosomes present in CEN.PK113-7D (green) and CEN.PK-EVO (purple). Graphs were obtained by using the average coverage value every 1000 positions and ggplot2 R package. This indicates that the genome of CEN.PK-EVO had no copy number variation nor big aneuploidies on its genome compared to CEN-PK113-7D.

165

Figure S 2
Phospholipid measurements of the chemostat culture at 30.0°C and 39.0°C. The standard deviation of both graphs based on three independent samples collected at three different time points during the steady state chemostat. Compared with the unevolved strain at the same temperature, * indicates a significant difference with a p-value (ANOVA and Tukey HSD test, α=0.05, n=3) of < 0.05.
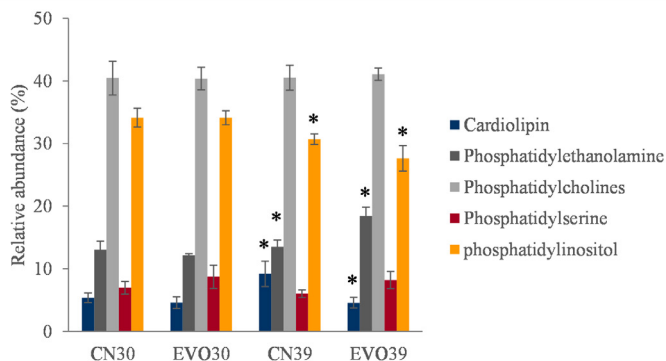
Figure S 3
Experimental overview. The details of the methods and materials can refer to the section of methods and materials.
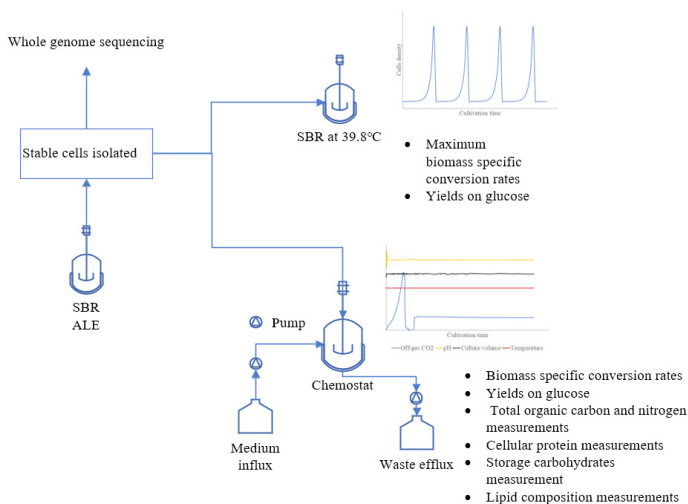
Table S 1
Apparent maximum specific growth rate (h⁻¹) in anaerobic SBR cultivations at 39.8°C. Standard errors of each strain were obtained from three independent batches.

	Apparent μmax
CEN.PK113-7D	0.081 ± 0.003
Evolved CEN.PK113-7D	0.281 ± 0.011

mmol·g$_{viable\ DW}^{-1}$·h^{-1}	CEN.PK113-7D		CEN.PK-EVO	
	30°C	39°C	30°C	39°C
$q_{acetate}$	0.01 ± 0.002	0.046 ± 0.046	0.011 ± 0.013	0.033 ± 0.01
q_{CO2}	3.341 ± 0.267	5.13 ± 0.475	3.576 ± 0.075	4.605 ± 0.191
$q_{ethanol}$	3.175 ± 0.269	4.989 ± 0.471	3.405 ± 0.095	4.485 ± 0.238
$q_{glycerol}$	0.312 ± 0.002	0.337 ± 0.059	0.317 ± 0.04	0.306 ± 0.067
$q_{lactate}$	0.014 ± 0.006	0.029 ± 0	0.015 ± 0.007	0.04 ± 0.007
q_{malate}	0.004 ± 0.001	0.012 ± 0.007	0.001 ± 0.002	0.01 ± 0.001
q_s	-1.956 ± 0.139	-2.945 ± 0.312	-2.073 ± 0.016	-2.689 ± 0.079
$q_{sucinnate}$	0.012 ± 0.001	0.073 ± 0.037	0.011 ± 0.001	0.088 ± 0.022

Table S 2
Reconciled specific conversion rates of CEN.PK113-7D and evolved CEN.PK113-7D with their standard errors during anaerobic chemostat cultivation at 30°C and 39°C at a dilution rate of 0.03 h-1. The nomenclature of s represents as substrate (glucose).

	CEN.PK113-7D	Evolved CEN.PK113-7D
30°C	0.051 ± 0.002	0.072 ± 0.001
39°C	0.044 ± 0.003	0.059 ± 0.003

Table S 3
Average cellular nitrogen contents (g total N·gDW-1) of CEN.PK113-7D and evolved CEN.PK113-7D during anaerobic steady-state chemostat cultivation at 30°C and 39°C. Standard errors were obtained from four measurements at different time points during the steady-states.

	CEN.PK113-7D		Evolved CEN.PK113-7D	
	30°C	39°C	30°C	39°C
Acetate	0.679 ± 0.051	1.485 ± 0.059	0.407 ± 0.055	1.182 ± 0.055
Lactate	0.827 ± 0.054	1.143 ± 0.057	1.087 ± 0.097	1.792 ± 0.041
Succinate	0.708 ± 0.057	2.871 ± 0.212	0.548 ± 0.075	3.643 ± 0.083

Table S 4
Average acid-(by) products (mmol·L-1) of CEN.PK113-7D and evolved CEN.PK113-7D during anaerobic steady-state chemostat cultivation at 30°C and 39°C. Standard errors were obtained in duplicate chemostat experiments where four measurements at different time points were used for each duplicate.

Table S 5
DNA content of the
reference strains
(S288c and FY1679),
CEN.PK113-7D, and
CEN.PK-EVO for the
ploidy estimation.
Values expressed
as mean and their
standard deviation.
The analysis indicated
significantly different
values (ANOVA and
Tukey HSD test,
α=0.05, n=2) compared
with the parental
strain.

Table S 6
Variants identified
from genome
sequencing of CEN.
PK-EVO which were
not found in CEN.
PK113-7D.

Strains	DNA content
S288c	1.00 ± 0.05
FY1679	2.14 ± 0.13
CEN.PK113-7D	1.09 ± 0.03
CEN.PK-EVO	1.13 ± 0.01

Gene Systematic Name	Gene Standard Name	Gene Name	Amino acids	Codons
YBR147W	RTC2	Restriction of Telomere Capping	Q/*	Caa/Taa
YBR227C	MCX1	Mitochondrial ClpX	Q/*	Caa/Taa
YDL089W	NUR1	NUclear Rim1	R/*	Cga/Tga
YDR097C	MSH6	MutS Homolog	Y/*	taC/taG
YDR406W	PDR15	Pleiotropic Drug Resistance	W/*	tgG/tgA
YIL130W	ASG1	Activator of Stress Genes	Q/*	Cag/Tag
YFL049W	SWP82	SWi/snf-associated Protein	W/*	tGg/tAg
YGR040W	KSS1	Kinase Suppressor of Sst2 mutations	S/*	tCa/tAa
YJL196C	ELO1	ELOngation defective	Q/*	Cag/Tag
YLR419W	-	-	Q/*	Caa/Taa
YOR064C	YNG1	Yeast iNG1 homolog	W/*	tGg/tAg
YPR030W	CSR2	Chs5 Spa2 Rescue	Q/*	Caa/Taa
YPR117W	-	-	Q/*	Caa/Taa
YAL039C	CYC3	CYtochrome C	V/M	Gtg/Atg
YAR002C-A	ERP1	Emp24p/Erv25p Related Protein	A/T	Gcc/Acc
YAR014C	BUD14	BUD site selection	D/V	gAt/gTt
YBL104C	SEA4	SEh1-Associated	G/C	Ggt/Tgt
YBL099W	ATP1	ATP synthase	H/Y	Cat/Tat
YBL040C	ERD2	Endoplasmic reticulum Retention Defective	S/T	aGt/aCt
YBL039C	URA7	URAcil requiring	E/G	gAa/gGa
YBL037W	APL3	clathrin Adaptor Protein complex Large chain	K/N	aaG/aaT
YBL034C	STU1	Suppressor of TUbulin	A/T	Gca/Aca
YBR012C			P/S	Cca/Tca
YBR112C	CYC8	CYtochrome C	P/H	cCt/cAt
YBR157C	ICS2	Increased Copper Sensitivity	V/I	Gtc/Atc
YBR158W	AMN1	Antagonist of Mitotic exit Network	P/L	cCa/cTa
YBR179C	FZO1	FuZzy Onions homolog	V/M	Gtg/Atg
YBR203W	COS111	Ciclopirox Olamine Sensitive	G/C	Ggt/Tgt
YBR208C	**DUR1,2**	**Degradation of URea**	**G/R**	**Ggg/Agg**
YBR296C	PHO89	PHOsphate metabolism	D/V	gAc/gTc
YCR011C	ADP1	ATP-Dependent Permease	G/S	Ggt/Agt
YCR028C	FEN2	FENpropimorph resistance	A/T	Gca/Aca
YDL222C	FMP45	Found in Mitochondrial Proteome	G/R	Gga/Aga
YDL193W	NUS1	Nuclear Undecaprenyl pyrophosphate Synthase	E/K	Gaa/Aaa
YDL171C	GLT1	GLuTamate synthase	T/A	Act/Gct
YDL171C	GLT1	GLuTamate synthase	K/N	aaG/aaT
YDL134C	PPH21	Protein PHosphatase	G/C	Ggc/Tgc
YDL017W	CDC7	Cell Division Cycle	T/I	aCa/aTa
YDL006W	PTC1	Phosphatase type Two C	A/T	Gca/Aca
YDR011W	SNQ2	Sensitivity to 4-NitroQuinoline-N-oxide	S/Y	tCc/tAc
YDR019C	GCV1	GlyCine cleaVage	S/F	tCc/tTc
YDR020C	DAS2	Dst1-delta 6-Azauracil Sensitivity	T/I	aCt/aTt
YDR043C	NRG1	Negative Regulator of Glucose-repressed genes	C/Y	tGt/tAt
YDR080W	VPS41	Vacuolar Protein Sorting	V/A	gTt/gCt
YDR207C	UME6	Unscheduled Meiotic gene Expression	L/S	tTa/tCa
YDR217C	RAD9	RADiation sensitive	E/K	Gaa/Aaa
YDR218C	SPR28	SPorulation Regulated	G/R	Ggg/Agg
YDR229W	IVY1	Interacting with Vps33p and Ypt7p	A/T	Gcc/Acc

YDR346C	SVF1	SurVival Factor	M/V	Atg/Gtg
YDR356W	SPC110	Spindle Pole Component	I/N	aTt/aAt
YDR430C	**CYM1**	**CYtosolic Metalloprotease**	**G/D**	**gGt/gAt**
YDR523C	SPS1	SPorulation Specific	W/L	tGg/tTg
YIL177C	-		L/M	Ttg/Atg
YIL137C	TMA108	Translation Machinery Associated	D/N	Gac/Aac
YIL134W	FLX1	FLavin eXchange	A/V	gCa/gTa
YIL108W	-		S/P	Tca/Cca
YIR025W	MND2	Meiotic Nuclear Divisions	V/A	gTt/gCt
YEL077C	-		L/M	Ttg/Atg
YEL062W	NPR2	Nitrogen Permease Regulator	S/T	Tcc/Acc
YEL016C	NPP2	ecto-Nucleotide Pyrophosphatase/Phosphodiesterase	D/Y	Gac/Tac
YER026C	CHO1	CHOline requiring	T/A	Aca/Gca
YER065C	ICL1	IsoCitrate Lyase	A/T	Gca/Aca
YER071C	TDA2	Topoisomerase I Damage Affected	L/M	Ctg/Atg
YER079W			S/N	aGc/aAc
YER162C	RAD4	RADiation sensitive	N/D	Aac/Gac
YER190W	YRF1-2		L/M	Ttg/Atg
YFR026C	ULI1	Upr-L-Inducible gene	A/V	gCa/gTa
YFR030W	MET10	METhionine requiring	G/D	gGt/gAt
YGL216W	KIP3	KInesin related Protein	V/I	Gtt/Att
YGL195W	GCN1	General Control Nonderepressible	A/V	gCa/gTa
YGL173C	XRN1	eXoRiboNuclease	P/H	cCt/cAt
YGL158W	RCK1	Radiation sensitivity Complementing Kinase	G/D	gGc/gAc
YGL155W	CDC43	Cell Division Cycle	R/H	cGt/cAt
YGL124C	MON1	MONensin sensitivity	F/L	Ttc/Ctc
YGL115W	SNF4	Sucrose NonFermenting	S/P	Tcc/Ccc
YGL049C	TIF4632	Translation Initiation Factor	C/Y	tGt/tAt
YGL013C	PDR1	Pleiotropic Drug Resistance	S/P	Tca/Cca
YGL008C	PMA1	Plasma Membrane ATPase	D/N	Gat/Aat
YGR014W	MSB2	Multicopy Suppression of a Budding defect	S/N	aGc/aAc
YGR041W	BUD9	BUD site selection	A/V	gCt/gTt
YGR148C	RPL24B	Ribosomal Protein of the Large subunit	E/D	gaA/gaC
YGR162W	TIF4631	Translation Initiation Factor	E/G	gAa/gGa
YGR170W	PSD2	PhosphatidylSerine Decarboxylase	D/N	Gat/Aat
YGR198W	YPP1	alpha-sYnuclein Protective Protein	F/L	Ttc/Ctc
YGR215W	RSM27	Ribosomal Small subunit of Mitochondria	H/D	Cat/Gat
YGR270W	YTA7	Yeast Tat-binding Analog	S/Y	tCt/tAt
YGR270W	YTA7	Yeast Tat-binding Analog	A/T	Gcc/Acc
YGR271W	SLH1	SKI2-Like Helicase	P/L	cCt/cTt
YGR296W	YRF1-3		L/M	Ttg/Atg
YHL019C	APM2	clathrin Adaptor Protein complex Medium chain	N/D	Aac/Gac
YHL019W-A			L/S	tTg/tCg
YHR011W	DIA4	Digs Into Agar	P/S	Cct/Tct
YHR042W	NCP1	NADP-Cytochrome P450 reductase	A/V	gCc/gTc
YHR047C	AAP1	Arginine/alanine AminoPeptidase	R/C	Cgt/Tgt
YHR063C	PAN5	PANtothenate biosynthesis	Q/R	cAa/cGa
YHR064C	SSZ1		L/S	tTg/tCg
YHR086W	NAM8	Nuclear Accommodation of Mitochondria	Q/R	cAa/cGa
YHR098C	SFB3	Sed Five Binding	I/V	Att/Gtt
YHR106W	TRR2	ThioRedoxin Reductase	V/I	Gta/Ata
YHR150W	PEX28	PEroXisome related	V/I	Gta/Ata
YHR182C-A	-		T/A	Acc/Gcc
YJL225C	-		E/K	Gaa/Aaa
YJL095W	BCK1	Bypass of C Kinase	S/N	aGt/aAt
YJL086C	-		E/K	Gaa/Aaa
YJL048C	UBX6	UBiquitin regulatory X	Y/H	Tac/Cac
YJR031C	GEA1	Guanine nucleotide Exchange on ARF	D/Y	Gat/Tat
YJR036C	HUL4	Hect Ubiquitin Ligase	L/M	Ctg/Atg
YJR147W	HMS2	High-copy Mep Suppressor	G/D	gGt/gAt
YKL182W	FAS1	Fatty Acid Synthetase	V/M	Gtg/Atg
YKL166C	TPK3	Takashi's Protein Kinase	T/S	Acc/Tcc
YKL024C	URA6	URAcil requiring	A/V	gCt/gTt
YKR016W	MIC60	MItochondrial contact site and Cristae organizing s	S/R	agC/agA

Table S 6
(continued)

YKR024C	DBP7	Dead Box Protein	A/V	gCc/gTc
YKR043C	SHB17	SedoHeptulose 1,7-Bisphosphatase	R/C	Cgt/Tgt
YKR054C	DYN1	DYNein	E/G	gAa/gGa
YKR082W	NUP133	NUclear Pore	E/K	Gaa/Aaa
YLL040C	VPS13	Vacuolar Protein Sorting	V/A	gTt/gCt
YLR019W	PSR2	Plasma membrane Sodium Response	A/T	Gca/Aca
YLR045C	STU2	Suppressor of TUbulin	N/S	aAc/aGc
YLR067C	PET309	PETite colonies	P/L	cCc/cTc
YLR081W	GAL2	GALactose metabolism	F/S	tTc/tCc
YLR083C	EMP70		E/G	gAa/gGa
YLR108C			A/T	Gca/Aca
YLR131C	ACE2	Activator of CUP1 Expression	P/Q	cCg/cAg
YLR131C	ACE2	Activator of CUP1 Expression	R/Q	cGa/cAa
YLR253W	MCP2	Mdm10 Complementing Protein	I/F	Atc/Ttc
YLR314C	CDC3	Cell Division Cycle	P/S	Cct/Tct
YLR353W	BUD8	BUD site selection	A/T	Gct/Act
YLR410W	VIP1		P/L	cCc/cTc
YLR466W	YRF1-4		L/M	Ttg/Atg
YLR467W	YRF1-5		F/L	ttC/ttG
YLR467W	YRF1-5		P/S	Cct/Tct
YLR467W	YRF1-5		L/M	Ttg/Atg
YML124C	TUB3	TUBulin	R/C	Cgt/Tgt
YML109W	ZDS2	Zillion Different Screens	A/T	Gcc/Acc
YML065W	ORC1	Origin Recognition Complex	G/D	gGc/gAc
YMR012W	CLU1	CLUstered mitochondria	E/K	Gaa/Aaa
YMR049C	ERB1	Eukaryotic Ribosome Biogenesis	E/D	gaG/gaC
YMR089C	YTA12	Yeast Tat-binding Analog	R/C	Cgt/Tgt
YMR124W	EPO1	Endoplasmic reticulum POlarization	A/V	gCa/gTa
YMR137C	PSO2	PSOralen derivative sensitive	E/D	gaG/gaT
YMR190C	SGS1	Slow Growth Suppressor	D/N	Gat/Aat
YMR192W	GYL1	GYp Like	A/V	gCa/gTa
YMR229C	RRP5	Ribosomal RNA Processing	A/T	Gcc/Acc
YMR251W	GTO3	Glutathione Transferase Omega-like	V/I	Gta/Ata
YNL339C	YRF1-6	-	L/M	Ttg/Atg
YNL326C	PFA3	Protein Fatty Acyltransferase	A/S	Gcc/Tcc
YNL321W	VNX1	Vacuolar Na+/H+ eXchanger	R/H	cGt/cAt
YNL224C	SQS1	SQuelch of Splicing suppression	S/N	aGt/aAt
YNL186W	UBP10	UBiquitin-specific Protease	P/S	Cca/Tca
YNL017C	-	-	H/Y	Cat/Tat
YNR013C	PHO91	PHOsphate metabolism	H/Y	Cat/Tat
YNR018W	RCF2	Respiratory superComplex Factor	A/T	Gct/Act
YNR023W	SNF12	Sucrose NonFermenting	C/Y	tGc/tAc
YNR041C	COQ2	COenzyme Q	T/I	aCc/aTc
YNR042W	-	-	V/M	Gtg/Atg
YOL125W	TRM13	TRna Methyltransferase	G/D	gGc/gAc
YOL105C	WSC3	cell Wall integrity and Stress response Component	A/V	gCa/gTa
YOL105C	WSC3	cell Wall integrity and Stress response Component	L/V	Ctg/Gtg
YOL070C	NBA1	Nap1p and Bud neck Associated	P/L	cCc/cTc
YOL060C	MAM3	-	S/P	Tca/Cca
YOL058W	ARG1	ARGinine requiring	A/V	gCa/gTa
YOL022C	TSR4	Twenty S rRNA accumulation	M/I	atG/atT
YOR043W	WHI2	WHIskey	Y/C	tAc/tGc
YOR073W	SGO1	ShuGOshin (Japanese for "guardian spirit")	P/L	cCa/cTa
YOR096W	RPS7A	Ribosomal Protein of the Small subunit	V/I	Gtt/Att

YOR116C	RPO31	RNA POlymerase	G/D	gGc/gAc
YOR119C	RIO1	RIght Open reading frame	G/C	Ggt/Tgt
YOR127W	RGA1	Rho GTPase Activating Protein	S/Y	tCc/tAc
YOR140W	SFL1	Suppressor gene for FLocculation	G/R	Ggg/Agg
YOR218C			V/I	Gtc/Atc
YOR270C	VPH1	Vacuolar pH	R/H	cGt/cAt
YOR328W	PDR10	Pleiotropic Drug Resistance	P/H	cCt/cAt
YOR396W	YRF1-8	-	F/L	ttC/ttG
YOR396W	YRF1-8	-	P/S	Cct/Tct
YOR396W	YRF1-8	-	L/M	Ttg/Atg
YPL283C	YRF1-7	-	L/M	Ttg/Atg
YPL235W	RVB2	RuVB-like	R/I	aGa/aTa
YPL200W	CSM4	Chromosome Segregation in Meiosis	V/I	Gta/Ata
YPL187W	MF(ALPHA)	Mating Factor ALPHA	N/I	aAc/aTc
YPL055C	LGE1	LarGE cells	T/I	aCc/aTc
YPL001W	HAT1	Histone AcetylTransferase	A/T	Gct/Act
YPR030W	CSR2	Chs5 Spa2 Rescue	D/N	Gat/Aat
YPR052C	NHP6A	Non-Histone Protein	V/L	Gtc/Ctc
YPR053C			K/N	aaG/aaC
YPR057W	BRR1	Bad Response to Refrigeration	A/V	gCc/gTc
YPR099C			H/Y	Cat/Tat
YPR100W	MRPL51	Mitochondrial Ribosomal Protein, Large subunit	C/Y	tGc/tAc
YPR104C	FHL1	Fork Head-Like	S/T	aGt/aCt
YPR149W	NCE102	NonClassical Export	V/A	gTt/gCt
YPR194C	OPT2	OligoPeptide Transporter	L/S	tTa/tCa

Table S 6
(continued)

Table S 7
Gene Ontology
Enrichment for the list
of genes with variants
with moderate or
high impact. Max BH
corrected p-value 0.05.

GO term description	Gene identities	Term	No. of genes in term	p-value
Organelle organization	YAR002CA | YAR014C | YBL034C | YBR112C | YBR158W | YBR179C | YBR227C | YDL006W | YDL017W | YDL089W | YDL134C | YDL222C | YDR080W | YDR097C | YDR207C | YDR218C | YDR229W | YDR356W | YEL062W | YEL077C | YER071C | YER162C | YER190W | YFL049W | YGL049C | YGL115W | YGL158W | YGL173C | YGL216W | YGR148C | YGR162W | YGR270W | YGR296W | YHR098C | YHR150W | YIL177C | YIR025W | YJL225C | YJR031C | YKL166C | YKR016W | YKR054C | YKR082W | YLL040C | YLR045C | YLR067C | YLR253W | YLR314C | YLR466W | YLR467W | YML065W | YML109W | YML124C | YMR012W | YMR089C | YMR124W | YMR137C | YMR190C | YMR229C | YNL186W | YNL326C | YNL339C | YNR018W | YOL060C | YOR043W | YOR064C | YOR073W | YOR119C | YOR127W | YOR396W | YPL001W | YPL055C | YPL200W | YPL235W | YPL283C | YPR052C | YPR100W | YPR194C	GO:0006996	78	1.11E-04
DNA duplex unwinding	YEL077C | YER190W | YGR296W | YIL177C | YJL225C | YLR466W | YLR467W | YMR190C | YNL339C | YOR396W | YPL235W | YPL283C	GO:0032508	12	5.74E-04
Biological regulation	YAR002CA | YAR014C | YBL034C | YBL040C | YBL104C | YBR112C | YBR158W | YBR203W | YBR227C | YDL006W | YDL017W | YDL089W | YDL134C | YDL171C | YDR011W | YDR019C | YDR043C | YDR080W | YDR097C | YDR207C | YDR217C | YDR356W | YDR523C | YEL062W | YER071C | YER162C | YER190W | YFL049W | YFR026C | YGL008C | YGL013C | YGL049C | YGL115W | YGL124C | YGL158W | YGL173C | YGL195W | YGL216W | YGR014W | YGR040W | YGR162W | YGR270W | YGR271W | YGR296W | YHR064C | YHR086W | YHR106W | YIL130W | YIL137C | YIR025W | YJR031C | YJR147W | YKL166C | YKR082W | YLL040C | YLR019W | YLR067C | YLR083C | YLR131C | YLR253W | YLR466W | YLR467W | YML065W | YML109W | YMR137C | YMR190C | YMR192W | YNL186W | YNL224C | YNL321W | YNL339C | YNR013C | YNR018W | YNR023W | YOL060C | YOL070C | YOL105C | YOR043W | YOR064C | YOR073W | YOR119C | YOR127W | YOR140W | YOR270C | YPL001W | YPL055C | YPL187W | YPL200W | YPL235W | YPL283C | YPR030W | YPR052C | YPR100W | YPR104C | YPR149W | YPR194C	GO:0065007	96	6.15E-04
DNA geometric change	YEL077C | YER190W | YGR296W | YIL177C | YJL225C | YLR466W | YLR467W | YMR190C | YNL339C | YOR396W | YPL235W | YPL283C	GO:0032392	12	0.000812
mitotic cell cycle process	YBL034C | YBR158W | YDL017W | YDL089W | YDL134C | YDR217C | YDR218C | YDR356W | YGL158W | YGL173C | YGL216W | YGR014W | YGR041W | YIR025W | YKR054C | YLR045C | YLR131C | YLR314C | YLR353W | YML065W | YML109W | YML124C | YMR190C | YOL070C | YOR073W | YOR119C | YOR127W	GO:1903047	27	0.006037
Cellular component organization	YAL039C | YAR002CA | YAR014C | YBL034C | YBR112C | YBR158W | YBR179C | YBR227C | YDL006W | YDL017W | YDL089W | YDL134C | YDL222C | YDR043C | YDR080W | YDR097C | YDR207C | YDR218C | YDR229W | YDR356W | YDR523C | YEL062W | YEL077C | YER071C | YER162C | YER190W | YFL049W | YGL008C | YGL049C | YGL115W | YGL158W | YGL173C | YGL216W | YGR014W | YGR040W | YGR148C | YGR162W | YGR270W | YGR296W | YHR086W | YHR098C | YHR150W | YIL177C | YIR025W | YJL225C | YJR031C | YKL166C | YKR016W | YKR054C | YKR082W | YLL040C | YLR045C | YLR067C | YLR253W | YLR314C | YLR466W | YLR467W | YML065W | YML109W | YML124C | YMR012W | YMR089C | YMR124W | YMR137C | YMR190C | YMR229C | YNL186W | YNL326C | YNL339C | YNR018W | YOL060C | YOL105C | YOR043W | YOR064C | YOR073W | YOR119C | YOR127W | YOR270C | YOR396W | YPL001W | YPL055C | YPL200W | YPL235W | YPL283C | YPR030W | YPR052C | YPR057W | YPR100W | YPR149W | YPR194C	GO:0016043	90	0.006564
DNA conformation change	YBR112C | YEL077C | YER162C | YER190W | YGR296W | YIL177C | YJL225C | YKR082W | YLR466W | YLR467W | YML065W | YML109W | YMR190C | YNL186W | YNL339C | YOR396W | YPL235W | YPL283C	GO:0071103	18	0.006928
Mitotic cell cycle	YBL034C | YBR158W | YDL017W | YDL089W | YDL134C | YDR217C | YDR218C | YDR356W | YDR523C | YGL158W | YGL173C | YGL216W | YGR014W | YGR041W | YIR025W | YKR054C | YLR045C | YLR131C | YLR314C | YLR353W | YML065W | YML109W | YML124C | YMR190C | YOL070C | YOR073W | YOR119C | YOR127W	GO:0000278	28	0.007811

Regulation of cellular process	YAR014C | YBL034C | YBL104C | YBR112C | YBR158W | YBR203W | YBR227C | YDL006W | YDL017W | YDL089W | YDL134C | YDR043C | YDR080W | YDR097C | YDR207C | YDR217C | YDR356W | YDR523C | YEL062W | YER071C | YER162C | YFL049W | YFR026C | YGL008C | YGL013C | YGL049C | YGL115W | YGL158W | YGL173C | YGL195W | YGL216W | YGR014W | YGR040W | YGR162W | YGR270W | YGR271W | YHR086W | YIL130W | YIL137C | YIR025W | YJR031C | YJR147W | YKL166C | YKR082W | YLL040C | YLR019W | YLR067C | YLR131C | YML065W | YML109W | YMR190C | YMR192W | YNL186W | YNR013C | YNR018W | YNR023W | YOL070C | YOL105C | YOR043W | YOR064C | YOR073W | YOR119C | YOR127W | YOR140W | YPL001W | YPL187W | YPL200W | YPL235W | YPR030W | YPR052C | YPR100W | YPR104C | YPR149W | YPR194C	GO:0050794	75	0.015995
Chromosome organization	YBR112C | YDL017W | YDL089W | YDR097C | YDR207C | YDR356W | YEL077C | YER162C | YER190W | YFL049W | YGL216W | YGR270W | YGR296W | YIL177C | YIR025W | YJL225C | YKR054C | YKR082W | YLR466W | YLR467W | YML065W | YML109W | YML124C | YMR137C | YMR190C | YNL186W | YNL339C | YOR064C | YOR073W | YOR396W | YPL001W | YPL055C | YPL200W | YPL235W | YPL283C | YPR052C	GO:0051276	36	0.018212
Regulation of TORC1 signaling	YBL104C | YEL062W | YGL008C | YGL195W | YLR019W | YOR043W	GO:1903432	6	0.019688
Telomere maintenance via recombination	YER190W | YGR296W | YLR466W | YLR467W | YMR190C | YNL339C | YPL283C	GO:0000722	7	0.020722
DNA duplex unwinding	YEL077C | YER190W | YGR296W | YIL177C | YJL225C | YLR466W | YLR467W | YMR190C | YNL339C | YOR396W | YPL235W | YPL283C	GO:0032508	12	5.74E-04
Biological regulation	YAR002CA | YAR014C | YBL034C | YBL040C | YBL104C | YBR112C | YBR158W | YBR203W | YBR227C | YDL006W | YDL017W | YDL089W | YDL134C | YDL171C | YDR011W | YDR019C | YDR043C | YDR080W | YDR097C | YDR207C | YDR217C | YDR356W | YDR523C | YEL062W | YER071C | YER162C | YER190W | YFL049W | YFR026C | YGL008C | YGL013C | YGL049C | YGL115W | YGL124C | YGL158W | YGL173C | YGL195W | YGL216W | YGR014W | YGR040W | YGR162W | YGR270W | YGR271W | YGR296W | YHR064C | YHR086W | YHR106W | YIL130W | YIL137C | YIR025W | YJR031C | YJR147W | YKL166C | YKR082W | YLL040C | YLR019W | YLR067C | YLR083C | YLR131C | YLR253W | YLR466W | YLR467W | YML065W | YML109W | YMR137C | YMR190C | YMR192W | YNL186W | YNL224C | YNL321W | YNL339C | YNR013C | YNR018W | YNR023W | YOL060C | YOL070C | YOL105C | YOR043W | YOR064C | YOR073W | YOR119C | YOR127W | YOR140W | YOR270C | YPL001W | YPL055C | YPL187W | YPL200W | YPL235W | YPL283C | YPR030W | YPR052C | YPR100W | YPR104C | YPR149W | YPR194C	GO:0065007	96	6.15E-04
DNA geometric change	YEL077C | YER190W | YGR296W | YIL177C | YJL225C | YLR466W | YLR467W | YMR190C | YNL339C | YPL235W | YPL283C	GO:0032392	12	0.000812
mitotic cell cycle process	YBL034C | YBR158W | YDL017W | YDL089W | YDL134C | YDR217C | YDR218C | YDR356W | YGL158W | YGL173C | YGL216W | YGR014W | YGR041W | YIR025W | YKR054C | YLR045C | YLR131C | YLR314C | YLR353W | YML065W | YML109W | YML124C | YMR190C | YOL070C | YOR073W | YOR119C | YOR127W	GO:1903047	27	0.006037
Cellular component organization	YAL039C | YAR002CA | YAR014C | YBL034C | YBR112C | YBR158W | YBR179C | YBR227C | YDL006W | YDL017W | YDL089W | YDL134C | YDL222C | YDR043C | YDR080W | YDR097C | YDR207C | YDR218C | YDR229C | YDR356W | YDR523C | YEL062W | YEL077C | YER071C | YER162C | YER190W | YFL049W | YGL008C | YGL049C | YGL115W | YGL158W | YGL173C | YGL216W | YGR014W | YGR040W | YGR148C | YGR162W | YGR270W | YGR296W | YHR086W | YHR098C | YHR150W | YIL177C | YIR025W | YJL225C | YJR031C | YKL166C | YKR016W | YKR054C | YKR082W | YLL040C | YLR045C | YLR067C | YLR253W | YLR314C | YLR466W | YLR467W | YML065W | YML109W | YML124C | YMR012W | YMR089C | YMR124W | YMR137C | YMR190C | YMR229C | YNL186W | YNL326C | YNL339C | YNR018W | YOL060C | YOL105C | YOR043W | YOR064C | YOR073W | YOR119C | YOR127W | YOR270C | YOR396W | YPL001W | YPL055C | YPL200W | YPL235W | YPL283C | YPR030W | YPR052C | YPR057W | YPR100W | YPR149W | YPR194C	GO:0016043	90	0.006564

Table S 7
(continued)

DNA conformation change	YBR112C | YEL077C | YER162C | YER190W | YGR296W | YIL177C | YJL225C | YKR082W | YLR466W | YLR467W | YML065W | YML109W | YMR190C | YNL186W | YNL339C | YOR396W | YPL235W | YPL283C	GO:0071103	18	0.006928
Mitotic cell cycle	YBL034C | YBR158W | YDL017W | YDL089W | YDL134C | YDR217C | YDR218C | YDR356W | YDR523C | YGL158W | YGL173C | YGL216W | YGR014W | YGR041W | YIR025W | YKR054C | YLR045C | YLR131C | YLR314C | YLR353W | YML065W | YML109W | YML124C | YMR190C | YOL070C | YOR073W | YOR119C | YOR127W	GO:0000278	28	0.007811
Regulation of cellular process	YAR014C | YBL034C | YBL104C | YBR112C | YBR158W | YBR203W | YBR227C | YDL006W | YDL017W | YDL089W | YDL134C | YDR043C | YDR080W | YDR097C | YDR207C | YDR217C | YDR356W | YDR523C | YEL062W | YER071C | YER162C | YFL049W | YFR026C | YGL008C | YGL013C | YGL049C | YGL115W | YGL158W | YGL173C | YGL195W | YGL216W | YGR014W | YGR040W | YGR162W | YGR270W | YGR271W | YHR086W | YHR106W | YIL130W | YIL137C | YIR025W | YJR031C | YJR147W | YKL166C | YKR082W | YLL040C | YLR019W | YLR067C | YLR131C | YML065W | YML109W | YMR190C | YMR192W | YNL186W | YNR013C | YNR018W | YNR023W | YOL070C | YOL105C | YOR043W | YOR064C | YOR073W | YOR119C | YOR127W | YOR140W | YPL001W | YPL187W | YPL200W | YPL235W | YPR030W | YPR052C | YPR100W | YPR104C | YPR149W | YPR194C	GO:0050794	75	0.015995
Chromosome organization	YBR112C | YDL017W | YDL089W | YDR097C | YDR207C | YDR356W | YEL077C | YER162C | YER190W | YFL049W | YGL216W | YGR270W | YGR296W | YIL177C | YIR025W | YJL225C | YKR054C | YKR082W | YLR466W | YLR467W | YML065W | YML109W | YML124C | YMR137C | YMR190C | YNL186W | YNL339C | YOR064C | YOR073W | YOR396W | YPL001W | YPL055C | YPL200W | YPL235W | YPL283C | YPR052C	GO:0051276	36	0.018212
Regulation of TORC1 signaling	YBL104C | YEL062W | YGL008C | YGL195W | YLR019W | YOR043W	GO:1903432	6	0.019688
Telomere maintenance via recombination	YER190W | YGR296W | YLR466W | YLR467W | YMR190C | YNL339C | YPL283C	GO:0000722	7	0.020722
Regulation of TOR signaling	YBL104C | YEL062W | YGL008C | YGL195W | YLR019W | YOR043W	GO:0032006	6	0.035297
TORC1 signaling	YBL104C | YEL062W | YGL008C | YGL195W | YLR019W | YOR043W	GO:0038202	6	0.035297
Rellular component organization or biogenesis	YAL039C | YAR002C-A | YAR014C | YBL034C | YBR112C | YBR158W | YBR179C | YBR227C | YDL006W | YDL017W | YDL089W | YDL134C | YDL222C | YDR043C | YDR080W | YDR097C | YDR207C | YDR218C | YDR229W | YDR356W | YDR523C | YEL062W | YEL077C | YER071C | YER162C | YER190W | YFL049W | YGL008C | YGL049C | YGL115W | YGL158W | YGL173C | YGL216W | YGR014W | YGR040W | YGR148C | YGR162W | YGR270W | YGR296W | YHR064C | YHR086W | YHR098C | YHR150W | YIL137C | YIL177C | YIR025W | YJL225C | YJR031C | YKL166C | YKR016W | YKR024C | YKR054C | YKR082W | YLL040C | YLR045C | YLR067C | YLR253W | YLR314C | YLR466W | YLR467W | YML065W | YML109W | YML124C | YMR012W | YMR049C | YMR089C | YMR124C | YMR137C | YMR190C | YMR229C | YNL186W | YNL224C | YNL326C | YNL339C | YNR018W | YOL022C | YOL060C | YOL105C | YOR043W | YOR064C | YOR073W | YOR096W | YOR119C | YOR127W | YOR270C | YOR396W | YPL001W | YPL055C | YPL200W | YPL235W | YPL283C | YPR030W | YPR052C | YPR057W | YPR100W | YPR149W | YPR194C	GO:0071840	97	0.036626

Pathway enrichment description	Gene identities	Pathway	No. of genes in term	p-value
Phosphatidylethanolamine biosynthesis I	CHO1 | PSD2	PWY-5669	2	1.74E-03
Phospholipid biosynthesis	CHO1 | PSD2	PHOSLIPSYN2-PWY-1	2	1.15E-02
De novo biosynthesis of pyrimidine ribonucleotides	URA7 | URA6	PYRIMID-RNTSYN-PWY	2	1.92E-02
Urea degradation I	DUR1 | 2	PWY-5703	1	2.52E-02
Superpathway of pyrimidine ribonucleotides de novo biosynthesis	URA7 | URA6	PWY0-162	2	2.85E-02
Superpathway of phospholipid biosynthesis	CHO1 | PSD2	PWY3O-2	2	4.51E-02
Fatty acids biosynthesis	FAS1	PWY3O-31723	1	4.99E-02

Table S 8
Pathway enrichment for the list of genes with variants with moderate or high impact in CEN.PK-EVO.

175

	CN30	EVO30	CN39	EVO39
C8	0.645 ± 0.052	0.383 ± 0.103	0.102 ± 0.004	0.224 ± 0.048
C10	2.92 ± 0.23	2.2 ± 0.13	2.52 ± 0.41	1.26 ± 0.15
C12	3.85 ± 0.34	8.41 ± 0.38	3.49 ± 0.27	6.17 ± 0.45
C14	5.93 ± 0.61	12.11 ± 0.56	3.13 ± 0.51	10.57 ± 1.21
C14:1	0.175 ± 0.014	2.409 ± 0.218	0.165 ± 0.008	0.23 ± 0.061
C16	29.6 ± 0.8	19.6 ± 1	31.6 ± 1.6	27.7 ± 1.1
C16:1	8.04 ± 0.83	13.74 ± 0.09	10.99 ± 1.51	4.78 ± 0.42
C18	1.6 ± 0.24	2.51 ± 0.23	0.44 ± 0.04	1.46 ± 0.2
C18:1	41.1 ± 0.1	30.7 ± 1.3	42.6 ± 1.7	40.7 ± 0.5

Table S 9
Fatty acids composition of the chemostat culture at 30.0°C and 39.0°C for both unevolved and the evolved strains. The relative abundance based on the total sum of the identified fatty acids in each strain which was normalized by the weight of the sample analysed. The standard deviation based on three independent samples collected at three different time points during the steady state chemostat. CN30 and CN39 indicated as the chemostat culture of CEN.PK113-7D at 30.0°C and 39.0°C, respectively. EVO30 and EVO39 indicated as the chemostat culture of CEN.PK-EVO at 30.0°C and 39.0°C, respectively.

Chapter 5

Global Proteomic Analysis of *Saccharomyces* cerevisiae to Identify Mechanisms for High Temperature Tolerance under Anaerobic Conditions

177

Shotgun proteomics was used to generate proteome profiles of anaerobically grown chemostat cultures of CEN.PK113-7D and the high temperature evolved CEN.PK113-7D at 30.0°C and 39.0°C. The analysis of the proteome profiles revealed that the responses to 39.0°C involved general (the same for both strains) and strain-specific mechanisms. Overall, we observed that both strains showed a strong repression of several proteins involved in central carbon metabolism and translation, and an increased expression of proteins involved in protein folding at 39.0°C. Significant differences in quantity and capacity of several glycolytic enzymes were observed in both strains at high cultivation temperature, most likely to maintain metabolite homeostasis. Intracellular metabolite quantification indeed confirmed that except for fructose 1,6 bisphosphate, of which the level was four to fivefold reduced in both strains at high temperature, the levels of all glycolytic intermediates were not affected by temperature. The proteome analysis suggested that the evolved strain counteracted the thermal stress through multiple mechanisms, such as better nutrient recycling by autophagy, better cytoplasmic pH regulation, increased trehalose accumulation, decrease of Ras activation, increased translation capacity and decreased proteome allocation in central carbon metabolism.

1

Introduction

The response of *Saccharomyces cerevisiae* yeast to supra-optimal temperatures is of a great relevance to second-generation biofuel production, e.g. reducing cooling costs and accomplishment of simultaneous saccharification of cellulosic feedstocks at supra-optimal temperatures (≥40°C). With the advance of high-throughput omics technologies (genomics, transcriptomics, proteomics, and metabolomics), many efforts have been made to systematically identify the molecular responses of yeast to prolonged thermal stress [1–4]. Most of these studies have been performed under aerobic rather than anaerobic conditions, while the latter is more relevant for biofuel production processes. In a previous study, we analysed the differences in the physiological response of a number of industrial *S. cerevisiae* strains and the well characterized laboratory strain *S. cerevisiae* (CEN.PK113-7D) during growth at supra-optimal temperatures under anaerobic conditions [4]. Although the laboratory strain was used as a reference for comparison with the industrial strains and the investigated strains were all *S. cerevisiae* yeasts, differences between each selected industrial strain may have interfered with specific temperature effects, thus hampering to draw clear conclusions. Moreover, the industrial strains used were less well characterized than the reference strain. In order to specifically pinpoint adaptive strategies where yeast develops to cope with prolonged thermal stress, we applied adaptive laboratory evolution of the well-studied laboratory strain CEN.PK113-7D, resulting in an evolved strain with improved growth performance at ~40°C under anaerobic conditions. Subsequently, we compared its physiological response to supra-optimal temperatures together with the unevolved CEN.PK113-7D and carried out whole genome sequencing of both strains (Chapter 4).

Temperature affects not only protein stability but also reaction rate which is often described using an Arrhenius function [5]. The

maximum rate of an enzymatic reaction depends on the amount of active enzyme and has a positive correlation with increasing temperature, which is well described by an enzyme-assisted Arrhenius model [6]. Furthermore there is a clear positive correlation between increased cultivation temperature and energy expenses in non-growth associated processes in cells, such as protein (re)folding and degradation of denatured proteins [7]. Glycolysis is the main catabolic pathway to generate energy for cellular maintenance and cell growth under anaerobic conditions.

In this work, we aimed to gain more insight into the influence of the mutations found in the evolved strain (Chapter 4) on protein expression and their contribution to the improved growth of the evolved strain at supra-optimal temperatures. To this end, cell samples taken from steady state chemostat cultivations of both strains cultivated at 30°C and 39 °C were subjected to global proteome analysis. Furthermore, we analysed the effects of the cultivation as well as the assay temperature on the enzymatic capacities of most of the glycolytic enzymes under in vivo like conditions. As in vivo enzyme activities also depend on the concentrations of substrates, effectors and products, we also quantified the metabolites in the central carbon metabolism to characterise possible metabolic adjustment of enzyme activities to the cultivation temperatures. With respect to the interconnected multi-layer regulations from gene and protein expression to flux, we aim to understand the strain-specific response of the evolved *S. cerevisiae* strain to prolonged thermal stress under anaerobic conditions.

2
Methods and materials

2.1
Yeast strains and growth conditions

The *S. cerevisiae* strains used in this study were the laboratory strain CEN.PK113-7D (Fungal Biodiversity Centre, Utrecht, The Netherlands) and the high temperature evolved CEN.PK113-7D which was derived from the laboratory strain by in-vitro evolution as described in Chapter 4. Pre-cultures were prepared by introducing two frozen culture stocks into 1000mL Erlenmeyer flasks containing 400 mL of filter sterilized synthetic medium [8] supplemented with 15 g·L⁻¹ glucose monohydrate. The flasks were incubated overnight in an orbital shaker at 30°C and at a rotation speed of 220 *rpm*. The pre-cultures were used to inoculate the chemostat cultivations, which were carried out as described previously (Chapter 4). After achieving a steady state, broth samples were withdrawn for proteome analysis. After centrifugation at 5000 *rpm* and at 4°C during 2 minutes, the supernatant was discarded and the cell pellet was washed with the same volume of cold Mi-Q water and again centrifuged at 4°C and at 5000 *rpm* for 2 minutes. The supernatant was discarded, and the biomass pellet was immediately frozen in liquid nitrogen and stored at -80°C until the analysis described below.

2.2
Intracellular metabolites analysis

Samples containing approximately 2 mg dry-weight of cells from the chemostat fermentations described previously (Chapter 4) were obtained by immediately quenching of 1.3 ± 0.2 mL of culture broth into 8.0 mL of 100 % -40°C methanol using a rapid sampling setup [9]. Directly after sampling, the exact weight of each sample was determined by weighing each tube before and after sampling. Cells from each sample were separated by filtration and subsequently washed by cold filtration with 80 % (v/v) -40°C methanol. The intracellular metabolites were then extracted from the cells with the boiling ethanol method [10]. C¹³ labelled cell extract was added as an internal standard for IDMS-based quantification [11] at the beginning of the extraction process. The resulting extracts were stored at -80°C

until evaporation under vacuum (120 mins, 30°C, ≤ 5 mbar) using a RapidVac (Labconco, USA). After evaporation, the dried residues with C¹³ labelled internal standard were resuspended in 600 µL Mi-Q water, followed by centrifugation at 4°C and 13 000 x g for 5 mins. Supernatants were collected until further analysis.

The quantification of fructose-1,6-biphosphate, glucose-1-phosphate, phosphoenolpyruvate, pyruvate, trehalose-6-phosphate, and succinate in the supernatant samples was performed by using anion-exchange LC-MS/MS [12]. For the quantification of the other metabolites in the central carbon pathways (glycolysis, pentose phosphate pathway, and tricarboxylic cycle), 100 µL of supernatant samples were freeze-dried and derivatized [13]. The resulting derivatives were analysis by GC-MS [13]. For the quantification of amino acids, 3.0 g L⁻¹ NaCl was added to the cell extract of which 100 µL was freeze-dried and derivatized as previously described [9]. The resulting derivatives were injected for GC-MS analysis [9]. The metabolites were quantified by using the isotope dilution mass spectrometry (IDMS) method [11]. All quantifications were performed with four biological samples collected from duplicate chemostat fermentations.

Biomass pellets collected from three separate sampling time points during steady-state chemostat cultivation were thawed on ice. From each biomass pellet 50 mg was transferred to a 1.5 mL protein LoBind tube (Eppendorf, 022431081) and dissolved in 300 µL of cold cell lysis buffer containing 1.0 % SDS (Sigma-Aldrich, 71736-100ML, 10 % in H2O), 90 mM triethylammonium bicarbonate (Sigma-Aldrich, T7408-100ML, 1.0 M TEAB), 3.0 µL Protease Inhibitor Cocktail (Sigma-Aldrich, P8215-5ML, for use with fungal and yeast extracts), 7.5 µL Phosphatase Inhibitor Cocktail Set II (Millipore, 524625-1ML). The cell lysis buffer was prepared fresh prior to each experiment. The cell suspension was homogenized with 0.17 g glass beads (Sigma-Aldrich, G8772, acid-washed, 425-600 µm) using a bead beater (BioSpec Products, mini-Beadbeater-16) for 10 interval cycles. Each cycle consisted of 1-minute beadbeating and 1-minute resting on ice. The lysate was centrifuged at 14000 x g for 10 minutes at 4°C (Eppendorf, Centrifuge 5424R). A volume of 250 µL supernatant was pipetted to a new LoBind Eppendorf tube. The sample was mixed with 25 µL of 50 mM dithiothreithol (Sigma-Aldrich, 43815-5G) and incubated at 37°C and at 300 rpm for 1 hour in a heating block

2.3
Proteomics experiment

2.3.1
Protein extraction and in-solution proteolytic digestion

(Eppendorf, Thermomixer C with Thermotop). Then the sample was alkylated by adding 87.5 μL of 200 mM acrylamide (Sigma-Aldrich, A9099-25G) and incubated for 1 hour at room temperature in the dark (samples covered with aluminium foil). Each sample was split into two equal volumes in new LoBind Eppendorf tubes, and 725 μL of -20°C acetone (Sigma-Aldrich, 650501-1L) was added to each volume of sample. After briefly vortexing, the mixture was incubated at -20°C for 1 hour to precipitate the proteins, followed by centrifugation at 4°C and at 14000 x g for 10 minutes. The supernatant was removed, and the pellet was then washed with 100 μL -20°C acetone by vortexing for 1 minute. After centrifugation at 14000 x g for 10 minutes at 4°C, the tubes were again gently inverted to remove the supernatant. The pellet was then resuspended in 100 μL of 100 mM ammonium bicarbonate (Sigma-Aldrich, 09830-500G). To digest the proteins, 2.5 μL of 0.1 μg μL-1 trypsin (Promega, Sequencing Grade Modified Trypsin, V5111A) in 1 mM HCl was added to the suspension where after it was incubated overnight at 37°C.

The result mixture was desalted and purified by using solid phase extraction. Each column of a 96-column μElution plate (Waters, Oasis HLB μElution 30μm, 186001828BA) was first conditioned with 750 μL of 100 % methanol (Honeywell Riedel-de-Haën, 34860-2.5L) and equilibrated with two times 500 μL of LC-MS grade water (Thermo Fisher Scientific, LC/MS optima, W6-1). The samples were loaded on the columns for filtration. Each column was then washed with 700 μL 5 % methanol followed by a second wash of 300 μL 5 % methanol. The samples were eluted with 200 μL of 80 % methanol containing 0.01 % trifluoroacetic acid (Acros Organics, 293811000) followed by a second elution with 200 μL of 80% methanol containing 1.0 mM ammonium bicarbonate. The samples were stored at -80°C for 1 hour followed by evaporation using a SpeedVac vacuum concentrator (Thermo Fisher Scientific, integrated SpeedVac SPD1010230) at 45°C for approximately 2 hours. The dried samples were stored at -20°C until tandem mass tag (TMT) labelling, as described below.

2.3.2
Protein peptides labelling with TMT reagents

The dried samples were dissolved in 100 mM TEAB and the protein concentration was estimated by the measurement at 280 nm on a NanoDrop spectrophotometer (Thermo Fisher Scientific, ND-1000). The samples were diluted to a protein concentration of approximately 2.5 μg μL-1 using 100 mM TEAB. The TMT

sixplex isobaric label reagents (Thermo Scientific, TMT sixplex label reagent set, 90061) were equilibrated in 40 μL of 100 % anhydrous acetonitrile prior use (Sigma-Aldrich, 271004-1L). Of each sample 20 μL was used and 5 μL of TMT sixplex isobaric label reagent was added according to the prepared scheme (table S1). The reaction mixture was incubated at 25°C and at 400 rpm for 1 hour. The reaction was stopped by adding 5 % hydroxylamine (Sigma-Aldrich, 50 wt. % in water, 467804-10ML) to a final concentration of 0.4 % and followed by incubation at 25°C and at 400 rpm for 15 minutes. Of each comparison condition, 10 μL of each biological replicate was pooled according to table S1. Each pooled sample was mixed with 240 μL of LC/MS water to dilute the acetonitrile concentration to ≤ 5 %. The pooled samples were frozen at -80°C for 1 hour and subsequent followed by drying using a SpeedVac vacuum concentrator at 45°C for approximately 2 hours. The samples were again desalted and purified using solid phase extraction as described above. The sample elution was dried using a SpeedVac vacuum concentrator at 45°C for approximately 2 hours and then dissolved in 15 μL of LC/MS water containing 0.1 % formic acid (Thermo Fisher Scientific, LC/MS optima, A117-50) and 3 % acetonitrile (Thermo Fisher Scientific, LC/MS optima, A955-1) to obtain a final concentration of 0.3 - 0.4 μg μL-1 labelled peptides for LC-MS measurement.

An aliquot corresponding to approx. 250 ng TMT labelled protein digest was analysed using an one dimensional shot-gun proteomics approach [14]. The peptides were separated using a nano-liquid-chromatography system consisting of an ESAY nano LC 1200, equipped with an Acclaim PepMap RSLC RP C18 capillary column (50 μm x 150 mm, 2μm) coupled online through a nano-spray source to an QE plus Orbitrap mass spectrometer (Thermo, Germany). The flow rate was maintained at 350 nL/min over a linear gradient from 7% to 25% solvent B over 98 minutes, and finally to 60% B over 20 minutes. Data were acquired from 5 to 125 min. Solvent A was H2O containing 0.1% formic acid, and solvent B consisted of 80% acetonitrile in H2O and 0.1% formic acid. The Orbitrap was operated in data depended acquisition mode acquiring peptide signals form 385-1450 m/z at 70K resolution, with an AGS target of 3e6. The top 10 signals were isolated at a window of 1.2 m/z and fragmented using a NCE of 32. Fragments were acquired at 35K resolution with an AGS target of 1e5. Unassigned, single charged as well as 7+ and higher were excluded from fragmentation. Data were analysed against the

2.3.3
LC-MS/MS
measurements
(shot-gun
proteomics)

proteome database from *Saccharomyces* cerevisiae (Uniprot, strain ATCC 204508 / S288C, Tax ID: 559292, July 2018) using PEAKS Studio X (Bioinformatics Solutions Inc, Canada) [15] allowing for 20 ppm parent ion and 0.02 m/z fragment ion mass error, 2 missed cleavages, acrylamide as fixed and methionine oxidation and N/Q deamidation as variable modifications. Quantitative analysis was performed using the PEAKS Q software using ANOVA. The following parameters were applied for quantification: peptide spectrum matches were filtered against 1% false discovery rates (FDR), protein identifications required ≥ 2 unique peptides, a minimum quality ≥ 15, a reporter ion intensity of ≥ 1E4, modified peptides were included, reporter ions present in all channels was required and reference channel present was set to true. Signal normalisation was set to auto-normalisation and quantification mass tolerance was set to equal or less 15 ppm. Data were further visualised/processed as described below.

2.3.4
Statistical
analysis

The average abundance of each protein which was detected from both duplicate injections of each combined sample was calculated from three biological replicates by using the software package PEAKS Q (Bioinformatics Solutions Inc, Canada). By this, the fold-change of the corresponding detected proteins between the conditions was established. We first performed statistical analysis on the protein discovery level, by using the target/decoy approach and by estimating false discovery rate (FDR) for peptide or protein identifications which allows multiple testing correction[16], and second by determining the statistical significance for every protein fold change by using two-sample t-test. The default proteins fold change threshold corresponded to a statistical significance of q-value 0.05 or below, which is specified otherwise in the respective tables or figures separately. The data as obtained by the bioinformatics software PEAKS were further processed by Matlab to visualise the data using volcano or scatter plots (as established by Pabst and den Ridder, manuscript in preparation, 2021) and tables.

2.3.5
Functional
annotation and
enrichment
analysis

To explore the biological processes among the proteins which have significant fold-change either higher than 2.0 or lower than 0.5 by comparison on the volcano plot, we used the *Saccharomyces* genome database (http://yeastgenome.org) to perform functional annotations of the selected proteins at gene ontology slim term mapper.

We examined the data sets between the chemostat cultures at 30°C and at 39°C for CEN.PK113-7D and the evolved CEN. PK113-7D (data sets CN3039 and EVO3039) for the enriched functional terms by using STRING [17] (https://string-db. org/). The protein network database was imported from the STRING v11.0 for functional enrichment analysis with an FDR threshold of 0.05. The resulting enriched terms of each analysis were sorted by FDR value (≤0.05). With the output data (CN3039 and EVO3039), we created Venn diagrams using Venny online software (Venny, http://bioinfogp.cnb.csic.es/tools/venny/index. html) to identified the differential expressed proteins in common and in different.

The proteins involved in glycolysis, glycogen metabolism, pentose phosphate pathway, pyruvate metabolisms, trehalose metabolism, and tricarboxylic acid cycle of *S. cerevisiae* were obtained from the UniProtKB database (https://www.uniprot.org/). The average output data sets (CN3039, EVO3039, and CNEVO39) were filtered against the target proteins. Metabolic networks were formulated in the software Omix v1.9.34 [18]. The fold-change differences for the target proteins at each comparison condition were visualized on the constructed networks by different node symbols in the software Omix v1.9.34 [19].

2.3.6
Data
visualization
with Omix

The frozen biomass pellet (approximately 30 mg dry weight) was first defrosted on ice and was resuspended in 20.0 mL cold in-vivo like buffer containing 1.0 mM dithiothreitol (DTT). The in-vivo like buffer was prepared freshly from the buffer stocks [20] prior the experiment and contained 300 mM potassium, 50 mM phosphate, 245 mM glutamate, 20 mM sodium, and 2.0 mM free magnesium, and 0.5 mM calcium at a pH of 6.8. The suspension pellet (10 mL) was vortexed with approximately 3.2 g glass beads (acid- washed, 425-600 μm, G8772 sigma) four interval cycles of 30 seconds followed with 30 seconds resting on ice. The result supernatant was centrifuged at 4°C and at 13000 rpm for 5 minutes. The supernatant was transferred into separate Eppendorf tubes and kept on ice.

2.4
Enzyme
Activity
measurements

2.4.1
Cell free extract
preparation

2.4.2
Enzymatic assays

The activity of hexokinase (HXK, EC 2.7.1.1), phosphoglucoisomerase (PGI, EC 5.3.1.9), phosphofructokinase (PFK, EC 2.7.1.11), aldolase (ALD, EC 4.1.2.13), glyceraldehyde-3-phosphate dehydrogenase (GAPDH, EC 1.2.1.12), 3-phosphoglycerate kinase (PGK, EC 2.7.2.3), phosphglycerate mutase (PGM, EC 5.4.2.1), pyruvate kinase (PYK, EC 2.7.1.40),and pyruvate decarboxylase (PDC, EC 4.1.1.1) in cell free extract were measured as previously described [20], except that hexokinase was assayed with 10.0 mM glucose, 2.0 mM ATP, 1.2 mM NADP and glucose-6-phosphate. Each assay was carried out in triplicates with 4 times diluted cell free extract at assay temperatures of 30°C and 39°C. Enzymatic activity was measured for 15 minutes where the absorbance at the last three minutes were used to calculate the specific activity.

2.4.3
Quantification of total protein content in cell free extract

The total protein concentration in cell free extract was determined as described in [21] where bovine serum albumin was used as standard. Triplicate measurements were obtained for each diluted cell free extract.

3
Results and Discussion

To investigate their proteome response to elevated cultivation temperature, we grew both an evolved, improved thermo-tolerant strain (EVO) (Chapter 4) and the unevolved strain CEN. PK113.7D (CN) at optimal (30.0°C) and supra-optimal (39.0°C) temperatures in duplicate, anaerobic, glucose limited chemostat cultures at a constant growth rate of 0.03 h-1. Therefore, for each strain, difference in protein expression should solely be induced by the cultivation temperature. The reconciled biomass specific conversion rates for both strains indicated that the duplicate experiments were very similar (Table S 2), which confirmed the reproducibility of the chemostat experiments. Therefore, samples from one of the duplicate chemostat cultures were collected at three time points during the steady state and were subjected to comparative proteome analysis.

The global proteome analysis of the chemostat cultures at 39.0°Crevealed that both strains had a similar number of differentially expressed proteins compared to cultivation at 30.0°C, namely in total 423 (268 upregulated and 155 downregulated) for the unevolved (CN39/CN30) and 414 (169 upregulated and 245 downregulated) for the evolved strain (EVO39/EVO30) (Figure S1). These changes in the proteome were not all strain specific, both strains had 200 (107 upregulated and 93 downregulated) differentially expressed proteins in common as response to elevated cultivation temperature. When comparing the evolved strain with the unevolved strain during the cultivation at 39.0°C(EVO39/CN39), 181 proteins were differentially expressed (48 upregulated and 133 downregulated) in the evolved strain compared to the unevolved strain (Figure 6).

All acquired differentially expressed proteins were visualised in a volcano plot (Figure S2) which combines statistical significance (t-test) with the fold-change of a differentially expressed protein

between two conditions for each comparison. The most significant differentially expressed proteins were identified from the global proteome data set at each comparison condition, based on the criterion that the differentially expressed protein between two conditions had at least a two-fold higher or lower abundance (Table S4).

The aim of the in-depth analysis of the differently expressed proteins described below was firstly to identify possible mechanisms for the improved growth performance of the evolved strain during cultivation at supra-optimal temperatures (chapter 4) and secondly to identify possible mechanisms behind the common responses to supra-optimal temperature in both strains. Therefore, three categories of responses are addressed:

1) the common responses of both strains growing at elevated cultivation temperature, 2) the specific response of the evolved strain growing at elevated cultivation temperature, 3) and the different responses of both strains growing at 39°C.
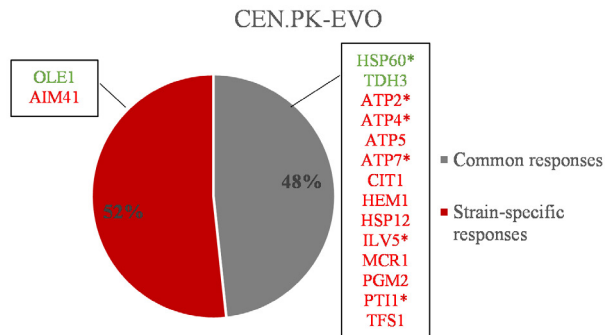
Figure 1

Differentially expressed proteins (in total 414 proteins) during chemostat cultivation of the evolved strain at 39.0°C compared to 30.0°C. The percentages of various responses were calculated based on the Venn diagram (Figure S1). The common responses (grey) refer to the differentially expressed proteins which were also found in the chemostat culture of unevolved strain at 39.0°C compared to 30.0°C. The strain-specific responses (red) refer to the differentially expressed proteins only found in the evolved strain between different cultivation temperatures. Proteins indicated in green were at least 2-fold upregulated, whereas proteins indicated in red were at least 2-fold downregulated in the evolved strain. The symbol (*) indicates the proteins that have also a 2-fold change or more in the unevolved strain between 39.0°C and 30.0°C (CN3039).

As mentioned above, both strains had 200 differentially expressed proteins in common as a response to growth at elevated cultivation temperatures (grey in Figure 1). From a KEGG-pathway enrichment analysis, it appears that the common responses of both strains at elevated cultivation temperature were predominantly in central carbon metabolism, translation, and protein folding (Table 1). From these proteins, we found 6 proteins which changed at least two-fold in both strains as response to the increase cultivation temperature (indicated with a star in the right box in Figure 1). From the five proteins which were at least two-fold downregulated in both strains as response to cultivation at 39.0°C; three (ATP2, ATP4, and ATP7) are subunits of the mitochondrial F1Fo ATP synthase complex. Although ATP generation through this complex plays no role during strictly anaerobic growth, anaerobically grown yeast cells, supplemented with unsaturated fatty acids and ergosterol, have been shown to contain mitochondria which are morphologically similar to aerobic mitochondria and contain active ATP synthase [22]. It has been reported that *S. cerevisiae* growing at temperatures above 37°C under aerobic conditions results in a steep decrease in the efficiency of oxidative phosphorylation and a severe alternation of mitochondrial morphology, without clear cristae [23]. Our observation of the significant decrease of several subunits of the F1Fo ATP synthase during growth at 39.0°C could, therefore, possibly be related to an alteration of the mitochondrial inner membrane structure. This could lead to a reduced membrane surface for the ATP synthase complex subunits to attach.

3.1
Common proteome responses to increased cultivation temperature

Table 1

Table 1 Enrichment analysis for KEGG pathways of the up-(green) and downregulated (red) proteins which were found in both CEN. PK113-7D and the evolved CEN.PK113-7D between 30°C and 39°C.

Category description	Protein identity	No. of proteins in cluster	No. of proteins in genome	FDR value
Ribosome	RPL4A | RPS9B | RPL13A | RPL35A | RPS11A | RPL12A | RPL34A | RPL23B | RPS26B | RPL24A | RPL7A | RPL28 | RPS2 | RPS26A | RPS25A | RPL24B | RPS20 | RPL2B | RPL34B | RPS5 | RPS4A | RPL37A | RPS28B | RPS25B | RPL6B | RPS18B | RPL6A | RPL13B | RPS16A | RPL16B | RPS3 | RPL18A | RPL3 | RPS28A | RPL20B | RPS12 | RPS9A | RPL5 | RPL1A | RPS23B	40	147	1.24E-36
Protein processing in endoplasmic reticulum	SSA1 | PDI1 | SSA4 | KAR2 | SSA2 | SEC61 | HSC82 | YDJ1 | SSE1 | HSP82	10	86	1.32E-05
Glycolysis / Gluconeogenesis	CDC19 | GPM2 | TPI1 | TDH3 | ENO2 | PDC1	6	55	2.10E-03
Biosynthesis of antibiotics	CYS3 | CDC19 | GPM2 | TPI1 | ADE5,7 | TDH3 | ENO2 | MET3 | PDC1	9	226	4.49E-02
Metabolic pathways	PGI1 | ARO4 | GLK1 | IDP1 | GCV1 | HEM13 | SDH4 | HEM1 | HPT1	52	716	3.35E-24
Biosynthesis of secondary metabolites	PGI1 | ARO4 | GLK1 | IDP1 | GCV1 | HEM13 | SDH4 | HEM1 | HPT1 | PDA1 | LPD1 | HXK1 | LSC2 | IMD2 | KGD1 | GUT2 | ILV3 | MDH1 | SDH1 | SDH2 | SHM2 | ILV5 | ERG6 | PGM2 | ZWF1 | CIT1 | ACC1 | MVD1 | LYS9 | ALD4 | ALD6 | ASN1 | GPH1	33	295	2.55E-19
Biosynthesis of amino acids	ARO4 | IDP1 | PYC1 | CYS4 | ILV3 | SHM2 | ILV5 | CIT1 | LYS9	9	120	3.40E-04
Carbon metabolism	PGI1 | GLK1 | IDP1 | GCV1 | SDH4 | PDA1 | LPD1 | HXK1 | PYC1 | LSC2 | KGD1 | MAE1 | MDH1 | SDH1 | SDH2 | SHM2 | ZWF1 | CIT1	18	112	1.10E-12
Purine metabolism	HPT1 | RNR4 | IMD2 | RNR2 | PGM2	5	99	3.03E-02
Oxidative phosphorylation	COR1 | IPP1 | ATP3 | SDH4 | ATP5 | COX4 | COX6 | ATP2 | ATP7 | SDH1 | SDH2 | ATP4 | QCR2	13	72	7.74E-10
Glycolysis / Gluconeogenesis	PGI1 | GLK1 | PDA1 | LPD1 | HXK1 | PGM2 | ALD4 | ALD6	8	55	1.32E-05
Pyruvate metabolism	DLD1 | PDA1 | LPD1 | PYC1 | MAE1 | MDH1 | ACC1 | ALD4 | ALD6	9	43	2.06E-07
Starch and sucrose metabolism	PGI1 | GLK1 | HXK1 | SUC2 | PGM2 | GPH1	6	40	2.10E-04
2-Oxocarboxylic acid metabolism	IDP1 | ILV3 | ILV5 | CIT1	4	35	5.20E-03
Amino sugar and nucleotide sugar metabolism	PGI1 | GLK1 | HXK1 | MCR1 | PGM2	5	33	6.00E-04
Citrate cycle (TCA cycle)	IDP1 | SDH4 | PDA1 | LPD1 | PYC1 | LSC2 | KGD1 | MDH1 | SDH1 | SDH2 | CIT1	11	32	7.75E-11
Glycine, serine and threonine metabolism	GCV1 | HEM1 | LPD1 | CYS4 | SHM2	5	31	5.00E-04
Alanine, aspartate and glutamate metabolism	CPA2 | GDH1 | ASN1	3	29	2.22E-02
Glyoxylate and dicarboxylate metabolism	GCV1 | LPD1 | MDH1 | SHM2 | CIT1	5	28	3.80E-04
Pentose phosphate pathway	PGI1 | PGM2 | ZWF1	3	28	2.12E-02
Glutathione metabolism	IDP1 | RNR4 | RNR2 | ZWF1	4	24	1.80E-03
Galactose metabolism	GLK1 | HXK1 | SUC2 | PGM2	4	23	1.70E-03
Tryptophan metabolism	KGD1 | ALD4 | ALD6	3	17	6.30E-03
Porphyrin and chlorophyll metabolism	HEM13 | HEM1	2	17	4.70E-02
Pantothenate and CoA biosynthesis	CAB2 | ILV3 | ILV5	3	15	5.10E-03
One carbon pool by folate	GCV1 | SHM2	2	15	4.06E-02
Sulfur metabolism	MET10 | MET5	2	15	4.06E-02
Lysine degradation	KGD1 | LYS9 | ALD4 | ALD6	4	14	4.00E-04
Histidine metabolism	ALD4 | ALD6	2	14	3.73E-02
Peroxisome	IDP1 | SOD1 | CAT2	3	38	3.59E-02

3.1.1
Up- and downregulated proteins involved in central carbon metabolism

Of the 107 upregulated proteins in both strains 6 were involved in metabolic pathways, all related to glycolysis/gluconeogenesis. Of the 93 downregulated proteins more than half (52 proteins) were involved in metabolic pathways (Table 1). We used heat maps to visualize the differential fold-changes of the proteins involved in different parts of (central) metabolism, namely glycolysis (Figure 2), pentose phosphate pathway (PPP) (Figure 3), TCA cycle (Figure 4), as well as glycogen and trehalose metabolism (Figure 5).

In the upper part of glycolysis between glucose and glyceraldehyde 3-phosphate (GAP), hexokinase 1 (HXK1), glucokinase (GLK1) and phosphoglucose isomerase (PGI1) were downregulated in both strains at 39.0°C, while triose phosphate isomerase (TPI1) was upregulated (Figure 2). There are no significant differences at the intracellular levels of G6P and F6P (Table S9), neither between the two cultivation temperatures nor between the two strains. It appears that these levels are tightly controlled, in this case by lowering the capacity of glucose phosphorylation and conversion to F6P through lowering the HXK1/GLK1 and PGI enzyme levels. From *in-vitro* enzyme activity measurements under *in-vivo* liked conditions we indeed found that the capacities of glucose phosphorylation were the same at 30.0°C and 39.0°C for both strains (section 3.4, Table 4, HXK, columns D/A). This was not the case for PGI, where the capacity increased more than two-fold during cultivation at 39.0°C in both strains (Table 4, PGI, columns D/A). However, this did not result in significant differences between mass action ratio's (MAR) for PGI for the four different conditions (Calculated from the measured G6P and F6P levels (Table S9); CN 39.0°C: 0.16; CN 30.0°C: 0.21; EVO 39.0°C: 0.21; EVO 30.0°C: 0.18).

Glucose-6-phosphate dehydrogenase (ZWF1), responsible for the first and the rate limiting step of PPP at which NADPH is regenerated, was downregulated in both strains at 39.0°C (Figure 3). This could have compensated a temperature induced capacity increase of the enzyme, as for both strains no significant changes occurred in the measured intermediates of the PPP during the cultivations at 39.0°C (Table S9).

In the lower part of glycolysis, glyceraldehyde-3-phosphate dehydrogenase isoenzyme 3 (TDH3), enolase isoenzyme 2 (ENO2), pyruvate kinase (CDC19), and the major pyruvate decarboxylase (PDC1) were all upregulated at 39.0°C in both strains. The upregulation of TDH (GAPDH), CDC19 (PYK) and PDC at 39.0°C was confirmed for both strains by the in-vitro enzyme capacity analysis (Table 4, columns D/A). The capacities of GAPDH, PYK and PDC in the 39 °C chemostat cultivations, due to the upregulation and the increased temperature (Table 4, columns D/A), were respectively increased 3.9-, 3.6- and 2.6- fold for the unevolved and respectively 5.8-, 7.8- and 3.4-fold for the evolved strain. The increased capacity of GAPDH in the 39.0°C cultivations might have been the reason of the 3.7- and

4.8-fold decreased levels of fructose-1,6-bisphosphate (FBP) for the unevolved and evolved strain, respectively (Table S9). It has been shown that FBP is a potent activator of Ras [24], a major regulator of cell proliferation in yeast. It has also been reported that the suppression of Ras activity results in a decreased sensitivity to heat shock [25]. An increased capacity of PYK is expected to cause a depletion of the intermediates of lower glycolysis (3-phosphoglyceric acid 3PG, 2-phosphoglyceric acid 2PG, phosphoenolpyruvic acid PEP) and an increase in the pyruvate level after a glucose pulse [26]. However, this cannot be observed from the intracellular metabolite measurements (Table S9), possibly because the effect of the capacity increase of PYK was counteracted by the capacity increase of GAPDH. The increased capacity of PDC1 coincided with the increased acetate production of both strains at 39.0°C (Table S2 and Table S3), although the mitochondrial (ALD4) and cytosolic (ALD6) aldehyde dehydrogenases catalysing the conversion of acetaldehyde to acetate were downregulated.
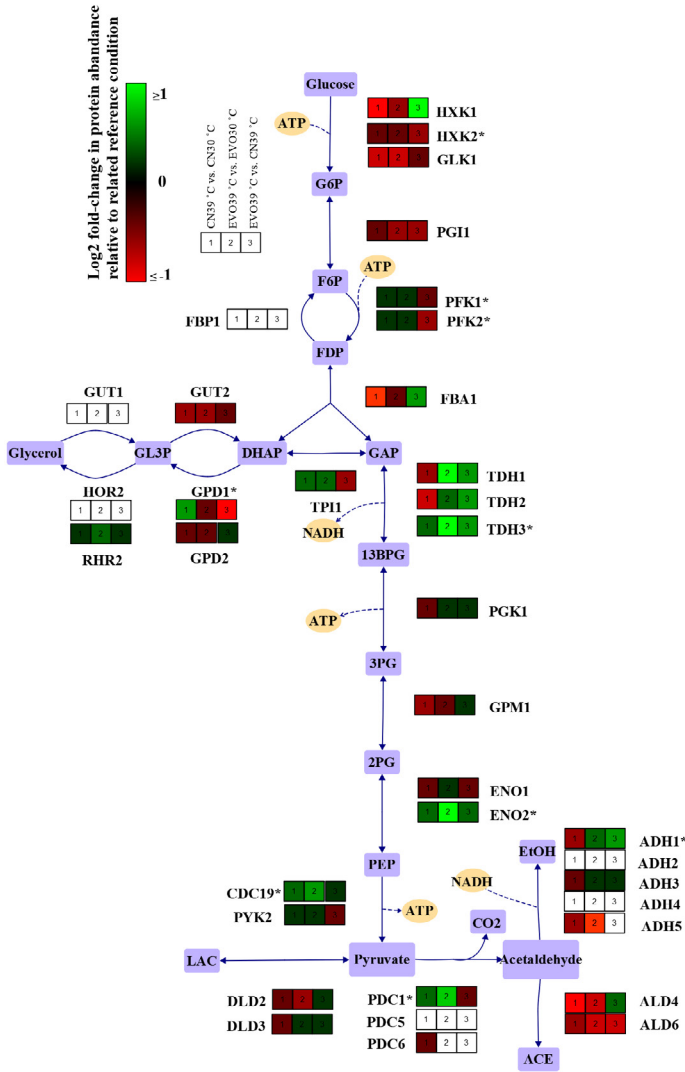
Figure 2
Abundance ratio
of differentially
expressed proteins in
glycolysis and pyruvate
metabolism for the
comparison conditions
(CN3039, EVO3039,
and CNEVO39).

Figure 3
Abundance ratio of
differentially expressed
proteins in PPP for the
comparison conditions
(CN3039, EVO3039,
and CNEVO39).

194
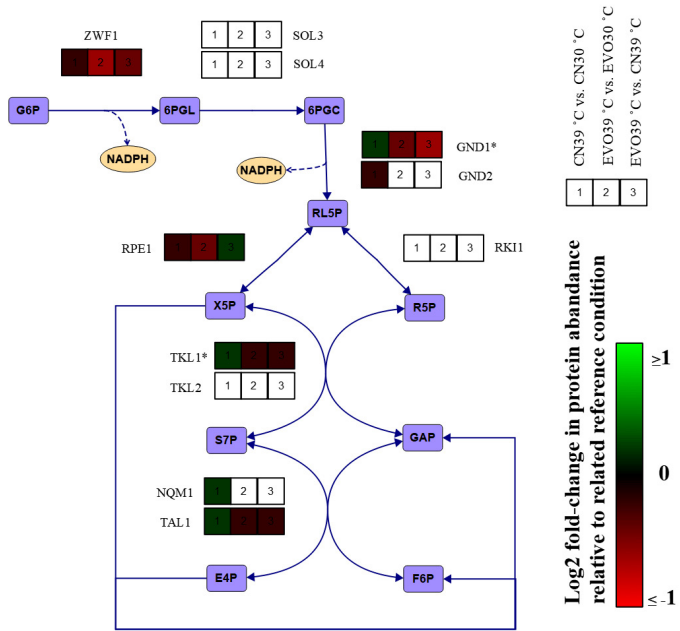
Figure 4
Abundance ratio of
differentially expressed
proteins in TCA cycle
for the comparison
conditions (CN3039,
EVO3039, and
CNEVO39).
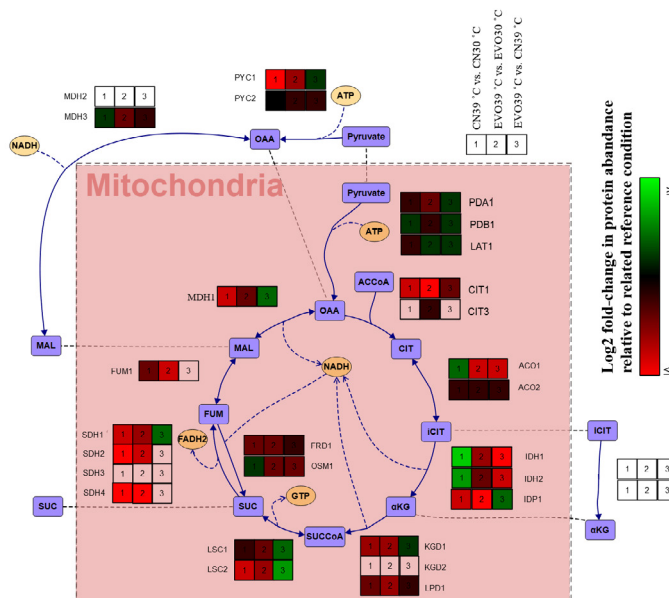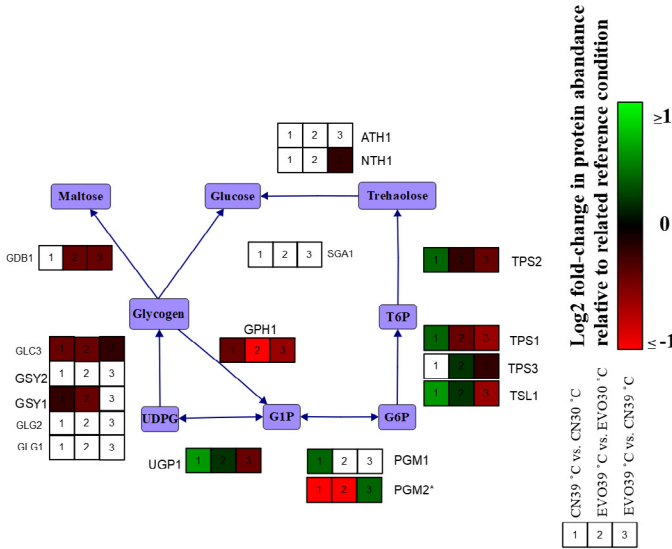
Figure 5
Abundance ratio of differential expressed proteins in glycogen and trehalose metabolism for the comparison conditions (CN3039, EVO3039, and CNEVO39).

The TCA pathway has been shown to operate in a reductive and an oxidative branch instead of a cycle under anaerobic conditions in *S. cerevisiae*, whereby the succinate dehydrogenase (SDH) complex is inactive [27]. Nevertheless, three of the four subunits of SDH were present, namely the flavoprotein subunit (SDH1), iron-sulfur protein subunit (SDH2), and membrane anchor subunit (SDH4). They were downregulated in both strains at 39.0°C (Table 2). In the reductive branch of the TCA (from oxaloacetate to fumarate), mitochondrial malate dehydrogenase (MDH1), fumarase (FUM1), and fumarate reductase (FRD1) were downregulated. Most of the mitochondrial enzymes in the oxidative branch of the TCA also showed significantly reduced levels: the E1 alpha subunit of pyruvate dehydrogenase complex (PDA1), citrate synthase (CIT1), NADP-specific isocitrate dehydrogenase (IDP1), a subunit of the alpha-ketoglutarate dehydrogenase complex (KGD1), and the beta subunit of succinyl-CoA ligase (LSC2). Furthermore, the anaplerotic enzyme pyruvate carboxylase (PYC1) was also less abundant in both strains at 39.0°C. The observed downregulated enzymes could have occurred to counteract the increased capacities of the pathway enzymes at 39.0°C. No clear correlations were found between the observed downregulations in the two TCA branches and the intracellular TCA metabolites measurements.

Although CIT1 was downregulated in both strains at 39.0°C, this corresponded with an increased citrate level in the unevolved and a decreased citrate level in the evolved strain (Table S9). Except for malate, where the intracellular level increased in both strains during cultivation at 39.0°C, the levels of the other measured TCA intermediates were similar.

3.1.2
Proteins involved in amino acid biosynthesis and purine metabolism

Several proteins involved in amino acid biosynthesis were downregulated at 39.0°C in both strains (Table 1). 3-deoxy-D-arabino-heptulosonate-7-phosphate (DAHP) synthase (ARO4) catalyzes the first and rate controlling step in the biosynthesis of the aromatic amino acids and is feedback inhibited by tyrosine or high concentrations of phenylalanine or tryptophan. This appears in agreement with the significantly higher intracellular levels of these amino acids in both strains at 39.0°C (Table S10). Compared to the 30.0°C chemostat cultures, the intracellular levels of phenylalanine, tryptophan, and tyrosine for the unevolved strain grown at 39.0°C were respectively 33.8-, 10.1-, and 59.4-fold higher, whereas for the evolved they were respectively 19.8-, 26.9-, and 54.5-fold higher.

Dihydroxy acid dehydratase (ILV3) and acetohydroxyacid reductoisomerase (ILV5) involved in the biosynthesis of the branched-chain amino acids, leucine, isoleucine, and valine were both downregulated at 39°C in both strains, whereby ILV5 was downregulated at least two-fold (Table S4). Of the three branched chained amino acids, the free level of isoleucine was decreased more than two-fold in both strains, the level of valine was decreased in the unevolved strain, but increased in the evolved strain, while the level of leucine was increased significantly (more than 15-fold) in both strains at 39.0°C (Table S10). This shows that there was a limited correlation between the decreased levels of enzymes involved in branched chain amino acid biosynthesis and the free levels of the corresponding amino acids.

Enzymes involved in asparagine synthesis (ASN1), cysteine synthesis (CYS4) and lysine synthesis (LYS9) were also downregulated at 39.0°C in both strains. We observed a significant increase of asparagine but a significant decrease of lysine in both strains at 39.0°C (Table S10). NADP-dependent glutamate dehydrogenase (GDH1), essential for ammonium assimilation through amination of alpha-ketoglutarate (AKG) to glutamate was also downregulated. This coincided with a significant

reduction of the free levels of glutamate and glutamine in both strains at 39.0°C (Table S10). Glutamine is required for the synthesis of purine bases. There were two downregulated proteins involved in the synthesis of 5,10-methylenetetrahydrfolate (THF) which is a precursor for purine, pyrimidine, and amino acid biosynthesis; cytosolic serine hydroxymethyltransferase (SHM2) which converts serine to glycine and THD, and the T-subunit of the mitochondrial glycine decarboxylase complex (GCV1) which is involved in the catabolism of glycine to 5,10-methylene-THF in the cytoplasm.

Simultaneously we found reduced expression levels of several proteins (HPT1, IMD2, RNR2, and RNR4) involved in purine synthesis. HPT1 catalyses the transfer of 5-phosphoribosyl-α-1-pyrophosphate (PRPP) to a purine base, to form pyrophosphate and a purine nucleotide. IMD2 (inosine monophosphate dehydrogenase) catalyses the rate-limiting step in guanosine triphosphate (GTP) biosynthesis. RNR2 and RNR4 are the subunits of ribonucleotide-diphosphate reductase (RNR) which catalyses the synthesis of deoxyribonucleotide triphosphate (dNTP). Both strains showed a more than two-fold of reduction in a component of the cleavage and polyadenylation factor (CPF) complex (PTI1) (Table S4) which participates in the 3' end formation of snoRNA and mRNA. snoRNA has a predominant function in ribosome biosynthesis [28]. The reduced levels of proteins involved in the synthesis of precursors for purine biosynthesis, as well as the two-fold downregulation of PTI1 in both strains at 39.0°C infers the decrease of transcription activity at high temperature in both strains.

Enriched pathways in both strains at 39.0°C were predominately in ribosome and protein processing in the endoplasmic reticulum (Table 1). According to the enriched GO terms in Table S5, 40 of the 97 upregulated proteins in both strains are involved in rRNA processing and export from the nucleus, ribosome biosynthesis and assembly, as well as tRNA import into the nucleus. Simultaneously, 49 proteins contribute to the process of cytoplasmic translation. There were upregulated proteins involved in the process of translational fidelity regulation (RPS2, RPS5, RPS9A, RPS9B, RPS23A, and RPS23B). Protein translation is dependent on ribosomal proteins, and their abundance is correlated to growth rate [29]. A study showed that yeast cells with more proteome allocation for ribosomes showed improved

3.1.3
Proteins
involved in
translation and
protein folding

growth rate under anaerobic conditions [30]. As high temperature affects the stability of the protein structure, it is not surprising that proteins involved in misfolded protein folding (SSA1, SSA2, SSA4, SSE1) and protection from aggregation (HSP78, HSP60, HSP10) were upregulated at 39.0°C in both strains. Furthermore, there was a more than two-fold increase of expression of HSP60 in both strains at 39.0°C (Table S4). HSP60 is a chaperonin which is required for ATP dependent de novo protein folding and translocation, as well as protein refolding after heat shock [31,32]. Clearly, both strains required an increased amount of energy for the maintenance of their protein pools at high temperature, resulting a decrease of the biomass yield at 39.0°C (Table S3). This was more pronounced for the unevolved strain than for the evolved strain, showing the adaptation growing at increased temperatures of the evolved strain.

3.2
The evolved strain-specific responses at high temperature

Apart from the differentially expressed proteins found in both strains between 39.0°C and 30.0°C, there were 62 upregulated proteins and 152 downregulated proteins which were expressed differently only in the evolved strain compared to the unevolved strain (Figure S1). From these, two proteins (OLE1 and AIM41) changed at least two-fold in the evolved strain during chemostat cultivation at 39.0°C compared to 30.0°C (Figure 1). OLE1 was upregulated and is a stearoyl-CoA-desaturase which involves in the synthesis of ergosterol under aerobic conditions and also appears to be required for the proper distribution of mitochondria between mother and daughter cells [33,34]. AIM41 was downregulated and is a protein with unknown function of which the null mutant displays a reduced frequency of mitochondrial genome loss [35]. From a STRING enrichment analysis (Table 2), the unique proteome responses of the evolved strain at elevated cultivation temperature were found to be predominantly in ribosomal proteins, metabolic pathways, aminoacyl-tRNA biosynthesis, and proteasome.

Category description	Protein identity	No. of proteins in cluster	No. of proteins in genome	FDR value
Ribosome	RPL4B | RPP2B | RPL30 | RPL26B | RPS0A | RPS21B | RPS0B | RPL38 | RPP0 | RPL26A | RPS29A | RPS19B | RPP2A | RPS19A | RPL36B | RPL43A	16	147	2.72E-12
Metabolic pathways		18	716	1.70E-04
Glycolysis / Gluconeogenesis	PGK1 | TDH1 | TDH2 | ADH3 | ADH1	5	55	1.10E-03
Biosynthesis of antibiotics	PGK1 | ADK1 | SER3 | SER33 | TDH1 | TDH2 | ADE13 | ADH3 | ADH1	9	226	1.10E-03
Biosynthesis of amino acids	PGK1 | THR4 | SER3 | SER33 | TDH1 | TDH2	6	120	3.30E-03
Biosynthesis of secondary metabolites	RIB5 | PGK1 | THR4 | ADK1 | TDH1 | TDH2 | ADE13 | ADH3 | ADH1	9	295	3.70E-03
Glycine, serine and threonine metabolism	THR4 | SER3 | SER33	3	31	1.15E-02
Carbon metabolism	PGK1 | SER3 | SER33 | TDH1 | TDH2	5	112	1.15E-02
Vitamin B6 metabolism	PDX3 | THR4	2	13	2.28E-02
Tyrosine metabolism	ADH3 | ADH1	2	14	2.33E-02
Fatty acid degradation	ADH3 | ADH1	2	19	3.61E-02
Thiamine metabolism	ADK1 | PHO8	2	19	3.61E-02
Fatty acid metabolism	CEM1 | OLE1	2	22	3.95E-02
Methane metabolism	SER3 | SER33	2	25	4.60E-02
Metabolic pathways		57	716	2.32E-18
Biosynthesis of secondary metabolites	ADH5 | SHM1 | LEU2 | CIT2 | MDH3 | GLT1 | SAM2 | GLC3 | PMI40 | HIS1 | ARG5,6 | ALD5 | MET6 | LEU1 | POX1 | GUS1 | ASN2 | PRS3 | ARG4 | GND1 | ERG9 | BAT1 | ERG20 | YNK1 | GPT2 | SAM1 | ACO1 | IMD3 | COQ5 | ILV2 | IDH1 | LEU4 | ARG1 | IDH2 | LSC1 | FUM1 | TKL1	37	295	5.30E-17
Biosynthesis of amino acids	SHM1 | LEU2 | CIT2 | LYS21 | GLT1 | SAM2 | HIS1 | ARG5,6 | MET6 | LEU1 | PRS3 | ARG4 | BAT1 | SAM1 | ACO1 | ILV2 | IDH1 | LEU4 | ARG1 | IDH2 | GLN1 | TKL1	22	120	8.63E-13
Biosynthesis of antibiotics	ADH5 | SHM1 | CIT2 | MDH3 | LYS21 | GLT1 | PMI40 | ARG5,6 | ALD5 | ERG25 | PRS3 | ARG4 | GND1 | ERG9 | BAT1 | ERG20 | YNK1 | GFA1 | ACO1 | ILV2 | IDH1 | ARG1 | IDH2 | LSC1 | FUM1 | TKL1	26	226	4.64E-11
2-Oxocarboxylic acid metabolism	LEU2 | CIT2 | LYS21 | ARG5,6 | LEU1 | BAT1 | ACO1 | ILV2 | IDH1 | LEU4 | IDH2	11	35	1.48E-08
Alanine, aspartate and glutamate metabolism	GLT1 | ASN2 | ARG4 | URA2 | GFA1 | ARG1 | GLN1	7	29	7.05E-05
Citrate cycle (TCA cycle)	CIT2 | MDH3 | ACO1 | IDH1 | IDH2 | LSC1 | FUM1	7	32	1.10E-04
Valine, leucine and isoleucine biosynthesis	LEU2 | LEU1 | BAT1 | ILV2 | LEU4	5	12	1.40E-04
Carbon metabolism	SHM1 | CIT2 | MDH3 | PRS3 | GND1 | ACO1 | IDH1 | IDH2 | LSC1 | FUM1 | TKL1	11	112	2.60E-04
Cysteine and methionine metabolism	MDH3 | SAM2 | SAH1 | MET6 | BAT1 | SAM1	6	40	2.10E-03
Pyruvate metabolism	ACH1 | MDH3 | LYS21 | ALD5 | LEU4 | FUM1	6	43	2.70E-03
Glyoxylate and dicarboxylate metabolism	SHM1 | CIT2 | MDH3 | ACO1 | GLN1	5	28	2.80E-03
Arginine biosynthesis	ARG5,6 | ARG4 | ARG1 | GLN1	4	17	4.10E-03
Purine metabolism	PRS3 | YNK1 | IMD3 | APT1 | GUA1 | RPA49 | ISN1 | RPA135	8	99	6.40E-03
C5-Branched dibasic acid metabolism	LEU2 | ILV2	2	3	1.72E-02
Fatty acid degradation	ADH5 | ALD5 | POX1	3	19	3.86E-02
Aminoacyl-tRNA biosynthesis	GUS1 | VAS1 | DED81 | YNL247W | ALA1	5	39	8.20E-03
Proteasome	RPT2 | RPT3 | RPT6 | RPT1 | RPT5	5	35	6.00E-03

199

Table 2
Enrichment analysis for KEGG pathways of the up-(green) and downregulated (red) proteins which were uniquely found in the evolved CEN.PK113-7D at 39.0°C relative to 30.0°C, all of which are the red area in the Venn diagrams (Figure S1).

Aminoacyl-tRNAs (aa-tRNAs) have an essential role in translation by serving as substrates to pair an amino acid with the corresponding tRNA and for misacylated translation [36]. It has been shown that the expression of aminoacyl-tRNA synthetases has a positive correlation to glycolytic activity [37]. Multiple proteins involved in central metabolism, such as the TCA pathway, were downregulated in the evolved strain at 39.0°C. The downregulation of Aminoacyl-tRNA synthetases was in agreement with the reduced level of proteins involved in

3.2.1
Aminoacyl-tRNA biosynthesis

central carbon metabolism and indicated the lower capacity of translation in the evolved strain at 39.0°C. In yeast roughly 15% of the total protein consists of glycolytic enzymes [38,39], and there is a positive relation between glycolytic protein abundance and growth rate, although most of the glycolytic enzymes are not used at their full capacity [30,40]. The lower capacity of translation in the evolved strain did not influence the total protein content where both strains showed similar total protein contents at 39.0°C (chapter 4), but lower the energy burden in maintaining the overcapacity of protein production.

3.2.2 Nutrient recycling by autophagy

Carboxypeptidase Y inhibitor (TFS1) is a member of the phosphatidylethanolamine-binding protein (PEBP) family. TFS1 inhibits Ira2P, a GTPase-activating protein which negatively controls Ras activity by converting it from the GTP-to the inactive GDP-bound form. Downregulation of TFS1 would result in release of Ira2p inhibition and, therefore, downregulation of Ras activity which regulates a variety of functions, such as cell cycle progression and can have profound implications for life span [25]. These authors also showed that deletion of TFS1 in yeast results in a fivefold to tenfold decreased sensitivity to heat shock, while overexpression results in the opposite, a fivefold to tenfold increased sensitivity to heat shock. Therefore, we hypothesize that the observed more than twofold downregulation of TFS1 in the evolved strain at 39.0°C has contributed to an increased tolerance of the evolved strain to the cultivation at supra-optimal temperature.

TFS1 also suppresses the activity of carboxypeptidase Y which is essential for the breakdown of the autophagy bodies in the vacuole and results in an efflux of macromolecules [41,42]. Downregulation of TFS1 could have resulted in higher activity of autophagy to allow cellular recycling process. Autophagy occurs in response to nutrient limiting conditions and has two types in yeast cells: microautophagy and macroautophagy [43]. During the process of macroautophagy initiated by the inactivation of TORC1, autophagosomes containing damaged organelles or cytosolic proteins are delivered to the vacuole and are subsequently degraded to recycle the macromolecules for cellular use [44,45]. Meanwhile, we also observed an upregulation of Rab family GTPase (YPT7) (Table S6) which regulates the fusion of autophagosomes with lysosomes at the late step of autophagy[46–48]. The formation of the autophagosomes requires

the fatty acid desaturase (OLE1) to deliver the transmembrane protein (ATG9) to the pre-autophagosomal structure [49]. Ogasawara et al. showed that an OLE1 knockout mutant was defective in membrane elongation during autophagosome formation. We found that OLE1 was upregulated more than 2-fold in the chemostat culture of the evolved strain at 39.0°C(Figure 1). There is a review about how autophagy has a positive effect on the chronological and replicative life span of yeast [50]. Consistent with this finding, the chemostat culture of the evolved strain had a lower death rate than the unevolved strain at 39.0°C (Chapter 4). Although it is not clear what triggered the activation of autophagy in this case, we hypothesize that the increase of autophagy activity in the evolved strain at high temperature may facilitate the removal of cytotoxic intermediates accumulated due to increased amounts of misfolded proteins or damaged organelles in the cytoplasm at supra-optimal temperature. As a result, this may protect the cells from proteotoxicity, resulting in a lower death rate. The ubiquitin proteasome system (UPS) and autophagy are the two protein degradation pathways to recycle the macromolecules. UPS is selective to targeted proteins, whereas autophagy is non-selective to clear protein aggregates and membrane associated proteins [51]. Five of the six distinct ATPases of the regulatory particle in proteasomes (RPT1, RPT2, RPT3, RPT5, and RPT6) which are required to mediate the unfolding of the targeted protein by proteasome [52] were all downregulated in the evolved strain at 39.0°C (Table 2). An increase of misfolded proteins/aggregates are expected at high temperature, but the downregulation of these ATPases indicated that autophagy seemed to be the dominant pathway for protein degradation in the evolved strain at high temperature.

An upregulation of plasma membrane ATPase 1 (*PMA1*) was one of the distinct features found in the evolved strain at 39.0°C (Table S6). *PMA1* plays an essential role in cytosolic pH regulation by pumping protons out of the cells. It has been shown that a reduced level of *PMA1* during glucose starvation results in a rapid drop of the intracellular pH [53]. Tight control of the intracellular pH is essential for all cellular activities, such as genetic materials synthesis (RNA and DNA) and cell proliferation [54]. It has been shown that the intracellular pH of yeast cells decreases at high temperature [55] due to an increase in membrane permeability which facilitates the net proton influx [56]. In a previous study, we observed an increase of acetic acid production in chemostat

3.2.3
Cytoplasmic pH
regulation

cultures of both strains at 39.0°C (Table S3). Because the pH in the chemostat cultures was controlled at 5.00 ± 0.05, more than 50% of the excreted acetic acid (pKa = 4.76) was present in the undissociated form, which can easily diffuse across the plasma membrane into the cells. At the near neutral intracellular pH, the dissociation of acids leads to the release of protons inside the cell which have to be exported by *PMA1*. The increased abundance of *PMA1* indicates a higher capacity of the evolved strain to pump protons out of the cell, likely resulting in improved cytoplasmic pH regulation at the high cultivation temperature. We also observed a missense mutation in *PMA1* close to the active site (at position 378) in the evolved strain (Table S8) from our previous study (Chapter 4). It is not clear whether the mutation has had a direct effect on the upregulation of the protein.

3.3 Responses of the evolved strain relative to the unevolved strain during cultivation at 39.0°C

From the proteome comparison between the evolved and the unevolved strains during chemostat cultivation at 39.0°C, we identified 48 upregulated and 133 downregulated proteins in the evolved strain. From a STRING enrichment analysis of these 181 differentially expressed proteins, the different responses in the evolved strain were predominantly found in central carbon metabolism, amino acid biosynthesis, purine biosynthesis, fatty acid biosynthesis, protein synthesis, translocation and degradation (Table 3).
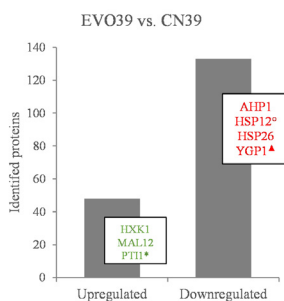
Figure 6

The differentially expressed proteins between the evolved and unevolved strain during chemostat cultivation at 39.0°C. Proteins indicated in green were at least 2-(log2) fold upregulated, whereas proteins indicated in red were at least 2-(log2) fold downregulated in the evolved strain. The symbol (*) indicates the proteins which had also an at least 2-(log2) fold change in both strains between 39.0°C and 30.0°C (CN39/CN30 and EVO39/EVO30). The symbol (▲) indicates the proteins which had also an at least 2-(log2) fold change in the evolved strain at 39.0°C (EVO39/EVO30). The symbol (°) indicates the proteins which had also an at least 2-(log2) fold change in the unevolved strain between 39.0°C and 30.0°C (CN39/CN30).

According to the enriched pathways for the up- and downregulated proteins (Table 3), of the 190 differentially expressed proteins 71 were predominantly in metabolic pathways, whereby 26 proteins were upregulated and 45 downregulated in the evolved strain. Compared to the unevolved strain, the evolved strain at 39.0°C showed a lower abundance of some proteins involved in glycolysis (PGI1, PFK2, TPI1, ALD5, ALD6) (Figure 2), storage carbohydrate metabolism (Figure 5) and the oxidative TCA branch (Figure 4). Moreover, the proteins involved in the connection steps between the glycolysis, storage carbohydrate metabolism, and PPP (ZWF1 and TSL1) were downregulated in the evolved strain. A number of proteins involved in the oxidative branch of the TCA were also less abundant, namely mitochondrial citrate synthase (CIT1), aconitate hydratase (ACO1), and NAD-dependent isocitrate dehydrogenase (IDH1 and IDH2). Repression of various enzymes involved in metabolic pathways, such as TCA cycle and PPP seems also a distinct feature of thermotolerant industrial strains, possibly to decrease the energy demand [2].

Although up and downregulations of the proteins involved in central carbon metabolism occurred in the evolved strain, the capacity of energy production was maintained at a fixed slow growth rate (0.03 h-1) (Chapter 4). Both strains at 39.0°C showed similar fermentative capacity, but the evolved strain had 37.7 % increase in trehalose accumulation (Chapter 4). Trehalose was shown to improve cell membrane integrity at thermal stress [57] but also to involve in denatured protein repair [58]. Furthermore, trehalose-6-phosphate (T6P) acts as a competitive inhibitor of hexokinase and thereby controls the glycolytic flux [59]. Remarkably, HXK1 was more than 2-fold upregulated in the evolved strain relative to the unevolved strain at 39.0°C, while HXK2 and GLK1 were downregulated (Figure 2). However, the enzyme activity assays did not show a significant change in hexokinase capacity at 39.0°C for both strains (column D/A in Table 4).

The upregulation of glyceraldehyde-3-phosphate dehydrogenase (TDH1 and TDH3) in the evolved strain at 39.0°C (Figure 3) corresponded with a significant increase in the measured enzyme capacity (Table 4), most probably to maintain the flux through the lower part of the glycolysis while several steps in the upper part were downregulated (see 3.1.1). Besides, GAPDH plays important role in maintaining NAD+ and NADH ratio. This must have been

3.3.1
Proteins involved in central carbon metabolism

203

the reason for the significant decrease of the intracellular FBP concentration in both strains. TDH3, the dominant isoenzyme of glyceraldehyde-3-phosphate dehydrogenase [60] plays a moonlighting role in aging regulation via Sir2-induced transcriptional silencing which can slow down the telomeres shorting [61,62]. However, the degree of silencing a telomere has no correlation to GADPH activity [61] but has a positive correlation with an increase of NAD+ level [63].

3.3.2 Downregulated proteins involved in protein synthesis, translocation, and degradation

Three of the four enriched pathways among the 140 downregulated proteins in the evolved strain at 39.0°C were protein processing in the ER, RNA transport, and proteasome (Table 3). The downregulation of proteins in the enriched pathway of RNA transport are involved in translation initiation (FUN12, RPG1, NIP1, CDC33, GCD1), in translation elongation (TEF1), in maintenance of nuclear organisation, RNA processing and transport (GSP1 and GSP2), export of RNA from the nucleus (SEC13) and export of protein, and ribosomal subunits from the nucleus (CRM1). SEC13 is a structural component of 3 complexes (Nup84p nuclear pore subcomplex, COPII vesicle coat required for ER-to-Golgi transport and SEACAT) whereby the latter has a role in TORC1 activation. There was a more than 2-fold decrease of HSP26 in the evolved strain at 39.0°C (Figure 6) which is required for mRNA binding activity [64] and the suppression of unfolded protein aggregation in the cytosol [65,66]. The latter might indicate less problems with protein folding in the evolved strain at high temperature. Regarding protein processing in the ER, HSP26, PDI1, KAR2, SSA2, SSE1, YDJ1, and HSP82 were all lower in abundance in the evolved strain at 39.0°C. These proteins are known to be heat shock proteins involved in protein folding, suppression of unfolded protein aggregation and recognition of unfolded proteins. UFD2 is a E4 ubiquitin chain-elongation enzyme and is involved in polyubiquitin chain assembly and targeting the ubiquitinated proteins to the proteasome. Furthermore, several downregulated proteins, RPT3, RPN9, RPN1, 11, PRE2 are known to be the subunits of the proteasome. The downregulation of these proteins, which are related to protein folding, suppression of unfolded protein aggregation, recognition of unfolded protein and protein degradation, in the evolved strain indicates the better resistance to heat. Protein turnover is an energy-requiring process because of the translocation of the ubiquitinated protein by proteasome [67] and the re-synthesis of degraded proteins. Besides, the turnover of nuclear and ribosomal

proteins occurs at a higher rate than of the structural membrane and organelle specific proteins [68]. The downregulation of the proteins involved in protein translation and protein turnover could indicate that the protein turnover rate in the evolved strain seems to be lower than in the unevolved strain during growth at 39.0ºC. Therefore, this observation possibly explains the decreased the energy demand for maintenance in the evolved strain at supra-optimal cultivation temperature.

Of the 45 downregulated proteins in the evolved strain involved in metabolic pathways (Table 3) 5 were involved in the biosynthesis of amino acids, namely leucine (LEU2, LEU4), methionine and threonine (HOM6 and SAM1), as well as glutamate (GLT1). Furthermore, arginase (CAR1) which catabolizes arginine to urea and ornithine when nitrogen sources are limited was also reduced in the evolved strain at 39.0ºC. Of the 26 upregulated proteins involved in metabolic pathways in the evolved strain 4 were involved in the biosynthesis of amino acids, namely serine (SER3), glycine (SHM2), methionine and cysteine (MET17), and histidine (HIS7). Some of these upregulated proteins are metabolically connected to the purine pathway [69] and are involved in the synthesis of precursors of purine biosynthesis, such as glycine. Imidazole glycerol phosphate synthase (HIS7) and O-acetyl homoserine-O-acetyl serine sulfhydrylase (MET17) are also involved in the formation of other purine precursors. HIS7 catalyses the biosynthesis of AICAR which is an intermediate for the formation of inosine monophosphate (IMP). MET17 catalyses the formation of homocysteine which is not only used in the biosynthesis of cysteine and methionine but also the formation of THF, while serine is required for THF formation. Glycine and THF are the components of purine molecules. Of the 26 upregulated proteins another 4 also take part in the formation of nucleosides, namely inosine (ADE1 and ADE17), guanosine (IMD2), and adenosine bisphosphate (ADK1). Purine nucleotides play an important role in cellular metabolism, as they are the constituents of genetic materials, phosphate donors, and the major carriers of cellular energy [70]. The upregulation of proteins metabolically connected to the purine de novo synthesis pathway could indicate an increase abundance of the purine nucleotide pool. Meanwhile, PTI1 was significantly downregulated (>2-fold) in both strains at 39.0ºC compared to 30.0ºC. Compared to the unevolved strain at 39.0ºC, the significantly higher expression of PTI1 in the evolved strain (Figure 6) could indicate a higher transcription capacity.

3.3.3
Higher capacity in purine nucleotide pool synthesis

205

Table 3
Enrichment analysis
for KEGG pathways
of up-(green) and
downregulated (red)
proteins for the
evolved CEN.PK113-
7D relative to the
unevolved CEN.PK113-
7D strain at 39°C.

Category description	Protein identity	No. of proteins in cluster	No. of proteins in genome	FDR value
Metabolic pathways		26	716	2.26E-13
Biosynthesis of amino acids	HIS7 | SER3 | TDH3 | ENO2 | TDH1 | FBA1 | GPM1 | SHM2 | MET17	9	120	6.51E-07
Galactose metabolism	HXK1 | MAL12 | SUC2 | PGM2	4	23	1.20E-04
Fructose and mannose metabolism	SEC53 | HXK1 | FBA1	3	22	2.00E-03
Purine metabolism	ADE1 | ADK1 | IMD2 | PGM2 | ADE17	5	99	2.00E-03
Glycine, serine and threonine metabolism	SER3 | GPM1 | SHM2	3	31	4.20E-03
Histidine metabolism	HIS7 | ALD4	2	14	1.17E-02
One carbon pool by folate	SHM2 | ADE17	2	15	1.17E-02
Pentose phosphate pathway	FBA1 | PGM2	2	28	2.99E-02
Glyoxylate and dicarboxylate metabolism	MDH1 | SHM2	2	28	2.99E-02
Cysteine and methionine metabolism	MDH1 | MET17	2	40	4.69E-02
Ribosome	RPS0A | RPS0B | RPL37A | RPL6A	4	147	2.99E-02
Metabolic pathways		45	716	7.50E-10
Biosynthesis of amino acids	LEU2 | GLT1 | TPI1 | HOM6 | SAM1 | ACO1 | TAL1 | PFK2 | IDH1 | LEU4 | CIT1 | IDH2 | CAR1	13	120	5.54E-05
Fatty acid biosynthesis	FAS1 | ACC1 | FAA1 | FAS2	4	11	1.80E-03
2-Oxocarboxylic acid metabolism	LEU2 | ACO1 | IDH1 | LEU4 | CIT1 | IDH2	6	35	1.80E-03
Carbon metabolism	PGI1 | TPI1 | GND1 | ACO1 | TAL1 | PFK2 | IDH1 | ZWF1 | CIT1 | IDH2	10	112	1.80E-03
Pyruvate metabolism	GLO2 | ALD5 | LEU4 | ACC1 | ALD6	5	43	1.64E-02
Valine, leucine and isoleucine degradation	ALD5 | ERG13 | ALD6	3	13	2.06E-02
Porphyrin and chlorophyll metabolism	HEM13 | HEM2 | GUS1	3	17	3.46E-02
Glycolysis / Gluconeogenesis	PGI1 | TPI1 | ALD5 | PFK2 | ALD6	5	55	3.46E-02
Starch and sucrose metabolism	PGI1 | UGP1 | FKS1 | TSL1	4	40	4.55E-02
Protein processing in endoplasmic reticulum	HSP26 | PDI1 | UFD2 | KAR2 | SSA2 | SEC13 | YDJ1 | SSE1 | SAR1 | HSP82	10	86	3.10E-04
RNA transport	FUN12 | RPG1 | CRM1 | SEC13 | GSP1 | NIP1 | CDC33 | GSP2 | GCD1 | TEF1	10	83	2.80E-04
Proteasome	RPT3 | RPN9 | RPN11 | RPN1 | PRE2	5	35	8.50E-03

3.3.4
Downregulated
proteins
involved in
fatty acids and
sterol formation

During chemostat cultivation at 39.0°C, several proteins involved in fatty acid biosynthesis showed reduced abundances in the evolved strain (Table 3). These were acetyl-CoA carboxylase (ACC1), involved in the rate limiting step for de novo biosynthesis of long-chain fatty acids, and the subunits FAS1 and FAS2 of the fatty acid synthetase complex which takes part in the initiation and elongation steps of long-chain saturated fatty acid biosynthesis, as well as the long chain fatty acyl-CoA synthetase FAA1. From measurements of the fatty acid compositions of both strains at both cultivation temperatures. The evolved strain had a 32.3 % higher content of medium chain fatty acids than the unevolved strain at 39.0°C (Chapter 4). However, the lower abundance of FAS1 and FAS2 in the evolved strain did not correlate with the higher saturated fatty acid content (15.9 %) found in the evolved strain at 39.0°C (Chapter 4). From the whole genome sequencing of the evolved strain (Chapter 4), we found there was a single nucleotide variant in FAS1, resulting in a codon that codes for a different amino acid (Table S8). This missense mutation

locates outside the region of the active site for enzymatic activity, and therefore, is less likely to have contributed to changes in structural properties of the protein.

Compared to the unevolved strain at 39.0°C, the evolved strain had reduced levels of five proteins involved ergosterol biosynthesis (Table S7). However, for several reactions in the ergosterol biosynthesis pathway molecular oxygen is required [71] and therefore those reactions are not relevant under the anaerobic conditions of our chemostat cultures. In addition, ergosterol was a constituent of the chemostat feed medium. Therefore, it could be energetically efficient to downregulate these proteins in the evolved strain under anaerobic conditions. The import of exogenous ergosterol in *S. cerevisiae* occurs exclusively under anaerobic conditions and is carried out by two ABC transporters: AUS1 and PDR11 [72] and the uptake rate is reported to be inversely proportional to the intracellular ergosterol content [73]. The evolved strain had a 74% higher ergosterol content than the unevolved strain at 39.0°C (Chapter 4) which implies that this strain had a higher cell specific ergosterol uptake rate than the unevolved strain, which contradicts with the findings mentioned above. However, it is not clear what contributed to the larger pool of ergosterol in the evolved strain under the anaerobic condition.

To investigate the impact of increased cultivation temperature on the capacities of the glycolytic enzymes, we measured the enzyme activities in the cell free extracts of the chemostat cultures at 30.0°C and 39.0°C of both strains under in vivo like conditions [20]. The enzymatic assays were carried out at both 30.0°C and 39.0°C (Table 4). A comparison of the measured in vivo like enzymatic activities carried out at the cultivation temperature of the chemostats (D/A) indicated that the majority of the enzymes of both strains showed at least a 1.5-fold increase of their maximum capacity at increased cultivation temperature with as only exceptions hexokinase (HXK) and phosphoglycerate kinase (PGK). During cultivation at 39.0°C, the capacities of aldehyde dehydrogenase (ALD), glyceraldehyde-3-phosphate dehydrogenases(GAPDH), and pyruvate kinase (PYK) were respectively 1.9-fold, 1.5-fold, and 2-fold higher than in the unevolved strain. GAPDH and PYK are regulated by protein kinase via phosphorylation [74,75] which is known to be regulated by temperature [76,77].

*3.4
High temperature impact on the capacities of the glycolytic enzymes*

A comparison of the measured enzyme activities at same assay temperature for the chemostat cultures grown at the two different temperatures (C/A and D/B) could reveal the impact of cultivation temperature on the enzyme amounts, assuming that the cultivation temperature has no influence on the specific enzyme activities of each, such as through differences in the post-translational modifications. Compared to the chemostat culture at 30.0°C, both strains showed significant increases of PGI, PFK, GAPDH, PGM, PYK, and PDC at 39.0°C (p-value < 0.05) and in the evolved strain also ALD, with average increases at the two assay temperatures of 1.4- to 4.2-fold. These observations are, except for PGI and PGM which were both slightly downregulated, in agreement with increased protein abundances in both strains between 39.0°C and 30.0°C (CN39/CN30 and EVO39/EVO30) measured by LC-MS/MS (Figure 3). This could indicate that in case of PGI and PGM post translational modifications have occurred during cultivation at 39.0°C resulting in increased enzyme capacities. However, these enzymes are not considered as key regulatory steps of glycolysis, such as PFK1, PFK2, and the pyruvate kinase CDC19, which are known to be hubs of PTM's [78]. The protein levels of both PFK's were only slightly upregulated at 39.0°C in both strains, while the enzyme abundances quantified via the enzyme activity measurements were respectively 2.2 and 2.7-fold in the unevolved and evolved strains. The increase in abundances of PYK were respectively 2.0 and 4.0-fold at 39.0°C in the unevolved and evolved strains, while the increases in protein abundances were less than two-fold. For these enzymes, PTM's could have resulted in increased enzyme capacities at 39.0°C.

a)

	A	B	C	D		D/A	C/A	D/B	Average	B/A	D/C	Average
CT	30°C	30°C	39°C	39°C								
AT	30°C	39°C	30°C	39°C								
HXK	1.92 ± 0.17	2.50 ± 0.22	1.42 ± 0.41	1.74 ± 0.50		0.9	0.7	0.7	0.7	1.3	1.2	1.3
PGI	4.66 ± 0.40	5.75 ± 0.50	9.20 ± 0.67	11.0 ± 0.8		2.4*	2.0*	1.9*	1.9	1.2	1.2	1.2
PFK	0.35 ± 0.03	0.50 ± 0.04	0.77 ± 0.06	1.13 ± 0.08		3.2*	2.2*	2.3*	2.2	1.4*	1.5*	1.5
ALD	4.32 ± 0.37	6.57 ± 0.61	4.26 ± 0.33	6.34 ± 0.53		1.5*	1.0	1.0	1.0	1.5*	1.5*	1.5
GAPDH	1.87 ± 0.19	2.49 ± 0.23	6.07 ± 0.38	7.19 ± 0.45		3.9*	3.3*	2.9*	3.1	1.3	1.2	1.3
PGK	32.4 ± 1.4	36.3 ± 1.5	21.3 ± 1.0	31.9 ± 5.7		1.0	0.7*	0.9	0.8	1.1	1.5*	1.3
PGM	18.7 ± 0.8	28.8 ± 2.3	24.9 ± 1.1	40.9 ± 4.0		2.2*	1.3*	1.4*	1.4	1.5*	1.6*	1.6
PYK	4.0 ± 0.4	6.7 ± 0.8	7.7 ± 1.3	14.3 ± 2.4		3.6*	1.9*	2.1*	2.0	1.7*	1.9*	1.8
PDC	0.94 ± 0.08	1.25 ± 0.11	2.19 ± 0.37	2.50 ± 0.43		2.6*	2.3*	2.0*	2.2	1.3	1.1	1.2

b)

	A	B	C	D		D/A	C/A	D/B	Average	B/A	D/C	Average
CT	30°C	30°C	39°C	39°C								
AT	30°C	39°C	30°C	39°C								
HXK	1.67 ± 0.08	2.26 ± 0.11	1.51 ± 0.33	1.89 ± 0.49		1.1	0.9	0.8	0.9	1.3*	1.3	1.3
PGI	4.08 ± 0.21	4.66 ± 0.21	8.51 ± 0.96	9.87 ± 1.12		2.4*	2.1*	2.1*	2.1	1.1	1.2	1.2
PFK	0.34 ± 0.02	0.51 ± 0.02	0.94 ± 0.05	1.34 ± 0.07		3.9*	2.7*	2.6*	2.7	1.5*	1.4*	1.5
ALD	3.35 ± 0.18	4.60 ± 0.24	7.25 ± 0.40	9.85 ± 0.53		2.9*	2.2*	2.1*	2.2	1.4*	1.4*	1.4
GAPDH	1.96 ± 0.15	2.53 ± 0.21	7.84 ± 1.20	11.4 ± 1.7		5.8*	4.0*	4.5*	4.2	1.3	1.5	1.4
PGK	29.5 ± 1.6	33.9 ± 2.1	23.0 ± 3.4	28.8 ± 16.9		1.0	0.8	0.8	0.8	1.1	1.2	1.2
PGM	15.7 ± 1.1	25.7 ± 2.3	26.5 ± 3.9	43.0 ± 12.7		2.7	1.7*	1.7	1.7	1.6*	1.6	1.6
PYK	2.87 ± 0.20	6.03 ± 0.45	12.1 ± 1.2	22.2 ± 2.4		7.8*	4.2*	3.7*	4.0	2.1*	1.8*	2.0
PDC	0.81 ± 0.06	1.07 ± 0.08	2.39 ± 0.24	2.72 ± 0.27		3.4*	3.0*	2.5*	2.8	1.3*	1.1	1.2

Table 4
Measured capacities of glycolytic enzymes for a) CEN.PK113-7D and b) CEN.PK-EVO at different cultivation temperatures (CT) and at different assay temperatures (AT). The following abbreviations are used: HXK, hexokinase; PGI, glucose-6-phosphate isomerase; PFK, phosphofructokinase; ALD, aldolase; GAPDH, glyceraldehyde-3-phophate dehydrogenase; PGK, 3-phosphoglycerate kinase; PGM, phosphoglycerate mutase; PYK, pyruvate kinase; PDC, pyruvate decarboxylase. *p-value is lower than 0.05 which was determined by a two-sample T-test with unequal-variance.

As we carried out the enzyme activity assays at 30.0°C and 39.0°C, we could also investigate the temperature dependencies of the glycolytic enzymes' capacities. For both strains, the glycolytic enzyme activities of cultures grown at the same temperatures but assayed at 39.0°C were higher than that were assayed at 30.0°C (B/A and D/C) whereby the fold increase of the activity ranged from 1.2 to 2.0. PYK showed the most significant increase of 1.8- and 2.0-fold for the unevolved and the evolved strain respectively. However, there were no significant differences in the temperature dependencies of the individual glycolytic enzymes between the different strains (p-value > 0.05).

4
Conclusion

In order to elucidate the impacts of the genomic changes and the cause of the superior growth and lower cell death rate at supra-optimal temperatures in the evolved CEN.PK113-7D strain, we used shotgun proteomics to analyse the proteome of the anaerobically grown chemostat cultures for CEN.PK113-7D and the high temperature evolved CEN.PK113-7D strain cultivated at 30.0°C and 39.0°C. The changes on the proteomic level between the unevolved and the evolved strain at the optimal and supra-optimal cultivation temperatures revealed common and strain-specific responses to cultivation at 39.0°C. The common responses found in both strains involved up- and downregulation of proteins in central carbon metabolism, and upregulation of proteins involved in translation and protein folding. The strain-specific responses of the evolved strain were high expression of ribosomal proteins, aminoacyl-tRNA biosynthesis and proteasome. We also quantified the capacities of the glycolytic enzymes in the anaerobic chemostat cultures of both strain under in vivo like conditions at 30.0°C and 39.0°C. Although no mutations were found within the coding sequences for the glycolytic enzymes in the evolved strain, significant differences were observed between the unevolved and the evolved strain in quantity and capacity of these enzymes at elevated cultivation temperatures, specifically ALD, GAPDH and PYK. This indicates that changes must have occurred in genetic control mechanisms of the evolved strain as a result of evolution. The proteome analysis suggested that the evolved strain counteracted the thermal stress through multiple mechanisms, that is better nutrient recycling by autophagy, better cytoplasmic pH regulation, increased trehalose accumulation, decrease of Ras activation, increased translation capacity and decreased proteome allocation in central carbon metabolism, while retaining the capacity of metabolic enzymes. Overall, the proteome allocation in the evolved strain allowed lowering the maintenance energy and relieve the potential factors attributed

to cell death. In order to validate these hypotheses, future experiments should be performed to understand the precise impact of the changes which occurred in these mechanisms in the evolved strain.

References

[1]   K. Strassburg, D. Walther, H. Takahashi, S. Kanaya, J. Kopka, Dynamic Transcriptional and Metabolic Responses in Yeast Adapting to Temperature Stress, OMICS. 14 (2010) 249–259. https://doi.org/10.1089/omi.2009.0107.

[2]   W. Shui, Y. Xiong, W. Xiao, X. Qi, Y. Zhang, Y. Lin, Y. Guo, Z. Zhang, Q. Wang, Y. Ma, Understanding the Mechanism of Thermotolerance Distinct From Heat Shock Response Through Proteomic Analysis of Industrial Strains of *Saccharomyces* cerevisiae, Mol Cell Proteomics. 14 (2015) 1885–1897. https://doi.org/10.1074/mcp.M114.045781.

[3]   L. Caspeta, Y. Chen, J. Nielsen, Thermotolerant yeasts selected by adaptive evolution express heat stress response at 30 °C, Scientific Reports. 6 (2016) 27003. https://doi.org/10.1038/srep27003.

[4]   T. Pinheiro, K.Y.F. Lip, E. Garcia-Rios, A. Querol, J.A. Teixeira, W. van Gulik, J.M. Guillamon, L. Domingues, Differential proteomic analysis by SWATH-MS unravels the most dominant mechanisms underlying yeast adaptation to non-optimal temperatures under anaerobic conditions, BioRxiv. (2020) 2020.01.06.895581. https://doi.org/10.1101/2020.01.06.895581.

[5]   K.J. Laidler, The development of the Arrhenius equation, J. Chem. Educ. 61 (1984) 494. https://doi.org/10.1021/ed061p494.

[6]   J.P. DeLong, J.P. Gibert, T.M. Luhring, G. Bachman, B. R eed, A. Neyer, K.L. Montooth, The combined effects of reactant kinetics and enzyme stability explain the temperature dependence of metabolic rates, Ecol Evol. 7 (2017) 3940–3950. https://doi.org/10.1002/ece3.2955.

[7]   R. Lum, J.M. Tkach, E. Vierling, J.R. Glover, Evidence for an Unfolding/Threading Mechanism for Protein DiS. A. Ghisaigregation by *Saccharomyces* cerevisiae Hsp104, J. Biol. Chem. 279 (2004) 29139–29146. https://doi.org/10.1074/jbc.M403777200.

[8]   C. Verduyn, E. Postma, W.A. Scheffers, J.P. van Dijken, Physiology of *Saccharomyces* Cerevisiae in Anaerobic Glucose-Limited Chemostat Culturesx, Microbiology. 136 (1990) 395–403. https://doi.org/10.1099/00221287-136-3-395.

[9]   A.B. Canelas, A. ten Pierick, C. Ras, R.M. Seifar, J.C. van Dam, W.M. van Gulik, J.J. Heijnen, Quantitative Evaluation of Intracellular Metabolite Extraction Techniques for Yeast Metabolomics, Anal. Chem. 81 (2009) 7379–7389. https://doi.org/10.1021/ac900999t.

[11]   L. Wu, M.R. Mashego, J.C. van Dam, A.M. Proell, J.L. Vinke, C. Ras, W.A. van Winden, W.M. van Gulik, J.J. Heijnen, Quantitative analysis of the microbial metabolome by isotope dilution mass spectrometry using uniformly 13C-labeled cell extracts as internal standards, Analytical Biochemistry. 336 (2005) 164–171. https://doi.org/10.1016/j.ab.2004.09.001.

[12]   J.C. van Dam, M.R. Eman, J. Frank, H.C. Lange, G.W.K. van Dedem, S.J. Heijnen, Analysis of glycolytic intermediates in *Saccharomyces* cerevisiae using anion exchange chromatography and electrospray ionization with tandem mass spectrometric detection, Analytica Chimica Acta. 460 (2002) 209–218. https://doi.org/10.1016/S0003-2670(02)00240-4.

[13]   S. Niedenführ, A. ten Pierick, P.T.N. van Dam, C.A. Suarez Mendez, K. Nöh, S.A. Wahl, Natural isotope correction of MS/MS measurements for metabolomics and 13C fluxomics, Biotechnology and Bioengineering. 113 (2016) 1137–1147. https://doi.org/10.1002/bit.25859.

[14]   T. Köcher, P. Pichler, R. Swart, K. Mechtler, Analysis of protein mixtures from whole-cell extracts by single-run nanoLC-MS/MS using ultralong gradients, Nat Protoc. 7 (2012) 882–890. https://doi.org/10.1038/nprot.2012.036.

[15]   T. Välikangas, T. Suomi, L.L. Elo, A comprehensive evaluation of popular proteomics software workflows for label-free proteome quantification and imputation, Brief. Bioinformatics. 19 (2018) 1344–1355. https://doi.org/10.1093/bib/bbx054.

[16]   W.S. Noble, How does multiple testing correction work?, Nat Biotechnol. 27 (2009) 1135–1137. https://doi.org/10.1038/nbt1209-1135.

[17]   D. Szklarczyk, A.L. Gable, D. Lyon, A. Junge, S. Wyder, J. Huerta-Cepas, M. Simonovic, N.T. Doncheva, J.H. Morris, P. Bork, L.J. Jensen, C. von Mering, STRING v11: protein–protein association networks with increased coverage, supporting functional discovery in genome-wide experimental datasets, Nucleic Acids Res. 47 (2019) D607–D613. https://doi.org/10.1093/nar/gky1131.

[18]   P. Droste, W. Wiechert, K. Nöh, Semi-automatic drawing of metabolic networks, Information Visualization. 11 (2012) 171–187. https://doi.org/10.1177/1473871611413565.

[19]   P. Droste, S. Miebach, S. Niedenführ, W. Wiechert, K. Nöh, Visualizing multi-omics data in metabolic networks with the software Omix—A case study, Biosystems. 105 (2011) 154–161. https://doi.org/10.1016/j.biosystems.2011.04.003.

[20]   K. van Eunen, J. Bouwman, P. Daran-Lapujade, J. Postmus, A.B. Canelas, F.I.C. Mensonides, R. Orij, I. Tuzun, J. van den Brink, G.J. Smits, W.M. van Gulik, S. Brul, J.J. Heijnen, J.H. de Winde, M.J.T. de Mattos, C. Kettner, J. Nielsen, H.V. Westerhoff, B.M. Bakker, Measuring enzyme activities under standardized in vivo-like conditions for systems biology, FEBS J. 277 (2010) 749–760. https://doi.org/10.1111/j.1742-4658.2009.07524.x.

[21]   O. Ernst, T. Zor, Linearization of the Bradford Protein Assay, J Vis Exp. (2010). https://doi.org/10.3791/1918.

[22]   K. Watson, J.M. Haslam, A.W. Linnane, BIOGENESIS OF MITOCHONDRIA : XIII. The Isolation of Mitochondrial Structures from Anaerobically Grown *Saccharomyces* cerevisiae, Journal of Cell Biology. 46 (1970) 88–96. https://doi.org/10.1083/jcb.46.1.88.

[23]   J. Postmus, I. Tuzun, M. Bekker, W.H. Müller, M.J. Teixeira de Mattos, S. Brul, G.J. Smits, Dynamic regulation of mitochondrial respiratory chain efficiency in *Saccharomyces* cerevisiae, Microbiology. 157 (2011) 3500–3511. https://doi.org/10.1099/mic.0.050039-0.

[24]   K. Peeters, F. Van Leemputte, B. Fischer, B.M. Bonini, H. Quezada, M. Tsytlonok, D. Haesen, W. Vanthienen, N. Bernardes, C.B. Gonzalez-Blas, V. Janssens, P. Tompa, W. Versées, J.M. Thevelein, Fructose-1,6-bisphosphate couples glycolytic flux to activation of Ras, Nat Commun. 8 (2017) 922. https://doi.org/10.1038/s41467-017-01019-z.

[25]   H. Chautard, M. Jacquet, F. Schoentgen, N. Bureaud, H. Bénédetti, Tfs1p, a Member of the PEBP Family, Inhibits the Ira2p but Not the Ira1p Ras GTPase-Activating Protein in *Saccharomyces* cerevisiae, Eukaryot Cell. 3 (2004) 459–470. https://doi.org/10.1128/EC.3.2.459-470.2004.

[26]   K. Otterstedt, C. Larsson, R.M. Bill, A. Ståhlberg, E. Boles, S. Hohmann, L. Gustafsson, Switching the mode of metabolism in the yeast *Saccharomyces* cerevisiae, EMBO Reports. 5 (2004) 532–537. https://doi.org/10.1038/sj.embor.7400132.

[27]   C. Camarasa, J.-P. Grivet, S. Dequin, Investigation by 13C-NMR and tricarboxylic acid (TCA) deletion mutant analysis of pathways for succinate formation in *Saccharomyces* cerevisiae during anaerobic fermentation, Microbiology (Reading, Engl.). 149 (2003) 2669–2678. https://doi.org/10.1099/mic.0.26007-0.

[28]   F. Dupuis-Sandoval, M. Poirier, M.S. Scott, The emerging landscape of small nucleolar RNAs in cell biology, Wiley Interdiscip Rev RNA. 6 (2015) 381–397. https://doi.org/10.1002/wrna.1284.

[29]   E. Metzl-Raz, M. Kafri, G. Yaakov, I. Soifer, Y. Gurvich, N. Barkai, Principles of cellular resource allocation revealed by condition-dependent proteome profiling, ELife. 6 (n.d.). https://doi.org/10.7554/eLife.28034.

[30]   J. Björkeroth, K. Campbell, C. Malina, R. Yu, F.D. Bartolomeo, J. Nielsen, Proteome reallocation from amino acid biosynthesis to ribosomes enables yeast to grow faster in rich media, PNAS. 117 (2020) 21804–21812. https://doi.org/10.1073/pnas.1921890117.

[31]   J. Reinders, K. Wagner, R.P. Zahedi, D. Stojanovski, B. Eyrich, M. van der Laan, P. Rehling, A. Sickmann, N. Pfanner, C. Meisinger, Profiling phosphoproteins of yeast mitochondria reveals a role of phosphorylation in assembly of the ATP synthase, Mol Cell Proteomics. 6 (2007) 1896–1906. https://doi.org/10.1074/mcp.M700098-MCP200.

[32]   M.Y. Cheng, F.U. Hartl, J. Martin, R.A. Pollock, F. Kalousek, W. Neupert, E.M. Hallberg, R.L. Hallberg, A.L. Horwich, Mitochondrial heat-shock protein hsp60 is essential for assembly of proteins imported into yeast mitochondria, Nature. 337 (1989) 620–625. https://doi.org/10.1038/337620a0.

[33]   J.E. Stukey, V.M. McDonough, C.E. Martin, The OLE1 gene of *Saccharomyces* cerevisiae encodes the delta 9 fatty acid desaturase and can be functionally replaced by the rat stearoyl-CoA desaturase gene, J. Biol. Chem. 265 (1990) 20144–20149.

[34]   S.J. McConnell, L.C. Stewart, A. Talin, M.P. Yaffe, Temperature-sensitive yeast mutants defective in mitochondrial inheritance., J Cell Biol. 111 (1990) 967–976. https://doi.org/10.1083/jcb.111.3.967.

[35]   D.C. Hess, C.L. Myers, C. Huttenhower, M.A. Hibbs, A.P. Hayes, J. Paw, J.J. Clore, R.M. Mendoza, B.S. Luis, C. Nislow, G. Giaever, M. Costanzo, O.G. Troyanskaya, A.A. Caudy, Computationally Driven, Quantitative Experiments Discover Genes Required for Mitochondrial Biogenesis, PLoS Genet. 5 (2009). https://doi.org/10.1371/journal.pgen.1000407.

[36]   M. Ibba, D. Söll, Aminoacyl-tRNAs: setting the limits of the genetic code, Genes Dev. 18 (2004) 731–738. https://doi.org/10.1101/gad.1187404.

[37]   M.J.L. de Groot, P. Daran-Lapujade, B. van Breukelen, T.A. Knijnenburg, E.A.F. de Hulster, M.J.T. Reinders, J.T. Pronk, A.J.R. Heck, M. Slijper, Quantitative proteomics and transcriptomics of anaerobic and aerobic yeast cultures reveals post-transcriptional regulation of key cellular processes, Microbiology,. 153 (2007) 3864–3878. https://doi.org/10.1099/mic.0.2007/009969-0.

[38]   Y. Eguchi, K. Makanae, T. Hasunuma, Y. Ishibashi, K. Kito, H. Moriya, Estimating the protein burden limit of yeast cells by measuring the expression limits of glycolytic proteins, ELife. 7 (2018) e34595. https://doi.org/10.7554/eLife.34595.

[39]   B. Bolognesi, B. Lehner, Reaching the limit, ELife. 7 (2018) e39804. https://doi.org/10.7554/eLife.39804.

[40]   R. Yu, K. Campbell, R. Pereira, J. Björkeroth, Q. Qi, E. Vorontsov, C. Sihlbom, J. Nielsen, Nitrogen limitation reveals large reserves in metabolic and translational capacities of yeast, Nature Communications. 11 (2020) 1881. https://doi.org/10.1038/s41467-020-15749-0.

[41]   R. Caesar, A. Blomberg, The Stress-induced Tfs1p Requires NatB-mediated Acetylation to Inhibit Carboxypeptidase Y and to Regulate the Protein Kinase A Pathway *, Journal of Biological Chemistry. 279 (2004) 38532–38543. https://doi.org/10.1074/jbc.M402939200.

[42]   J. Mima, H. Fukada, M. Nagayama, M. Ueda, Specific membrane binding of the carboxypeptidase Y inhibitor I(C), a phosphatidylethanolamine-binding protein family member, FEBS J. 273 (2006) 5374–5383. https://doi.org/10.1111/j.1742-4658.2006.05530.x.

[43]   F. Reggiori, D.J. Klionsky, Autophagic Processes in Yeast: Mechanism, Machinery and Regulation, Genetics. 194 (2013) 341–361. https://doi.org/10.1534/genetics.112.149013.

[44]   Y. Feng, D. He, Z. Yao, D.J. Klionsky, The machinery of macroautophagy, Cell Research. 24 (2014) 24–41. https://doi.org/10.1038/cr.2013.168.

[45]   J.-C. Farré, S. Subramani, Mechanistic insights into selective autophagy pathways: lessons from yeast, Nat Rev Mol Cell Biol. 17 (2016) 537–552. https://doi.org/10.1038/nrm.2016.74.

[46]   F. Schimmöller, H. Riezman, Involvement of Ypt7p, a small GTPase, in traffic from late endosome to the vacuole in yeast, J Cell Sci. 106 (Pt 3) (1993) 823–830.

[47]   Y. Chen, F. Zhou, S. Zou, S. Yu, S. Li, D. Li, J. Song, H. Li, Z. He, B. Hu, L.O. Björn, Z. Lipatova, Y. Liang, Z. Xie, N. Segev, A Vps21 endocytic module regulates autophagy, Mol Biol Cell. 25 (2014) 3166–3177. https://doi.org/10.1091/mbc.E14-04-0917.

[48]   H.J. kleine Balderhaar, H. Arlt, C. Ostrowicz, C. Bröcker, F. Sündermann, R. Brandt, M. Babst, C. Ungermann, The Rab GTPase Ypt7 is linked to retromer-mediated receptor recycling and fusion at the yeast late endosome, J Cell Sci. 123 (2010) 4085–4094. https://doi.org/10.1242/jcs.071977.

[49]   Y. Ogasawara, S. Kira, Y. Mukai, T. Noda, A. Yamamoto, Ole1, fatty acid desaturase, is required for Atg9 delivery and isolation membrane expansion during autophagy in *Saccharomyces* cerevisiae, Biol Open. 6 (2016) 35–40. https://doi.org/10.1242/bio.022053.

[50]   J.K. Tyler, J.E. Johnson, The role of autophagy in the regulation of yeast life span, Ann N Y Acad Sci. 1418 (2018) 31–43. https://doi.org/10.1111/nyas.13549.

[51]   Y.T. Kwon, A. Ciechanover, The Ubiquitin Code in the Ubiquitin-Proteasome System and Autophagy, Trends Biochem Sci. 42 (2017) 873–886. https://doi.org/10.1016/j.tibs.2017.09.002.

[52]   D. Finley, H.D. Ulrich, T. Sommer, P. Kaiser, The Ubiquitin–Proteasome System of *Saccharomyces* cerevisiae, Genetics. 192 (2012) 319–360. https://doi.org/10.1534/genetics.112.140467.

[53]   B.P. Young, J.J.H. Shin, R. Orij, J.T. Chao, S.C. Li, X.L. Guan, A. Khong, E. Jan, M.R. Wenk, W.A. Prinz, G.J. Smits, C.J.R. Loewen, Phosphatidic Acid Is a pH Biosensor That Links Membrane Biogenesis to Metabolism, Science. 329 (2010) 1085–1088. https://doi.org/10.1126/science.1191026.

[54]   R. Orij, S. Brul, G.J. Smits, Intracellular pH is a tightly controlled signal in yeast, Biochimica et Biophysica Acta (BBA) - General Subjects. 1810 (2011) 933–944. https://doi.org/10.1016/j.bbagen.2011.03.011.

[55]   T. Aabo, J. Glückstad, H. Siegumfeldt, N. Arneborg, Intracellular pH distribution as a cell health indicator in *Saccharomyces* cerevisiae, J R Soc Interface. 8 (2011) 1635–1643. https://doi.org/10.1098/rsif.2011.0148.

[56]   P.J. Coote, M.V. Jones, I.J. Seymour, D.L. Rowe, D.P. Ferdinando, A.J. McArthur, M.B. Cole, Activity of the plasma membrane H+-ATPase is a key physiological determinant of thermotolerance in *Saccharomyces* cerevisiae, Microbiology. 140 (1994) 1881–1890. https://doi.org/10.1099/13500872-140-8-1881.

[57]   R.S.S. Magalhães, B. Popova, G.H. Braus, T.F. Outeiro, E.C.A. Eleutherio, The trehalose protective mechanism during thermal stress in *Saccharomyces* cerevisiae: the roles of Ath1 and Agt1, FEMS Yeast Res. 18 (2018). https://doi.org/10.1093/femsyr/foy066.

[58]   M. Simola, A.-L. Hänninen, S.-M. Stranius, M. Makarow, Trehalose is required for conformational repair of heat-denatured proteins in the yeast endoplasmic reticulum but not for maintenance of membrane traffic functions after severe heat stress, Molecular Microbiology. 37 (2000) 42–53. https://doi.org/10.1046/j.1365-2958.2000.01970.x.

[59]   S. Hohmann, W. Bell, M.J. Neves, D. Valckx, J.M. Thevelein, Evidence for trehalose-6-phosphate-dependent and -independent mechanisms in the control of sugar influx into yeast glycolysis, Mol Microbiol. 20 (1996) 981–991. https://doi.org/10.1111/j.1365-2958.1996.tb02539.x.

[60]   D. Solis-Escalante, N.G.A. Kuijpers, N. Barrajon-Simancas, M. van den Broek, J.T. Pronk, J.-M. Daran, P. Daran-Lapujade, A Minimal Set of Glycolytic Genes Reveals Strong Redundancies in *Saccharomyces* cerevisiae Central Metabolism, Eukaryotic Cell. 14 (2015) 804–816. https://doi.org/10.1128/EC.00064-15.

[61]   A.E. Ringel, R. Ryznar, H. Picariello, K. Huang, A.G. Lazarus, S.G. Holmes, Yeast Tdh3 (Glyceraldehyde 3-Phosphate Dehydrogenase) Is a Sir2-Interacting Factor That Regulates Transcriptional Silencing and rDNA Recombination, PLoS Genet. 9 (2013). https://doi.org/10.1371/journal.pgen.1003871.

[62]   B.K. Kennedy, The Enigmatic Role of Sir2 in Aging, Cell. 123 (2005) 548–550. https://doi.org/10.1016/j.cell.2005.11.002.

[63]   J.J. Sandmeier, I. Celic, J.D. Boeke, J.S. Smith, Telomeric and rDNA silencing in *Saccharomyces* cerevisiae are dependent on a nuclear NAD(+) salvage pathway, Genetics. 160 (2002) 877–889.

[64]   S. Lindquist, G. Kim, Heat-shock protein 104 expression is sufficient for thermotolerance in yeast., Proc Natl Acad Sci U S A. 93 (1996) 5301–5306.

[65]   M. Haslbeck, A. Miess, T. Stromer, S. Walter, J. Buchner, Disassembling Protein Aggregates in the Yeast Cytosol: THE COOPERATION OF HSP26 WITH SSA1 AND HSP104*, Journal of Biological Chemistry. 280 (2005) 23861–23868. https://doi.org/10.1074/jbc.M502697200.

[66]   M. Haslbeck, N. Braun, T. Stromer, B. Richter, N. Model, S. Weinkauf, J. Buchner, Hsp42 is the general small heat shock protein in the cytosol of *Saccharomyces* cerevisiae, EMBO J. 23 (2004) 638–649. https://doi.org/10.1038/sj.emboj.7600080.

[67]   M. Correa Marrero, I. Barrio-Hernandez, Toward Understanding the Biochemical Determinants of Protein Degradation Rates, ACS Omega. (2021). https://doi.org/10.1021/acsomega.0c05318.

[68]   M. Martin-Perez, J. Villén, Determinants and regulation of protein turnover in yeast, Cell Syst. 5 (2017) 283-294.e5. https://doi.org/10.1016/j.cels.2017.08.008.

[69]   P.O. Ljungdahl, B. Daignan-Fornier, Regulation of Amino Acid, Nucleotide, and Phosphate Metabolism in *Saccharomyces* cerevisiae, Genetics. 190 (2012) 885–929. https://doi.org/10.1534/genetics.111.133306.

[70]   R.J. Rolfes, Regulation of purine nucleotide biosynthesis: in yeast and beyond, Biochem Soc Trans. 34 (2006) 786–790. https://doi.org/10.1042/BST0340786.

[71]   J.-F. Liu, J.-J. Xia, K.-L. Nie, F. Wang, L. Deng, Outline of the biosynthesis and regulation of ergosterol in yeast, World J Microbiol Biotechnol. 35 (2019) 98. https://doi.org/10.1007/s11274-019-2673-2.

[72]   P. Kohut, D. Wüstner, L. Hronska, K. Kuchler, I. Hapala, M. Valachovic, The role of ABC proteins Aus1p and Pdr11p in the uptake of external sterols in yeast: dehydroergosterol fluorescence study, Biochem Biophys Res Commun. 404 (2011) 233–238. https://doi.org/10.1016/j.bbrc.2010.11.099.

[73]   M. Zavrel, S.J. Hoot, T.C. White, Comparison of Sterol Import under Aerobic and Anaerobic Conditions in Three Fungal Species, Candida albicans, Candida glabrata, and *Saccharomyces* cerevisiae, Eukaryot Cell. 12 (2013) 725–738. https://doi.org/10.1128/EC.00345-12.

[74]   P. Portela, S. Howell, S. Moreno, S. Rossi, In Vivo and in Vitro Phosphorylation of Two Isoforms of Yeast Pyruvate Kinase by Protein Kinase A *, Journal of Biological Chemistry. 277 (2002) 30477–30487. https://doi.org/10.1074/jbc.M201094200.

[75]   M. Cytryńska, M. Frajnt, T. Jakubowicz, *Saccharomyces* cerevisiae pyruvate kinase Pyk1 is PKA phosphorylation substrate in vitro, FEMS Microbiology Letters. 203 (2001) 223–227. https://doi.org/10.1111/j.1574-6968.2001.tb10845.x.

[76]   E. Kanshin, P. Kubiniok, Y. Thattikota, D. D'Amours, P. Thibault, Phosphoproteome dynamics of *Saccharomyces* cerevisiae under heat shock and cold stress, Molecular Systems Biology. 11 (2015) 813. https://doi.org/10.15252/msb.20156170.

[77]   C. Zhao, U.S. Jung, P. Garrett-Engele, T. Roe, M.S. Cyert, D.E. Levin, Temperature-Induced Expression of Yeast FKS2 Is under the Dual Control of Protein Kinase C and Calcineurin, Mol Cell Biol. 18 (1998) 1013–1022.

[78]   F. Tripodi, R. Nicastro, V. Reghellin, P. Coccetti, Post-translational modifications on yeast carbon metabolism: Regulatory mechanisms beyond transcriptional control, Biochimica et Biophysica Acta (BBA) - General Subjects. 1850 (2015) 620–627. https://doi.org/10.1016/j.bbagen.2014.12.010.

Supplementary materials

	TMT[6]-126	TMT[6]-127	TMT[6]-128	TMT[6]-129	TMT[6]-130	TMT[6]-131
CN3039	CN 39°C t2	CN 39°C t3	CN 39°C t4	CN 30°C t2	CN 30°C t3	CN 30°C t4
EVO3039	EVO 30°C t2	EVO 30°C t3	EVO 30°C t4	EVO 39°C t2	EVO 39°C t3	EVO 39°C t4
CNEVO39	CN 39°C t2	CN 39°C t3	CN 39°C t4	EVO 39°C t2	EVO 39°C t3	EVO 39°C t4

Table S1

TMT labelling scheme for the chemostat culture collected at the steady-state. Each comparison condition, indicated on the most left of the table, consisted of three biological replicates of two types of chemostat samples which categorized by four colours (green, yellow, blue, and red); CN represents CEN.PK113-7D, whereas EVO represents the evolved CEN.PK113-7D; 30°C and 39°C refer to the cultivation temperature of the chemostat fermentations; t2, t3, and t4 indicate the time points where the biomass samples were withdrawn during the steady-state of the chemostat. The TMT labelling agents, indicated on the top of the table, were used to label the corresponding replicate samples.

	CEN.PK113-7D		CEN.PK-EVO	
$mmol \cdot g_{viable\,DW}^{-1} \cdot h^{-1}$	30˚C	39˚C	30˚C	39˚C
$q_{acetate}$	0.01 ± 0.002	0.046 ± 0.046	0.011 ± 0.013	0.033 ± 0.01
q_{CO2}	3.341 ± 0.267	5.13 ± 0.475	3.576 ± 0.075	4.605 ± 0.191
$q_{ethanol}$	3.175 ± 0.269	4.989 ± 0.471	3.405 ± 0.095	4.485 ± 0.238
$q_{glycerol}$	0.312 ± 0.002	0.337 ± 0.059	0.317 ± 0.04	0.306 ± 0.067
$q_{lactate}$	0.014 ± 0.006	0.029 ± 0	0.015 ± 0.007	0.04 ± 0.007
q_{malate}	0.004 ± 0.001	0.012 ± 0.007	0.001 ± 0.002	0.01 ± 0.001
q_s	-1.956 ± 0.139	-2.945 ± 0.312	-2.073 ± 0.016	-2.689 ± 0.079
$q_{sucinnate}$	0.012 ± 0.001	0.073 ± 0.037	0.011 ± 0.001	0.088 ± 0.022

Table S2

Reconciled specific conversion rates of CEN.PK113-7D and evolved CEN.PK113-7D with their standard errors during anaerobic chemostat cultivation at 30˚C and 39 C at a dilution rate of 0.03 h-1. The nomenclature of s represents as substrate (glucose).

mol·mol$_{glucose}^{-1}$	CEN.PK113-7D		CEN.PK-EVO	
	30 °C	39 °C	30 °C	39 °C
Y$_{acetate}$	0.006 ± 0.001	0.016 ± 0.003	0.005 ± 0.001	0.012 ± 0.002
Y$_{biomass}$	0.559 ± 0.011	0.374* ± 0.013	0.509 ± 0.017	0.423* ± 0.013
Y$_{CO2}$	1.70 ± 0.02	1.74 ± 0.07	1.73 ± 0.06	1.71 ± 0.06
Y$_{ethanol}$	1.61 ± 0.02	1.69 ± 0.07	1.64 ± 0.06	1.67 ± 0.06
Y$_{glycerol}$	0.169 ± 0.004	0.115 ± 0.008	0.153 ± 0.006	0.114 ± 0.005
Y$_{lactate}$	0.005 ± 0.001	0.010 ± 0.001	0.007 ± 0.002	0.015 ± 0.001
Y$_{malate}$	0.002 ± 0.000	0.004 ± 0.000	0.001 ± 0.000	0.004 ± 0.000
Y$_{succinate}$	0.006 ± 0.001	0.025* ± 0.004	0.005 ± 0.001	0.033* ± 0.002

Table S3

Yield of biomass and main products on glucose of CEN.PK113-7D and CEN.PK-EVO during characterisation by chemostat with their standard errors, calculated from the biomass specific conversion rates shown in Chapter 4. Compared with the unevolved strain at the same temperature, * indicate a significant difference with a p-value (paired T-test) of < 0.05.

	Most significantly upregulated proteins	Most significantly downregulated proteins
CN39/CN30	CPR6, HSP60, HSP82, YGP1	ALD4, ATP2, ATP4, ATP5, ATP7, ATP17, COX4, COX14, HXK1, ILV5, PTI1, QCR10, SDH2
EVO39/EVO30	HSP60, OLE1, TDH3	AIM41, ATP2, ATP4, ATP5, ATP7, CIT1, HEM1, HSP12, ILV5, MCR1, PGM2, PTI1, TFS1
EVO39/CN39	HXK1, MAL12, PTI1	AHP1, HSP12, HSP26, YGP1

Table S4

The differential expressed proteins at each comparison condition which have log2(fold change) difference either ≥ 1 or ≤ -1 on the volcano plot (Figure S1) and with the p-values of two injections ≤ 0.05. Protein indicated in red are differentially expressed in both strains as response to 39.0°C.

a)

CN39/CN30   EVO39/EVO30

161   107   62

b)

CN39/CN30   EVO39/EVO30

62   93   152
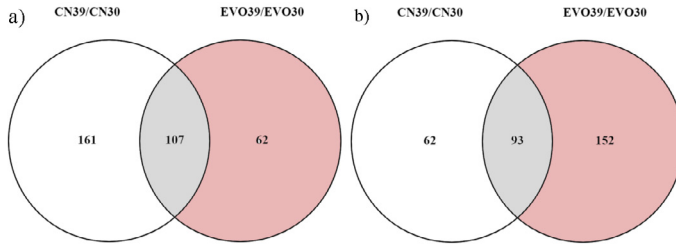
Figure S1

Venn diagrams indicate the overlap of differential expressed proteins between the two strains in comparison between 30°C and 39°C; a) based on upregulated proteins for all comparison conditions; b) based on downregulated proteins for all comparison conditions. The proteins in each protein profiles had a p-value <0.05. The grey cluster indicates the expressed proteins which differentially expressed at similar magnitude between both strains. The red cluster indicated the differentially expressed proteins in the evolved strain between different cultivation temperatures.
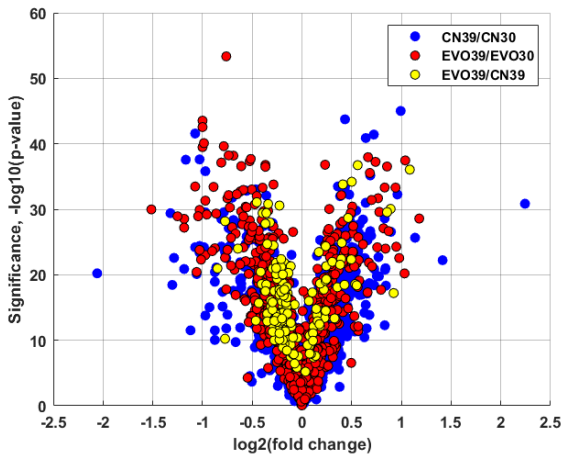
Figure S2

Volcano plot of all acquired data of three comparison conditions. The -log10 transformed significance of the differential expressed proteins in each comparison condition are plotted against the corresponding log2 transformed ratio of the fold change. The p-value provides evidence (95% significant confidence) of each acquired measurement at a predefined level where the proportion of false positives among all the acquired data of each comparison condition identified as being differentially expressed between two conditions. The negative log10 transformed p-value would indicate the differentially expressed proteins with a low p-value at the upper parts of the plot. The binary logarithm transformed fold-change would indicate the differentially expressed proteins with large fold-change values (larger or less than 2) either at most left (less than -1 of a vertical threshold line) or most right part (higher than 1 of a vertical threshold line) of the plot.

Table S5
Enrichment analysis
for GO processes of
the up-(green) and
downregulated (red)
proteins in common in
both strains between
two temperatures,
based on the proteins
found in the grey area
of Figure S1

Category description	Protein identity	No. of proteins in cluster	No. of proteins in genome	FDR value
cytoplasmic translation	SSA1 | RPL23A | RPL4A | RPS11B | RPL13A | RPS16B | RPL35B | RPL35A | RPS11A | RPL12B | RPS18A | RPL12A | RPL34A | RPL23B | RPS26B | RPL2A | RPL24A | RPL7A | RPL28 | RPL1B | RPS26A | RPS25A | RPL24B | RPS20 | RPS4B | RPL2B | RPL34B | RPS5 | RPS4A | RPL37A | RPS28B | RPS25B | RPL6B | RPS18B | RPL6A | RPL13B | RPS16A | RPL20A | RPL16B | RPS3 | RPL18B | RPL18A | RPL3 | RPS28A | RPL20B | RPS12 | RPS9A | RPL5 | RPL1A	49	171	1.28E-45
translation	SSA1 | RPL23A | RPL4A | RPS11B | RPS9B | RPL13A | RPS16B | RPL35B | RPL35A | RPS11A | RPL12B | RPS18A | RPL12A | RPL34A | RPL23B | RPS26B | RPL2A | RPL24A | RPL7A | RPL28 | RPS2 | RPL1B | RPS26A | RPS25A | RPS23A | RPL24B | RPS20 | RPS4B | RPL2B | RPL34B | RPS5 | RPS4A | RPL37A | RPS28B | RPS25B | RPL6B | RPS18B | RPL6A | RPL13B | RPS16A | RPL20A | RPL16B | RPS3 | RPL18B | RPL18A | RPL3 | RPS28A | RPL20B | RPS12 | RPS9A | RPL5 | RPL1A | TEF1 | RPS23B	54	372	1.20E-37
peptide metabolic process	SSA1 | RPL23A | RPL4A | RPS11B | RPS9B | RPL13A | RPS16B | RPL35B | RPL35A | RPS11A | RPL12B | RPS18A | RPL12A | RPL34A | RPL23B | RPS26B | RPL2A | RPL24A | RPL7A | RPL28 | RPS2 | RPL1B | RPS26A | RPS25A | RPS23A | RPL24B | RPS20 | RPS4B | RPL2B | RPL34B | RPS5 | RPS4A | RPL37A | RPS28B | RPS25B | RPL6B | RPS18B | RPL6A | RPL13B | RPS16A | RPL20A | RPL16B | RPS3 | RPL18B | RPL18A | RPL3 | RPS28A | RPL20B | RPS12 | RPS9A | RPL5 | RPL1A | TEF1 | RPS23B	54	411	7.13E-36
organonitrogen compound biosynthetic process	SSA1 | CYS3 | CDC19 | RPL23A | RPL4A | RPS11B | RPS9B | RPL13A | RPS16B | RPL35B | RPL35A | RPS11A | TPI1 | RPL12B | RPS18A | RPL12A | RPL34A | RPL23B | RPS26B | RPL2A | RPL24A | RPL7A | RPL28 | RPS2 | RPL1B | RPS26A | ADE5,7 | RPS25A | RPS23A | RPL24B | TDH3 | RPS20 | ENO2 | RPS4B | RPL2B | RPL34B | MET3 | ADO1 | RPS5 | RPS4A | RPL37A | RPS28B | RPS25B | KAP95 | RPL6B | RPS18B | RPL6A | RPL13B | RPS16A | RPL20A | RPL16B | RPS3 | RPL18B | RPL18A | RPL3 | RPS28A | RPL20B | RPS12 | RPS9A | RPL5 | RPL1A | TEF1 | RPS23B	63	897	8.67E-29
cellular protein metabolic process	SSA1 | RPL23A | RPL4A | RPS11B | RPS9B | GRX1 | PDI1 | RPL13A | RPS16B | RPL35B | RPL35A | RPS11A | CPR1 | CPR5 | RPL12B | RPS18A | RPL12A | RPL34A | RPL23B | RPS26B | MDJ1 | RPL2A | RPL24A | RPL7A | RPL28 | RPS2 | RPL1B | RPS26A | RPS25A | RPS23A | RPL24B | RPS20 | RPS4B | RPL2B | RPL34B | KAR2 | RPS5 | RPS4A | SSA2 | RPL37A | CPR6 | RPS28B | RPS25B | SEC61 | RPL6B | RPS18B | RPL6A | RPL13B | RPS16A | RPL20A | YDJ1 | RPL16B | RPS3 | RPL18B | RPL18A | RPL3 | RPS28A | RPL20B | RPS12 | RPS9A | RPL5 | RPL1A | YME1 | TEF1 | RPS23B	65	1242	6.58E-23
protein metabolic process	SSA1 | RPL23A | RPL4A | RPS11B | RPS9B | GRX1 | PDI1 | RPL13A | RPS16B | RPL35B | RPL35A | RPS11A | CPR1 | CPR5 | RPL12B | RPS18A | RPL12A | RPL34A | RPL23B | RPS26B | MDJ1 | RPL2A | RPL24A | RPL7A | RPL28 | RPS2 | RPL1B | RPS26A | RPS25A | RPS23A | RPL24B | RPS20 | RPS4B | RPL2B | RPL34B | KAR2 | RPS5 | RPS4A | SSA2 | RPL37A | CPR6 | HSP60 | RPS28B | RPS25B | SEC61 | RPL6B | RPS18B | RPL6A | RPL13B | RPS16A | RPL20A | YDJ1 | RPL16B | RPS3 | RPL18B | RPL18A | RPL3 | RPS28A | RPL20B | RPS12 | RPS9A | RPL5 | RPL1A | HSP82 | YME1 | TEF1 | RPS23B	67	1374	2.64E-22
organonitrogen compound metabolic process	SSA1 | CYS3 | CDC19 | RPL23A | RPL4A | RPS11B | RPS9B | GRX1 | PDI1 | RPL13A | RPS16B | RPL35B | RPL35A | RPS11A | TPI1 | CPR1 | CPR5 | RPL12B | RPS18A | RPL12A | RPL34A | RPL23B | RPS26B | MDJ1 | RPL2A | RPL24A | RPL7A | RPL28 | RPS2 | RPL1B | RPS26A | ADE5,7 | RPS25A | RPS23A | RPL24B | TDH3 | RPS20 | ENO2 | RPS4B | RPL2B | RPL34B | KAR2 | MET3 | ADO1 | RPS5 | RPS4A | SSA2 | PDC1 | RPL37A | CPR6 | HSP60 | RPS28B | RPS25B | KAP95 | SEC61 | RPL6B | RPS18B | RPL6A | RPL13B | RPS16A | RPL20A | YDJ1 | RPL16B | RPS3 | RPL18B | RPL18A | RPL3 | RPS28A | RPL20B | RPS12 | RPS9A | RPL5 | RPL1A | HSP82 | YME1 | TEF1 | RPS23B	77	1939	2.64E-22

cellular nitrogen compound biosynthetic process	SSA1 | CDC19 | RPL23A | RPL4A | RPS11B | RPS9B | RPL13A | RPS16B | RPL35B | RPL35A | RPS11A | TPI1 | RPL12B | RPS18A | RPL12A | RPL34A | RPL23B | RPS26B | RPL2A | RPL24A | RPL7A | RPL28 | RPS2 | RPL1B | RPS26A | ADE5,7 | RPS25A | RPS23A | RPL24B | TDH3 | RPS20 | ENO2 | RPS4B | RPL2B | RPL34B | ADO1 | RPS5 | RPS4A | RPL37A | RPS28B | RPS25B | RPL6B | RPS18B | RPL6A | RPL13B | RPS16A | RPL20A | RPL16B | RPS3 | RPL18B | RPL18A | RPL3 | RPS28A | RPL20B | RPS12 | RPS9A | RPL5 | RPL1A | TEF1 | RPS23B	60	1288	7.61E-18
ribosome biogenesis	RPS11B | RPS9B | RPS16B | RPL35B | RPL35A | RPS11A | RPL12B | RPS18A | RPL12A | ARB1 | RPL34A | RPS26B | RPL24A | RPL7A | RPS2 | RPL1B | RPS26A | RPS23A | RPL24B | RPS20 | RPL34B | RPS5 | RPL37A | RPS28B | RPL6B | RPS18B | RPL6A | RPS16A | RPS3 | RPL3 | RPS28A | RPS9A | RPL5 | RPL1A | RPS23B	35	403	3.13E-16
ribonucleoprotein complex biogenesis	RPS11B | RPS9B | RPS16B | RPL35B | RPL35A | RPS11A | RPL12B | RPS18A | RPL12A | ARB1 | RPL34A | RPS26B | RPL24A | RPL7A | RPS2 | RPL1B | RPS26A | RPS23A | RPL24B | RPS20 | RPL34B | RPS5 | RPL37A | RPS28B | RPL6B | RPS18B | RPL6A | RPS16A | HSC82 | RPS3 | RPL3 | RPS28A | RPS9A | RPL5 | RPL1A | HSP82 | RPS23B	37	485	1.30E-15
organic substance biosynthetic process	SSA1 | CYS3 | CDC19 | RPL23A | RPL4A | RPS11B | RPS9B | RPL13A | RPS16B | RPL35B | RPL35A | RPS11A | TPI1 | RPL12B | RPS18A | RPL12A | RPL34A | RPL23B | RPS26B | RPL2A | RPL24A | RPL7A | RPL28 | RPS2 | RPL1B | RPS26A | ADE5,7 | RPS25A | RPS23A | RPL24B | TDH3 | RPS20 | ENO2 | RPS4B | RPL2B | RPL34B | GPP1 | KAR2 | MET3 | ADO1 | RPS5 | RPS4A | PDC1 | RPL37A | RPS28B | RPS25B | KAP95 | RPL6B | RPS18B | RPL6A | RPL13B | RPS16A | RPL20A | RPL16B | RPS3 | RPL18B | RPL18A | RPL3 | RPS28A | RPL20B | RPS12 | RPS9A | RPL5 | RPL1A | TEF1 | RPS23B	66	1826	9.02E-15
gene expression	SSA1 | RPL23A | RPL4A | RPS11B | RPS9B | NFS1 | RPL13A | RPS16B | RPL35B | RPL35A | RPS11A | TRM1 | RPL12B | RPS18A | RPL12A | RPL34A | RPL23B | RPS26B | RPL2A | RPL24A | RPL7A | RPL28 | RPS2 | RPL1B | RPS26A | RPS25A | RPS23A | RPL24B | RPS20 | RPS4B | RPL2B | RPL34B | RPS5 | RPS4A | RPL37A | HSP60 | RPS28B | RPS25B | RPL6B | RPS18B | RPL6A | RPL13B | RPS16A | RPL20A | RPL16B | RPS3 | RPL18B | RPL18A | RPL3 | RPS28A | RPL20B | RPS12 | RPS9A | RPL5 | RPL1A | HSP82 | YME1 | TEF1 | RPS23B	59	1466	1.72E-14
cellular biosynthetic process	SSA1 | CYS3 | CDC19 | RPL23A | RPL4A | RPS11B | RPS9B | RPL13A | RPS16B | RPL35B | RPL35A | RPS11A | TPI1 | RPL12B | RPS18A | RPL12A | RPL34A | RPL23B | RPS26B | RPL2A | RPL24A | RPL7A | RPL28 | RPS2 | RPL1B | RPS26A | ADE5,7 | RPS25A | RPS23A | RPL24B | TDH3 | RPS20 | ENO2 | RPS4B | RPL2B | RPL34B | GPP1 | KAR2 | MET3 | ADO1 | RPS5 | RPS4A | RPL37A | RPS28B | RPS25B | KAP95 | RPL6B | RPS18B | RPL6A | RPL13B | RPS16A | RPL20A | RPL16B | RPS3 | RPL18B | RPL18A | RPL3 | RPS28A | RPL20B | RPS12 | RPS9A | RPL5 | RPL1A | TEF1 | RPS23B	65	1803	2.06E-14
cellular macromolecule biosynthetic process	SSA1 | RPL23A | RPL4A | RPS11B | RPS9B | RPL13A | RPS16B | RPL35B | RPL35A | RPS11A | RPL12B | RPS18A | RPL12A | RPL34A | RPL23B | RPS26B | RPL2A | RPL24A | RPL7A | RPL28 | RPS2 | RPL1B | RPS26A | RPS25A | RPS23A | RPL24B | RPS20 | RPS4B | RPL2B | RPL34B | KAR2 | RPS5 | RPS4A | RPL37A | RPS28B | RPS25B | RPL6B | RPS18B | RPL6A | RPL13B | RPS16A | RPL20A | RPL16B | RPS3 | RPL18B | RPL18A | RPL3 | RPS28A | RPL20B | RPS12 | RPS9A | RPL5 | RPL1A | TEF1 | RPS23B	55	1294	4.13E-14
protein folding	SSA1 | PDI1 | CPR1 | AHA1 | HSP78 | CPR5 | SSA4 | MDJ1 | SSA2 | CPR6 | HSP60 | HSC82 | YDJ1 | HCH1 | HSP10 | STI1 | SSE1 | HSP82 | YME1	19	108	3.41E-13
nitrogen compound metabolic process	SSA1 | CYS3 | CDC19 | RPL23A | RPL4A | RPS11B | RPS9B | NFS1 | GRX1 | PDI1 | RPL13A | RPS16B | RPL35B | RPL35A | RPS11A | TPI1 | TRM1 | CPR1 | CPR5 | RPL12B | RPS18A | RPL12A | RPL34A | RPL23B | RPS26B | MDJ1 | YPT1 | RPL2A | RPL24A | RPL7A | RPL28 | RPS2 | RPL1B | RPS26A | ADE5,7 | RPS25A | RPS23A | RPL24B | TDH3 | RPS20 | ENO2 | RPS4B | RPL2B | RPL34B | KAR2 | MET3 | ADO1 | RPS5 | RPS4A | SSA2 | PDC1 | RPL37A | CPR6 | HSP60 | RPS28B | RPS25B | KAP95 | SEC61 | RPL6B | RPS18B | RPL6A | RPL13B | RPS16A | HSC82 | RPL20A | YDJ1 | RPL16B | RPS3 | RPL18B | RPL18A | RPL3 | RPS28A | RPL20B | RPS12 | RPS9A | RPL5 | RPL1A | HSP82 | YME1 | TEF1 | RPS23B	81	3056	9.29E-13

Table S5
(continued)

cellular macromolecule metabolic process	SSA1 | RPL23A | RPL4A | RPS11B | RPS9B | GRX1 | PDI1 | RPL13A | RPS16B | RPL35B | RPL35A | RPS11A | TRM1 | CPR1 | CPR5 | RPL12B | RPS18A | RPL12A | RPL34A | RPL23B | RPS26B | MDJ1 | YPT1 | RPL2A | RPL24A | RPL7A | RPL28 | RPS2 | RPL1B | RPS26A | RPS25A | RPS23A | RPL24B | RPS20 | RPS4B | RPL2B | RPL34B | KAR2 | RPS5 | RPS4A | SSA2 | RPL37A | CPR6 | RPS28B | RPS25B | SEC61 | RPL6B | RPS18B | RPL6A | RPL13B | RPS16A | HSC82 | RPL20A | YDJ1 | RPL16B | RPS3 | RPL18B | RPL18A | RPL3 | RPS28A | RPL20B | RPS12 | RPS9A | RPL5 | RPL1A | YME1 | TEF1 | RPS23B	68	2185	3.22E-12
primary metabolic process	SSA1 | CYS3 | CDC19 | RPL23A | RPL4A | RPS11B | RPS9B | NFS1 | GRX1 | PDI1 | RPL13A | RPS16B | RPL35B | RPL35A | RPS11A | TPI1 | TRM1 | CPR1 | CPR5 | RPL12B | RPS18A | RPL12A | RPL34A | RPL23B | RPS26B | MDJ1 | YPT1 | RPL2A | RPL24A | RPL7A | RPL28 | RPS2 | RPL1B | RPS26A | ADE5,7 | RPS25A | RPS23A | RPL24B | TDH3 | RPS20 | ENO2 | RPS4B | RPL2B | RPL34B | GPP1 | KAR2 | MET3 | ADO1 | RPS5 | RPS4A | SSA2 | PDC1 | RPL37A | CPR6 | HSP60 | RPS28B | RPS25B | KAP95 | SEC61 | RPL6B | RPS18B | RPL6A | RPL13B | RPS16A | HSC82 | RPL20A | YDJ1 | RPL16B | RPS3 | RPL18B | RPL18A | RPL3 | RPS28A | RPL20B | RPS12 | RPS9A | RPL5 | RPL1A | HSP82 | YME1 | TEF1 | RPS23B	82	3255	1.02E-11
cellular component biogenesis	RPS11B | RPS9B | NFS1 | ABP1 | RPS16B | RPL35B | RPL35A | RPS11A | RPL12B | RPS18A | RPL12A | ARB1 | RPL34A | RPS26B | YPT1 | RPL24A | RPL7A | RPS2 | RPL1B | RPS26A | RPS23A | RPL24B | RPS20 | RPL34B | KAR2 | RPS5 | NAP1 | RPL37A | HSP60 | RPS28B | KAP95 | RPL6B | RPS18B | RPL6A | RPS16A | HSC82 | RPS3 | HSP10 | RPL3 | VPS21 | RPS28A | RPS9A | RPL5 | RPL1A | HSP82 | RPS23B	46	1073	3.21E-11
protein refolding	SSA1 | HSP78 | MDJ1 | CPR6 | HSP60 | HSC82 | YDJ1 | HSP10 | SSE1 | HSP82	10	16	3.43E-11
ribosome assembly	RPS11B | RPS11A | RPL12B | RPL12A | RPS26B | RPL24A | RPS26A | RPL24B | RPS5 | RPS28B | RPL6B | RPL6A | RPL3 | RPS28A | RPL5	15	78	7.43E-11
metabolic process	SSA1 | CYS3 | CDC19 | RPL23A | RPL4A | RPS11B | RPS9B | NFS1 | HBN1 | GRX1 | PDI1 | GPM2 | RPL13A | RPS16B | RPL35B | RPL35A | RPS11A | TPI1 | TRM1 | CPR1 | CPR5 | RPL12B | RPS18A | RPL12A | RPL34A | RPL23B | RPS26B | MDJ1 | YPT1 | RPL2A | RPL24A | RPL7A | RPL28 | RPS2 | RPL1B | RPS26A | ADE5,7 | RPS25A | RPS23A | RPL24B | TDH3 | RPS20 | ENO2 | RPS4B | RPL2B | RPL34B | GPP1 | KAR2 | MET3 | ADO1 | RPS5 | RPS4A | SSA2 | PDC1 | RPL37A | CPR6 | HSP60 | RPS28B | RPS25B | KAP95 | SEC61 | RPL6B | RPS18B | RPL6A | RPL13B | RPS16A | HSC82 | RPL20A | YDJ1 | RPL16B | RPS3 | RPL18B | RPL18A | RPL3 | VPS21 | RPS28A | RPL20B | RPS12 | RPS9A | RPL5 | RPL1A | HSP82 | YME1 | TEF1 | RPS23B	85	3661	1.55E-10
cellular process	SSA1 | CYS3 | CDC19 | RPL23A | RPL4A | RPS11B | RPS9B | NFS1 | HBN1 | GRX1 | PDI1 | ABP1 | RPL13A | RPS16B | RPL35B | RPL35A | RPS11A | TPI1 | TRM1 | CPR1 | AHA1 | HSP78 | CPR5 | RPL12B | RPS18A | RPL12A | RPL34A | SSA4 | RPL23B | RPS26B | MDJ1 | YPT1 | RPL2A | RPL24A | RPL7A | RPL28 | RPS2 | RPL1B | RPS26A | ADE5,7 | RPS25A | RPS23A | RPL24B | TDH3 | RPS20 | ENO2 | RPS4B | RPL2B | RPL34B | GPP1 | KAR2 | MET3 | ADO1 | RPS5 | RPS4A | NAP1 | SSA2 | PDC1 | RPL37A | CPR6 | HSP60 | RPS28B | RPS25B | KAP95 | SEC61 | RPL6B | RPS18B | RPL6A | ASC1 | RPL13B | RPS16A | HSC82 | RPL20A | YDJ1 | RPL16B | RPS3 | HCH1 | RPL18B | RPL18A | HSP10 | STI1 | RPL3 | VPS21 | RPS28A | RPL20B | RPS12 | RPS9A | SSE1 | RPL5 | RPL1A | HSP82 | YME1 | TEF1 | RPS23B	94	4626	1.62E-10
cellular nitrogen compound metabolic process	SSA1 | CDC19 | RPL23A | RPL4A | RPS11B | RPS9B | NFS1 | RPL13A | RPS16B | RPL35B | RPL35A | RPS11A | TPI1 | TRM1 | RPL12B | RPS18A | RPL12A | RPL34A | RPL23B | RPS26B | YPT1 | RPL2A | RPL24A | RPL7A | RPL28 | RPS2 | RPL1B | RPS26A | ADE5,7 | RPS25A | RPS23A | RPL24B | TDH3 | RPS20 | ENO2 | RPS4B | RPL2B | RPL34B | ADO1 | RPS5 | RPS4A | PDC1 | RPL37A | RPS28B | RPS25B | RPL6B | RPS18B | RPL6A | RPL13B | RPS16A | HSC82 | RPL20A | RPL16B | RPS3 | RPL18B | RPL18A | RPL3 | RPS28A | RPL20B | RPS12 | RPS9A | RPL5 | RPL1A | TEF1 | RPS23B	65	2182	1.96E-10

organic substance metabolic process	SSA1 | CYS3 | CDC19 | RPL23A | RPL4A | RPS11B | RPS9B | NFS1 | GRX1 | PDI1 | RPL13A | RPS16B | RPL35B | RPL35A | RPS11A | TPI1 | TRM1 | CPR1 | CPR5 | RPL12B | RPS18A | RPL12A | RPL34A | RPL23B | RPS26B | MDJ1 | YPT1 | RPL2A | RPL24A | RPL7A | RPL28 | RPS2 | RPL1B | RPS26A | ADE5,7 | RPS25A | RPS23A | RPL24B | TDH3 | RPS20 | ENO2 | RPS4B | RPL2B | RPL34B | GPP1 | KAR2 | MET3 | ADO1 | RPS5 | RPS4A | SSA2 | PDC1 | RPL37A | CPR6 | HSP60 | RPS28B | RPS25B | KAP95 | SEC61 | RPL6B | RPS18B | RPL6A | RPL13B | RPS16A | HSC82 | RPL20A | YDJ1 | RPL16B | RPS3 | RPL18B | RPL18A | RPL3 | RPS28A | RPL20B | RPS12 | RPS9A | RPL5 | RPL1A | HSP82 | YME1 | TEF1 | RPS23B	82	3417	1.98E-10
macromolecule metabolic process	SSA1 | RPL23A | RPL4A | RPS11B | RPS9B | NFS1 | GRX1 | PDI1 | RPL13A | RPS16B | RPL35B | RPL35A | RPS11A | TRM1 | CPR1 | CPR5 | RPL12B | RPS18A | RPL12A | RPL34A | RPL23B | RPS26B | MDJ1 | YPT1 | RPL2A | RPL24A | RPL7A | RPL28 | RPS2 | RPL1B | RPS26A | RPS25A | RPS23A | RPL24B | RPS20 | RPS4B | RPL2B | RPL34B | KAR2 | RPS5 | RPS4A | SSA2 | RPL37A | CPR6 | HSP60 | RPS28B | RPS25B | SEC61 | RPL6B | RPS18B | RPL6A | RPL13B | RPS16A | HSC82 | RPL20A | YDJ1 | RPL16B | RPS3 | RPL18B | RPL18A | RPL3 | RPS28A | RPL20B | RPS12 | RPS9A | RPL5 | RPL1A | HSP82 | YME1 | TEF1 | RPS23B	71	2613	3.81E-10
cellular metabolic process	SSA1 | CYS3 | CDC19 | RPL23A | RPL4A | RPS11B | RPS9B | NFS1 | GRX1 | PDI1 | RPL13A | RPS16B | RPL35B | RPL35A | RPS11A | TPI1 | TRM1 | CPR1 | CPR5 | RPL12B | RPS18A | RPL12A | RPL34A | RPL23B | RPS26B | MDJ1 | YPT1 | RPL2A | RPL24A | RPL7A | RPL28 | RPS2 | RPL1B | RPS26A | ADE5,7 | RPS25A | RPS23A | RPL24B | TDH3 | RPS20 | ENO2 | RPS4B | RPL2B | RPL34B | GPP1 | KAR2 | MET3 | ADO1 | RPS5 | RPS4A | SSA2 | PDC1 | RPL37A | CPR6 | RPS28B | RPS25B | KAP95 | SEC61 | RPL6B | RPS18B | RPL6A | RPL13B | RPS16A | HSC82 | RPL20A | YDJ1 | RPL16B | RPS3 | RPL18B | RPL18A | RPL3 | VPS21 | RPS28A | RPL20B | RPS12 | RPS9A | RPL5 | RPL1A | YME1 | TEF1 | RPS23B	81	3444	1.50E-09
rRNA export from nucleus	RPS18A | RPS26B | RPS2 | RPS26A | RPS5 | RPS28B | RPS18B | RPS3 | RPS28A	9	18	1.72E-09
ncRNA export from nucleus	RPS18A | RPS26B | RPS2 | RPS26A | RPS5 | RPS28B | RPS18B | RPS3 | RPS28A | TEF1	10	33	7.24E-09
organelle assembly	RPS11B | RPS11A | RPL12B | RPL12A | RPS26B | YPT1 | RPL24A | RPS26A | RPL24B | RPS5 | RPS28B | RPL6B | RPL6A | RPL3 | VPS21 | RPS28A | RPL5	17	159	7.59E-09
ribonucleoprotein complex subunit organization	SSA1 | RPS11B | RPS11A | RPL12B | RPL12A | RPS26B | RPL24A | RPS26A | RPL24B | RPS5 | RPS28B | RPL6B | RPL6A | HSC82 | RPL3 | RPS28A | RPL5 | HSP82	18	187	1.01E-08
rRNA processing	RPS11B | RPS9B | RPS16B | RPL35B | RPL35A | RPS11A | RPS18A | RPL7A | RPS2 | RPL1B | RPS23A | RPS20 | RPL37A | RPS28B | RPS18B | RPS16A | RPL3 | RPS28A | RPS9A | RPL1A | RPS23B	21	277	1.73E-08
ribonucleoprotein complex assembly	RPS11B | RPS11A | RPL12B | RPL12A | RPS26B | RPL24A | RPS26A | RPL24B | RPS5 | RPS28B | RPL6B | RPL6A | HSC82 | RPL3 | RPS28A | RPL5 | HSP82	17	175	2.75E-08
intracellular protein transport	SSA1 | RPS18A | ARB1 | SSA4 | RPS26B | RPS2 | RPS26A | KAR2 | RPS5 | NAP1 | SSA2 | HSP60 | RPS28B | KAP95 | SEC61 | RPS18B | YDJ1 | RPS3 | HSP10 | STI1 | VPS21 | RPS28A | HSP82 | YME1 | TEF1	25	439	8.57E-08
ribosomal large subunit biogenesis	RPL35B | RPL35A | RPL12B | RPL12A | RPL24A | RPL7A | RPL1B | RPL24B | RPL37A | RPL6B | RPL6A | RPL3 | RPL5 | RPL1A	14	121	1.13E-07
nucleocytoplasmic transport	SSA1 | RPS18A | ARB1 | RPS26B | RPS2 | RPS26A | RPS5 | NAP1 | SSA2 | RPS28B | KAP95 | RPS18B | YDJ1 | RPS3 | RPS28A | TEF1	16	169	1.17E-07
ncRNA processing	RPS11B | RPS9B | NFS1 | RPS16B | RPL35B | RPL35A | RPS11A | TRM1 | RPS18A | RPL7A | RPS2 | RPL1B | RPS23A | RPS20 | RPL37A | RPS28B | RPS18B | RPS16A | RPL3 | RPS28A | RPS9A | RPL1A | RPS23B	23	389	1.89E-07
maturation of SSU-rRNA	RPS11B | RPS9B | RPS16B | RPS11A | RPS18A | RPS23A | RPS20 | RPS28B | RPS18B | RPS16A | RPS28A | RPS9A | RPS23B	13	114	4.37E-07
ribosomal small subunit biogenesis	RPS11B | RPS9B | RPS16B | RPS11A | RPS18A | RPS23A | RPS20 | RPS5 | RPS28B | RPS18B | RPS16A | RPS28A | RPS9A | RPS23B	14	142	6.45E-07
rRNA-containing ribonucleoprotein complex export from nucleus	RPS18A | ARB1 | RPS26B | RPS2 | RPS26A | RPS5 | RPS28B | RPS18B | RPS3 | RPS28A	10	62	1.05E-06
RNA transport	RPS18A | ARB1 | RPS26B | RPS2 | RPS26A | RPS5 | SSA2 | RPS28B | KAP95 | RPS18B | YDJ1 | RPS3 | RPS28A | TEF1	14	166	3.77E-06

cellular protein localization	SSA1 | ABP1 | RPS18A | ARB1 | SSA4 | RPS26B | YPT1 | RPS2 | RPS26A | KAR2 | RPS5 | NAP1 | SSA2 | HSP60 | RPS28B | KAP95 | SEC61 | RPS18B | YDJ1 | RPS3 | HSP10 | STI1 | VPS21 | RPS28A | HSP82 | YME1 | TEF1	27	627	4.05E-06
ribosomal large subunit assembly	RPL12B | RPL12A | RPL24A | RPL24B | RPL6B | RPL6A | RPL3 | RPL5	8	42	7.07E-06
maturation of SSU-rRNA from tricistronic rRNA transcript (SSU-rRNA, 5.8S rRNA, LSU-rRNA)	RPS11B | RPS9B | RPS16B | RPS11A | RPS18A | RPS23A | RPS20 | RPS18B | RPS16A | RPS9A | RPS23B	11	103	8.73E-06
protein transport	SSA1 | CPR1 | RPS18A | ARB1 | SSA4 | RPS26B | YPT1 | RPS2 | RPS26A | KAR2 | RPS5 | NAP1 | SSA2 | HSP60 | RPS28B | KAP95 | SEC61 | RPS18B | YDJ1 | RPS3 | HSP10 | STI1 | VPS21 | RPS28A | HSP82 | YME1 | TEF1	27	655	8.73E-06
intracellular transport	SSA1 | RPS18A | ARB1 | SSA4 | RPS26B | YPT1 | RPS2 | RPS26A | KAR2 | RPS5 | NAP1 | SSA2 | HSP60 | RPS28B | KAP95 | SEC61 | RPS18B | YDJ1 | RPS3 | HSP10 | STI1 | VPS21 | RPS28A | HSP82 | YME1 | TEF1	26	624	1.14E-05
cellular protein-containing complex assembly	RPS11B | RPS11A | RPL12B | RPL12A | RPS26B | YPT1 | RPL24A | RPS26A | RPL24B | RPS5 | NAP1 | HSP60 | RPS28B | KAP95 | RPL6B | RPL6A | HSC82 | HSP10 | RPL3 | RPS28A | RPL5 | HSP82	22	477	1.91E-05
'de novo' protein folding	MDJ1 | HSP60 | HSC82 | YDJ1 | HSP10 | HSP82	6	24	4.44E-05
ribonucleoprotein complex export from nucleus	RPS18A | ARB1 | RPS26B | RPS2 | RPS26A | RPS5 | RPS28B | RPS18B | RPS3 | RPS28A | TEF1	11	127	4.83E-05
cellular component organization or biogenesis	SSA1 | RPS11B | RPS9B | NFS1 | ABP1 | RPS16B | RPL35B | RPL35A | RPS11A | CPR1 | HSP78 | RPL12B | RPS18A | RPL12A | ARB1 | RPL34A | RPS26B | MDJ1 | YPT1 | RPL24A | RPL7A | RPS2 | RPL1B | RPS26A | RPS23A | RPL24B | RPS20 | RPL34B | KAR2 | RPS5 | NAP1 | RPL37A | HSP60 | RPS28B | KAP95 | RPL6B | RPS18B | RPL6A | RPS16A | HSC82 | YDJ1 | RPS3 | HSP10 | STI1 | RPL3 | VPS21 | RPS28A | RPS9A | RPL5 | RPL1A | HSP82 | YME1 | RPS23B	53	2149	5.63E-05
protein localization	SSA1 | ABP1 | CPR1 | RPS18A | ARB1 | SSA4 | RPS26B | YPT1 | RPS2 | RPS26A | KAR2 | RPS5 | NAP1 | SSA2 | HSP60 | RPS28B | KAP95 | SEC61 | RPS18B | YDJ1 | RPS3 | HSP10 | STI1 | VPS21 | RPS28A | HSP82 | YME1 | TEF1	28	786	6.33E-05
regulation of translational fidelity	RPS9B | RPS2 | RPS23A | RPS5 | RPS9A | RPS23B	6	28	8.21E-05
protein targeting	SSA1 | SSA4 | KAR2 | SSA2 | HSP60 | KAP95 | SEC61 | YDJ1 | HSP10 | STI1 | VPS21 | HSP82 | YME1	13	198	9.29E-05
nitrogen compound transport	SSA1 | CPR1 | RPS18A | ARB1 | SSA4 | RPS26B | YPT1 | RPS2 | RPS26A | TDH3 | KAR2 | RPS5 | NAP1 | SSA2 | HSP60 | RPS28B | KAP95 | SEC61 | RPS18B | YDJ1 | RPS3 | HSP10 | STI1 | VPS21 | RPS28A | HSP82 | YME1 | TEF1	28	804	9.30E-05
SRP-dependent cotranslational protein targeting to membrane, translocation	SSA1 | SSA4 | KAR2 | SSA2 | SEC61	5	16	1.00E-04
protein-containing complex subunit organization	SSA1 | RPS11B | RPS11A | RPL12B | RPL12A | RPS26B | YPT1 | RPL24A | RPS26A | RPL24B | RPS5 | NAP1 | HSP60 | RPS28B | KAP95 | RPL6B | RPL6A | HSC82 | HSP10 | RPL3 | RPS28A | RPL5 | HSP82	23	592	1.40E-04
cellular component assembly	RPS11B | NFS1 | ABP1 | RPS11A | RPL12B | RPL12A | RPS26B | YPT1 | RPL24A | RPS26A | RPL24B | RPS5 | NAP1 | HSP60 | RPS28B | KAP95 | RPL6B | RPL6A | HSC82 | HSP10 | RPL3 | VPS21 | RPS28A | RPL5 | HSP82	25	714	2.90E-04
intracellular protein transmembrane transport	SSA1 | SSA4 | KAR2 | SSA2 | HSP60 | SEC61 | HSP10 | YME1	8	83	4.30E-04
protein targeting to ER	SSA1 | SSA4 | KAR2 | SSA2 | SEC61 | YDJ1	6	40	4.40E-04
establishment of protein localization to organelle	SSA1 | SSA4 | KAR2 | NAP1 | SSA2 | HSP60 | KAP95 | SEC61 | YDJ1 | HSP10 | STI1 | VPS21 | HSP82 | YME1	14	276	5.60E-04
organic substance transport	SSA1 | CPR1 | RPS18A | ARB1 | SSA4 | RPS26B | YPT1 | RPS2 | RPS26A | TDH3 | KAR2 | RPS5 | NAP1 | SSA2 | HSP60 | RPS28B | KAP95 | SEC61 | RPS18B | YDJ1 | RPS3 | HSP10 | STI1 | VPS21 | RPS28A | HSP82 | YME1 | TEF1	28	903	6.50E-04
protein targeting to mitochondrion	SSA1 | HSP60 | YDJ1 | HSP10 | STI1 | HSP82 | YME1	7	68	8.40E-04
ribosomal small subunit assembly	RPS11B | RPS11A | RPS5 | RPS28B | RPS28A	5	29	1.00E-03

response to heat	AHA1 | HSP78 | SSA4 | MDJ1 | HSC82 | YDJ1 | HCH1	7	73	1.20E-03
ADP metabolic process	CDC19 | TPI1 | TDH3 | ENO2 | PDC1	5	31	1.30E-03
protein localization to organelle	SSA1 | ABP1 | SSA4 | YPT1 | KAR2 | NAP1 | SSA2 | HSP60 | KAP95 | SEC61 | YDJ1 | HSP10 | STI1 | VPS21 | HSP82 | YME1	16	389	1.50E-03
protein targeting to membrane	SSA1 | SSA4 | KAR2 | SSA2 | KAP95 | SEC61	6	54	1.60E-03
maturation of LSU-rRNA	RPL35B | RPL35A | RPL7A | RPL1B | RPL37A | RPL1A	6	55	1.80E-03
protein import into mitochondrial intermembrane space	HSP60 | HSP10 | YME1	3	8	3.50E-03
pyruvate metabolic process	CDC19 | TPI1 | TDH3 | ENO2 | PDC1	5	42	4.10E-03
positive regulation of translational fidelity	RPS9B | RPS2 | RPS9A	3	9	4.50E-03
glycolytic process	CDC19 | TPI1 | TDH3 | ENO2	4	24	4.90E-03
ATP generation from ADP	CDC19 | TPI1 | TDH3 | ENO2	4	24	4.90E-03
pyruvate biosynthetic process	CDC19 | TPI1 | TDH3 | ENO2	4	24	4.90E-03
purine ribonucleoside monophosphate biosynthetic process	CDC19 | TPI1 | ADE5,7 | TDH3 | ENO2 | ADO1	6	70	5.50E-03
positive regulation of ATPase activity	AHA1 | MDJ1 | YDJ1 | HCH1	4	26	6.10E-03
nucleotide catabolic process	CDC19 | TPI1 | TDH3 | ENO2	4	30	9.80E-03
response to abiotic stimulus	AHA1 | HSP78 | SSA4 | MDJ1 | GPP1 | HSC82 | YDJ1 | HCH1 | HSP82	9	179	1.02E-02
cellular response to heat	AHA1 | HSP78 | SSA4 | HSC82 | HCH1	5	54	1.07E-02
import into nucleus	SSA1 | NAP1 | SSA2 | KAP95 | YDJ1	5	54	1.07E-02
purine ribonucleotide biosynthetic process	CDC19 | TPI1 | ADE5,7 | TDH3 | ENO2 | ADO1	6	85	1.28E-02
purine ribonucleoside monophosphate metabolic process	CDC19 | TPI1 | ADE5,7 | TDH3 | ENO2 | ADO1 | PDC1	7	118	1.36E-02
tRNA import into nucleus	SSA2 | YDJ1	2	3	1.36E-02
protein peptidyl-prolyl isomerization	CPR1 | CPR5 | CPR6	3	16	1.55E-02
gluconeogenesis	TPI1 | TDH3 | ENO2	3	16	1.55E-02
protein import	SSA1 | NAP1 | HSP60 | KAP95 | SEC61 | HSP10 | YME1	7	124	1.67E-02
nucleobase-containing small molecule biosynthetic process	CDC19 | TPI1 | TDH3 | ENO2 | ADO1	5	62	1.67E-02
organelle organization	SSA1 | RPS11B | ABP1 | RPS11A | CPR1 | HSP78 | RPL12B | RPL12A | RPS26B | MDJ1 | YPT1 | RPL24A | RPS26A | RPL24B | KAR2 | RPS5 | NAP1 | HSP60 | RPS28B | KAP95 | RPL6B | RPL6A | HSC82 | YDJ1 | HSP10 | STI1 | RPL3 | VPS21 | RPS28A | RPL5 | HSP82 | YME1	32	1362	1.68E-02
glucose metabolic process	TPI1 | TDH3 | ENO2 | PDC1	4	39	1.96E-02
nicotinamide nucleotide biosynthetic process	CDC19 | TPI1 | TDH3 | ENO2	4	41	2.29E-02
negative regulation of cell aging	SSA1 | SSA2	2	5	2.43E-02
positive regulation of nuclear-transcribed mRNA catabolic process, deadenylation-dependent decay	RPS28B | RPS28A	2	5	2.43E-02
tRNA transport	SSA2 | YDJ1 | TEF1	3	21	2.68E-02
maturation of LSU-rRNA from tricistronic rRNA transcript (SSU-rRNA, 5.8S rRNA, LSU-rRNA)	RPL35B | RPL35A | RPL7A | RPL37A	4	44	2.73E-02
nicotinamide nucleotide metabolic process	CDC19 | TPI1 | TDH3 | ENO2 | PDC1	5	75	3.15E-02
ATP biosynthetic process	CDC19 | TPI1 | TDH3 | ENO2	4	48	3.50E-02
purine ribonucleotide metabolic process	CDC19 | TPI1 | ADE5,7 | TDH3 | ENO2 | ADO1 | PDC1	7	147	3.50E-02
box C/D snoRNP assembly	HSC82 | HSP82	2	8	4.56E-02

Table S5
(continued)

chaperone-mediated protein complex assembly	HSP60 | HSP10	2	8	4.56E-02
carbohydrate biosynthetic process	TPI1 | TDH3 | ENO2 | GPP1 | KAR2	5	84	4.62E-02
ubiquitin-dependent ERAD pathway	PDI1 | KAR2 | SEC61 | YDJ1	4	54	4.86E-02
small molecule metabolic process	BDH1 | COR1 | ILS1 | ATP1 | ATP3 | PGI1 | ARO4 | GLK1 | IDP1 | DLD1 | GCV1 | SDH4 | ATP5 | HPT1 | PDA1 | LPD1 | MET10 | HXK1 | PYC1 | COX4 | CYS4 | RNR4 | LSC2 | COX6 | IMD2 | CAB2 | KGD1 | GUT2 | RNR2 | ILV3 | CPA2 | ATP2 | MET5 | ATP7 | MAE1 | MDH1 | SDH1 | MCR1 | FAS1 | SDH2 | SHM2 | ILV5 | ERG6 | CAT2 | NDI1 | PGM2 | ZWF1 | CIT1 | ACC1 | MVD1 | LYS9 | ALD4 | GDH1 | ALD6 | ATP4 | ASN1 | QCR2	57	755	2.54E-26
purine ribonucleotide metabolic process	COR1 | ATP1 | ATP3 | PGI1 | GLK1 | SDH4 | ATP5 | HPT1 | PDA1 | HXK1 | COX4 | LSC2 | COX6 | IMD2 | CAB2 | ATP2 | ATP7 | SDH1 | NDI1 | CIT1 | ACC1 | MVD1 | ATP4 | QCR2	24	147	4.87E-16
small molecule biosynthetic process	BDH1 | PGI1 | ARO4 | GLK1 | IDP1 | HPT1 | PDA1 | LPD1 | MET10 | HXK1 | PYC1 | CYS4 | IMD2 | ILV3 | CPA2 | MET5 | MCR1 | FAS1 | SHM2 | ILV5 | ERG6 | CIT1 | ACC1 | LYS9 | ALD4 | GDH1 | ALD6 | ASN1	28	345	2.79E-12
generation of precursor metabolites and energy	PET9 | COR1 | PGI1 | GLK1 | IDP1 | SDH4 | PDA1 | LPD1 | HXK1 | COX4 | LSC2 | COX6 | KGD1 | MDH1 | SDH1 | SDH2 | NDI1 | PGM2 | CIT1 | LYS9 | GPH1 | QCR2	22	204	9.92E-12
cofactor metabolic process	PGI1 | GLK1 | HEM13 | HEM1 | PDA1 | LPD1 | HXK1 | RNR4 | LSC2 | CAB2 | KGD1 | GUT2 | CCP1 | SHM2 | NDI1 | ZWF1 | CIT1 | ACC1 | MVD1 | ALD4 | ALD6	21	245	1.57E-09
ATP biosynthetic process	ATP1 | ATP3 | PGI1 | GLK1 | ATP5 | PDA1 | HXK1 | COX4 | ATP2 | ATP7 | ATP4	11	48	7.47E-09
monocarboxylic acid metabolic process	PGI1 | GLK1 | IDP1 | DLD1 | PDA1 | LPD1 | HXK1 | PYC1 | MAE1 | FAS1 | CAT2 | ACC1 | ALD4 | ALD6 | ASN1	15	158	2.16E-07
alpha-amino acid biosynthetic process	IDP1 | LPD1 | MET10 | CYS4 | ILV3 | CPA2 | MET5 | SHM2 | ILV5 | CIT1 | LYS9 | GDH1 | ASN1	13	123	6.44E-07
respiratory electron transport chain	COR1 | SDH4 | COX4 | COX6 | SDH1 | SDH2 | NDI1 | QCR2	8	45	7.75E-06
carbohydrate catabolic process	PGI1 | GLK1 | PDA1 | HXK1 | MAL11 | GUT2 | SUC2 | PGM2 | GPH1	9	84	5.76E-05
dicarboxylic acid metabolic process	ARO4 | IDP1 | LPD1 | KGD1 | MAE1 | CIT1 | GDH1	7	45	7.38E-05
ribonucleoside bisphosphate metabolic process	PDA1 | LSC2 | CAB2 | CIT1 | ACC1 | MVD1	6	29	8.03E-05
serine family amino acid metabolic process	GCV1 | LPD1 | MET10 | CYS4 | MET5 | SHM2	6	38	2.90E-04
glucose 6-phosphate metabolic process	PGI1 | GLK1 | HXK1 | PGM2 | ZWF1	5	22	2.90E-04
nucleobase-containing small molecule biosynthetic process	PGI1 | GLK1 | HPT1 | PDA1 | HXK1 | IMD2 | CIT1	7	62	4.20E-04
NADPH regeneration	ZWF1 | ALD4 | ALD6	3	5	1.20E-03
cofactor biosynthetic process	PGI1 | GLK1 | HEM13 | HEM1 | PDA1 | HXK1 | RNR4 | CAB2 | ACC1	9	147	2.50E-03
organic hydroxy compound metabolic process	BDH1 | DLD1 | GUT2 | MCR1 | ERG6 | MVD1 | ALD4 | ALD6	8	128	4.40E-03
valine metabolic process	LPD1 | ILV3 | ILV5	3	10	4.90E-03
glutamate biosynthetic process	IDP1 | CIT1 | GDH1	3	11	6.00E-03
cellular carbohydrate catabolic process	MAL11 | GUT2 | SUC2 | GPH1	4	30	8.20E-03
chronological cell aging	ACB1 | SOD1 | MDH1 | NDI1	4	32	9.90E-03
long-chain fatty acid biosynthetic process	FAS1 | ACC1	2	3	1.17E-02
ATP hydrolysis coupled ion transmembrane transport	ATP1 | ATP3 | ATP5 | ATP2	4	35	1.23E-02
glycine catabolic process	GCV1 | LPD1	2	4	1.64E-02
hydrogen peroxide metabolic process	LPD1 | CCP1	2	4	1.64E-02
positive regulation of translational elongation	EFT2 | EFT1	2	4	1.64E-02
organic hydroxy compound catabolic process	DLD1 | GUT2 | ALD6	3	19	1.89E-02

mannose metabolic process	GLK1 | HXK1	2	5	2.10E-02
2-oxoglutarate metabolic process	LPD1 | KGD1	2	5	2.10E-02
GMP biosynthetic process	HPT1 | IMD2	2	5	2.10E-02
anaerobic respiration	PET9 | SDH1	2	5	2.10E-02
negative regulation of endopeptidase activity	TFS1 | PBI2	2	5	2.10E-02
sulfur compound biosynthetic process	PDA1 | MET10 | CYS4 | MET5 | ACC1	5	78	2.97E-02
mitochondrial electron transport, succinate to ubiquinone	SDH4 | SDH1	2	7	3.26E-02
protoporphyrinogen IX biosynthetic process	HEM13 | HEM1	2	7	3.26E-02
apoptotic process	PET9 | OYE2 | CPR3	3	26	3.58E-02
secondary alcohol biosynthetic process	BDH1 | MCR1 | ERG6	3	26	3.58E-02
response to reactive oxygen species	SOD1 | CCP1 | ZWF1	3	27	3.86E-02
L-serine metabolic process	LPD1 | CYS4	2	8	3.86E-02
acyl-CoA biosynthetic process	PDA1 | ACC1	2	8	3.86E-02
aspartate family amino acid biosynthetic process	MET10 | MET5 | LYS9 | ASN1	4	55	4.09E-02
cellular nitrogen compound biosynthetic process	ILS1 | ATP1 | ATP3 | PGI1 | GLK1 | HEM13 | HEM1 | ATP5 | EFT2 | HPT1 | PDA1 | HXK1 | COX4 | PTI1 | RNR4 | IMD2 | CAB2 | RNR2 | CPA2 | ATP2 | ATP7 | YEF3 | CIT1 | ACC1 | EFT1 | WTM1 | ATP4 | ASN1	28	1288	4.98E-02

Table S5 (continued)

Category description	Protein identity	No. of proteins in cluster	No. of proteins in genome	FDR value
organonitrogen compound biosynthetic process	PDX3 | RIB5 | PGK1 | THR4 | RPL4B | RPP2B | HOM3 | PMA1 | RPL30 | RPL26B | ENO1 | SER33 | BNA3 | RPS21B | TDH2 | RPL43B | MET14 | ACS2 | RPL38 | RPP0 | RPL26A | ADE13 | RPS29A | RPS19B | RPP2A | SPE2 | RPS19A | RPL36B	28	897	1.80E-08
drug metabolic process	PDX3 | VMA2 | RIB5 | PGK1 | PMA1 | ENO1 | BNA3 | TDH2 | MET14 | ACS2 | ADE13 | ADH3 | SPE2	13	278	4.65E-05
carboxylic acid biosynthetic process	PGK1 | THR4 | HOM3 | CEM1 | OLE1 | ENO1 | SER33 | BNA3 | TDH2 | MET14 | SPE2	11	210	8.00E-05
purine ribonucleotide biosynthetic process	PGK1 | PMA1 | ENO1 | TDH2 | ACS2 | ADE13	6	85	0.0021
pyridine-containing compound metabolic process	PDX3 | PGK1 | PHO8 | ENO1 | TDH2 | ADH3	6	88	0.0023
proteasome storage granule assembly	VMA2 | PMA1	2	3	0.0085
protein import into nucleus	NTF2 | NSP1 | GSP1 | PSE1	4	51	0.0111
threonine biosynthetic process	THR4 | HOM3	2	6	0.0139
serine family amino acid biosynthetic process	HOM3 | SER33 | MET14	3	27	0.0139
rRNA-containing ribonucleoprotein complex export from nucleus	NSP1 | GSP1 | RPS19B | RPS19A	4	62	0.0147
nucleobase-containing small molecule biosynthetic process	PGK1 | ENO1 | TDH2 | SPE2	4	62	0.0147
sulfur compound biosynthetic process	HOM3 | MET14 | ACS2 | SPE2	4	78	0.0262
ribosome biogenesis	RPL30 | RPL26B | NSP1 | RPS21B | GSP1 | RPP0 | RPL26A | RPS19B | RPS19A	9	403	0.0302
regulation of vacuole fusion, non-autophagic	ENO1 | YPT7	2	14	0.0405
cellular protein metabolic process	FES1 | RPL4B | RPP2B | PHO8 | SMT3 | RPL30 | RPL26B | RPS21B | RPL43B | ACS2 | RPL38 | RPP0 | RPL26A | RPS29A | RPS19B | RPP2A | RPS19A | RPL36B	18	1242	0.0412

Table S6
Enrichment analysis for GO processes of the up-(green) and downregulated (red) proteins in the evolved strain between two temperatures, based on the proteins found in the red area of Figure S1.

Table S6
(continued)

Process	Genes			
water-soluble vitamin biosynthetic process	PDX3 | RIB5 | SPE2	3	49	0.0457
small molecule metabolic process	ACH1 | ADH5 | SHM1 | CIT2 | TRX3 | MDH3 | LYS21 | VMA1 | HOM2 | SAM2 | PMI40 | FAA2 | HIS1 | ARG5,6 | MET6 | MET10 | LEU1 | POX1 | PDX1 | ADE3 | PRS3 | ARG4 | DED81 | NCP1 | ERG9 | PPX1 | BAT1 | BNA1 | CYC1 | YNK1 | GFA1 | GPT2 | MTD1 | IMD3 | APT1 | COQ5 | ILV2 | GUA1 | YNL247W | ARG1 | PEX11 | CYT1 | GCY1 | LSC1 | ISN1 | ALA1 | GDH1 | FUM1 | PDH1 | GLN1 | TKL1	51	755	3.65E-15
oxidation-reduction process	RFS1 | ADH5 | CIT2 | TRX3 | MDH3 | HOM2 | MRP1 | TRR1 | GRX2 | GLC3 | ARG5,6 | GLC7 | MET10 | POX1 | ADE3 | SOD2 | NCP1 | ERG9 | BNA1 | CYC1 | MTD1 | IMD3 | COQ5 | YMR226C | PEX11 | CYT1 | GCY1 | LSC1 | CIR2 | GDH1 | FUM1 | TKL1	32	457	3.45E-09
cellular amino acid metabolic process	ADH5 | SHM1 | CIT2 | LYS21 | HOM2 | SAM2 | HIS1 | ARG5,6 | MET6 | MET10 | LEU1 | ADE3 | ARG4 | DED81 | BAT1 | BNA1 | GFA1 | ILV2 | GUA1 | YNL247W | ARG1 | ALA1 | GDH1 | GLN1	24	248	3.63E-09
nucleobase-containing small molecule metabolic process	ACH1 | ADH5 | MDH3 | VMA1 | PMI40 | PDX1 | ADE3 | PRS3 | BNA1 | CYC1 | YNK1 | GFA1 | GPT2 | MTD1 | IMD3 | APT1 | GUA1 | CYT1 | LSC1 | ISN1 | TKL1	21	290	4.24E-06
cellular process	TPD3 | HTA2 | ACH1 | PIM1 | NCL1 | PRE7 | TPS1 | ADH5 | SHM1 | APE3 | MAL31 | CIT2 | TRX3 | RPT2 | ARP2 | RPS29B | MDH3 | NUP84 | LYS21 | ARF2 | VMA1 | GCS1 | PAA1 | HOM2 | HMO1 | HTA1 | MRP1 | TRR1 | SAM2 | GRX2 | GLC3 | PRB1 | PMI40 | FAA2 | HIS1 | ARG5,6 | MET6 | GLC7 | ACT1 | MET10 | RET2 | LEU1 | SCL1 | STT3 | RPT6 | SDS23 | POX1 | PDX1 | ADE3 | PRS3 | SOD2 | ARG4 | DED81 | NCP1 | ERG9 | EGD2 | PPX1 | BAT1 | NUP159 | SFH5 | BNA1 | CYC1 | YNK1 | VMA5 | GFA1 | RPT1 | MIC60 | GPT2 | MTD1 | SPC3 | MRPL15 | IMD3 | APT1 | PRE8 | COQ5 | ILV2 | GUA1 | RRP5 | PRC1 | SRV2 | YCK2 | YNL247W | RPA49 | SIN3 | ARG1 | PEX11 | SFM1 | CKA2 | CYT1 | RPT5 | GCY1 | LSC1 | ISN1 | ALA1 | CIR2 | GDH1 | CAM1 | NOG1 | PEP4 | FUM1 | PDH1 | RPA135 | GLN1 | TKL1	104	4626	2.95E-05
purine ribonucleoside biosynthetic process	YNK1 | IMD3 | APT1 | GUA1 | ISN1	5	14	6.30E-04
glutamine family amino acid biosynthetic process	CIT2 | ARG5,6 | ARG4 | ARG1 | GDH1 | GLN1	6	28	9.10E-04
drug metabolic process	ACH1 | ADH5 | SHM1 | CIT2 | MDH3 | VMA1 | SAM2 | MET10 | BAT1 | CYC1 | GFA1 | APT1 | CYT1 | LSC1 | FUM1 | PDH1	16	278	0.0014
generation of precursor metabolites and energy	ADH5 | CIT2 | MDH3 | GRX2 | GLC3 | GLC7 | NCP1 | CYC1 | COQ5 | CYT1 | LSC1 | CIR2 | FUM1 | TKL1	14	220	0.0015
proteasome regulatory particle assembly	RPT2 | RPT6 | RPT1 | RPT5	4	11	0.003
coenzyme metabolic process	ACH1 | ADH5 | SHM1 | MDH3 | SAM2 | PDX1 | ADE3 | BNA1 | MTD1 | COQ5 | LSC1 | TKL1	12	181	0.0032
antibiotic metabolic process	ACH1 | ADH5 | CIT2 | MDH3 | LSC1 | FUM1 | PDH1	7	59	0.0036
sulfur compound metabolic process	ACH1 | HOM2 | SAM2 | GRX2 | MET6 | MET10 | PDX1 | ADE3 | BAT1 | LSC1	10	135	0.0045
cellular response to oxidative stress	NCL1 | TPS1 | TRX3 | MRP1 | TRR1 | GRX2 | ACT1 | SOD2 | GCY1	9	112	0.005
purine nucleotide biosynthetic process	PDX1 | ADE3 | YNK1 | MTD1 | IMD3 | APT1 | GUA1 | CYT1	8	88	0.0051
branched-chain amino acid biosynthetic process	HOM2 | LEU1 | BAT1 | ILV2	4	16	0.0067
one-carbon metabolic process	SHM1 | SAM2 | ADE3 | MTD1	4	18	0.0084
cellular response to reactive oxygen species	NCL1 | MRP1 | TRR1 | SOD2	4	19	0.0092
aspartate family amino acid biosynthetic process	LYS21 | HOM2 | MET6 | MET10 | ADE3 | BAT1	6	55	0.0092
fatty acid metabolic process	ACH1 | MDH3 | FAA2 | POX1 | PEX11 | PDH1	6	56	0.0095
glutamine metabolic process	GFA1 | GUA1 | GDH1 | GLN1	4	24	0.0156
dicarboxylic acid metabolic process	CIT2 | HOM2 | ADE3 | GDH1 | FUM1	5	45	0.019
purine nucleobase biosynthetic process	ADE3 | MTD1 | APT1	3	11	0.019
propionate metabolic process, methylcitrate cycle	ACH1 | PDH1	2	2	0.0203

Category description	Protein identity	No. of proteins in cluster	No. of proteins in genome	FDR value
cellular protein catabolic process	PIM1 | PRE7 | APE3 | RPT2 | PRB1 | SCL1 | RPT6 | RPT1 | PRE8 | PRC1 | RPT5 | PEP4	12	254	0.0224
cellular response to stress	HTA2 | NCL1 | TPS1 | TRX3 | RPT2 | NUP84 | HTA1 | MRP1 | TRR1 | GRX2 | PRB1 | GLC7 | ACT1 | RPT6 | SDS23 | SOD2 | YNK1 | RPT1 | SIN3 | CKA2 | RPT5 | GCY1 | PEP4	23	693	0.0237
protein catabolic process in the vacuole	APE3 | PRB1 | PRC1	3	13	0.0254
cellular amide metabolic process	ACH1 | SHM1 | RPT2 | RPS29B | MRP1 | GRX2 | PDX1 | ADE3 | DED81 | MTD1 | SPC3 | MRPL15 | PRC1 | YNL247W | ARG1 | LSC1 | ALA1 | CAM1	18	498	0.0304
ribonucleoside monophosphate metabolic process	ADH5 | VMA1 | PRS3 | CYC1 | IMD3 | APT1 | GUA1 | CYT1	8	136	0.0332
transfer RNA gene-mediated silencing	HTA1 | GLC7 | SIN3	3	15	0.0339
proteasomal ubiquitin-independent protein catabolic process	PRE7 | SCL1 | PRE8	3	15	0.0339
GTP biosynthetic process	YNK1 | IMD3	2	4	0.0409
carbohydrate metabolic process	TPS1 | ADH5 | MAL31 | CIT2 | MDH3 | GLC3 | PMI40 | GLC7 | GFA1 | YMR196W | GCY1	11	252	0.0481

Table S6 (continued)

231

Table S7
Enrichment analysis for GO processes of up-(green) and downregulated (red) proteins for both CEN.PK113-7D and the evolved CEN.PK113-7D at 39°C.

Category description	Protein identity	No. of proteins in cluster	No. of proteins in genome	FDR value
purine ribonucleoside monophosphate metabolic process	ADE1 | COR1 | ADK1 | HXK1 | TDH3 | COX6 | ENO2 | IMD2 | TDH1 | ATP2 | FBA1 | GPM1 | ADE17 | ADH1 | QCR2	15	118	9.83E-13
generation of precursor metabolites and energy	PET9 | COR1 | HXK1 | TDH3 | CIR1 | COX6 | ENO2 | MAM33 | KGD1 | TDH1 | FBA1 | MDH1 | GPM1 | PGM2 | ADH1 | QCR2	16	204	1.17E-11
pyruvate metabolic process	HXK1 | TDH3 | ENO2 | TDH1 | FBA1 | GPM1 | ADH1 | ALD4	8	42	1.09E-08
organonitrogen compound biosynthetic process	ADE1 | HIS7 | ADK1 | MRP1 | SER3 | SEC53 | HXK1 | TDH3 | RPS0A | ENO2 | IMD2 | TDH1 | ATP2 | FBA1 | GPM1 | DPS1 | RPS0B | SHM2 | RPL37A | MET17 | RPL6A | ADE17	22	897	9.11E-08
aerobic respiration	PET9 | COR1 | COX6 | MAM33 | KGD1 | MDH1 | QCR2	7	89	1.62E-05
apoptotic process	PET9 | TDH3 | CPR3 | POR1	4	26	2.40E-04
antibiotic metabolic process	KGD1 | MDH1 | ADH1 | ALD4	4	59	3.80E-03
ion transmembrane transport	PET9 | COR1 | CTP1 | COX6 | MIR1 | ATP2 | POR1 | QCR2	8	298	3.80E-03
endonucleolytic cleavage to generate mature 3'-end of SSU-rRNA from (SSU-rRNA, 5.8S rRNA, LSU-rRNA)	RPS0A | RPS0B	2	5	4.50E-03
electron transport chain	COR1 | CIR1 | COX6 | QCR2	4	74	7.60E-03
'de novo' IMP biosynthetic process	ADE1 | ADE17	2	9	9.90E-03
nucleotide-sugar metabolic process	SEC53 | PGM2	2	14	1.95E-02
cellular amino acid metabolic process	HIS7 | SER3 | DPS1 | SHM2 | MET17 | ADH1	6	248	2.31E-02
reactive oxygen species metabolic process	MRP1 | TDH3	2	18	2.75E-02
metabolic process	EFB1 | FUN12 | HHF1 | HHT1 | RPL4A | RPG1 | PGI1 | PCS60 | ENP1 | LEU2 | PDI1 | RPS14A | LHP1 | SLC1 | RPS16B | YDL124W | RPO21 | GLT1 | UFD2 | YPD1 | REG1 | HEM13 | TPI1 | CPR1 | GLO2 | RPT3 | RPN9 | SAH1 | ALD5 | SEC4 | RPN11 | YFR006W | PNC1 | HEM2 | RMD9 | AMS1 | SPT16 | GUS1 | SCM4 | ERG25 | VAS1 | ASN2 | ERG1 | PCT1 | CRM1 | MES1 | ZUO1 | ERG11 | RPN1 | MSC7 | GRE3 | OYE2 | GND1 | YIL108W | RPL16A | VTC4 | RNR2 | KAR2 | URA2 | ERG20 | RPS14B | OSM1 | HOM6 | PMT4 | UGP1 | TEF4 | APE2 | FAS1 | SSA2 | HSP104 | ADE16 | AHP1 | SAM1 | NMT1 | SEC13 | YEF3 | DCS1 | GSP1 | ACO1 | FKS1 | TAL1 | POB3 | TSL1 | ERG13 | PLB1 | PDS5 | YPK2 | RPS16A | PFK2 | NIP1 | IDH1 | YDJ1 | LEU4 | ZWF1 | CIT1 | ACC1 | CMK2 | CDC33 | DBP5 | IDH2 | TUF1 | BFR1 | WTM1 | GCD1 | MBF1 | FAA1 | ALD6 | CAR1 | NAB3 | NEW1 | FAS2 | RVB2 | HSP82 | TEF1 | PRE2	115	3661	2.40E-08
organonitrogen compound biosynthetic process	EFB1 | FUN12 | RPL4A | RPG1 | PGI1 | LEU2 | RPS14A | SLC1 | RPS16B | GLT1 | HEM13 | TPI1 | SAH1 | PNC1 | HEM2 | RMD9 | GUS1 | VAS1 | ASN2 | PCT1 | MES1 | ZUO1 | RPL16A | URA2 | RPS14B | HOM6 | PMT4 | TEF4 | ADE16 | NMT1 | YEF3 | RPS16A | PFK2 | NIP1 | IDH1 | LEU4 | CIT1 | ACC1 | CDC33 | DBP5 | IDH2 | TUF1 | GCD1 | CAR1 | TEF1	45	897	3.40E-06

Table S7
(continued)

oxidation-reduction process	LEU2 | PDI1 | YDL124W | GLT1 | REG1 | HEM13 | ALD5 | RMD9 | ERG25 | ERG1 | ERG11 | MSC7 | GRE3 | OYE2 | GND1 | RNR2 | OSM1 | HOM6 | UGP1 | FAS1 | ADE16 | AHP1 | ACO1 | IDH1 | ZWF1 | CIT1 | IDH2 | ALD6 | FAS2	29	445	7.20E-06
carboxylic acid biosynthetic process	PGI1 | LEU2 | GLT1 | TPI1 | ALD5 | ASN2 | URA2 | HOM6 | FAS1 | PFK2 | IDH1 | LEU4 | CIT1 | ACC1 | IDH2 | ALD6 | FAS2	17	210	2.70E-04
protein folding	HSP26 | PDI1 | CPR1 | HSP78 | ZUO1 | SSC1 | OSM1 | SSA2 | HSP104 | YDJ1 | SSE1 | HSP82	12	108	3.70E-04
translation	EFB1 | FUN12 | RPL4A | RPG1 | RPS14A | RPS16B | RMD9 | GUS1 | VAS1 | MES1 | ZUO1 | RPL16A | RPS14B | TEF4 | YEF3 | RPS16A | NIP1 | CDC33 | DBP5 | TUF1 | GCD1 | TEF1	22	372	9.60E-04
NADP metabolic process	PGI1 | TPI1 | GND1 | TAL1 | ZWF1 | ALD6	6	23	1.20E-03
coenzyme metabolic process	PGI1 | TPI1 | SAH1 | PNC1 | GND1 | OSM1 | SAM1 | TAL1 | PFK2 | ZWF1 | CIT1 | ACC1 | FAA1 | ALD6	14	181	2.20E-03
protein refolding	HSP78 | SSC1 | YDJ1 | SSE1 | HSP82	5	16	2.30E-03
organic substance catabolic process	PGI1 | PCS60 | PDI1 | UFD2 | REG1 | TPI1 | GLO2 | RPT3 | RPN9 | SAH1 | ALD5 | RPN11 | AMS1 | RPN1 | GRE3 | KAR2 | PMT4 | APE2 | SSA2 | SEC13 | DCS1 | PLB1 | PFK2 | YDJ1 | CIT1 | CDC33 | ALD6 | CAR1 | NAB3 | PRE2	30	658	2.30E-03
translational elongation	EFB1 | ZUO1 | TEF4 | YEF3 | TUF1 | TEF1	6	31	3.60E-03
protein metabolic process	EFB1 | FUN12 | HHF1 | RPL4A | RPG1 | PDI1 | RPS14A | RPS16B | UFD2 | YPD1 | REG1 | CPR1 | RPT3 | RPN9 | RPN11 | YFR006W | RMD9 | AMS1 | GUS1 | VAS1 | MES1 | ZUO1 | RPN1 | YIL108W | RPL16A | KAR2 | RPS14B | PMT4 | TEF4 | APE2 | SSA2 | HSP104 | NMT1 | SEC13 | YEF3 | YPK2 | RPS16A | NIP1 | YDJ1 | CMK2 | CDC33 | DBP5 | TUF1 | GCD1 | RVB2 | HSP82 | TEF1 | PRE2	48	1374	5.10E-03
protein unfolding	HSP78 | SSC1 | HSP104	3	3	5.20E-03
glutamate biosynthetic process	GLT1 | IDH1 | CIT1 | IDH2	4	11	5.90E-03
response to stress	HHT1 | HSP26 | SDS24 | PDI1 | YDL124W | RPO21 | UFD2 | YPD1 | REG1 | HSP78 | RPT3 | HSP12 | SPT16 | GRE3 | BZZ1 | GND1 | KAR2 | PMT4 | HSP104 | AHP1 | SEC13 | DCS1 | POB3 | TSL1 | PDS5 | YDJ1 | ZWF1 | CMK2 | LSP1 | ALD6 | RVB2 | HSP82	32	785	6.20E-03
ergosterol biosynthetic process	ERG25 | ERG1 | ERG11 | ERG20 | ERG13	5	25	8.90E-03
regulation of actin filament organization	EFB1 | BZZ1 | BBC1 | ARP3 | CRN1 | PFY1	6	40	8.90E-03
nucleocytoplasmic transport	ENP1 | CRM1 | ZUO1 | SSA2 | GSP1 | YDJ1 | ACC1 | DBP5 | GSP2 | WTM1 | NEW1 | TEF1	12	169	8.90E-03
carbohydrate metabolic process	PGI1 | LEU2 | REG1 | TPI1 | AMS1 | GRE3 | GND1 | KAR2 | UGP1 | HSP104 | FKS1 | TAL1 | TSL1 | PFK2 | ZWF1	15	252	8.90E-03
cellular amino acid metabolic process	LEU2 | GLT1 | SAH1 | GUS1 | VAS1 | ASN2 | MES1 | URA2 | HOM6 | SAM1 | IDH1 | LEU4 | CIT1 | IDH2 | CAR1	15	248	8.90E-03
ERAD pathway	PDI1 | UFD2 | RPT3 | KAR2 | PMT4 | SEC13 | YDJ1	7	62	1.14E-02
positive regulation of cellular component biogenesis	RPT3 | SPT16 | BZZ1 | ARP3 | CRN1 | POB3 | PFY1	7	67	1.38E-02
translational initiation	FUN12 | RPG1 | RMD9 | NIP1 | CDC33 | GCD1	6	52	1.83E-02
lipid biosynthetic process	SLC1 | SAH1 | ERG25 | ERG1 | PCT1 | ERG11 | ERG20 | FAS1 | ERG13 | ACC1 | FAS2	11	178	2.37E-02
response to abiotic stimulus	HSP26 | YPD1 | HSP78 | HSP12 | GRE3 | BZZ1 | HSP104 | YDJ1 | LSP1 | ALD6 | HSP82	11	179	2.45E-02
phosphorus metabolic process	PGI1 | SLC1 | YPD1 | TPI1 | SAH1 | PNC1 | PCT1 | GND1 | VTC4 | RNR2 | URA2 | ERG20 | OSM1 | HOM6 | UGP1 | ADE16 | TAL1 | TSL1 | PLB1 | YPK2 | PFK2 | ZWF1 | CIT1 | ACC1 | CMK2 | FAA1 | ALD6	27	705	2.45E-02
regulation of cellular component organization	EFB1 | SDS24 | CPR1 | RPT3 | SPT16 | BZZ1 | BBC1 | ARP3 | CDC42 | GSP1 | FKS1 | CRN1 | POB3 | YPK2 | PFY1 | BFR1 | WTM1 | SAR1 | HSP82	19	436	3.04E-02
membrane addition at site of cytokinesis	SEC4 | MYO2	2	2	3.09E-02
trehalose metabolic process	UGP1 | HSP104 | TSL1	3	11	3.20E-02
drug metabolic process	PGI1 | GLT1 | TPI1 | SAH1 | ALD5 | PNC1 | ASN2 | SAM1 | ACO1 | PFK2 | IDH1 | CIT1 | IDH2 | ALD6	14	278	3.22E-02
carbohydrate derivative metabolic process	PGI1 | PDI1 | TPI1 | SAH1 | AMS1 | GND1 | RNR2 | URA2 | PMT4 | UGP1 | ADE16 | TAL1 | PFK2 | ZWF1 | CIT1 | ACC1 | FAA1	17	378	3.37E-02
positive regulation of RNA polymerase II transcriptional preinitiation complex assembly	RPT3 | SPT16 | POB3	3	12	3.62E-02
organophosphate catabolic process	PGI1 | TPI1 | PLB1 | PFK2 | CIT1	5	46	4.11E-02
tRNA import into nucleus	SSA2 | YDJ1	2	3	4.33E-02
phosphatidylcholine metabolic process	SAH1 | PCT1 | PLB1	3	14	4.90E-02

Gene Systematic Name	Protein Standard Name	Protein Name	Amino acid change	Consequence	Impact	Fold-change difference
YDL171C	GLT1	Glutamate synthase [NADH]	p.Thr791Ala	Missense variant	Moderate	0.84
YDL171C	GLT1	Glutamate synthase [NADH]	p.Lys215Asn	Missense variant	Moderate	0.84
YIL108W	-	Putative metalloendopeptidase	p.Ser272Pro	Missense variant	Moderate	0.79
YKL182W	FAS1	Fatty acid synthase subunit beta	p.Val61Met	Missense variant	Moderate	0.69
YPL235W	RVB2	RuvB-like protein 2	p.Arg220Ile	Missense variant	Moderate	0.84
YGL008C	PMA1	Plasma Membrane ATPase 1	p.Asp420Asn	Missense variant	Moderate	1.60
YHR042W	NCP1	NADP-Cytochrome P450 reductase	p.Ala218Val	Missense variant	Moderate	0.70
YKR016W	MIC60	MICOS complex subunit MIC60	p.Ser409Arg	Missense variant	Moderate	0.74
YMR229C	RRP5	rRNA biogenesis protein RRP5	p.Ala354Thr	Missense variant	Moderate	0.91
YOL058W	ARG1	Argininosuccinate synthase	p.Ala164Val	Missense variant	Moderate	0.78

Table S8
The differentially expressed proteins found in EVO39/EVO30 and EVO39/CN39 which has mutations identified from genome sequencing of CEN.PK-EVO (Chapter 4).

$\mu mol \cdot gDW^{-1}$	CEN.PK113-7D		Evolved CEN.PK113-7D	
	30 ℃	39 ℃	30 ℃	39 ℃
GLU	1.92 ± 0.72	6.91 ± 1.76	10.1 ± 1.91	11.2 ± 1.66
G6P	2.94 ± 0.32	2.94 ± 0.32	3.02 ± 0.19	3.12 ± 0.36
F6P	0.61 ± 0.09	0.46 ± 0.02	0.55 ± 0.07	0.65 ± 0.10
F1,6P	12.0 ± 1.1	3.25 ± 0.10	19.3 ± 4.9	3.98 ± 0.56
DHAP	2.50 ± 0.21	1.30 ± 0.30	3.02 ± 0.36	1.56 ± 0.16
GAP	0.73 ± 0.48	0.40 ± 0.28	0.94 ± 0.24	0.54 ± 0.12
3PG	0.50 ± 0.05	0.51 ± 0.02	0.51 ± 0.11	0.41 ± 0.06
2PG	0.034 ± 0.002	0.040 ± 0.006	0.043 ± 0.015	0.037 ± 0.008
PEP	0.033 ± 0.004	0.030 ± 0.006	**0.077 ± 0.017**	0.040 ± 0.010
G1P	0.31 ± 0.06	0.15 ± 0.04	1.74 ± 0.34	0.12 ± 0.01
UDPG	1.81 ± 0.22	1.06 ± 0.05	**1.62 ± 0.26**	1.81 ± 0.21
RL5P	0.15 ± 0.02	0.12 ± 0.02	0.14 ± 0.03	0.13 ± 0.03
X5P	0.33 ± 0.04	0.24 ± 0.03	0.31 ± 0.04	0.26 ± 0.02
R5P	0.41 ± 0.04	0.32 ± 0.03	0.55 ± 0.05	0.33 ± 0.06
S7P	0.33 ± 0.04	0.28 ± 0.04	0.21 ± 0.02	0.23 ± 0.02
E4P	0.015 ± 0.001	0.010 ± 0.001	0.013 ± 0.002	0.011 ± 0.002
CIT	14.7 ± 2.54	20.0 ± 1.01	3.93 ± 0.10	2.03 ± 0.28
iCIT	0.13 ± 0.02	0.13 ± 0.02	0.036 ± 0.012	0.060 ± 0.016
αKG	0.57 ± 0.11	0.99 ± 0.18	0.41 ± 0.03	0.71 ± 0.05
SUS	5.13 ± 1.72	3.77 ± 1.86	4.96 ±1.49	3.79 ±0.57
FUM	0.46 ± 0.09	0.60 ± 0.13	0.41 ± 0.06	0.93 ±0.09
MAL	4.81 ± 0.88	7.08 ± 1.16	2.71 ± 0.77	7.26 ± 0.63

Table S9
Intracellular metabolites concentrations for the chemostat culture of CEN.PK113-7D and the evolved CEN.PK113-7D at 30°C and 39°C under anaerobic condition. The standard deviations were obtained from four separate biological samples obtained from the duplicate chemostat.

Table S10
Intracellular amino
acids concentrations
for the chemostat
culture of CEN.
PK113-7D and the
evolved CEN.PK113-
7D at 30°C and 39°C
under anaerobic
condition. The
standard deviations
were obtained from
four separate biological
samples obtained
from the duplicate
chemostat.

μmol·gDW^{-1}	CEN.PK113-7D		Evolved CEN.PK113-7D	
	30 °C	39 °C	30 °C	39 °C
Ala	49.2 ± 15	65.6 ± 28	55.0 ± 4.2	107 ± 5
Asn	5.86 ± 0.87	104 ± 23	6.16 ± 0.23	132 ± 8
Asp	16.7 ± 2.5	0.09 ± 0.02	22.8 ± 1.3	0.10 ± 0.00
Glu	77.2 ± 10.8	1.74 ± 0.21	123 ± 3	2.03 ± 0.01
Gln	27.7 ± 3.8	6.39 ± 1.40	36.2 ± 1.9	7.42 ± 0.37
Gly	4.41 ± 1.09	7.68 ± 2.09	5.37 ± 0.58	11.0 ± 0.7
His	1.50 ± 0.19	0.51 ± 0.12	1.63 ± 0.08	0.67 ± 0.10
Ile	1.86 ± 0.30	0.68 ± 0.13	1.24 ± 0.07	0.48 ± 0.01
Leu	0.93 ± 0.13	14.4 ± 3.8	0.74 ± 0.06	12.9 ± 0.3
Lys	1.85 ± 0.20	0.43 ± 0.07	3.43 ± 0.3	0.19 ± 0.03
Met	0.14 ± 0.02	8.96 ± 2.99	0.11 ± 0.01	10.2 ± 0.1
Phe	0.40 ± 0.05	13.5 ± 2.6	0.58 ± 0.04	11.5 ± 0.9
Pro	1.12 ± 0.26	1.32 ± 0.26	2.00 ± 0.20	1.34 ± 0.07
Ser	1.86 ± 0.46	2.78 ± 1.17	2.75 ± 0.15	2.29 ± 0.16
Thr	6.89 ± 1.41	2.86 ± 0.81	7.70 ± 0.3	3.66 ± 0.14
Trp	0.15 ± 0.02	1.52 ± 0.29	0.07 ± 0.01	1.88 ± 0.10
Tyr	0.50 ± 0.06	29.7 ± 6.6	0.69 ± 0.06	37.6 ± 1.5
Val	29.0 ± 5.2	14.4 ± 3.8	7.07 ± 0.2	12.9 ± 0.3

Abbreviations

Metabolites		Amino acids	
GLU	Glucose	Ala	Alanine
G6P	Glucose-6-phosphate	Asn	Asparagine
F6P	Fructose-6-phosphate	Asp	Aspartic acid
F1,6P	Fructose-1,6-bisphosphate	Glu	Glutamic acid
DHAP	Dihydroxyacetone phosphate	Gln	Glutamine
GAP	Glyceraldehyde-3-phosphate	Gly	Glycine
3PG	3-phosphoglyceric acid	His	Histidine
2PG	2-phosphoglyceric acid	Ile	Isoleucine
PEP	Phosphoenolpyruvic acid	Leu	Leucine
G1P	Glucose-1-phosphate	Lys	Lysine
UDPG	Uridine diphosphate glucose	Met	Methionine
RL5P	Ribulose-5-phosephate	Phe	Phenylalanine
X5P	Xylulose-5-phosphate	Pro	Proline
R5P	Ribose-5-phosphate	Ser	Serine
S7P	Sehoheptulose-7-phosphate	Thr	Threonine
E4P	Erythrose-4-phosphate	Trp	Tryptophan
CIT	Citrate	Tyr	Tyrosine
iCIT	Isocitrate	Val	Valine
αKG	α-ketoglutarate		
SUS	Succinate		
FUM	Fumarate		
MAL	Malate		

Chapter 6

Concluding remarks and outlook

The collaborative researches presented in this thesis aim to identify and understand the mechanisms employed by *S. cerevisiae* to cope with the stress during growth at sub-and supra-optimal temperatures under anaerobic conditions. To do so, we used a top-down holistic approach, thereby performing quantitative physiological studies under well-defined cultivation conditions, global proteome analysis, whole genome sequencing and capacity measurements of the glycolytic enzymes, where we tried to integrate and comprehend the information to study the biological system as a whole. We designed robust experimental set-ups and implemented realistic mathematical models for quantitative characterization of the different yeast strains under well-defined conditions. The large amount of data obtained from the omics analyses generated various hypotheses for mechanisms to counteract thermal stress in *S. cerevisiae*. The generated knowledge in this thesis can benefit the alcoholic beverages and biofuel industries to tailor yeast strains for industrial applications, allowing to explore the opportunities to improve productivity and to decrease energy expenses in process operations.

In **chapter 2**, we performed phenotypic screening and selected two industrial *S. cerevisiae* strains (ADY5 and Ethanol Red) which grew best at sub-optimal and supra-optimal temperatures, respectively. From the physiological characterization of the chemostat cultures of these selected industrial strains and the well characterized laboratory strain CEN.PK113-7D we observed, in addition to the large differences in the effect of cultivation temperature on the growth rate between the strains, also significant differences between strains and cultivation temperatures in terms of biomass and ethanol yields on glucose, total protein content, and storage carbohydrate contents. This implied that the physiological responses of the different yeast strains to different cultivation temperatures were very different,

in spite of the fact that they belong to the same species. The quantitative analysis of the chemostat cultures of the three selected strains revealed that energy allocation might be one of the strategies for the industrial strains ADY5 and Ethanol Red to perform better than the laboratory strain at sub-and supra-optimal temperatures, respectively; as both strains required less ATP to form biomass compared to CEN.PK113-7D at sub- and supra-optimal temperatures. Compared with CEN.PK113-7D, both industrial strains had relatively higher storage carbohydrate contents (glycogen and trehalose) at sub- and supra-optimal temperatures. The higher glycogen accumulation in the industrial strains could facilitate a transient increase of energy production for the progression during the cell cycle[1] and thereby benefit the growth under stressful conditions such as non-optimal temperature.

With the aim to obtain more insight in possible mechanisms responsible for the high temperature tolerance of Ethanol Red and the low temperature tolerance of ADY5 strain a global proteome analysis of the chemostat cultivated strains at 12, 30 and 39 °C (**chapter 3**). The results showed a broad remodelling of the proteome of all three strains at sub- and supra-optimal temperature, however, the differences between the strains were surprisingly large. This shows that apparently the proteome response to temperature highly depends on the genetic makeup of the strains and might also reflect the differences in thermotolerance between them. Nevertheless, we observed some similar responses, whereby during growth at low temperature a strong repression of translation-related proteins and induction of amino acid metabolism occurred, along with components involved in protein folding and degradation. During growth at high temperature all strains showed changes in proteins involved in central metabolism and amino acid biosynthesis.

ADY5 also showed a high expression of antioxidant proteins at sub-optimal temperature, which is remarkable as our experiments were carried out under anaerobic conditions. However, it has been suggested that transcription of antioxidant-encoding genes also might occur as part of a general stress response [2]. On the other hand, the increased expression of proteins involved in protein folding and degradation in Ethanol Red could prevent the accumulation of toxic components at supra-optimal temperatures in this strain. The increased expression of proteins involved

in ergosterol and proline production could also point towards mechanisms to increase the stability of the cell membrane under thermal stress [3–6]. These two features found in Ethanol Red seem to protect the cells from the physical impact of thermal stress, thus lowering the energy demand in cellular maintenance while growing at supra-optimal temperatures.

Since all strains being investigated in **chapter 2** and **chapter 3** are *S. cerevisiae*, we assumed that there were only minor genetic differences between them. However, the physiological characterization and the proteome analysis of the three strains in **chapter 2** and **chapter 3** indicate that they must have different regulatory systems in response to different cultivation temperatures. In order to future evaluate the potential strategies of ADY5 and Ethanol Red, the following experiments/studies are suggested.

For ADY5, if glycogen benefits the cells to obtain a transient increase of energy to progress cell cycle under sub-optimal temperature, the cell cycle of ADY5 can be investigated by flow cytometry. Knutsen et al. showed a flow cytometric method to differentiate the cells in G_1 phase and in G_2 phase where the cells in G_1 phase have two nuclei and in G_2 phase have only one nucleus [7]. The obtained light-scattering plot due to the effect of a fluorescent dye (Sytox Green) would allow to assess the progression of the cell cycle.

For Ethanol Red, the high expression of proteins involved in protein folding and degradation suggested that Ethanol Red had an efficient defence mechanism against the temperature stress to proteins. It has been shown that the decline of proteolytic activities attributes to cell aging because of the broad negative cellular consequences, such as translational inaccuracy and the disruption of the interaction between cellular components [8]. Among the three strains, Ethanol Red showed the lowest numbers of differentially expressed proteins at supra-optimal temperature, and therefore, it showed to have a robust system to maintain protein homeostasis. There are multiple complex mechanisms regulating proteostasis, such as chaperones, ubiquitin-proteasome, and autophagy [9,10]. It is worthwhile to further study these suggested mechanisms in order to elucidate the thermal impact on the decrease of protein homeostasis. On the other hand, ergosterol and proline are known to protect cells

from thermal stress by membrane stabilization, and therefore, the upregulation of proteins involved in ergosterol biosynthesis and proline biosynthesis in Ethanol Red implied that it has a prevailing membrane composition against thermal stress. It is worthwhile to analyse and compare the membrane composition in terms of lipid and amino acids between the three strains. This could give an insight into metabolic pathways attributing the synthesis of a favourable membrane composition for growing at supra-optimal temperatures. Since many fatty acid and amino acid supplements are available in the industrial market, the industry could possibly improve cell performance at supra-optimal temperature by giving appropriate supplements during process conditions.

In order to minimize the genetic differences between strains for the study of thermal tolerance, an evolved CEN.PK113-7D was generated by adaptive laboratory evolution (ALE) using long term sequential batch reactor (SBR) cultivation under anaerobic conditions. **Chapter 4** descripts the genotypic and phenotypic changes identified in the evolved strain at supra-optimal temperature under anaerobic conditions. The evolved strain showed significant improved growth performance at 39.8 °C under glucose excess and anaerobic conditions. We performed a physiological characterization of chemostat cultures of both strains at 39.0°C and found out that the evolved strain showed a slightly higher biomass yield with 37.7% increase of trehalose accumulation, 32.3% increase of medium chain fatty acids, 12% decrease of unsaturated fatty acids/saturated fatty acids ratio, and 75% increase of ergosterol content. From the whole genome sequencing of the unevolved and evolved strain, we identified several mutations, such as SNVs and INDELS, in the evolved strain. The enrichment analysis indicated that these mutations are involved in phosphatidylethanolamine (PE) biosynthesis, de novo pyrimidines biosynthesis, and TORC1 signalling. **Chapter 5** descripts the proteomic analysis of the chemostat cultures for the unevolved and evolved strains at different cultivation temperatures. This analysis allows to identify the common, the evolved strain-specific, and different responses between both strains at supra-optimal temperature under anaerobic conditions. **Chapter 5** also descripts the possible differences in enzyme capacity, enzyme quantity, and temperature dependency of glycolytic enzymes between both strains. The quantitative physiology characterizations, genomic, and proteomic analysis

in **chapter 4** and **chapter 5** generated new hypotheses that the improved thermotolerance (by decrease in death rate) of the evolved strain was attributed by proteome allocations where less ATP was required for maintenance, membrane composition with high PE and ergosterol, efficient cytoplasmic pH regulation, and autophagy resulting an efficient protein homeostasis. Since the evolved CEN.PK113-7D in **chapter 4** was obtained by a single evolution experiment, the possible mechanisms identified in **chapter 4** and **chapter 5** should in the future be evaluated by the following suggestions.

In order to identify the mutations attributed to the improved thermotolerance of the evolved strains, several ALE at identical conditions **(chapter 4)** should be repeated to obtain several stable isolates. All stable isolates should be characterized and analysed in terms of whole genome sequencing and proteomic analysis in anaerobic chemostat cultures. The mutations which do not contribute to the improved thermotolerance during ALE can be eliminated by identifying the common changes among the stable isolates obtained from independent ALE experiments.

Several mutations were found in the evolved strain **(chapter 4)**, and some of them are involved in the cellular processes which may attribute to the improved thermotolerance (mentioned above). The mutations which resulted in a stop codon resulted in a non-functional protein. A genetic knockout of the gene encoding these protein sequences can be implemented into the unevolved strain to verify the significance of this mutation. On the other hand, the missense mutations from the evolved strain can be implemented into the unevolved knockout mutant. In order to validate the influence of these mutations on thermotolerance, the resulting mutants can be characterized under well-defined anaerobic conditions at 39°C. It is worthy to mention that thermo-tolerance is a complicated quantitative trait determined by multiple genes [11,12]. Therefore, there may be additive effects from various mutations identified in the evolved strain. For industrial application, a subsequent reverse engineering of these mutations using different copy numbers should also be considered because diploid/polyploid strains are often used rather than haploid strains in industry. Compare to a haploid strain, a mutation impact on the physiology of a diploid strain depends on more genetics events, such as genome copy numbers and interaction between dominant and recessive alleles [13,14].

Several proteins in the evolved strain, such as TFS1 and OLE1, showed significant differential change in expression compared to the unevolved strain at 39°C. These differentially expressed proteins play roles in the breakdown of autophagic bodies in vacuole and autophagosome formation during autophagy (**chapter 5**). Several studies showed that there is a positive relation between autophagy and cell longevity due to the removal of protein aggregates and toxic components within organelles (part of proteostasis mechanisms) [15]. Moreover, autophagy also allows cellular adaptation to changing nutrient environments by the degradation of organelles which requires high energy for maintenance [16]. It has also been shown that the activity of autophagy is positively related to the cellular PE level [17], meanwhile, we observed a significant high content of PE in the chemostat culture of the evolved strain at 39°C (**chapter 4**). These distinct features of the evolved strain prevailed during growth at supra-optimal temperature because autophagy enables efficient cellular adaptation by nutrient recycling and protein homeostasis. There are several methods to study autophagy [18]. For example, the degradation of autophagic bodies can be determined by mass spectrometry-based proteomics incorporated with stable isotopes, such as ^{13}C and ^{15}N. This allows to investigate the degradation rate of the proteins by monitoring the isotope labelled peptides [19,20]. Another common method to monitor autophagy is transmission electron microscopy, where various autophagic structures, such as phagophore and autophagosome, can be identified [21]. If the evolved strain had comparatively higher autophagy than the unevolved strain, more autophagic structures should be expected in chemostat grown cells at 39°C. The lower cell death rate observed in the chemostat culture of the evolved strain at 39°C has generated more questions about the regulation of cell aging and cell death.

A multi-omics approach was used to study the impact of temperature on *S. cerevisiae* in this thesis. This generated tremendous quantitative descriptions/understanding of the cellular activities and regulations as responses to different cultivation temperatures under anaerobic conditions. The processing of these data requires not only robust computational handling but also a critical thinking during the interpretation of these analyses. The findings presented in this thesis are just the tip of the iceberg, where metabolic processes beyond central carbon metabolism, such as autophagy and proteostasis, should

also be addressed in order to elucidate the mechanistic strategies coping with temperature stress. A holistic characterization of an organism is an essential baseline for the design and optimization of a bioprocess in industry. With the advance of omics technology, computer assisted interpretation and integration of large data sets is in demand. The integration of different omics data with mechanistic modelling (kinetics) can further validate the experimental observations and provide optimize solutions for large-scale bioprocess development.

References

[1]   H.H.W. Silljé, J.W.G. Paalman, E.G. ter Schure, S.Q.B. Olsthoorn, A.J. Verkleij, J. Boonstra, C.T. Verrips, Function of Trehalose and Glycogen in Cell Cycle Progression and Cell Viability in Saccharomyces cerevisiae, J Bacteriol. 181 (1999) 396–400.

[2]   B.R. Gibson, S.J. Lawrence, C.A. Boulton, W.G. Box, N.S. Graham, R.S.T. Linforth, K.A. Smart, The oxidative stress response of a lager brewing yeast strain during industrial propagation and fermentation, FEMS Yeast Res. 8 (2008) 574–585. https://doi.org/10.1111/j.1567-1364.2008.00371.x.

[3]   T.M. Swan, K. Watson, Stress tolerance in a yeast sterol auxotroph: role of ergosterol, heat shock proteins and trehalose, FEMS Microbiology Letters. 169 (1998) 191–197. https://doi.org/10.1111/j.1574-6968.1998.tb13317.x.

[4]   T. Kaino, T. Tateiwa, S. Mizukami-Murata, J. Shima, H. Takagi, Self-Cloning Baker's Yeasts That Accumulate Proline Enhance Freeze Tolerance in Doughs, Appl. Environ. Microbiol. 74 (2008) 5845–5849. https://doi.org/10.1128/AEM.00998-08.

[5]   H. Takagi, Proline as a stress protectant in yeast: physiological functions, metabolic regulations, and biotechnological applications, Appl Microbiol Biotechnol. 81 (2008) 211–223. https://doi.org/10.1007/s00253-008-1698-5.

[6]   S. Bhattacharya, B.D. Esquivel, T.C. White, Overexpression or Deletion of Ergosterol Biosynthesis Genes Alters Doubling Time, Response to Stress Agents, and Drug Susceptibility in Saccharomyces cerevisiae, MBio. 9 (2018). https://doi.org/10.1128/mBio.01291-18.

[7]   J.H.J. Knutsen, I.D. Rein, C. Rothe, T. Stokke, B. Grallert, E. Boye, Cell-Cycle Analysis of Fission Yeast Cells by Flow Cytometry, PLOS ONE. 6 (2011) e17175. https://doi.org/10.1371/journal.pone.0017175.

[8]   R.C. Taylor, A. Dillin, Aging as an Event of Proteostasis Collapse, Cold Spring Harb Perspect Biol. 3 (2011) a004440. https://doi.org/10.1101/cshperspect.a004440.

[9]   B. Sampaio-Marques, P. Ludovico, Linking cellular proteostasis to yeast longevity, FEMS Yeast Research. 18 (2018). https://doi.org/10.1093/femsyr/foy043.

[10]   T.A. Chernova, K.D. Wilkinson, Y.O. Chernoff, Prions, Chaperones, and Proteostasis in Yeast, Cold Spring Harb Perspect Biol. 9 (2017) a023663. https://doi.org/10.1101/cshperspect.a023663.

[11]   Z. Wang, Q. Qi, Y. Lin, Y. Guo, Y. Liu, Q. Wang, QTL analysis reveals genomic variants linked to high-temperature fermentation performance in the industrial yeast, Biotechnology for Biofuels. 12 (2019) 59. https://doi.org/10.1186/s13068-019-1398-7.

[12]   Y. Yang, M.R. Foulquié-Moreno, L. Clement, É. Erdei, A. Tanghe, K. Schaerlaekens, F. Dumortier, J.M. Thevelein, QTL Analysis of High Thermotolerance with Superior and Downgraded Parental Yeast Strains Reveals New Minor QTLs and Converges on Novel Causative Alleles Involved in RNA Processing, PLoS Genet. 9 (2013). https://doi.org/10.1371/journal.pgen.1003693.

[13]   K. Krogerus, M. Arvas, M. De Chiara, F. Magalhães, L. Mattinen, M. Oja, V. Vidgren, J.-X. Yue, G. Liti, B. Gibson, Ploidy influences the functional attributes of de novo lager yeast hybrids, Appl Microbiol Biotechnol. 100 (2016) 7203–7222. https://doi.org/10.1007/s00253-016-7588-3.

[14]   A.R. Gorter de Vries, J.T. Pronk, J.-M.G. Daran, Industrial Relevance of Chromosomal Copy Number Variation in Saccharomyces Yeasts, Applied and Environmental Microbiology. 83 (n.d.) e03206-16. https://doi.org/10.1128/AEM.03206-16.

[15]   J.K. Tyler, J.E. Johnson, The role of autophagy in the regulation of yeast life span, Ann N Y Acad Sci. 1418 (2018) 31–43. https://doi.org/10.1111/nyas.13549.

[16]   D.L. Tuttle, A.S. Lewin, W.A. Dunn, Selective autophagy of peroxisomes in methylotrophic yeasts, Eur J Cell Biol. 60 (1993) 283–290.

[17]   P. Rockenfeller, M. Koska, F. Pietrocola, N. Minois, O. Knittelfelder, V. Sica, J. Franz, D. Carmona-Gutierrez, G. Kroemer, F. Madeo, Phosphatidylethanolamine positively regulates autophagy and longevity, Cell Death Differ. 22 (2015) 499–508. https://doi.org/10.1038/cdd.2014.219.

[18]   R. Torggler, D. Papinski, C. Kraft, Assays to Monitor Autophagy in Saccharomyces cerevisiae, Cells. 6 (2017) 23. https://doi.org/10.3390/cells6030023.

[19]   A.C. Zimmermann, M. Zarei, S. Eiselein, J. Dengjel, Quantitative proteomics for the analysis of spatio-temporal protein dynamics during autophagy, Autophagy. 6 (2010) 1009–1016. https://doi.org/10.4161/auto.6.8.12786.

[20]   A.R. Kristensen, S. Schandorff, M. Høyer-Hansen, M.O. Nielsen, M. Jäüättelaü, J. Dengjel, J.S. Andersen, Ordered Organelle Degradation during Starvation-induced Autophagy, Molecular & Cellular Proteomics. 7 (2008) 2419–2428. https://doi.org/10.1074/mcp.M800184-MCP200.

[21]   P. Ylä-Anttila, H. Vihinen, E. Jokitalo, E. Eskelinen, Chapter 10 Monitoring Autophagy by Electron Microscopy in Mammalian Cells, in: Methods in Enzymology, Academic Press, 2009: pp. 143–164. https://doi.org/10.1016/S0076-6879(08)03610-0.

Curriculum Vitae
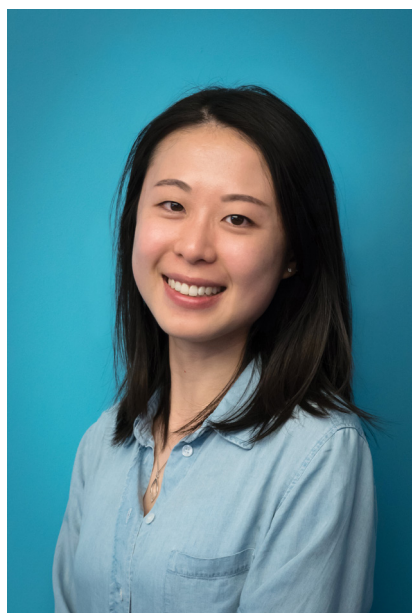
Ka Ying Florence Lip was born on 16th August 1989 and grew up in Hong Kong, China. Driven by adventure and motivated by her mother, she left her home country after high school and began her college journey in the United States in 2008. Interested in the diverse applications of microorganisms, she did her bachelor study at the University of California, Davis where she majored in biotechnology. After her bachelor study, she worked in Professor Kentaro Inoue's lab at UC Davis for nine months as a voluntary researcher to gain research experience and explore her research interest. The research focused on the functional organisation of a signal peptidase via biochemical, molecular biological and genetic approaches.

Her academic background and research experience inspired her to continue her study in the renewable energy sector and to put scientific discoveries into practical use. In 2013, She started her master at Wageningen UR, The Netherlands, and specialized in marine biotechnology. She did her master's thesis project on developing a genetic transformation platform for microalgae by electroporation in the department of bioprocess engineering under the supervision of dr. Marcus Sturme and dr. Lenny de Jaeger. Afterwards, Florence performed a six-month research internship on unravelling the effect of mutant forms of a C1 transcription factor from a filamentous fungus on cellulase production at Dyadic, The Netherlands, under the supervision of dr. Hans Visser and Rob Joosten. During her internship at Dyadic, she got inspired to push herself beyond her limitation of critical thinking.

With the encouragement of dr. Marcus Sturme on breaking out of her comfort zone, Florence decided to continue her scientific journey as a PhD candidate at the TU Delft in 2016. Her PhD project focused on studying temperature tolerance of *Saccharomyces* yeasts under the supervision of dr. Walter M. van Gulik, in collaboration with the University of Minho, Portugal, and IATA, Spain. During her PhD, she supervised four students during their thesis projects which contributed to this thesis. Apart from scientific research, Florence enjoyed working with her PhD fellows in the PhD committee of the BT department and the PhD council of the faculty wherein she assisted the organisation of the annual departmental symposium and collaborated with the faculty graduate school (GS) to improve the communication platform between PhDs and the GS. In September 2020, Florence joined the process development department in uniQure as a Jr.scientist (Cell Line & Upstream Process Development) to assist the development of production processes for gene therapies.

Publications

Lip, K.Y.F., García-Ríos, E., Costa, C.E., Guillamón, J.M., Domingues, L., Teixeira, J., van Gulik, W.M., 2020. **Selection and subsequent physiological characterization of industrial Saccharomyces cerevisiae strains during continuous growth at sub- and- supra-optimal temperatures**. Biotechnology Reports 26, e00462. https://doi.org/10.1016/j.btre.2020.e00462

Pinheiro, T., Lip, K.Y.F., García-Ríos, E., Querol, A., Teixeira, J., van Gulik, W., Guillamón, J.M., Domingues, L., 2020. **Differential proteomic analysis by SWATH-MS unravels the most dominant mechanisms underlying yeast adaptation to non-optimal temperatures under anaerobic conditions**. Scientific Reports 10, 22329. https://doi.org/10.1038/s41598-020-77846-w

Muñoz, C.F., de Jaeger, L., Sturme, M.H.J., Lip, K.Y.F., Olijslager, J.W.J., Springer, J., Wolbert, E.J.H., Martens, D.E., Eggink, G., Weusthuis, R.A., Wijffels, R.H., 2018. **Improved DNA/protein delivery in microalgae – A simple and reliable method for the prediction of optimal electroporation settings**. Algal Research 33, 448–455. https://doi.org/10.1016/j.algal.2018.06.021